THE INFLUENCE OF THE MECHANICAL PROPERTIES OF TRANS-TIBIAL PROSTHESES ON AMPUTEE PERFORMANCE

Matthew J. Major

Ph.D. Thesis

2010

THE INFLUENCE OF THE MECHANICAL PROPERTIES OF TRANS-TIBIAL PROSTHESES ON AMPUTEE PERFORMANCE

Matthew J. Major

Centre for Health, Sport and
Rehabilitation Sciences Research
School of Computing, Science and Engineering
University of Salford, Salford, UK

Submitted in Partial Fulfilment of the
Requirements of the Degree of Doctor of
Philosophy, June 2010

Table of Contents

List of Figures

List of Tables

Acknowledgements

As with all great pieces of work which prove to push the boundaries of thought and emotion, there are many thanks to be had. Nonetheless, I would still like to thank some people anyway. I should like to extend my sincere gratitude to my trio of supervisors, Professor David Howard and Drs Laurence Kenney and Martin Twiste, who provided enduring support, flawless mentoring, a never-ending stream of intellectual stimulation, and sometimes, even an egg in times of dire straits. Naturally, none of this work would have maintained the level of coherence and scientific prowess as displayed in its current form without their exceptional guidance. Additionally, I would like to thank Dr Roland Ennos of the University of Manchester for acting as my Virgil to lead me through the various levels of statistical 'Inferno.' I would like to thank Drs Anmin Liu and Richard Jones for sharing their expertise on certain aspects of this project. I would also like to sincerely thank Colin Smith for assisting in the design and fabrication of my experimental devices, repairing the results of my design flaws, and educating me on how Manchester 'used to be.' I would like to thank Ruth Nicholson for reluctantly agreeing to assist with the fabrication of the sockets for the participants in this study. Thank you to my office mates, who tolerated my quirky behaviour tempered with various degrees of eccentricity. A very heartfelt and sincere thank you must be made to my surrogate family across the Atlantic, the Levys, with specific gratitude to two important figures in my life on this island, Mark and Wendy. They provided me with a home away from home, easing the overall transition of becoming an American [Scientist] in Manchester and providing an essential basis of comfort and friendship. Thank you, Dorothea, for always putting me back together, propping me back up, and gently reminding me to pace myself whenever necessary. Your endearing support never faltered and for that I am forever grateful. Thank you, Mom and Dad. Finally, I believe the Chicagoan poet Ana Castillo said it best: "To all the trees that gave their life to the telling of these stories." Naturally, without their sacrifice, this thesis would not have achieved physical manifestation and be resting on a bookshelf somewhere, providing a vast playground for dust particles.

I express my sincere gratitude to you all.

Declaration

I declare that this thesis has been composed by myself and embodies the results of my own course of study and research whilst attending the University of Salford from January 2006 to June 2010. All sources and material have been acknowledged.

Abstract

Achieving the required functionality of a trans-tibial prosthesis during the stance phase of gait (e.g., shock absorption, close to normal roll-over characteristics, and smooth transition into swing) depends on the "Amputee Independent Prosthesis Properties" (*AIPP*), defined here as the mechanical properties of the prosthetic components distal to the socket that directly influence the performance of the amputee. Accordingly, if research studies are to inform the design of better prostheses, *AIPP* must be a primary consideration. Therefore, the objectives of this PhD study were: 1) develop a standardised method of *AIPP* characterisation, and 2) investigate the effects of *AIPP* on amputee performance through human performance testing.

For the first objective, a modified version of the roll-over shape model, referred to as the Salford *AIPP* model, was developed in order to characterise the mechanical properties of a trans-tibial prosthesis (i.e., foot and pylon). A custom-built test-rig was built in order to measure the parameters of this model.

For the second objective, a series of human performance studies were conducted which measured the biomechanical, physiological, and subjective performance of five amputees during four walking conditions: self-selected walking speed (SSWS) on the level, fast walking speed on the level, SSWS on a 5% grade incline, and SSWS on a 5% grade decline. A custom-built foot-ankle mechanism allowed for independent modulation of the prosthetic plantar and dorsiflexion stiffness. Four combinations of plantar and dorsiflexion stiffness were tested during each of the four walking conditions.

Results indicated that dorsiflexion stiffness is a dominant factor in trans-tibial amputee gait performance and decreased stiffness improved performance (e.g., increased gait symmetry and reduced metabolic energy expenditure). However, future work on identifying effective *AIPP* for improved gait performance must involve amputee gait simulation, in which results from this study may serve as a means of validation.

1. Chapter One: Introduction

During the stance phase of gait, a trans-tibial prosthesis must satisfy four basic functional requirements: a) providing early stance shock absorption; b) providing close to normal shank kinematics during stance by replicating the loaded roll-over shape of the normal foot; c) adapting to the ground surface by plantar flexing to a stable foot flat position; and d) contributing to push-off and a close to normal transition into swing phase. Achieving this functionality is dependent on the Amputee Independent Prosthesis Properties (*AIPP*), which are defined here as the mechanical properties which have a direct effect on the biomechanical and physiological performance of the amputee.

Identification of the relationships between *AIPP* and desirable gait[1] characteristics (e.g., reduced metabolic energy expenditure and increased comfort) can be achieved using one or both of the following approaches: 1) studies in which the *AIPP* of particular prostheses are identified, in a manner that is independent of the amputee, and subsequently the same prostheses are evaluated through amputee gait analysis and 2) a purely modelling-based approach, in which the *AIPP* are represented mathematically and their effects on gait are predicted using simulation. A better understanding of the relationships between *AIPP* and gait characteristics will provide a basis upon which improved prosthesis designs can be developed.

However, the majority of reported studies can be categorised as *either* human performance testing of commercial prosthetic components *or AIPP* characterisation. In only a few notable cases have authors reported studies in which these two approaches are combined. In addition, very little consistency exists in the methods used for *AIPP* characterisation, rendering comparison between results of such studies very difficult.

Human performance studies that fail to characterise the *AIPP* of the prostheses under evaluation can only provide information on relative performance, and provide no information about desirable *AIPP* upon which to base improved prosthetic designs. Further,

[1] Gait may include ambulation on flat ground, as well as stair ascent/descent and running.

a number of reviews of such studies of prosthetic feet (Hafner et al., 2002; Hofstad et al., 2004; van der Linde et al., 2004), dating back 27 years, have proved inconclusive, suggesting that there has been relatively little progress in recent years in the design of prosthetic feet. Therefore, improved approaches that address both the characterisation of prostheses' properties and the evaluation of their relationship with gait performance are required to advance the field.

This thesis addresses three objectives:

1) To develop a standardised method of *AIPP* characterisation,

2) To develop a "test" foot which allows *AIPP* to be systematically adjusted,

3) To use the "test" foot in a combined study of amputee gait and *AIPP* characterisation in order to provide further insight into the relationships between *AIPP* and amputee performance.

The remainder of this thesis is separated into six chapters (2-7). Chapter Two introduces a framework for studying prosthesis design, including *AIPP* characterisation, human performance and/or gait simulation studies, and detailed design. This framework provides a structure with which to review previous approaches to *AIPP* characterisation and their use in previous experimental and simulation studies. Chapter Three describes the development of a new method of *AIPP* characterisation for trans-tibial prostheses (i.e., the combined prosthetic components distal to the socket) through use of a modified version of the roll-over shape model, referred to as the Salford *AIPP* model. Furthermore, this chapter describes how components of the test-rig used for measuring the Salford *AIPP* model are assembled to form the Instrumented Trans-tibial Prosthesis (ITP) that was used during human performance testing.

Chapter Four presents the design of an experiment to investigate the effects of *AIPP* on amputee performance. The chapter begins with a description of a "test" foot, designed to allow the experimenter to systematically adjust particular *AIPP*s in order to investigate the effects of such changes on amputee performance. The chapter then describes how the test foot together with the Instrumented Trans-tibial Prosthesis (ITP) described in Chapter Three are used in an experimental gait study with amputees. The study design involved the

systematic variation of the *AIPP*, as determined by the settings of the "test foot", and assessment of their influence on the biomechanical (i.e., kinetics, kinematics, and temporal-spatial gait parameters), physiological (i.e., metabolic energy expenditure), and subjective (i.e., ratings on comfort, exertion, and stability) performance of amputees in a range of walking conditions.

The results of the human performance experiment described in Chapter Four (i.e., biomechanical, physiological, and subjective measures) are discussed in Chapter Five, with a particular focus on relationships between *AIPP* and specific measures of gait performance. Chapter Six discusses correlations between *AIPP* and gait performance, concepts in amputee gait simulation, and ideas for future work. Finally, Chapter Seven concludes the thesis by summarising each chapter, highlighting significant results, and describing the original contributions of this work.

2. Chapter Two: Literature review

2.1. Introduction

The required functionality of a trans-tibial prosthesis can be summarised as: a) providing early stance shock absorption; b) providing close to normal shank kinematics during stance by replicating the loaded roll-over shape of the normal foot; c) adapting to the ground surface by plantar-flexing to a stable foot flat position; and d) contributing to push-off and a close to normal transition into swing phase. Achieving this functionality depends on the "Amputee Independent Prosthesis Properties" (*AIPP*). In this context, *AIPP* are those mechanical properties that directly influence the comfort and performance of the amputee. For example, both the roll-over shape and the elastic properties of the prosthesis affect amputee gait directly. Conversely, the materials and other design details that realise these properties have an indirect influence. Moreover, apparently quite different designs could have the same *AIPP*. So it is clear that if research studies are to inform the design of better prostheses, *AIPP* must be a primary consideration.

Unfortunately, to date, the vast majority of studies investigating the effects of prosthesis design on amputee performance have compared different products in terms of their biomechanical and physiological effects, but without characterizing *AIPP* (Hafner et al., 2002; Hofstad et al., 2004; Twiste and Rithalia, 2003; van der Linde et al., 2004). As the primary information distinguishing the prostheses is their trade names, this approach can only indicate their relative performance, but cannot provide information on why a particular prosthesis performs better than the next. A smaller number of studies have characterised prostheses in terms of their *AIPP*; however, with notable exceptions (Hansen et al., 2006; Lehmann et al., 1993a; Lehmann et al., 1993b; Miller and Childress, 1997; Postema et al., 1997a) very few authors have combined both types of study in an attempt to understand the correlations between *AIPP* and their effects on amputee gait (comfort, biomechanics and physiological performance). Furthermore, these correlations can also be investigated through simulations of amputee gait which incorporate *AIPP* based prosthesis models. Only

in this way will more generic information, as opposed to product specific claims, become more widely available to inform future designs, prescription and alignment procedures.

Given a better understanding of *AIPP* and their influence on amputee gait, a better approach to prosthesis design can be envisaged (involving less trial and error) in which the first stage is to identify the required *AIPP*, either from published empirical data or by simulating amputee gait using an *AIPP* based prosthesis model. Then alternative design solutions (i.e., materials, geometry, and physical construction) can be assessed using standard engineering analysis techniques, such as finite element analysis (FEA), to establish whether the design solutions realise the required *AIPP*. This design process is outlined in Figure 2.1.1.

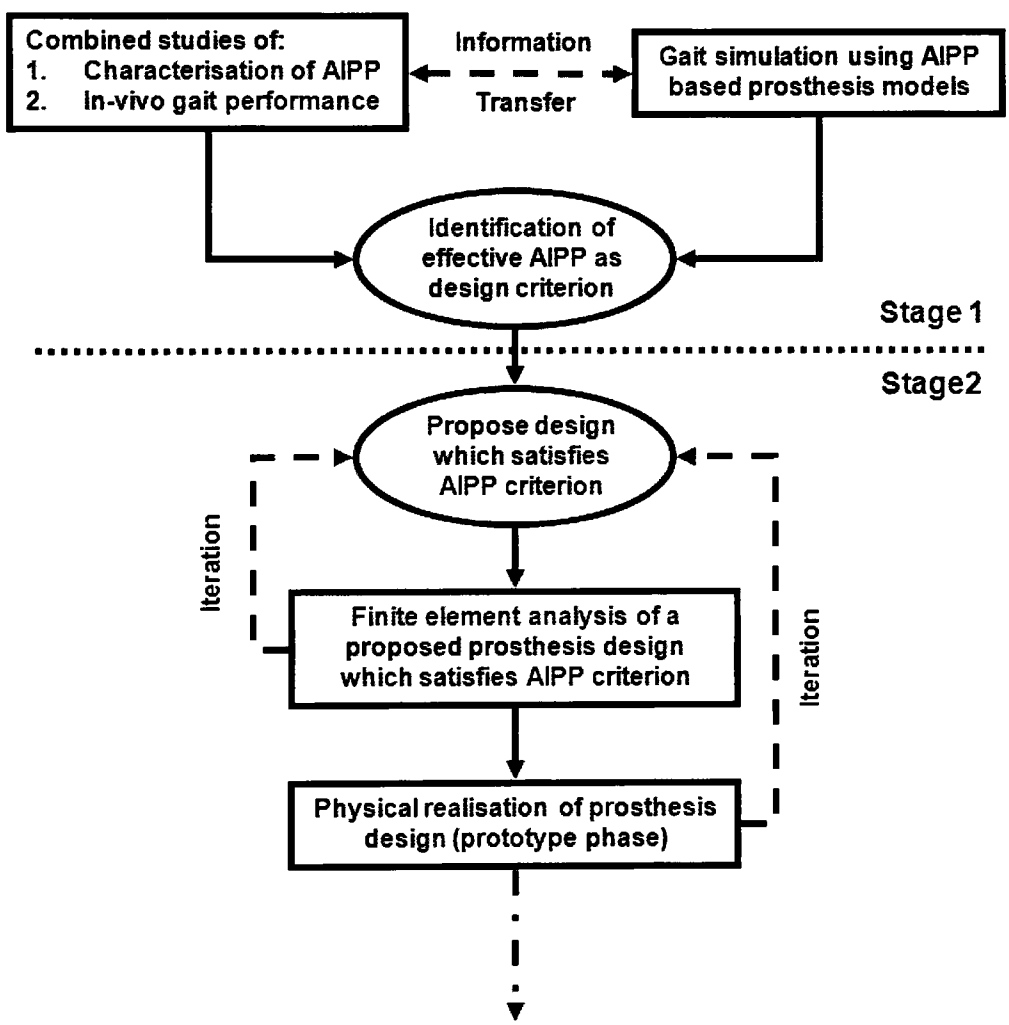

Figure 2.1.1. Prosthetic design process in two stages: 1) Characterisation and 2) Prototyping.

A major difficulty that limits R&D progress in lower limb prosthetics is the lack of an established framework for objectively and quantitatively describing "Amputee Independent Prosthesis Properties" (*AIPP*). Few studies involve the measurement of *AIPP* and, amongst those that do, there is very little consistency in the methods adopted. Therefore, the purpose of this chapter is to critically review alternative *AIPP* models and the methods previously used for measuring *AIPP*. For the purpose of this review, previous *AIPP* models are categorised as being either lumped parameter models or roll-over curve models. The scope of this review is limited to passive properties of trans-tibial prostheses and does not include components capable of internal power-generation.

2.2. Lumped parameter models

Probably the most common approach for the characterisation of prosthetic feet is the use of lumped parameter models. Such models use discrete mass, spring and damper elements to represent the mechanical behaviour of more complex, continuous structures to static and/or dynamic loading. As discussed in further detail below, these models are used as a means of characterising one or more properties of the foot or pylon, by observing the response to loads, usually at a small number of points on the plantar surface of the foot. The location at which loads are applied and the orientation of loads relative to the foot are usually chosen to be representative of one or more key points in the gait cycle, such as heel-strike. Lumped parameter models include the Maxwell (spring and damper in series), Voigt (spring and damper in parallel), and Kelvin, or Standard Linear Solid (Maxwell model in parallel with a spring) (Fung and Tong, 2001).

2.2.1. Justification of the lumped parameter modelling approach and the interpretation of the results

A number of different justifications are cited by authors in support of the use of lumped parameter modelling in studies of lower limb prostheses. Two studies reported that the motivation was simply to develop a standardised, accurate method of characterising the

mechanical properties of prosthetic feet with which to compare such feet (Geil, 2002; Kabra and Narayanan, 1991). Five further studies explicitly recognised that such an approach not only allows for comparison between feet (in some cases, with/without footwear), but also provides the *potential* to better understand how such properties relate to clinical benefits (Berge et al., 2004; Geil, 2001; Skinner et al., 1985; van Jaarsveld et al., 1990; Zeller, 2007). However, none of these studies reported experimental or simulation work that would be necessary to properly interpret their results.

Although these studies provide potentially valuable information for comparison purposes, a proper interpretation of the results for the purposes of improving future designs is only possible when integrated with in-vivo gait analysis and/or gait simulation as demonstrated in the design process in Figure 2.1.1. A small number of studies have addressed aspects of the interpretation of the results of lumped parameter models, as discussed below.

As will be discussed later in the chapter, two studies (Lehmann et al., 1993a; Lehmann et al., 1993b) used the lumped parameter approach, in conjunction with a gait lab study, to identify the relationships between mechanical properties (i.e., stiffness of the metatarsal head and heel region and natural frequency of oscillation of prosthetic feet) and amputee gait. These studies aimed to identify if changes in amputee gait performance (e.g., self-selected walking speed and metabolic cost) can be related to differences in the mechanical properties of the different prosthetic feet used. Miller and Childress (1997) used the lumped parameter approach to compare the mechanical properties of the physiological limb with prosthetic limb. Apart from characterising the *AIPP* of the prostheses used during performance analysis, the aim of this study was also to observe effects of including the telescoping function (i.e., vertical compliance) of a pylon on gait. Postema et al. (1997a) also used an *AIPP* approach to characterise the energy storage and return behaviour in a test-rig during simulated stance and compared the results with those calculated from gait analysis data. One study (Klute et al., 2004) focused on the shock absorption characteristics of prosthetic feet and characterised the mechanical properties of the heel region of various prosthetic feet, with and without shoes and under different impact velocities. Model characteristics from this study were used in a separate study to simulate the dynamic behaviour of the prosthetic limb (Klute and Berge, 2004) with the aim of identifying the

characteristics that minimised peak load and rate of loading on the residual limb at heel-strike. These studies are discussed in detail in sections 2.2.3 and 2.2.4.

Despite the frequent reporting of lumped parameter models, there is a no consensus in the literature over which particular model is best suited for the characterisation of prosthetic feet. Previous studies have, for example, used the Voigt (e.g., Berge et al. (2004) and Klute et al. (2004)) or Kelvin model (e.g., Geil (2002)) (see Figure 2.2.1.1a and 2.2.1.1b). A number of other studies have not specified a particular lumped parameter model and simply report the deflections at particular point(s) on the foot to a series of static loads and/or damping properties calculated from observing the response to a time-varying load (Geil, 2001; Kabra and Narayanan, 1991; Lehmann et al., 1993a; Lehmann et al., 1993b; van Jaarsveld et al., 1990; Zeller, 2007). In general, the justification for the choice of a particular modelling approach has often not been made clear, although the fit of the model to the observed data is, unsurprisingly, sometimes cited.

Most studies focus on one particular aspect of the foot's response, such as the response to impact loads at heel-strike and hence focus on one or two points on the foot. However, in one study, the foot was characterised by multiple, one degree of freedom spring and damper models, not explicitly coupled in either series or parallel, at 66 points along the foot (van Jaarsveld et al., 1990). This approach provides a representation of the foot's mechanical behaviour throughout the entirety of stance (i.e., heel-strike to toe-off). Apart from two studies identified by the authors (Kabra and Narayanan, 1991; Zeller, 2007), it is worth noting that all previous studies only consider the response to loading in the sagittal plane.

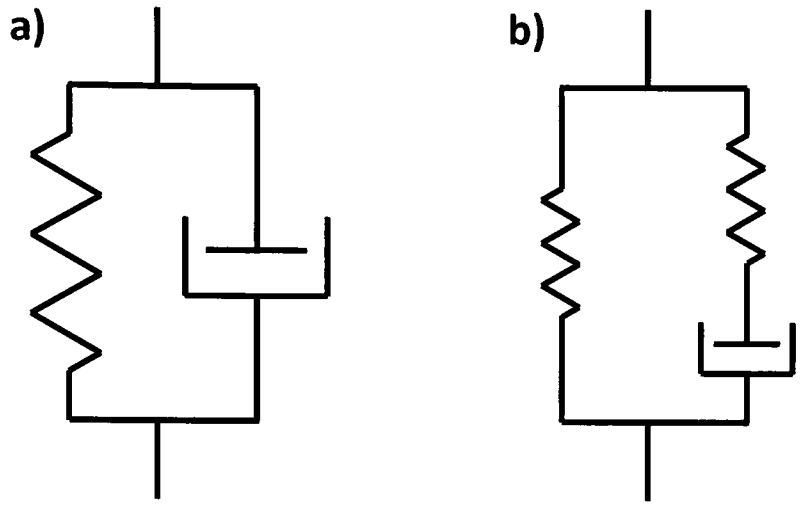

Figure 2.2.1.1. Schematic illustration of the Voigt (a) and Kelvin (b) lumped parameter model. For the adapted Voigt model used in the study by Klute et al. (2004), the equation of foot-ground reaction force, F_g, as a function of displacement, x, was: $F_g = ax^b + sign(\dot{x})cx^d|\dot{x}|^e$; where a is the linear stiffness coefficient, c, is the linear damping coefficient, and the sign($\dot{x}$) term is defined by the sign of the rate of deformation, $\dot{x}$ (1 for $\dot{x}>0$, 0 for $\dot{x}=0$, and -1 for $\dot{x}<0$). Note the inclusion of a position dependent factor in the damping element. By setting the exponent values of b and e to 1 and d to 0, this model would represent a linear spring and damper, as used in the model by Miller and Childress (1997).

2.2.2. Previously used experimental methods for measuring lumped parameter model parameters and associated issues

This section discusses the process of estimating values for model parameters (i.e., stiffness and/or damping coefficients). These values are determined experimentally using observation of the deflection and velocity of the component(s) to increasing levels of static and/or quasi-static loading or the response of the component(s) to dynamic loading, such as a step unloading or cyclical loading/unloading (Geil, 2001; Geil, 2002; Kabra and Narayanan, 1991; Klute et al., 2004; Lehmann et al., 1993a; Lehmann et al., 1993b; Miller and Childress, 1997; Postema et al., 1997a; Saunders et al., 2003; Skinner et al., 1985; van Jaarsveld et al., 1990; Zeller, 2007). During testing, the prosthetic foot is typically attached to a rigidly clamped pylon and oriented in such a way to allow loads to be applied to either a surface on the heel

or a surface on the metatarsal head region (forefoot). Load magnitudes and velocities, or kinetic energy values (in the case of impact studies) are typically chosen to correspond to values seen at heel-strike or at push-off. The direction of the applied loads usually approximately corresponds with the direction of the ground reaction force at the relevant point during gait. Deflections are then measured, typically along the axis of the direction in which the load is applied.

Additionally, stiffness and damping properties of vertical shock-absorbing pylons, represented as Voigt models, have been measured through the application of axial loads (Berge et al., 2004; Miller and Childress, 1997). Although a study has reported a method of measuring the rotational movements of torque shock-absorbing pylon adapters during gait (Twiste et al., 2004), no studies have been identified which characterise rotational stiffness of these adaptors.

Interestingly, there appears to be little consistency between the techniques used to measure (nominally) the same properties. Not only does the particular type of lumped parameter model chosen vary between studies, but so also do the orientation of the foot relative to the loads, as well as the magnitudes and timing of the applied loads, and the subsequent analysis of the results to derive model parameters.

For example, Figure 2.2.2.1 represents a typical setup as used in the study by Geil (2002), in which a material testing machine is used to subject a section of a prosthetic foot to controlled loading and unloading. The foot is located on a low friction plate and oriented in a plantar flexed position relative to a vertical rod (representing the pylon) in order to partially represent loading at late stance. In this study, stiffness and damping coefficients of a Kelvin model (Figure 2.2.1.1b) were estimated through the combined results of a stress-relaxation test, creep test, and constant strain test (all three tests are necessary produce three simultaneous equations in which to solve for the three model coefficients). Figure 2.2.2.2a shows an example of a custom test-rig used in the study by Miller and Childress (1997), to measure properties of a prosthetic foot and vertical shock-absorbing pylon. The 'ball' of the prosthetic foot was loaded by a plate to simulate late stance (Figure 2.2.2.2b) and stiffness coefficients of a Voigt model were estimated from the measured static force-

displacement relationship. The vertical shock-absorbing pylon was loaded vertically (Figure 2.2.2.2a) and the stiffness coefficients were estimated through the same technique. In this setup, the damping coefficients were estimated from the response decay resulting from either a step unloading, as in the case of estimating damping of the pylon alone, or by manually inducing an oscillation and then releasing the loading beam, as in the case with estimating damping of the pylon-foot assembly.

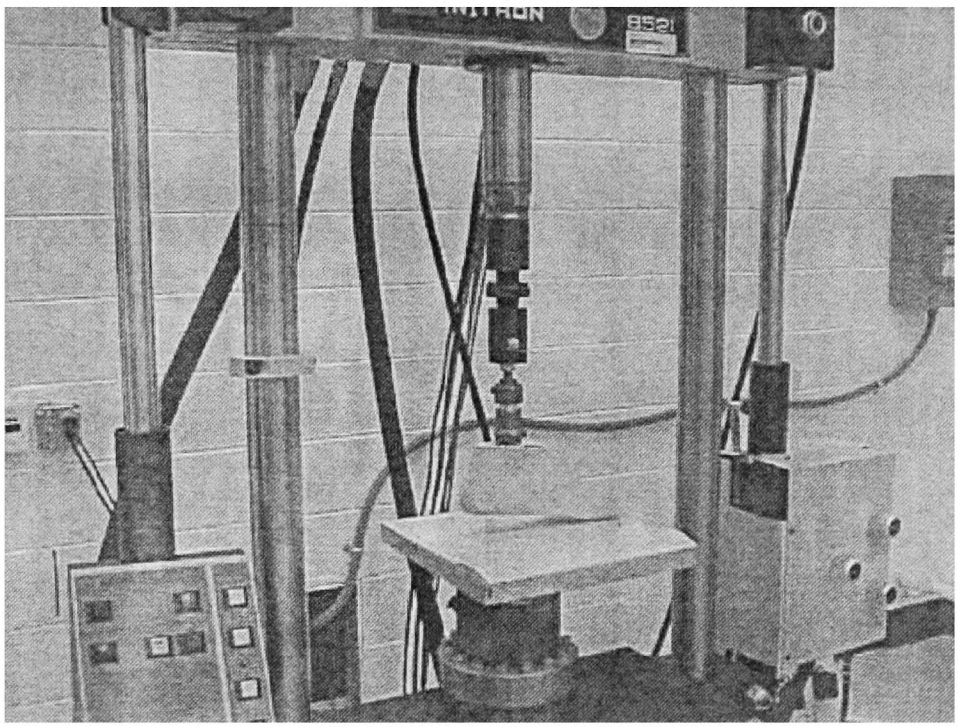

Figure 2.2.2.1. Experimental setup used in Geil (2002). Frictional forces parallel to the loading surface are minimised through a Teflon sheet loading interface.

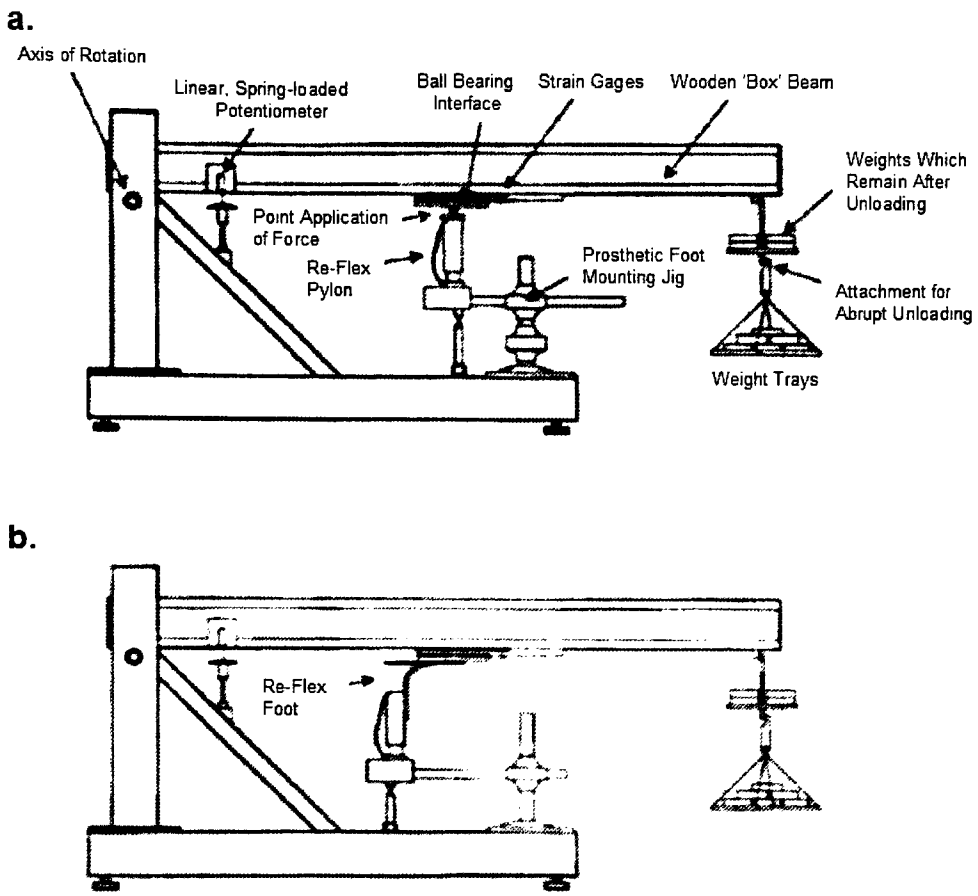

Figure 2.2.2.2. Experimental setup used in Miller and Childress (1997). Frictional forces parallel to the loading surface are minimised through a ball-bearing loading interface.

Two similar studies that aimed to characterise the stiffness properties of the Otto Bock SACH foot, but which each chose different approaches to loading and analysis were the studies by Saunders et al. (2003), and van Jaarsveld et al. (1990). Both of these studies reported linear stiffness at the 'heel strike' and 'toe off' position of an Otto Bock SACH foot, derived from the force-displacement plot when loading the foot within a material testing machine. Neither study explicitly used a specific lumped parameter model for this stiffness characterisation. The study by Saunders et al. (2003), positioned the foot such that the ankle joint angles matched those observed during gait: reported as 6 degrees plantar flexion and 2 degrees dorsiflexion for heel-strike and toe-off, respectively. However, the study by van Jaarsveld et al. (1990), positioned the pylon that was rigidly attached to the foot at -30 degrees and 35 degrees (with respect to the vertical axis) for heel-strike and toe-off, respectively. Further, each study used different approaches to the calculation of stiffness coefficients; Saunders et al. (2003) calculated the average slope of the force-

displacement curve up to a displacement of 13.77 mm and 17.77 mm for heel-strike and toe-off, respectively, while van Jaarsveld et al. (1990) used curve fitting to smooth the data and calculated the slope at either the maximum force or displacement, defined as 1000 N and 35 mm respectively, dependent on which occurred first during testing. Perhaps unsurprisingly, the two studies reported very different results for toe-off and heel-strike stiffness: 28.7 and 44 N/mm respectively in the study by van Jaarsveld et al. (1990) and 102.8 and 154.1 N/mm in the study by Saunders et al. (2003). Lehmann et al. (1993b), also reported a characterisation of the forefoot and heel stiffness of an Otto Bock SACH foot using different orientations of the loads relative to the foot to the papers of Saunders et al. (2003) and van Jaarsveld et al. (1990). By calculating the average slope of the force-displacement curves in this study, this resulted in estimates of approximately 71.6 and 32.4 N/mm for forefoot and heel stiffness, respectively. Contrary to the results from the studies by Saunders et al. (2003) and van Jaarsveld et al. (1990), the forefoot in this study was estimated as having greater stiffness than the heel. This may be the result of differences in characterisation techniques or potentially differences in the particular Otto Bock prosthetic foot model tested (which is not specified in any of the three studies).

Methods used to estimate damping properties also vary between studies. For instance, the studies by (Lehmann et al., 1993a; Lehmann et al., 1993b; Miller and Childress, 1997; Sam et al., 2000) estimated the damping properties through analysing the oscillation of the prosthetic forefoot resulting from a step unloading. Other studies, for example, have estimated damping properties from measuring the hysteresis during controlled loading and unloading of a region of the prosthetic foot (Geil, 2001; van Jaarsveld et al., 1990). The studies that used the step unloading technique reported either the damped natural frequency of oscillation (Lehmann et al., 1993a; Lehmann et al., 1993b) or damping ratio (Miller and Childress, 1997; Sam et al., 2000), as calculated from the oscillation decay using the log-decrement method. The damping ratio and damped natural frequency can be used to calculate the damping coefficient for use in a lumped parameter model, but are dependent on the applied mass used to induce the oscillations used for their calculation. However, only the studies by Lehmann et al. (1993a; 1993b) and Sam et al. (2000) explicitly stated the applied, albeit different, loads used during testing.

As discussed above there are a range of different testing methods reported in the literature. The combined effect of the different approaches to modelling and the different approaches to estimating model coefficients make any sensible comparison of results between studies very difficult.

2.2.3. Experimental studies that have used lumped parameter *AIPP*

As mentioned earlier, many previous studies have used lumped parameter models simply as a means of comparing prosthetic feet properties. Only a few studies have gone on to attempt to *interpret* the results of the lumped parameter models through human performance or gait simulation studies.

In the two studies by Lehmann et al. (1993a; 1993b), the linear stiffness properties of the heel and forefoot regions and the natural frequency of oscillation of the forefoot region of several different prosthetic feet were measured. A gait analysis study of amputees walking on the different feet was then carried out and the model coefficients of the different feet were correlated with gait analysis data. The authors reported that a greater range of prosthetic ankle angle during stance was associated with reduced forefoot stiffness (Lehmann et al., 1993a; Lehmann et al., 1993b), and increased maximum prosthetic side knee flexion moment during stance was associated with increased heel stiffness (Lehmann et al., 1993b). Furthermore, the authors observed that all of the tested prosthetic feet displayed quite different damped natural frequency of oscillation values to the values of 'stance phase' frequency. The authors defined 'stance phase frequency' as $1/2T$, where T was the average time from foot flat to toe-off as observed during gait analysis. They concluded that this mismatch between the natural frequency of the foot and the stance phase frequency may result in an untimely release of stored energy during the stance phase of amputee gait (Lehmann et al., 1993a; Lehmann et al., 1993b). Additionally, correlations were drawn between subjective feedback on comfort and the relative forefoot stiffness, and subjects showed a preference for prosthetic feet with increased forefoot compliance (Lehmann et al., 1993a).

Miller and Childress (1997), used a lumped parameter model to characterise the mechanical properties of a prosthesis and compare the model coefficients with those of the anatomical limb, as reported in previously published literature. In this study, Voigt models were used to represent a vertical shock-absorbing pylon and pylon-foot assembly. The authors noted that the overall stiffness coefficients for the pylon-foot assembly were remarkably insensitive to differences in the stiffness of the vertical shock-absorbing pylon. Further, the values of the model coefficients compared well to those of the physiological limb. The gait analysis part of the study simply observed differences in walking speed, vertical ground reaction force, and temporal parameters of gait with and without activation (i.e., enabling the telescoping function) of a vertical shock-absorbing pylon. Activation of the pylon, and hence increasing the vertical compliance of the prosthesis, was found to increase walking speed during fast walking, as well as decrease stance time of the prosthetic limb, increase vertical-ground reaction force, and increase peak-to-peak vertical trunk motion for both fast walking and jogging. In this study, subjects preferred the prosthesis with the pylon functional. Apart from in-vivo performance studies which compare differences in gait with and without the presence of vertical compliance in pylons (Adderson et al., 2007; Berge et al., 2005; Buckley et al., 2002; Gard and Konz, 2003; Jones et al., 2006; Klute et al., 2006; Miller and Childress, 1997; Twiste and Rithalia, 2003), the authors are not aware of any studies in which correlations between the *AIPP* model parameters of vertical shock-absorbing pylons and gait performance measures have been made.

The study by Postema et al. (1997a), characterised the damping properties of several prosthetic feet by measuring the hysteresis seen in response to a loading profile representative of the stance phase of gait. The prosthetic foot was loaded continuously on a surface whilst rolling from simulated heel-strike (pylon angle of 32 degrees with respect to the horizontal axis) to toe-off (pylon angle of 40 degrees with respect to the horizontal axis). Mechanical work was calculated at all intermediate pylon angles as the integral of force with respect to displacement. These results were used to compare the energy storage and release (and hence energy loss) as calculated from total ankle power during gait with that measured independent of the amputee in the test device. Results indicated that the energy storage measured within the test device was 2 to 3 times smaller than that calculated from total ankle power during gait, which the authors believe is primarily due to the differences in

method of calculating energy (i.e., integration of prosthetic ankle joint moment times angular displacement from gait versus integration of applied force times material deformation from the test device). This problem with the in-vivo measurement techniques for calculation of energy storage and return in prosthetic feet has been investigated in studies by Prince et al. (1994) and Geil et al. (2000). The study by Prince et al. (1994) presented an alternative method for calculating energy storage and return that accounted for both rotational and translational terms in the calculation of power. Furthermore, the study by Geil et al. (2000) compared a conventional analysis (including only rotational terms) with the analysis that accounted for the translational terms also. The authors reported that by including the translational term in their calculation of power, this resulted in estimated calculation of less energy stored and more energy returned during the stance phase of gait when using an energy storage and return (ESAR) foot as compared to calculating energy through rotational terms alone (Geil et al., 2000).

It is worth noting that for all of these studies comparing mechanical properties of the prosthesis with results from gait studies, the prosthesis was characterised off the body and standard clinical alignment approaches were then used to set up the device on the amputee. It is known that alignment can significantly affect the mechanical behaviour of prostheses (Hansen, 2008; Hansen et al., 2003) and it is not clear whether this factor may have affected gait study results and hence conclusions drawn.

2.2.4. Simulation studies that have used lumped parameter *AIPP*

Lumped parameter models have also been used in numerical simulation studies to predict the effects of different prosthesis properties on amputee gait. In a study by Klute and Berge (2004), the prosthetic limb of the amputee was modelled in order to simulate the influence of certain variables (i.e., prosthetic foot, shoes, amputee mass characteristics, and impact velocity) on the vertical component of the ground reaction force at heel-strike. Various prosthetic feet (with and without shoes) were characterised using the Voigt model as described previously (Klute et al., 2004). The amputee was also represented using several Voigt models to simulate the upper and lower rigid bodies and oscillating soft tissue masses

of the amputee. Results from this model were validated with results from in-vivo experimentation. A sensitivity analysis was then conducted with the lumped parameter model simulation by systematically adjusting the stiffness and damping coefficients of the prosthetic foot and shoe in order to observe their effect on the vertical ground reaction force. This simulation study in combination with the previous experimental characterisation study satisfies all the requirements for stage 1 of the design process in Figure 2.1.1. Within the limitations acknowledged by the author, this simulation can be used as a design tool for identifying the effective *AIPP* with respect to the design objective of minimising the vertical ground reaction force at heel-strike.

An additional simulation study utilised a numerical musculoskeletal model to investigate the effects of an ESAR prosthetic foot-ankle mechanism on trunk support, forward propulsion, leg swing initiation, and muscle activation patterns required to produce a normal, symmetric gait pattern (Zmitrewicz et al., 2007). The prosthetic foot-ankle mechanism was modelled as an articulated ankle joint that behaved as a viscoelastic torsional spring, parameters of which were derived from data reported in the experimental study by Lehmann et al. (1993b). This simulation identified how the ESAR prosthesis stored and returned energy during the stance phase of gait and how this compared to muscle contractions and associated work during non-amputee walking. Additionally, this study was able to identify muscle compensatory strategies employed by amputees to produce a symmetric gait pattern. This study demonstrates the usefulness of simulation in understanding amputee gait and its potential as a tool to systematically investigate the effects of different *AIPP* on gait performance.

2.3. Roll-over model

A model which begins to bridge the gap between characterising the mechanical properties of the prosthesis and its functional performance is the roll-over shape model (Hansen et al., 2000; Knox, 1996). The roll-over shape is a spatial mapping of the Centre of Pressure (CoP) location along the plantar surface of the foot relative to a shank-based coordinate frame. Through varying applied loads, a family of roll-over shapes can be produced which provide a

representation of foot stiffness. The roll-over shape can be measured both as *AIPP* from data generated using a test-rig (Curtze et al., 2009; Hansen, 2008; Hansen et al., 2000; Hansen et al., 2006; Sam et al., 2000; Sam et al., 2004), and in-vivo from continuous data produced during the stance phase of gait (Hansen et al., 2000; Hansen et al., 2003).

The in-vivo roll-over shape is a function both of the prosthetic foot's mechanical and alignment properties and the particular forces acting on the foot during the stance phase of gait. Hansen showed that prostheses with very different *AIPP* roll-over shapes can be aligned to produce the same in-vivo roll-over shape (Hansen et al., 2003) and hence the in-vivo roll-over shape is clearly not an *AIPP*. When establishing correlations between prosthetic properties and in-vivo gait performance, it is the *AIPP* roll-over shape which should represent these properties.

The roll-over shape model is a more intuitive representation of the mechanical properties of trans-tibial prostheses than many of the lumped parameter approaches discussed above, combining a representation of stiffness properties and geometry. In previous studies, damping properties have been measured in parallel with, but independent of, the roll-over shapes by applying a cyclical load to a section of the prosthetic foot (e.g., forefoot) (Sam et al., 2000; Sam et al., 2004), similar to the procedure described in the study of Miller and Childress (1997). However, the visco-elastic effects have yet to be integrated into the roll-over model. Additionally, the previously published versions of the roll-over shape model (Curtze et al., 2009; Hansen et al., 2000; Knox, 1996; Sam et al., 2000) do not include measurements of shear stiffness (i.e., linear stiffness in the direction normal to the vertical ground reaction force vector).

2.3.1. Experimental studies that have used *AIPP* roll-over shape

The roll-over shape model has also been used in combination with in-vivo gait analysis to explore the relationships between *AIPP* and gait. Hansen et al. (2006) investigated the relationship between roll-over shape arc length and gait kinematics and kinetics, using the custom-designed 'Shape&Roll' prosthetic foot. The Shape&Roll prosthetic foot was

constructed of copolymer plastic in which the changes to its in-vivo roll-over shape were achieved through cut-outs made in the dorsal aspect of the foot (Figure 2.3.1.1). Therefore, the foot became highly stiff in each of its loaded configuration and the changes in its behaviour were assumed to be primarily due to changes in geometry, not to the elastic properties of the foot. In this study, correlations were made between the roll-over shape arc length (SHORT, MEDIUM, and LONG as seen in Figure 2.3.1.1) and gait performance measures. For example, it was found that reducing the arc length resulted in reduced walking speed and prosthetic ankle moment dorsiflexion and an increased first peak of the vertical ground reaction force on the sound limb.

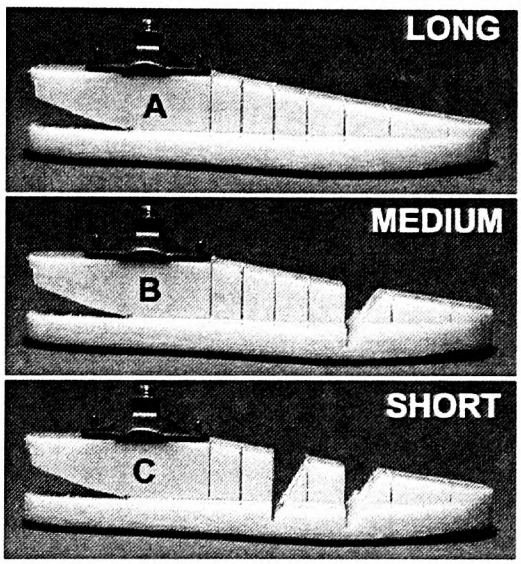

Figure 2.3.1.1. The Shape&Roll prosthetic foot that was used to create the long, medium, and short roll-over shape arc length test conditions (Hansen et al., 2006).

The roll-over shape model has also been used to characterise the effects of prosthesis alignment on gait. In a well designed study, Hansen et al. (2003) showed that prosthetists, when aligning different prostheses (of quite different *AIPP*), appear to converge on alignments for each of the prostheses that result in a single, common in-vivo roll-over shape. The study clearly demonstrated that prosthetic devices of very different *AIPP* could produce similar in-vivo roll-over shapes. Further, the study suggests that the differences in gait behaviour observed by clinicians when comparing feet are reasonably well explained by use of the roll-over model. Interestingly, however, the study did not go on to characterise in

detail the changes to the mechanical properties as a result of alignment. This is important as an additional study demonstrated that through changes in sagittal plane alignment, different *AIPP* can be obtained with the same prosthetic foot (Hansen, 2008) as alignment determines the points of contact of the foot during stance.

2.3.2. Simulation studies that have used *AIPP* roll-over shape

The roll-over shape model has recently been used in a numerical simulation to investigate the effects of prosthetic alignment, prosthetic mass and mass distribution, and varying roll-over shape radius on the kinematics of amputee gait (Srinivasan et al., 2009). Gait kinematics were predicted using a forward dynamic simulation of amputee gait and the roll-over shape was modelled as a circular arc. The study used an optimisation approach to vary the roll-over shape radius and prosthetic alignment characteristics with the objective of minimising both the total joint torque and joint power costs during gait. However, the roll-over model in this simulation was purely geometric and did not include stiffness and damping properties, factors which would influence joint torques and hence powers. Results indicated that lower total joint torque and joint power costs could be achieved by using a prosthetic roll-over shape radius that is equivalent to or slightly larger than the radius of the anatomical roll-over shape. Furthermore, the alignment which minimised total joint torque and joint power costs was found to be dependent on the roll-over shape radius.

2.3.3. The roll-over shape as a model for characterisation of prosthetic feet

Overall, the roll-over shape model provides a clear and convincing way of explaining the influence of prosthetic foot geometry and alignment on gait. However, the roll-over shape model, as described in the literature, does not explicitly account for visco-elastic behaviour. Therefore, two prostheses having the same in-vivo roll-over shape, but different visco-elastic properties may have different effects on gait, such as fatigue, or impact loads at heel-strike. Such effects might not be easily picked up during clinical gait observation used by prosthetists to align prostheses and this may explain the remarkable degree to which roll-over shape explains alignment (Hansen et al., 2003). However, as the roll-over shape does

not include viscoelastic effects it is limited when used as a model with which to investigate energy storage and return, or other dynamic effects.

2.4. Discussion

Proper characterisation of *AIPP* is essential to the first stage of the design process outlined in Figure 2.1.1. In order to improve on existing prosthesis designs, the properties of existing prostheses must be measured independent of the amputee before they are subjected to in-vivo performance testing.

An understanding of the correlations between *AIPP* and their effects on amputee gait can then be developed through combined studies of the characterisation of *AIPP* and gait performance. An *AIPP* model could also be used as part of a gait simulation to explore its effects on gait. The advantages of gait simulation-based exploration of the effects of *AIPP* on gait are that it allows for rapid and extensive design-test iterations that would not be possible with human subjects. Further, there are no constraints on the choice of *AIPP*s that can be tested within gait simulation. The predicted results from simulations may then be validated through carefully designed in-vivo experimentation. It is interesting to note that the vast majority of the in-vivo studies on gait performance identified by the author are constrained by the discrete set of *AIPP*s associated with commercially available feet. It is possible to envisage studies in which it would be advantageous to be able to vary a particular *AIPP* in a systematic manner, without varying other *AIPP*s. Such an approach may only be possible with an experimental foot designed for this purpose and this concept is explored in more detail in Chapter Four.

The output of such studies would be an (or a family of) optimal *AIPP,* which serve as the design criterion for the second stage of the design process. The *AIPP* can be represented as either a lumped parameter model or a roll-over shape model. While using a one degree of freedom lumped parameter model to represent a shock-absorber element is clearly a reasonable approximation, it is argued that such models do not adequately represent the complex behaviour of a prosthetic foot. In other domains, lumped parameter models are

most commonly employed to represent systems in which particular elements clearly dominate the behaviour (e.g., it is reasonable to model a car suspension system using a lumped parameter model in which the mass properties of the car body and the spring/damper properties of the suspension dominate the dynamics). However, with a small number of notable exceptions, most studies have chosen only to characterise behaviour of prosthetic feet at one or two locations. It is far from clear whether, for example, the stiffness at the heel or forefoot dominates the influence of prosthetic feet on gait and hence the benefit of simplifying the foot model to this extent is debatable. Also, as pointed out earlier, there has yet to be agreed a standard approach to lumped parameter model characterisation and this also greatly limits their utility. Most importantly, unless integrated with gait experimentation or gait simulation, interpreting the results of such simple models is extremely difficult, if not impossible.

By contrast, Hansen's series of papers in which the relationships between roll-over shape parameters and prosthetic gait are clearly shown, strongly suggest that this is the more promising approach. However, visco-elastic behaviour and the response to shear loads are not yet included in the standard roll-over shape model. Further, when using the *AIPP* roll-over shape model, it is important to maintain the same alignment of the foot relative to the pylon in any in-vivo studies.

The second stage of the design process could include finite element analysis to determine the geometry and properties of the foot that would deliver the required *AIPP*. In the study by Saunders et al. (2003), optimal material properties of a section of a prosthetic foot were identified through material behaviour simulation and used as an input into an FEA model of the foot. In the studies by Allard et al. (1995) and Jang et al. (2001), foot geometry optimisation was performed using FEA. Allard et al. (1995) used maximum energy storage capability of the prosthesis as the objective function driving the optimisation; Jang et al. (2001), used a representative set of normal gait data as input to an FE model of the foot. An optimisation was carried out with the objective of minimising predicted work at the knee. However, none of these studies included a predictive amputee gait model, in which the properties of the foot would influence gait behaviour. As a result, the chosen design criteria may, or may not yield improved amputee performance. For example, an increase in

maximum energy storage capability of the prosthesis might seem an intuitive approach to improving the energy returned at toe-off to facilitate smoother transition (or propulsion) into swing. However, if this increase in stored energy is returned to the amputee at an inappropriate time during gait, this could have a negative effect by increasing muscular demand to maintain stable gait dynamics (Lehmann et al., 1993b). This emphasises the need to choose appropriate design objectives based on amputee performance (e.g., reduced metabolic cost and increased stability) as is outlined in the design process of Figure 2.1.1.

The above discussion on measuring *AIPP* only applies to passive components, and does not relate to the recent developments in design of prosthetic foot-ankle systems with internal-power generation capabilities (e.g., Au et al. (2008), Collins and Kuo (2010), and Moser et al. (2009)). In these cases, energy is being generated by the prosthesis and variation in alignment during gait is occurring and hence the passive *AIPP* no longer apply. However, although these devices offer the promise of providing an amputee with improved gait performance, this does not eliminate the need for passive trans-tibial prosthetic components. Amputees in low-income and developing countries depend on passive components which are cheap, durable and require minimal maintenance. A similar argument also applies to developed countries where associated costs often limit a patient's selection of prosthetic components. Therefore, focus still needs to be maintained on improving the design of passive prosthetic components and further exploring their integral relationship with user performance.

3. Chapter Three: Amputee Independent Prosthesis Properties – Description, measurement and applications

3.1. Introduction

Modern trans-tibial prostheses are usually assembled from modular components, which are available in many different variants from many companies. The effects on the amputee in terms of comfort, gait biomechanics and physiological performance depend on the functional properties of the assembled prosthesis and these relationships are particularly complex.

To date, the vast majority of studies investigating the effects of prosthesis design on amputee performance have compared different products in terms of their biomechanical and physiological effects, but without characterizing the mechanical properties of the prostheses (van der Linde et al., 2004). In such papers, the primary descriptors distinguishing the prostheses are their trade names; and hence this approach can only indicate their relative performance, but cannot provide information on why a particular prosthesis performs better than the next. A smaller number of studies have characterised prostheses in terms of their mechanical properties, measured in ways that are independent of the amputee (Berge et al., 2004; Geil, 2001; Geil, 2002; Hansen et al., 2000; Kabra and Narayanan, 1991; Klute et al., 2004; Lehmann et al., 1993a; Lehmann et al., 1993b; Miller and Childress, 1997; Postema et al., 1997a; Sam et al., 2004; Skinner et al., 1985; van Jaarsveld et al., 1990). However, with notable exceptions (Hansen et al., 2006; Lehmann et al., 1993a; Lehmann et al., 1993b; Miller and Childress, 1997; Postema et al., 1997a), very few authors have combined both types of study in an attempt to understand the correlations between Amputee Independent Prosthesis Properties and the effects on amputee gait (comfort, biomechanics and physiological performance). Only in this way will more generic information, as opposed to product specific claims, become more widely available to inform future designs, prescription and alignment procedures.

If a greater number of future studies are to include the measurement of prosthesis properties, there is a need for a clear and comprehensive means of representing those properties, with supporting measurement techniques. This is particularly the case for stance phase properties, such as stiffness and damping, which are the subject of this chapter. Previous work can be loosely categorised as using one of two alternative representations: lumped parameter models or roll-over curves. However, these are not necessarily mutually exclusive.

A common representation of stance phase properties is the lumped parameter, or spring and damper, model (Klute and Berge, 2004; Miller and Childress, 1997). This model represents prosthesis elasticity (position-dependent forces) and damping (velocity-dependent forces). Such a model is useful in predicting the energy stored during load acceptance and returned during late stance to aid propulsion; the intended function of energy storage and return (ESAR) feet. These mechanical properties are typically quantified through either static or dynamic testing; both of which are performed in the sagittal plane, assuming that the medial-lateral forces experienced during gait are small in comparison to those in the sagittal plane (Perry, 1992).

Static quantification involves compressing the surface of the prosthetic foot under varying loads, at a series of foot angles which reflect the progression of the Centre of Pressure (CoP) during the stance phase of walking (Lehmann et al., 1993a; Lehmann et al., 1993b). The resulting load-versus-deformation plots provide information on prosthesis compliance at the specified foot angles (van Jaarsveld et al., 1990). The loads are applied either through active mechanical drives (e.g., universal materials testing machines) (Geil, 2001; Geil, 2002; Lehmann et al., 1993a; Lehmann et al., 1993b; van Jaarsveld et al., 1990) or gravity driven mechanisms (e.g., custom testing rigs) (Miller and Childress, 1997). Vertical shock-absorbing pylons (VSAPs) are also subjected to static testing, independent of the prosthetic foot (Berge et al., 2004; Miller and Childress, 1997).

In dynamic testing, the prosthesis or VSAP is subjected to a controlled loading and unloading process; again at foot angles reflecting CoP progression. This information can be used to quantify damping (energy dissipation) coefficients (Berge et al., 2004; Klute et al., 2004; van

Jaarsveld et al., 1990) and natural frequencies (Lehmann et al., 1993a; Lehmann et al., 1993b; Miller and Childress, 1997). Dynamic testing can also be conducted using active mechanical drives (Berge et al., 2004; Geil, 2001; Geil, 2002; van Jaarsveld et al., 1990) or gravity driven mechanisms; in the latter case, the prosthetic component is quickly unloaded to produce an oscillatory response representative of a second-order, underdamped system (Lehmann et al., 1993a; Lehmann et al., 1993b; Miller and Childress, 1997).

Lumped parameter models have their limitations. For example, when prosthesis compliance is represented by a set of load-versus-deformation plots, these are difficult to interpret in biomechanical terms and do not incorporate information on prosthesis geometry and alignment.

The roll-over shape, as described by Hansen et al. (2000), is a more intuitive representation of the mechanical behaviour of a prosthesis during gait. As the prosthetic foot-ankle complex compresses through stance phase, the resulting trajectory of the CoP forms a curve as the shank rolls over the stance foot. Specifically, the roll-over shape is the path followed by the CoP described in a coordinate frame attached to the prosthesis shank. The roll-over curve is a function of the geometry, construction, materials, and alignment of the prosthesis. In the study by Hansen et al. (2000), the roll-over curves of four different prosthetic feet were measured using a similar testing rig to that of Miller and Childress (1997). In their method, the prosthetic foot is tested at five different angles to a loading beam, reflecting the ground to pylon angles seen during stance phase (60°, 75°, 90°, 97°, and 105°).

Whilst the methods discussed above provide valuable data, they fail to give a comprehensive description of stance phase properties. In particular, both shear stiffness and damping properties are usually absent. Furthermore, with the exception of roll-over models, prosthesis geometry and alignment are not explicitly represented. We believe that a roll-over model offers a compact and intuitive means of representing both stance phase stiffness and geometry/alignment. However, in most cases, roll-over models have not been applied in a way that is independent of the amputee. Therefore, in this chapter, a model of Amputee Independent Prosthesis Properties (*AIPP*), for trans-tibial prostheses, is proposed which provides a comprehensive representation of stance phase properties and incorporates the

best features of both lumped parameter and roll-over models. Additionally, we describe the test-rig, instrumentation, and procedures that were established to measure *AIPP*. Finally, preliminary results are presented and conclusions drawn with regard to the methods proposed.

3.2. Methods

The objectives of this work were: to first define a comprehensive way to describe stance phase properties (stiffness and damping); then to develop test methods to capture those properties; and finally to present preliminary results using the proposed methods. Therefore, the methods section deals with:

- the *AIPP* description of stance phase properties;
- test-rig design;
- measurement of compliance normal to the support surface;
- measurement of compliance tangential to the support surface;
- measurement of damping.

3.2.1. Amputee Independent Prosthesis Properties (*AIPP*)

Both the lumped parameter and roll-over shape models provide valuable information on mechanical properties that one technique cannot capture on its own. For example, the roll-over shape model includes information on prosthesis geometry and alignment as well as compliance, whereas the lumped parameter model is particularly useful for describing damping properties. Therefore, the representation of Amputee Independent Prosthesis Properties (*AIPP*) we are proposing is a combination of both techniques, and this is accomplished by supplementing the roll-over shape with additional lumped parameter data. In almost all of the published work a single roll-over curve is presented; but unfortunately a single curve cannot distinguish between a compliant foot, where roll-over shape is a result of elastic deflections, and a rigid foot of the same shape. Only when a set of curves is presented for different loads, do these provide a proper representation of compliance normal to the

support surface. Furthermore, the roll-over curve does not present information on compliance tangential to the support surface or on damping. Therefore, the proposed *AIPP* model includes:

1. Normal compliance (perpendicular to the ground surface), which is related to the prostheses' ability to store and return elastic energy.
2. Shear compliance (parallel to the ground surface), which is also related to the prostheses' ability to store and return elastic energy.
3. Normal damping (perpendicular to the ground surface), which is related to the extent to which the prosthesis dissipates energy.

The data presentation approach is described in the section 3.3.

3.2.2. Test-rig design

A test-rig (Figure 3.2.2.1) has been developed to measure *AIPP* in a standardised way, independent of the amputee. The test-rig was constructed of pre-manufactured, commercially available aluminium profiles and articulated joints[2]. The design of the test-rig is based around the use of a six-channel load-cell[3] to measure the three-dimensional forces and moments applied to the proximal part of the prosthesis. Details on the calibration procedure of this load-cell are found in Appendix A.1. An adaptor was made to connect the load-cell to the prosthesis pylon, and a standard Otto Bock pyramid adaptor[4] is used to attach the foot to the pylon, which allows for adjustments in angular alignment.

[2] Bosch Rexroth AG, Lohr am Main, Germany

[3] Load-cell model 51E20A, JR3 Inc., CA, USA

[4] Otto Bock Gmbh, Duderstadt, Germany

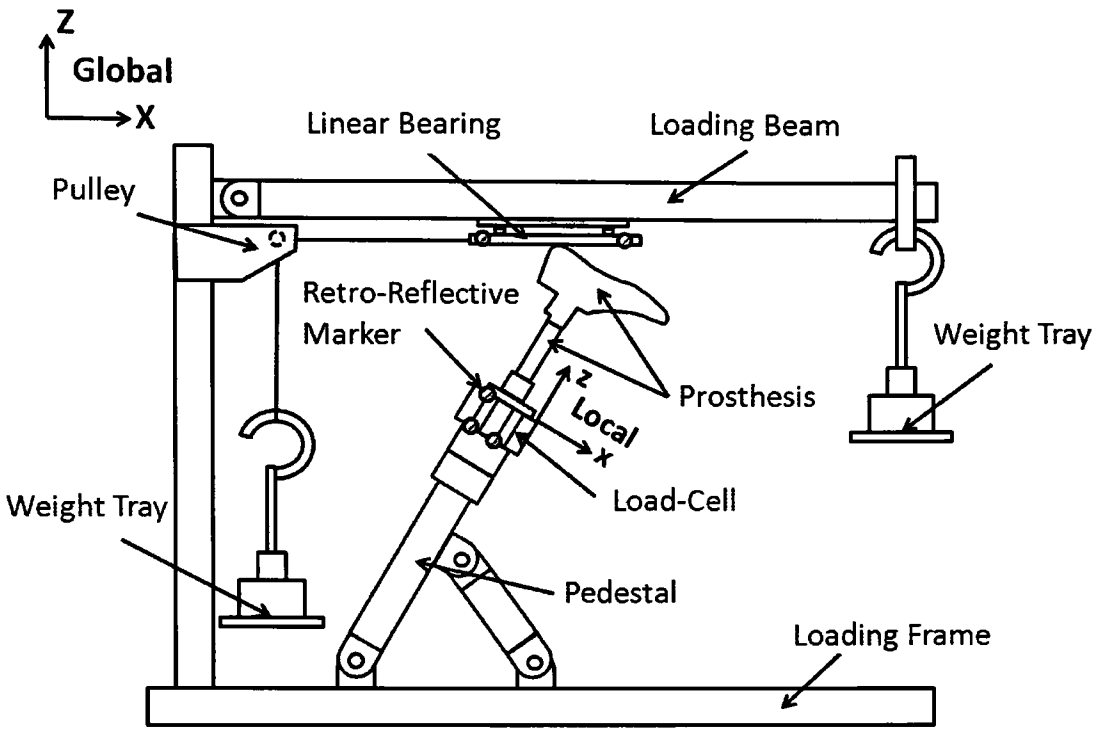

Figure 3.2.2.1. The test-rig consists of nine primary components: loading frame, loading beam, pedestal, linear bearing, pulley, weight tray for application of normal force, weight tray for application of shear force, load-cell, and prosthesis. Both the loading beam and pedestal are connected to the loading frame by near-frictionless hinge joints. Six retro-reflective markers are used in total, three to define the load-cell coordinate frame (origin at its geometric centre) and three to define the foot contact surface.

The load-cell is attached to the central pedestal of the test-rig which allows rotation of the prosthesis in the sagittal (global x-z) plane to adjust the angle between the pylon and the foot contact surface (loading beam) to replicate the angles seen between the tibia and ground in normal gait. A near-frictionless linear bearing, installed between the foot contact surface and the loading beam, decouples normal and shear forces and simplifies the calculations used to identify the centre of pressure in the load-cell coordinate frame (fixed with respect to the pylon).

Force and moment data from the load-cell are recorded at a frequency of 1000 Hz and filtered through a 5 Hz low-pass Butterworth filter. The relative position and orientation of the load-cell, with respect to the loading surface, is measured by capturing the positions of

six retro-reflective markers using a multi-camera motion capture system[5]. Marker position data is sampled at 100 Hz and filtered through a 6 Hz low-pass Butterworth filter.

An advantage of the approach we have adopted is that exactly the same load-cell and prosthesis alignment with respect to the load-cell can be used both in the test-rig and for in-vivo testing. This is possible because the load-cell and prosthesis can be removed from the test-rig and attached to an amputee's socket without interfering with the set-up. Conversely, in previously reported studies, the test-rig and in-vivo measurement set-ups have been different, hence introducing additional sources of measurement error. Furthermore, amputee specific alignments of prosthetic components distal to the socket have not usually been accounted for during test-rig measurement of mechanical properties. The alignment of the prosthesis is critical in determining its roll-over shape and, hence, mechanical behaviour during gait (Hansen, 2008).

Thus, a secondary outcome of the test-rig design adopted here is the ability to achieve a seamless transition from test-rig to instrumented trans-tibial prosthesis for in-vivo testing (Figure 3.2.2.2). All of the components that are attached to the test-rig pedestal (load-cell, prosthetic pylon, and prosthetic foot) can be attached to the socket using a standard Otto Bock pyramid adaptor, which also allows for alignment adjustments proximal to the load-cell. This instrumented prosthesis can be used to measure the forces and moments at the distal end of the socket; and hence enables derivation of ground reaction forces and moments, without the limitations imposed by the use of force plates, and also derivation of the in-vivo roll-over shape.

[5] Vicon, Vicon Motion Systems Ltd, Oxford, UK

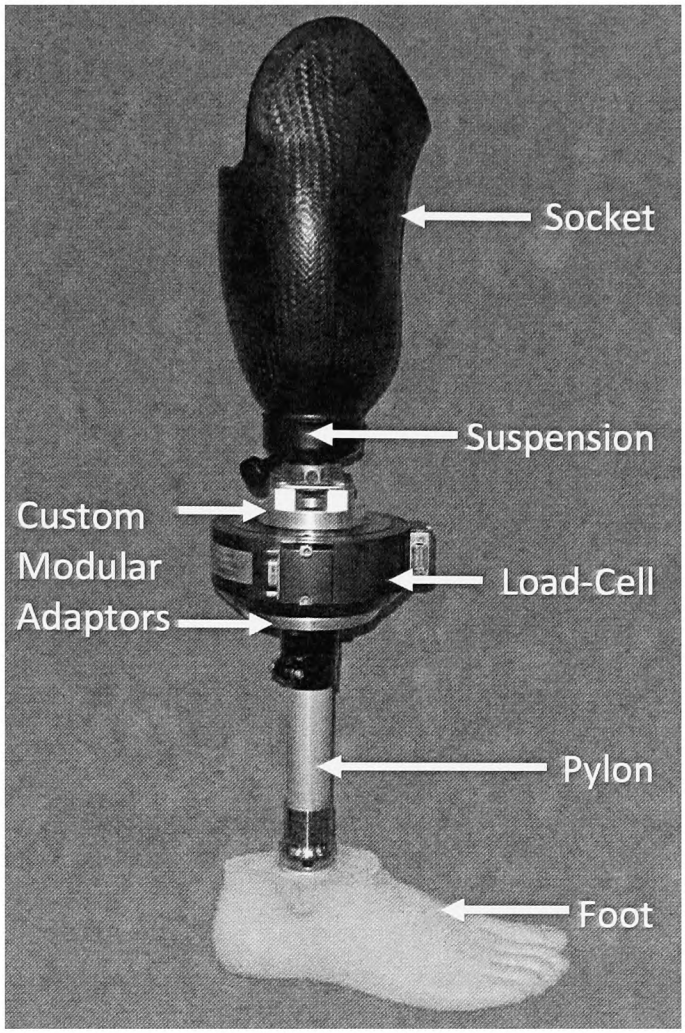

Figure 3.2.2.2. The instrumented trans-tibial prosthesis consists of four primary components: socket, load-cell, pylon, and foot. Custom modular adaptors are used between load-cell and socket, and between load-cell and pylon. Standard Otto Bock pyramid adaptors are located between load-cell adaptor and socket, and between pylon and foot, which allow for alignment adjustments in all three planes.

3.2.3. Measurement of normal compliance (roll-over curves)

To measure a set of roll-over curves (normal compliance), the pylon is placed at a series of angles with respect to the foot contact surface and, at each angle, different normal loads (perpendicular to the foot contact surface) are applied to the foot. The foot's longitudinal axis (connecting the mid-point of the posterior surface of the heel to the anterior surface of

the foot between the first and second toe) is aligned so that it lies in the sagittal plane. The normal load is achieved by adding weights to a tray at the free end of the pivoted beam while adjusting the foot contact surface so that it is nominally horizontal. Thus, the load applied at any point along the loading beam is proportional to the load at the end of the beam and the length of the loading beam. Note that precise adjustment of the load applied is not necessary as the actual force system applied to the prosthesis is measured by the load-cell.

The centre of pressure on the foot contact surface, in the pylon (load-cell) sagittal plane, is calculated from the sagittal plane load-cell readings and the sagittal plane coordinates of the retro-reflective markers. Referring to Figure 3.2.3.1, the load-cell readings can be used to calculate the moment arm, R, locating the line of action of the force applied to the foot by the loading beam, F_A, as follows:

$$R = \frac{M_{LY}}{(F_{LZ}\cos\theta + F_{LX}\sin\theta)/\cos\phi} \quad , \tag{3.1}$$

where M_{LY} is the sagittal plane moment about the load-cell geometric centre,

F_{Lx} and F_{Lz} are the sagittal plane forces acting at the load-cell centre,

θ is the angle of the pylon from vertical (obtained from markers), and

ϕ is the angle of the loading beam from horizontal (obtained from markers).

Then from the geometry of the test-rig, the coordinates of the centre of pressure (roll-over point) can be calculated as follows

$$X = D\sin(\beta) \quad , \tag{3.2}$$

and

$$Z = L - D\cos(\beta) \quad , \tag{3.3}$$

where $D = R + L\cos(\beta)$, $\beta = 90 - \theta + \phi$, and L is the distance along the pylon axis between the load-cell geometric centre and the loading surface (obtained from markers).

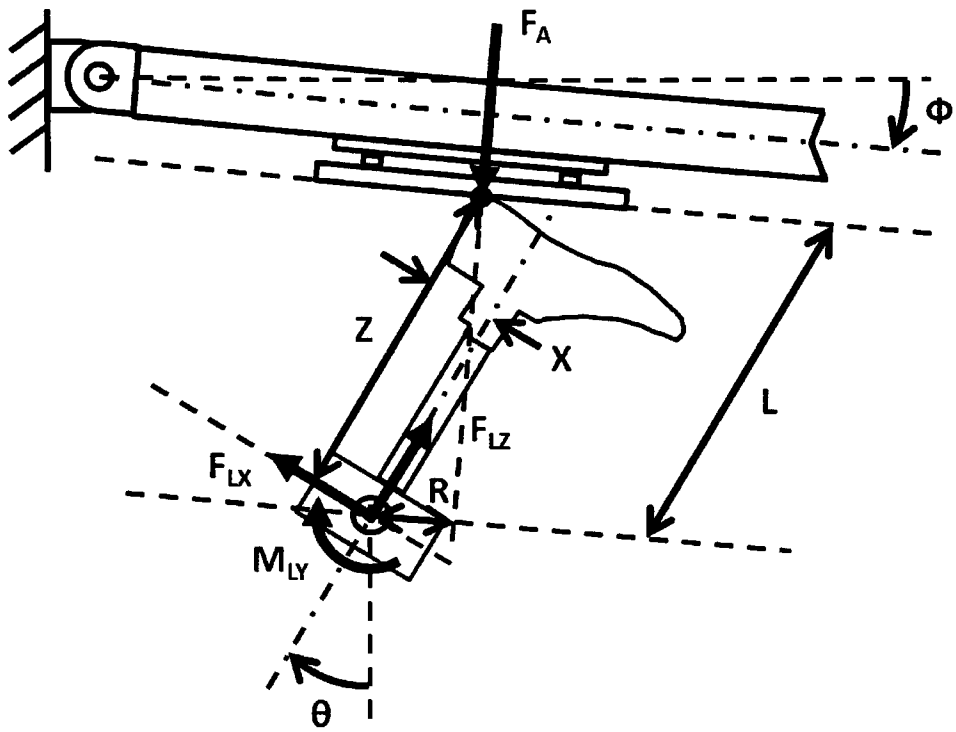

Figure 3.2.3.1. Free-body diagram of the loading scenario during measurement of a single roll-over point (represented by a solid circle).

3.2.4. Measurement of tangential compliance

The shear (tangential) force is applied by adding weights to a tray at the free end of the cord that runs over the pulley and is attached to the linear bearing. The pulley can be translated vertically to ensure that the force applied is parallel to the foot contact surface. To maintain sufficient friction between the foot and contact surface, a normal load corresponding to body weight is first applied. Subsequently, a tangential load is applied and the displacement of the linear bearing is recorded to measure shear compliance. To ensure that the displacement is due only to the compliance of the prosthetic components and not the test-rig, it is measured relative to the distal face of the load-cell where it attaches to the pylon.

3.2.5. Measurement of damping

For any given pylon angle, at which the normal and shear compliance is measured, a measure of normal damping is also obtained by inducing an oscillatory response by: 1) adding a nominal weight to the tray; 2) pulling hard on the tray; and 3) quickly releasing the tray. This quick unloading produces an oscillatory response, from which the damping ratio ζ (a dimensionless measure) can be calculated as follows:

$$\zeta = \frac{\delta}{\sqrt{4\pi^2 + \delta^2}} , \tag{3.4}$$

where $\delta = \frac{1}{n} \ln(x_i / x_{i+n})$, (3.5)

x_i is the amplitude of oscillation peak i, and

x_{i+n} is the amplitude of oscillation peak $i+n$.

The damping ratio depends on stiffness, damping and effective suspended mass ($\zeta = c/(2\sqrt{km})$), where the effective suspended mass depends on the geometry and mass properties of the test-rig. Therefore, either the damping ratio should be based on a standardised suspended mass or the damping coefficient c (Nsm^{-1}) should be quoted.

3.3. Results

The angles of the pylon with respect to the foot contact surface were chosen to reflect the angle of the physiological shank with respect to the ground at specific points in a normal gait cycle (Figure 3.3.1a). However, due to the design of the test-rig, the actual orientations of the pylon and foot were as seen in Figure 3.3.1b. The measurements of prosthesis deflection versus applied load (perpendicular to the foot contact surface) reveal the normal compliance at different pylon angles and can be represented by a set of roll-over curves corresponding to the four different loads (Figure 3.3.2). These show how the prosthesis will deflect during

the stance phase of gait for varying loads, as well as how the centre of pressure progresses along the foot contact surface.

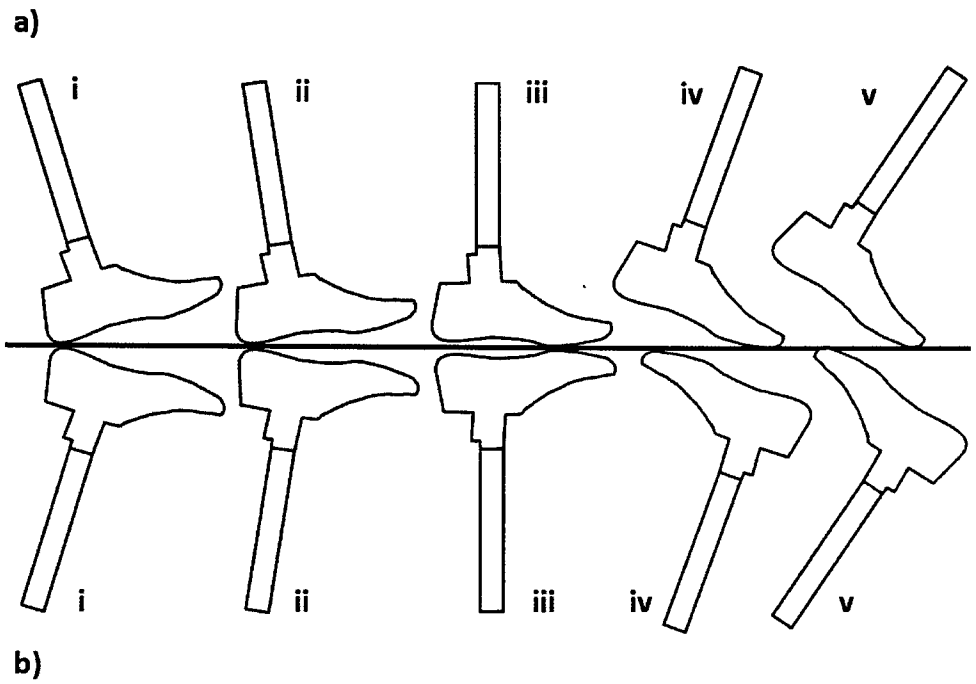

Figure 3.3.1. The five reference angles of the physiological shank with respect to the ground (solid black line) and the associated gait events (or timings) during the stance phase of normal walking are: i) 73° [initial contact], ii) 81° [half-way between initial contact and shank vertical] , iii) 90° [shank vertical], iv) 110° [half-way through terminal stance], and v) 124° [toe-off] (a). The test-rig pylon angles with respect to the foot contact surface (solid black line) that correspond to the five physiological angles are: i) 107°, ii) 99°, iii) 90°, iv) 110°, and v) 124° (b). In the first three positions, the toes of the prosthesis are pointing away from the loading beam pivot (located at the left-hand end of the solid black line), and in the remaining two positions, the foot has been rotated by 180° and the toes are pointing towards the pivot.

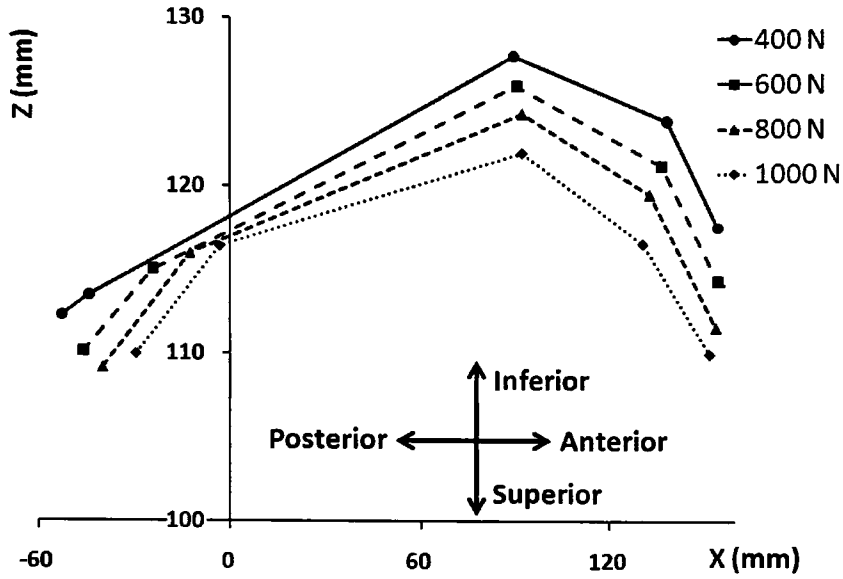

Figure 3.3.2. A family of roll-over curves for a 27 cm length Flex-Foot™ with cosmetic cover[6] attached to a rigid aluminium pylon of 34 mm outer diameter and loaded with 400, 600, 800 and 1000 Newtons. The foot is aligned to the pylon in a "neutral" position (each side of the pyramid adapter equidistant from the inside surface of the pylon tube). The four roll-over curves each consist of five points which correspond to five shank angles with respect to the ground. Data are presented in the load-cell (pylon) coordinate frame (origin at load-cell geometric centre, z- and x-axes in the sagittal plane, z-axis along the pylon).

Repeatability was assessed by measuring the roll-over curves on three separate occasions (sessions). Between each session, the motion capture system and load-cell were recalibrated, and the prosthesis was removed and reinserted into the test-rig. The maximum differences in the x and z coordinates were 4.8 mm and 1.3 mm respectively. When the set-up is not disturbed or re-calibrated, the errors associated with repeated loading and unloading are less than 1 mm. So better results are obtained if the set of roll-over points, corresponding to one pylon angle, is recorded without disturbing the set-up, apart from changing the load.

Figure 3.3.2 only provides information on normal compliance at different pylon angles with respect to the ground. In Figure 3.3.3 we show one approach to including additional information with the roll-over curves. The shear compliance (tangential to the foot contact

[6] Flex-Foot, Össur hf., Reykjavik, Iceland

surface) is represented by showing the deflection of the roll-over points resulting from a shear load of 240 Newtons (denoted by triangles). The shear load used is slightly greater than the average maximum anterior-posterior force seen during gait (23% of body weight, (Perry, 1992)). Except for the left most roll-over point, the shear load has been applied in one direction only because of the layout of the test-rig. However, the direction of the applied shear loads are the same as seen in normal gait. In the case of the left most roll-over point (initial contact), both posterior and anterior shear loads have been applied (by rotating the foot through 180° between measurements) and the corresponding deflections were 4.2 mm and 5.6 mm respectively; demonstrating that shear compliance can differ in the anterior and posterior directions.

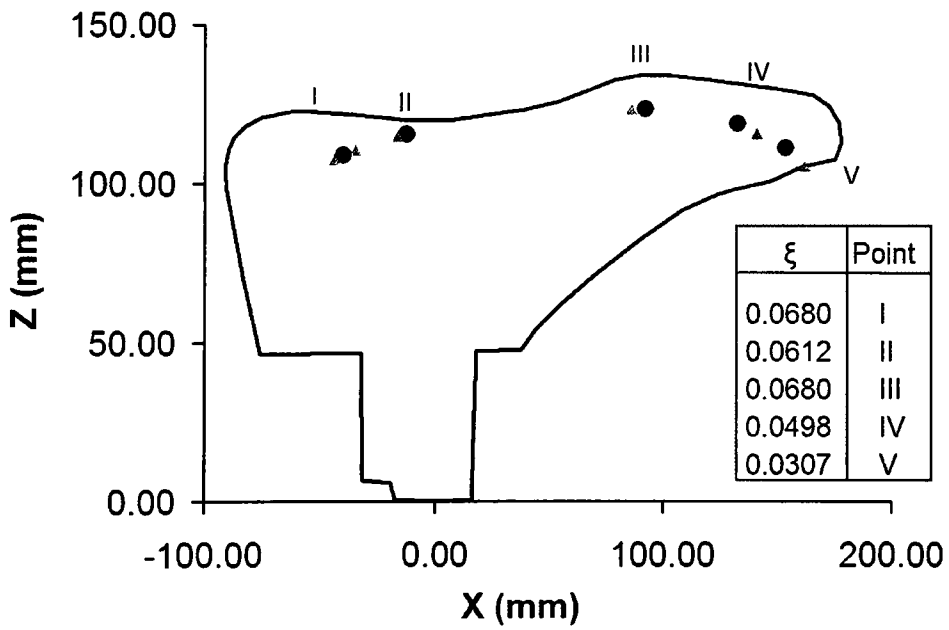

Figure 3.3.3. Amputee Independent Prosthesis Properties (AIPP) for a 27 cm length Flex-Foot™ with cosmetic cover attached to a 34 mm outer diameter rigid aluminium tube in "neutral" alignment, consisting of five roll-over points (corresponding to the five pylon angles defined in Figure 3.3.1) for a normal load of 800 N, superimposed on an outline of the prosthetic foot. At each point, a grey triangle shows the shear deflection for a tangential load of 240 N with the pylon at the angle associated with that roll-over point. The shear deflection is the gross displacement of the prosthetic foot as a whole relative to the loading surface resulting from an applied normal load of 800 N. The legend on the right lists the normal damping ratios at the five roll-over points for an effective suspended mass of 40 kg.

Although a set of roll-over curves can provide a clear graphical presentation of both normal and shear compliances at different pylon angles, they are not well suited to presenting damping information. Therefore, in Figure 3.3.3, the normal damping ratios are simply listed for the five roll-over points. This approach is acceptable for a small number of roll-over points.

3.4. Discussion

In this chapter, a comprehensive representation of stance phase properties, for trans-tibial prostheses, has been proposed that is independent of the amputee and incorporates the best features of both lumped parameter and roll-over models. These Amputee Independent Prosthesis Properties (*AIPP*) include: a set of roll-over curves for different normal loads to represent normal compliance; tangential deflections at the specified roll-over points to represent shear compliance; and the normal damping ratios at the specified roll-over points. Furthermore, we have developed a test-rig, instrumentation, and the corresponding test procedures to capture this data in a standardised way. Furthermore, the design allows for a seamless transition from test-rig to instrumented trans-tibial prosthesis for in-vivo testing.

By adopting the roll-over concept, the proposed *AIPP* model incorporates information on prosthesis geometry and alignment, which is not usually present in lumped parameter models. Because the combined mechanical properties of all prosthetic components distal to the socket are measured, the *AIPP* captures those characteristics of the prosthesis (distal to the socket) that influence stance phase behaviour and hence amputee performance and comfort. This data is more relevant than the properties of individual prosthetic components (e.g., pylon compliance) and is independent of manufacturer claims.

Limitations of the approach include the use of a multi-camera motion capture system to measure the relative positions of the key reference points used in the calculations. Whilst this is not a problem for the authors, it would prevent the use of our test-rig design in establishments that do not have such a system (they are far too expensive to purchase just for this purpose). In such a case, the test-rig would need to be re-designed so that other

position measurement devices are used (e.g., linear potentiometers (Miller and Childress, 1997)). The commercial load-cell that we adopted is relatively large, heavy (1.07 kg) and expensive for our application. A smaller and lighter device would be particularly beneficial for in-vivo testing (see Figure 3.2.2.2). In a similar installation for in-vivo testing, a custom-built strain gauged component was used in place of a commercial load-cell (Sanders et al., 1997). Finally, the test-rig does not readily allow shear compliance measurement in both directions; although the measurement directions do correspond to those observed in normal gait.

The majority of in-vivo studies compare different commercially available prostheses in terms of their biomechanical and physiological effects; but only distinguish the designs by quoting their trade names. This approach can only indicate their relative performance, but cannot explain why a particular prosthesis performs better than the next. The widespread adoption of an agreed standard for representing Amputee Independent Prosthesis Properties (*AIPP*) would encourage more researchers to look for correlations between *AIPP* and the effects on amputee gait (comfort, biomechanics and physiological performance). Only in this way will more generic information, as opposed to product specific claims, become more widely available to inform future designs, prescription and alignment procedures. Such studies would also inform revisions to the proposed *AIPP* model. For example, if it is shown that changes in shear compliance have little effect on amputee gait, then these measurements could be left out. Conversely, it may be shown that shear damping should also be included.

The *AIPP* model could also be used in computer model based simulation studies, eventually leading to virtual prototyping tools that can be used in design. In this context, it should be noted that the *AIPP* model only represents the behaviour of the prosthetic components distal to the socket. To create a virtual model that can predict the pressures acting on the residual limb, this would have to be combined with a model of the socket and residual limb.

4. Chapter Four: Human performance study methodology

4.1. Introduction

In parallel to previous *AIPP* studies (discussed in Chapter Two), numerous in-vivo studies have been conducted which have produced comprehensive data on the effects of various trans-tibial components on user performance (Hafner et al., 2002; Hofstad et al., 2004; van der Linde et al., 2004). However, there appears to be very little quantitative evidence supporting manufacturers' claims that particular foot designs provide the user with a biomechanical (i.e., joint kinematics and kinetics, and temporal-spatial gait parameters) or physiological (i.e., metabolic costs) advantage compared to alternative designs during human performance studies.

The primary focus of most previous human performance studies has been to compare commercially available prosthetic components that represent different instances of prosthetic design but not to characterise them by their mechanical function. For example, energy storage and return (ESAR) feet, such as the Flex-Foot, are often compared against conventional non-dynamic feet, such as the Solid Ankle Cushion Heel (SACH) foot. Similarly, the Vertical Shock-Absorbing Pylon (VASP) is compared to the rigid pylon. A common hypothesis has been that the use of ESAR feet during gait should result in lower metabolic cost than conventional feet, considering ESAR feet store energy during the loading phase of stance in order to return this energy during terminal stance. Unfortunately, these studies have often failed to identify consistent differences in the biomechanical and physiological measures of gait between various prosthetic designs.

With three notable exceptions (Casillas et al., 1995; Macfarlane et al., 1991a; Perry and Shanfield, 1993), the majority of previous human performance studies included as part of the literature review have investigated the effects of prosthetic components on user performance whilst walking on level ground (Barr et al., 1992; Barth et al., 1992; Culham et al., 1986; Doane and Holt, 1983; Goh et al., 1984; Hsu et al., 2006; Hsu et al., 1999; Lehmann et al., 1993a; Lehmann et al., 1993b; Marinakis, 2004; Menard et al., 1992; Nielsen et al.,

1989; Perry et al., 1997; Powers et al., 1994; Rao et al., 1998; Schmalz et al., 2002; Snyder et al., 1995; Torburn et al., 1990; Torburn et al., 1995; Underwood et al., 2004), and apart from seven (Hsu et al., 2006; Hsu et al., 1999; Lehmann et al., 1993a; Lehmann et al., 1993b; Nielsen et al., 1989; Schmalz et al., 2002; Torburn et al., 1990), exclusively at self-selected walking speed. However, select human performance studies have reported a reduction in metabolic energy cost when using certain ESAR feet as compared to conventional feet for more active conditions (e.g., incline/decline walking (Casillas et al., 1995) and increased walking speed (Hsu et al., 2006; Hsu et al., 1999; Schmalz et al., 2002)). Despite somewhat inconclusive results from human performance studies, investigations of the practical and perceived benefits of various prosthetic components have indicated that certain prostheses are more suitable for particular walking conditions other than self-selected walking speed on level ground (Alaranta et al., 1991; Alaranta et al., 1994; Macfarlane et al., 1991b; Nielsen et al., 1989; Underwood et al., 2004). For example, subjective feedback from unilateral trans-tibial amputees has identified a more pronounced preference for a flexible, dynamic prosthetic foot as compared to a conventional, non-dynamic foot for tasks of increased activity and difficulty (e.g., increased walking speeds (Alaranta et al., 1994), incline/decline walking (Alaranta et al., 1991; Alaranta et al., 1994; Macfarlane et al., 1991b), walking upstairs (Alaranta et al., 1991), or standing and walking on an uneven ground (Nielsen et al., 1989; Underwood et al., 2004)). Perhaps such differences in preference are reflective of the noted differences in the *AIPP* of these two designs as reported by previous *AIPP* characterisation studies. Therefore, the inconclusive results of previous human performance studies might partially be due to the fact that certain prosthetic foot designs are not tested under gait conditions in which they might provide the greatest benefit.

Because of the difficulty of generalising previous *AIPP* results and the ambiguous results from human performance studies, the relationship between the *AIPP* and user performance remains ill-defined. Therefore, the objective of this study was to develop a method of systematically investigating the influence of the mechanical properties of the trans-tibial prosthesis (i.e., its *AIPP*) on the biomechanical and physiological performance of the amputee user during various gait conditions. It is reasonable to assume that particular mechanical properties are best suited to specific walking conditions to produce a near optimal gait and hence lower metabolic energy expenditure. Initial hypothesis include the

belief that a more compliant forefoot is beneficial for incline walking as this allows increased dorsiflexion, and a more compliant rearfoot for decline walking as this allows for increased plantar flexion. Furthermore, a more compliant rearfoot would encourage early foot flat following heel-strike as the foot adapts to the walking surface. However, a stiffer rearfoot would improve shock absorption at fast walking speeds with increased loading of the prosthetic limb. It was hoped that results from this study would: 1) allow an understanding of how mechanical properties should vary to produce a near optimal gait for different walking conditions, 2) assist clinicians in prescribing appropriate prosthetic components based on quantitative evidence, and 3) develop design guidelines for future prostheses.

4.2. Custom Foot-Ankle Mechanism

Almost all human performance studies compare commercially available prosthetic components, and, as such cannot vary *AIPP* in a systematic and controlled manner. In particular, it is difficult to change one property without also changing other properties. As the primary focus of this study was to develop a method of systematically investigating the effects of different *AIPP* on amputee performance, a method of overcoming this limitation was developed. A Custom Foot-Ankle Mechanism (CFAM) was designed and fabricated which was capable of independent adjustment of rearfoot (i.e., plantar flexion) and forefoot (i.e., dorsiflexion) stiffness of the ankle joint (Figure 4.2.1). Consequently, the study was entirely uncoupled from the use of commercial prosthetic components and a range of *AIPP* could be tested during various walking conditions. Furthermore, as mentioned in Chapter Two, changing prosthetic components and alignment will alter the *AIPP* of a prosthesis in a complex manner. Therefore, the concept of the CFAM was to be able to modify the rearfoot and forefoot stiffness without changing other *AIPP* parameters at the same time.

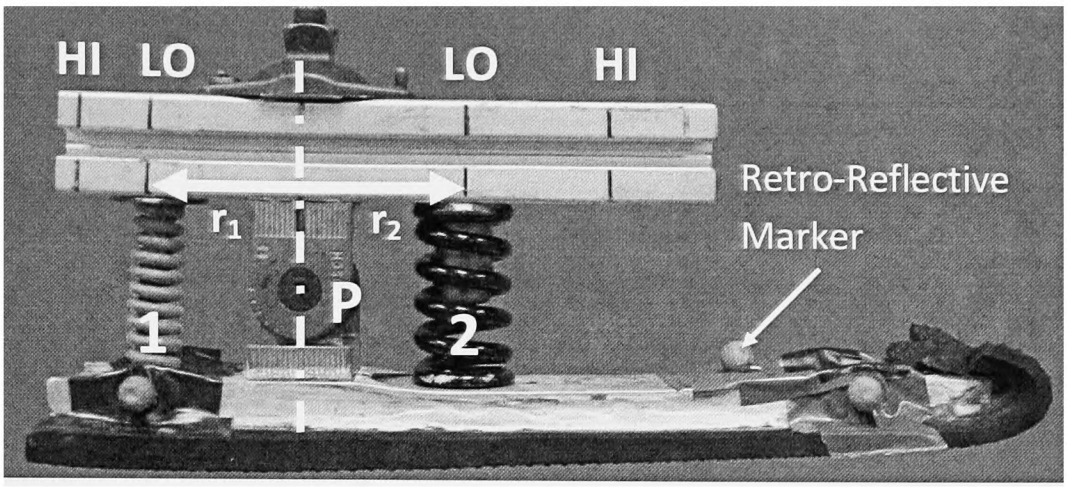

Figure 4.2.1. Custom Foot-Ankle Mechanism with retro-reflective markers used for motion capture. Spring positions are marked with vertical black lines on the upper rail and are representative of high rearfoot stiffness (HI – Left of vertical dashed line), low rearfoot stiffness (LO – Left of vertical dashed line), low forefoot stiffness (LO – Right of vertical dashed line), and high forefoot stiffness (HI – Right of vertical dashed line).

The design of the CFAM was based on a similar principle to a single-axis prosthetic foot, in which the rearfoot and forefoot stiffness of an articulated ankle joint is dictated by the stiffness of two rubber bumpers in the aft and fore position (Seymour, 2002). Ankle motion is only allowed in the sagittal plane, with any out-of-plane motion provided by the foot shell, keel and heel. Similarly, the CFAM has an articulated ankle joint[7] (labelled *P,* Figure 4.2.1), in which the rearfoot and forefoot stiffness are determined by two linear compression springs, labelled *1* and *2* respectively, that are translated along an upper track[8] to vary their distances from the central joint (r_1 and r_2). The ankle rearfoot stiffness ($K_{rot,1}$) and forefoot stiffness ($K_{rot,2}$) is described by the following equation:

$$K_{rot,i} = K_{lin,i} \times r_i^2 \qquad \text{for } i = 1, 2 \qquad (4.1)$$

where $K_{lin,i}$ is the linear stiffness of the respective spring (*1* and *2*). The lower track is a custom made aluminium profile with treaded rubber shoe sole material adhered to the

[7] 30X30 millimetre swivel joint, Bosch Rexroth, Lohr am Main, Germany

[8] 30X30 millimetre profile, Bosch Rexroth, Lohr am Main, Germany

plantar surface, and can be separated from the upper profile at the central joint. Therefore, the rearfoot and forefoot stiffness can be adjusted without altering the alignment of the CFAM as prescribed by a prosthetist during fitting. The individual components of the CFAM are displayed and labelled in Figure 4.2.2 and relevant dimensions are detailed in Figure 4.2.3.

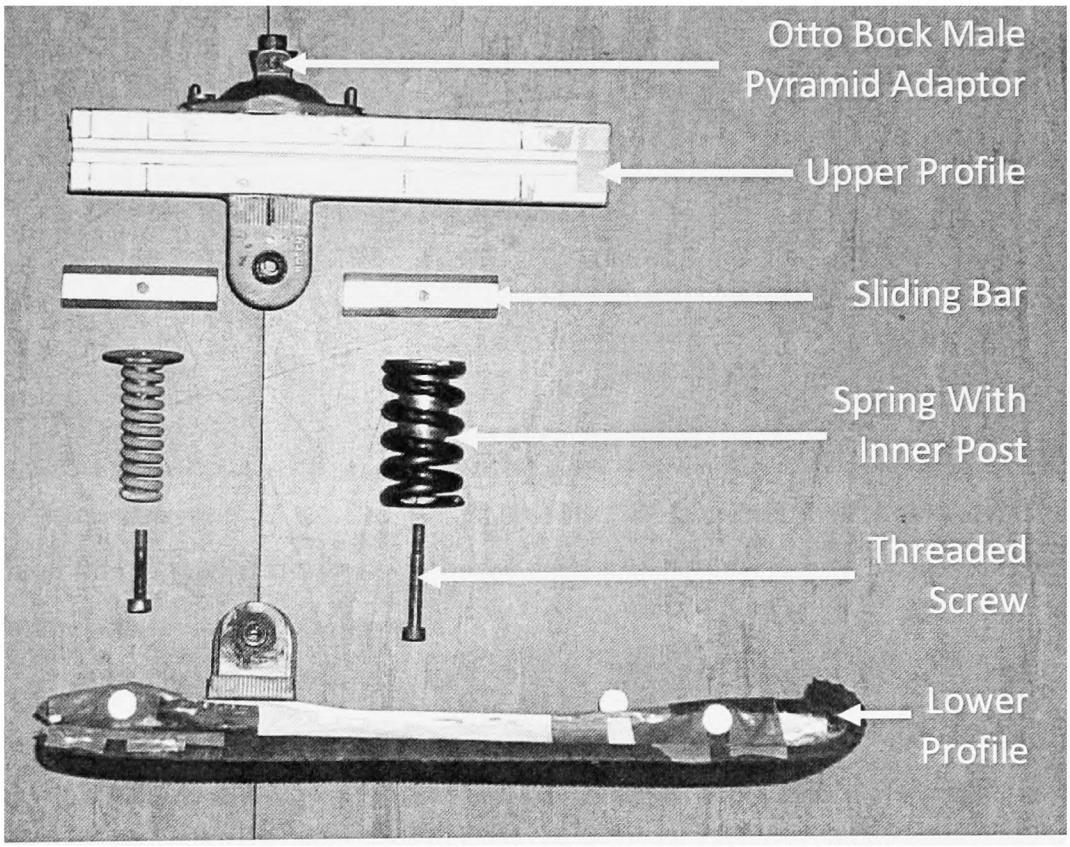

Figure 4.2.2. Exploded assembly view of individual components of the CFAM.

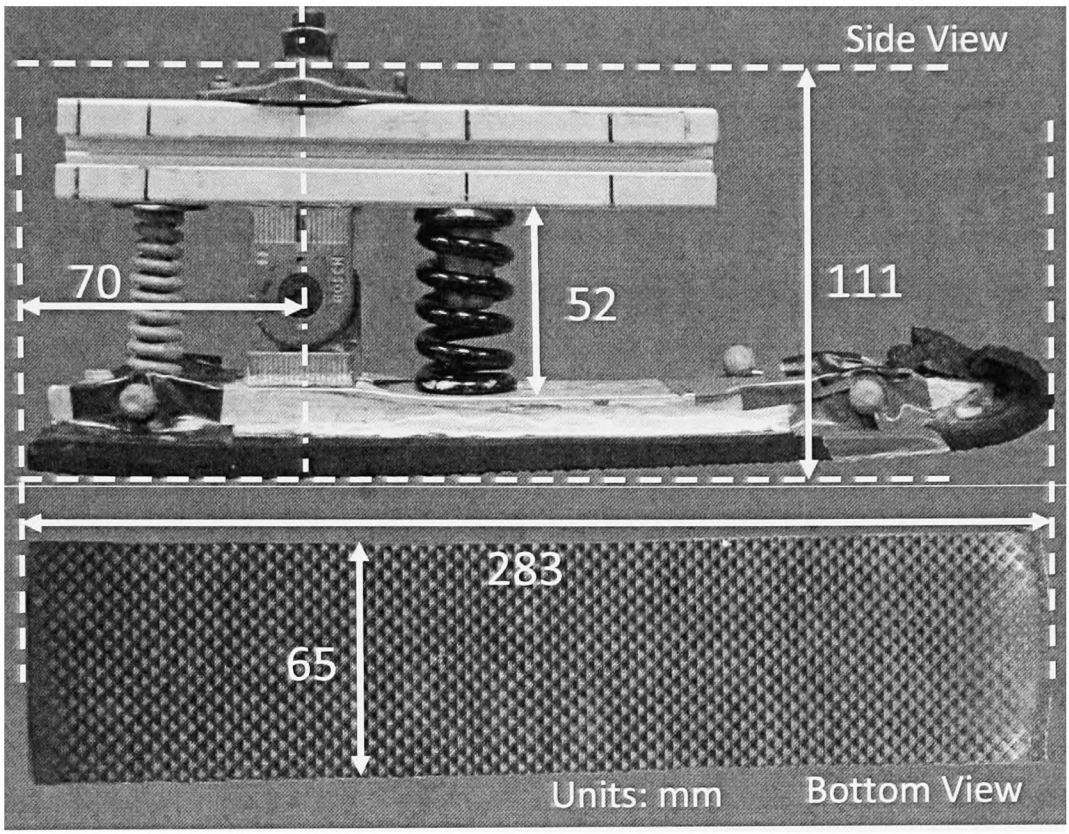

Figure 4.2.3. Relevant dimensions of the CFAM. The foot height of 111 millimetres is measured from the plantar surface of the foot to the bottom surface of the pylon when it is fixed to the male pyramid adaptor.

The length of the CFAM matched that of the average shoe size (283 mm) and also the ankle position, anterior to the heel, matched that of the average anatomical ankle (24% of foot length) (Tilley, 2002; UK, 2007). The CFAM is intended to be used without a foot shell or shoe in order to reduce any confounding variables contributing to its *AIPP*.

The design inherently restricted any rotational movement in the transverse plane. This was accomplished by fixing the springs, Otto Bock male pyramid adaptor, and upper arm of the central joint to the upper profile with threaded screws and sliding bars that slot into the profile groove. The lower arm of the central joint is joined with the lower profile through a mortise and tenant joint and a threaded screw. Where possible, components have been permanently fixed with the help of Loctite[9].

[9] Loctite 290 Threadlocker, Henkel AG & Co. KGaA, Düsseldorf, Germany

4.2.1. Spring selection

The choice of linear compression springs was constrained by three factors: 1) size restrictions of the CFAM, 2) able to provide the range of rearfoot and forefoot stiffness to be tested during gait analysis, and 3) the compressed length during operation could not be less than the solid (fully compressed) length. The intention was to test different levels of ankle stiffness that reflected the range found in commercial prosthetic foot design, the extremes of this range being based on the non-articulated SACH foot and an ESAR foot. Even though the CFAM allows for a range of stiffness to be tested, the objective was to test combinations of rearfoot and forefoot stiffness which reflect commercially available prosthetic devices. A suitable mechanical characterisation (*AIPP*) study was identified which measured the force versus displacement of three prosthetic feet (SACH Foot[10], Flex Foot[11], and Seattle Foot[12]) at the forefoot (metatarsal head region) and rearfoot (heel region) (Lehmann et al., 1993b). In this study, the location of the force point of application for the forefoot was identified as 14 centimetres anterior to the longitudinal axis of the pylon; however the rearfoot point of application was only identified as the 'posterior extremity of the heel.' Acquiring similar prosthetic feet from the University of Salford Prosthetic and Orthotics Department and measuring from pylon axis to heel extremity revealed an average distance of approximately 5.5 centimetres. The force versus displacement plots presented in this study appeared to be fairly linear, and therefore a linear best fit approximation was used to calculate the linear stiffness. Rotational stiffness was then calculated using Equation 4.1 and a linear approximation was taken. The approximated linear and rotational stiffness of the three feet are presented in Table 4.2.1.1. From these values, the maximum (HI) and minimum (LO) rearfoot and forefoot stiffnesses were identified (Table 4.2.1.1, bold face italics) and chosen as the stiffnesses which would be used to define the foot setups to be tested (see Figure 4.2.1).

[10] SACH Foot, Otto Bock Orthopaedic Industry, Inc., Minneapolis, MN, USA

[11] Flex Foot, Flex Foot, Inc., Laguna Hills, CA, USA

[12] Seattle Foot, Model + Instrument Development, Seattle, WA, USA

Table 4.2.1.1. Linear approximations of linear and rotational stiffness as calculated from force versus displacement data presented by (Lehmann et al., 1993b).

	Linear Stiffness (N/cm)		Rotational Stiffness (N-cm/rad)	
Foot Type	Forefoot	Rearfoot	Forefoot	Rearfoot
SACH	716	324	***139571 (HI)***	***9416 (LO)***
Flex Foot	208	486	***39428 (LO)***	14366
Seattle Foot	418	680	81084	***20282 (HI)***

Following an iterative process, appropriate springs were sourced that fit within the space provided by the CFAM and possess a linear stiffness which would provided a rotational stiffness closely matching the desired test stiffness. The resulting four locations of the springs are displayed in Figure 4.2.1. Position for rearfoot stiffness *HI*, rearfoot stiffness *LO*, forefoot stiffness *HI*, and forefoot stiffness *LO* are located at the following distances from the central joint, respectively: 6.32, 4.31, 4.75, and 8.93 cm. The rearfoot and forefoot linear compression springs, both 5.08 centimetres in height, possesses a linear stiffness of 507.7 and 1751 N/cm, respectively.

4.2.2. Stress analysis, failure modes analysis, and testing

The assembled components which constitute the frame of the CFAM (i.e., upper and lower profiles and central joint) were subjected to a theoretical force and stress analysis in order to determine how they performed when subjected to load. The material used for the solid lower profile was Dural, an aluminium alloy. The theoretical scenario of an 80 kilogram subject applying forces to the CFAM during gait was analysed. The typical maximum force observed during gait (120% of body weight) (Perry, 1992) was systematically applied at various points along the plantar surface of the lower profile. Furthermore, a conservative approach was taken where the assembled linear compression springs were assumed to be rigid struts (i.e., no vertical compliance permitted). Each component's yield stress and theoretical stress are presented in Table 4.2.2.1. The maximum theoretical force applied to the central joint (*P*) resulting from this analysis was approximately 4073 Newtons. The joint could sustain up to a maximum operational force of 10000 Newtons, providing a safety factor of 2.5. A safety factor of at least 1.5 was considered ample, in which all components

satisfied this criterion. Considering that the majority of gait related forces and moments occur within the sagittal plane, an out-of-plane analysis was not conducted.

Table 4.2.2.1. Theoretical stress analysis of the upper and lower profiles of the CFAM. The analysis is based on the following scenario: A load of 1.2 times the average male body weight of 80 kg (approximately 942 Newtons) applied to the anterior end of the forefoot (21.3 centimetres from the pivot) and the forefoot spring is located 4 centimetres from the pivot (4.75 centimetres being the minimal distance used during testing). The upper profile acts as a cantilever beam and the lower profile acts as a simply supported beam during loading.

	Yield Stress (N/cm^2)	Actual Stress (N/cm^2)	Safety Factor	Maximum Deflection (cm)
Lower Profile	42000	25724.92	1.6	3.46
Upper Profile	19500	10941.54	1.8	0.06

Following the initial design of the CFAM, any additional potential modes of failure were identified and, if necessary, addressed before testing. These modes of failure can be found in Appendix B.1.1. Before any human performance testing was conducted, the CFAM was trialled on healthy subjects using modified Aircast[13] boots as displayed in Figure 4.2.2.1. The CFAM was tested on two healthy subjects during overground walking on the level, as well as treadmill walking at self-selected and fast speeds on the level, and at self-selected speeds on a 5% grade incline and 5% grade decline. This ensured its safety before any amputee subject testing took place.

[13] Aircast XP Diabetic Walker, DJO Incorporated, Surrey, UK

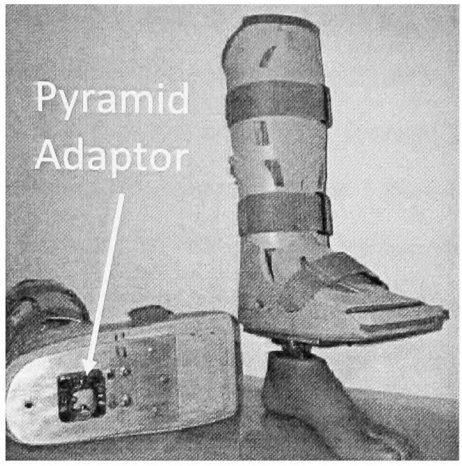

Figure 4.2.2.1. Modified Aircast boots with Otto Bock female pyramid adaptor fixed to the plantar surface allowing for commercial prosthetic feet to be attached. The boots immobilise the user's ankle joint and foot through Velcro straps and an inner inflatable bladder.

4.2.3. Foot characterisation

The springs were assembled into the CFAM and tested at each level of rearfoot and forefoot stiffness using the test-rig and method presented in Chapter Three at the appropriate pylon angle during gait and at loads of 400, 600, 800, and 1000 Newtons. For the purpose of discussion and presentation, the CFAM setups (i.e., combinations of forefoot and rearfoot stiffness) will be abbreviated as seen in Table 4.2.3.1.

Table 4.2.3.1. CFAM setup abbreviations.

Forefoot Stiffness	Rearfoot Stiffness	Foot Setup
LO	LO	*LOLO*
LO	HI	*LOHI*
HI	LO	*HILO*
HI	HI	*HIHI*

The CFAM *AIPP* roll-over profiles of the two extreme conditions, setups *HIHI* and *LOLO*, are noticeably different (Figure 4.2.3.1 and 4.2.3.2) and thus satisfied their purpose. The family of roll-over curves of the CFAM for two stiffness combination setups (*HIHI* and *LOLO*) at four different loading conditions (400, 600, 800, and 1000 Newtons) are displayed in Figure 4.2.3.1. Figure 4.2.3.2 displays these two setups as a full *AIPP* characterisation with

associated damping coefficients. Only two setups are presented because the rearfoot and forefoot roll-over points are entirely independent of each other and each setup permutation shares the same roll-over point at a pylon angle of 0 degrees to the vertical. Therefore, all setups can be derived from the two setups presented in Figure 4.2.3.1. Second-order best fit curves have been found for each set of roll-over points for the four combinations of foot setups at a load of 800 N; the equations of which can be found in Table 4.2.3.2. Neither spring was observed to reach maximum compression (i.e., solid length) during testing.

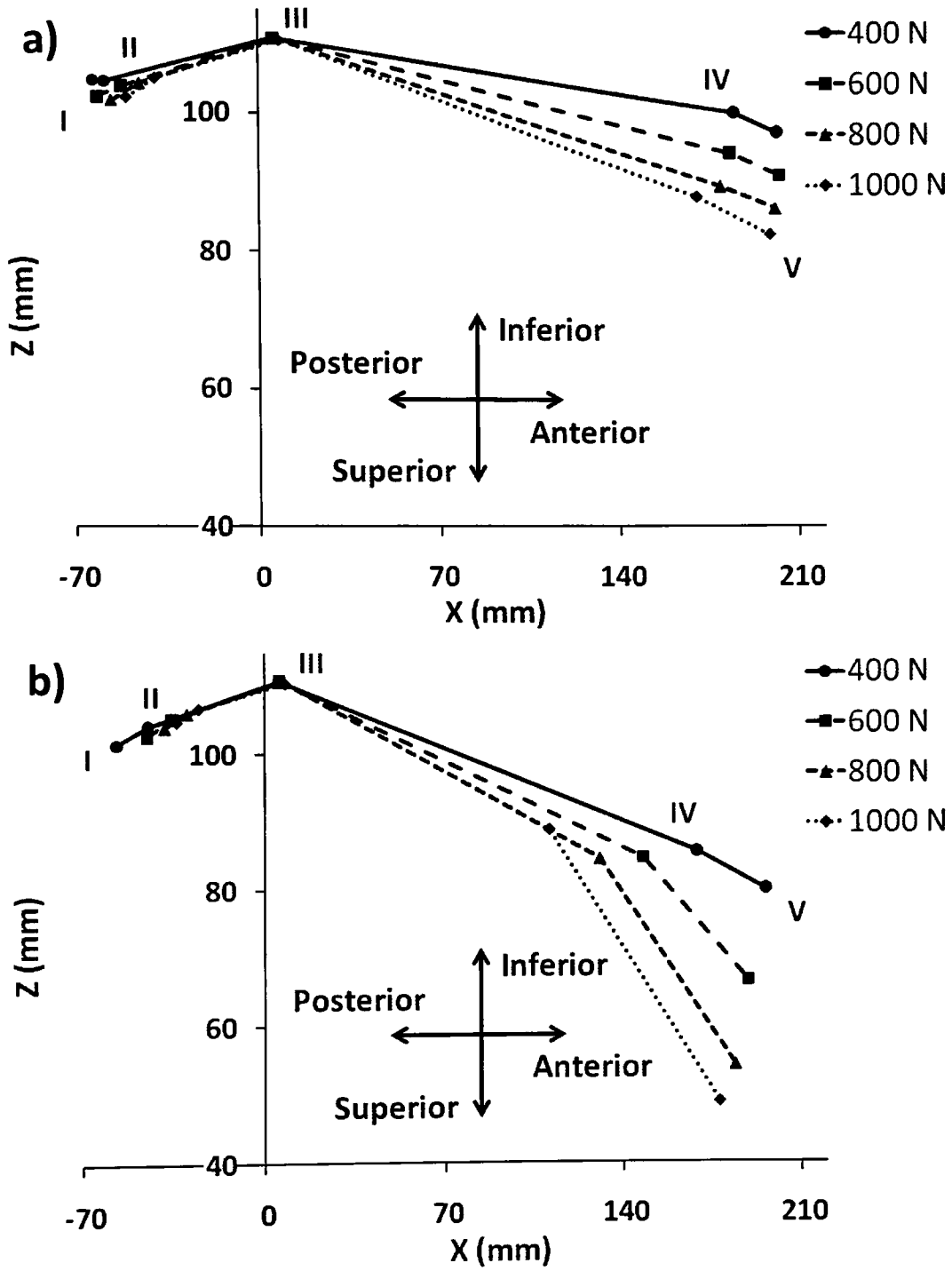

Figure 4.2.3.1. Family of roll-over curves of CFAM stiffness combination setups HIHI (a) and LOLO (b) at four loading conditions (400, 600, 800, and 1000 Newtons) with points corresponding to each of the five pylon angles defined in Figure 3.3.1. There is no displacement present at position III as the CFAM joint is completely rigid. The origin is located at the mid-point of the top surface of the female pyramid adaptor (i.e., distal end) of the pylon.

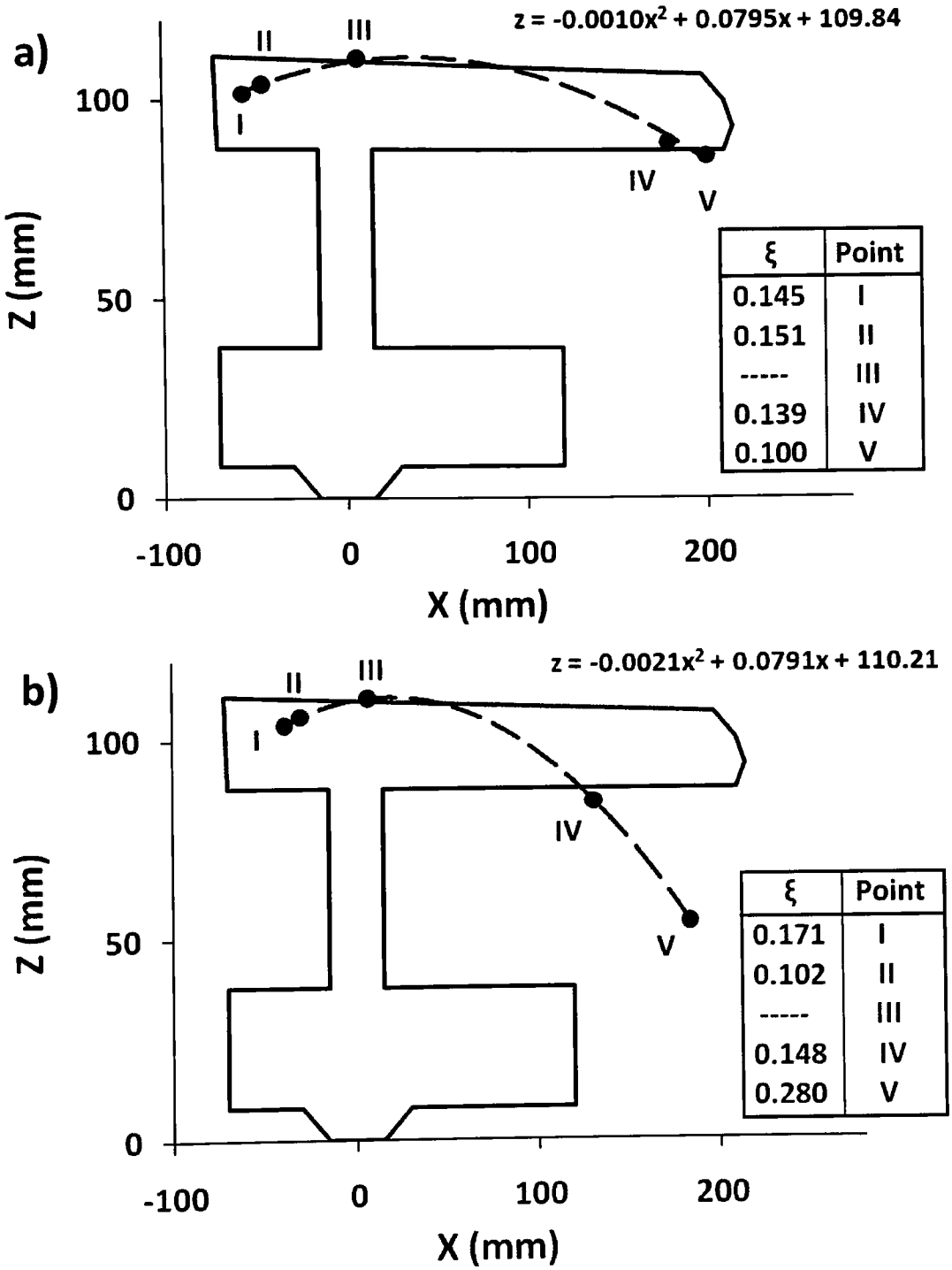

Figure 4.2.3.2. AIPP characterisation of CFAM stiffness combination setups HIHI (a) and LOLO (b) at a load of 800 Newtons. A second-order equation is fit to the five roll-over points (corresponding to the five pylon angles defined in Figure 3.3.1) and presented superimposed on the foot outline in order to define the roll-over curve. The foot is presented in the orientation as it was fixed into the test-rig.

Table 4.2.3.2. Second-order best fit curve equations of four foot setups. Orientation and origin of the curve is as represented in Figure 4.2.3.2.

Foot setup combination	Equation of second-order best fit
LOLO	$z = -0.0021x^2 + 0.0791x + 110.21$
LOHI	$z = -0.0019x^2 + 0.0533x + 110.65$
HILO	$z = -0.0011x^2 + 0.0899x + 109.64$
HIHI	$z = -0.0010x^2 + 0.0795x + 109.84$

When compared to the roll-over points measured for the forefoot HI and LO stiffness settings, the roll-over points for the rearfoot HI and LO stiffness settings appear to be much more similar when measured at different loads (Figure 4.2.3.1). The reason for this is because when the rearfoot was loaded and the foot was placed into plantar flexion during testing, the plantar surface of the foot often met with the loading surface (i.e., reached foot flat) and would thereby restrict any further plantar flexion motion. This is also partially the reason why the rearfoot spring never reached maximum compression during testing. This behaviour of early foot flat is common amongst single-axis feet. However, whereas in commercial single-axis feet the soft foot shell would allow for additional linear compression, further plantar flexion or linear compression of the spring was restricted when the CFAM reached foot flat due to a very stiff lower profile. The lower profile of the CFAM was intentionally stiff in order to ensure that the *AIPP* (i.e., forefoot and rearfoot stiffness) were dictated solely by the linear springs and not by material compression which would introduce an uncontrolled variable.

The concept behind the CFAM was to effectively alter the foot stiffness and hence, the *AIPP* roll-over shape, in which damping properties were controlled for in the design process. This is apparent in the relative differences in damping coefficients between the two conditions as seen in Figure 4.2.3.2. Additionally, when compared to the damping coefficients of the Flex-Foot presented in Chapter Three (Figure 3.3.3.), the CFAM is significantly more damped. For example, the CFAM setup *LOLO* possesses damping coefficients that are 251% and 912% greater than that of the Flex-Foot at positions I and V, respectively. This relatively high damping may partially be due to sliding between the springs and the lower profile during cyclical loading, as the springs are only fixed to the upper rail, and between the upper and

lower profile of the central pivot during rotation. These actions would cause the system to lose a portion of returned potential elastic energy through friction.

4.3. Instrumented Trans-tibial Prosthesis

A custom-built Instrumented Trans-tibial Prosthesis (ITP) was designed and fabricated in order to provide continuous measurement of forces and loads during human performance testing, as well as the in-vivo roll-over shape, unconstrained by the limitations imposed by the use of force plates. Design of the ITP was subjected to several design constraints: 1) able to attach to any commercial prosthetic foot with an Otto Bock male pyramid adaptor, 2) capable of continuous, non-invasive 3-axis force and moment measurement, 3) able to be attached to different sockets, and 4) capable of providing the amputee with quick and easy methods of locking into the socket and prosthesis.

The assembled ITP can be seen in Figure 4.3.1 with a standard SACH foot attached. As one of the design objectives of the ITP was its capability to measure the in-vivo roll-over shape during gait, this device was designed in tandem with the test-rig presented in Chapter Three. Considering that the in-vivo roll-over shape would be compared to the *AIPP* roll-over shape, it is important to reduce measurement error and thus standardise the measurement technique and equipment used in both assessments. Accordingly, the same components that are attached to the test-rig pedestal (load-cell, prosthetic pylon, and prosthetic foot) are attached to the socket using a standard Otto Bock pyramid adaptor. Additionally, a seamless transition from test-rig to ITP (and vice-versa) can be achieved without disassembling the load-cell, pylon, and prosthetic foot. Potentially, the *AIPP* roll-over shape can be measured following the alignment of the prosthesis as prescribed by a prosthetist, which would include unique rotational alignment of the foot.

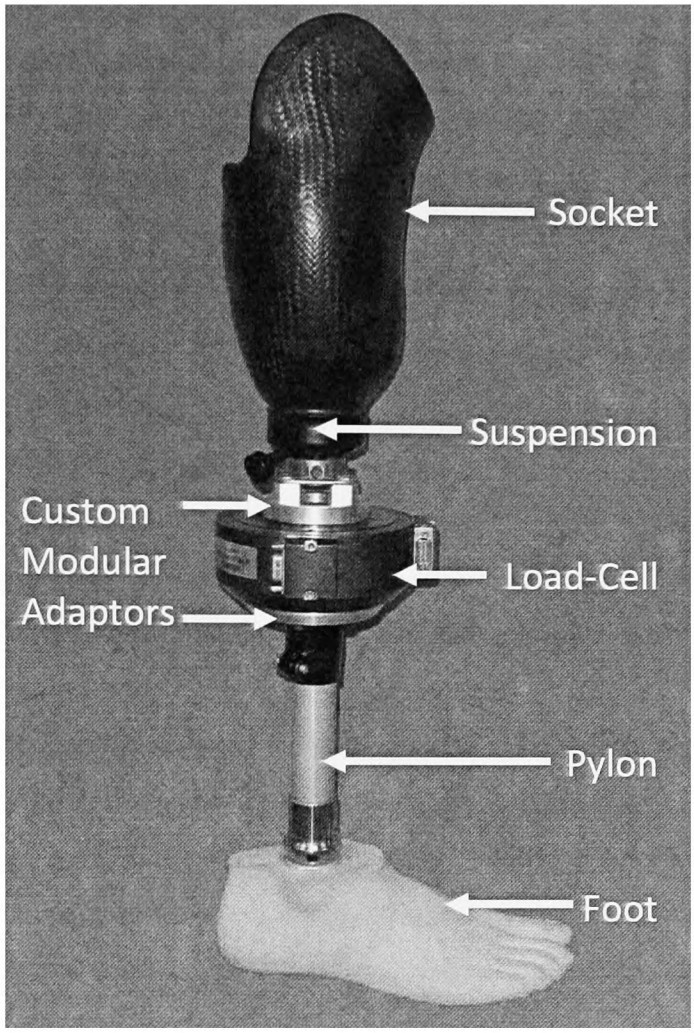

Figure 4.3.1. The ITP consists of four primary components: socket, load-cell, pylon, and foot.

Custom modular Dural adaptors were designed and fabricated to be attached to the both sides of the load-cell in order to accommodate an Otto Bock female pyramid adaptor at the proximal end for attachment of the socket and a tube clamp at the distal end for attachment of a standard 34 millimetre outer diameter pylon. Therefore, the ITP can accommodate any socket and any pylon/prosthetic foot assembly with the appropriate male pyramid adaptor and alignment adjustment of these devices can be made in all three planes. These modular adaptors were designed to be as light-weight and low-profile as possible.

The suspension technique used for the ITP is a shuttle-lock pin suspension. The distal end of the suspension is fitted with a male pyramid adaptor which secures to the prosthesis. Each

subject used a silicon Iceross[14] liner fitted with a locking pin at the distal end which is inserted and secured within the suspension mechanism. Between the liner and socket is a thin pelite foam liner in order to improve comfort by providing a soft cushion interface. Each subject was cast using the Icecast[15] pressure casting technique and subsequently provided with a custom total surface bearing socket and liner. This process satisfied two objectives: 1) eliminate the use of the subjects' prosthetic components as provided by their rehabilitation centre and 2) ensure that each subject used the same socket and suspension technique. The second objective is of primary importance as this eliminated any confounding effects produced by using different components.

Following the initial design of the ITP, potential modes of failure were identified and, if necessary, addressed before testing. These modes of failure can be found in Appendix B.1.2.

The ITP was used to continuously measure forces and moments at the distal end of the socket, and hence allow calculation of the ground reaction forces and the in-vivo roll-over shape. The system of equations used to calculate these parameters are found in Appendix C.1. The information required for these calculations includes continuous force and moment measurements from the load-cell and motion capture data for the prosthetic limb and walking surface.

4.3.1. Mass properties of the ITP

The weight of each of the ITP components, including the CFAM, is presented in Table 4.3.1.1. For an 80 kilogram individual, the mass of the lower leg (i.e., foot and shank) is approximately 4.8 kilograms (Dempster, 1955). Based on previous work conducted on a population of trans-tibial amputees (Twiste, 2004) as intended for this study the average residuum length is approximately 34% of the intact shank length and utilised a typical (copolymer, draped) socket of mass 0.4 kilograms. By assuming that the ratio of residuum mass to intact shank mass would equal the ratio of residuum length to intact shank length,

[14] Iceross liner, Össur hf., Reykjavik, Iceland
[15] Icecast Anatomy, Össur hf., Reykjavik, Iceland

the average residuum mass was calculated as approximately 1.25 kilograms. Consequently, the total mass of the below-knee prosthetic limb (i.e., residuum, socket, custom adaptors, load-cell, pylon, and CFAM) was approximately 4.62 kilograms (96% of the average intact lower leg).

Table 4.3.1.1. Mass of each component which assemble to make the ITP for human performance testing.

Component	Mass (kg)
CFAM	1.1
Distal load-cell adaptor	0.3
Proximal load-cell adaptor	0.4
Load-cell	1.07
Typical pylon	0.1

A moment table was used to locate the CoM of the load-cell, distal modular adaptor assembly, and the CFAM in the sagittal plane. A schematic of this process is displayed in Figure 4.3.1.1. The height and CoM of each component of the ITP distal to the socket is presented in the schematic of Figure 4.3.1.2, as is the CoM of the total assembly of the ITP which is a function of pylon length. A range of different lengths of aluminium pylons were tested (49 to 106 millimetres) and regardless of their length, the mass was approximately 0.1 kilograms as the majority of their weight is centred on the distal pyramid adaptor. Therefore, they were included during measurement of the CFAM CoM. For pylon lengths of 49 and 106 mm, the CoM of the assembled ITP is located 137 mm and 160 mm distal from the end of the socket, respectively. This places the CoM at approximately the distal end of the distal load-cell adaptor, with little difference (23 mm) between relatively large differences in pylon length. If the residuum and socket are included in the CoM calculation, using a maximum residuum length of 150 millimetres (for an individual of 1753 millimetre height, the average residuum length was 139 millimetres measuring from tibial plateau to end of socket) and a mass of 1.25 kilograms, the maximum total CoM location is 226 millimetres from the tibial plateau (based on 106 millimetre pylon length).

Previous studies have shown that increasing the mass of a trans-tibial prosthesis does not have a significant effect on the metabolic cost (ml O_2/kg/m) of the amputee during walking

at various speeds so long as the CoM locations are similar. A study by Lehmann et al. (1998) found that the mass of the prosthetic limb (including residuum) could be increased to 70% of the equivalent intact leg mass whilst walking at a self-selected (average 88 m/min) and 120 m/min speed without affecting metabolic cost as long as the CoM of the prosthesis remained at a similar location distal to the knee joint (47% of the intact tibial length). Additionally, a study by Lin-Chan et al. (2003), found that increasing the prosthetic limb mass (including residuum) up to 100% of the intact leg mass during multiple-speed treadmill walking (range of 54 to 107 m/min) does not affect metabolic efficiency as long as increased mass is attached to the original CoM location of the prosthesis (55% of the intact tibial length distal to the knee). The authors commented that the step frequency variability for an increase in prosthetic limb mass up to 100% was within natural gait variation, and concluded that this condition provided a stable gait. Overall, it appears that with sufficient time to accommodate to the prosthesis and so long as mass and CoM position are within the limits described above, trans-tibial amputees are able to tolerate large variations in prosthetic limb mass.

As mentioned above, the mass of the ITP is 3.37 kilograms without the residuum, which is 96% of the intact leg for an average 80 kilogram individual with the residuum included. Additionally, the maximum CoM location of an average prosthetic limb fit with the ITP would be 226 millimetres from the tibial plateau, or approximately 55% of the distance of the intact tibial length. Both of these measures fall within the range of prosthetic mass and CoM position tested in the previous studies mentioned above. This gave confidence that the subjects involved in this study would be able to tolerate the relatively heavy ITP (compared to the average trans-tibial prosthesis mass of 1.68 kilograms (Lin-Chan et al., 2003)) without any significant adverse effects to metabolic cost and stability.

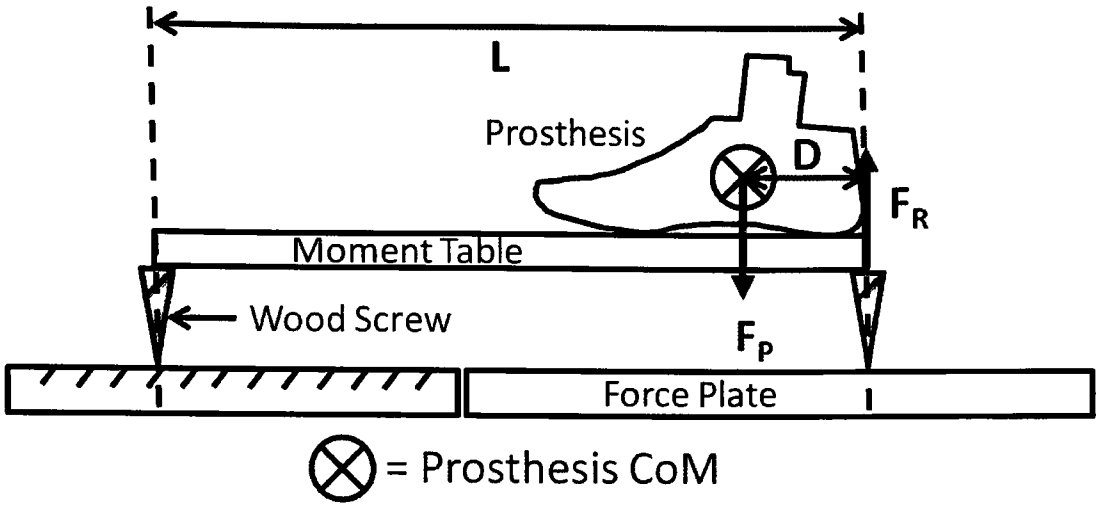

Figure 4.3.1.1. The moment table acts as a tripod supported by three wood screws, in which the single end point is placed on a force plate[16] and the other two end points are placed on level ground. The force plate is zeroed to remove mass effects of the moment table and the component is then lined up with the edge of the platform that is supported by the single screw. The component's CoM along the longitudinal axis of the moment table (D) is calculated through the following moment balance equation around the two end point side: $D = L \times (F_p - F_R)/F_p$, where L is the length of the moment table, F_p is the weight of the component, and F_R is the force measured by the force plate.

[16] Force plate model 9286a, Kistler Instruments Ltd., Alton, UK

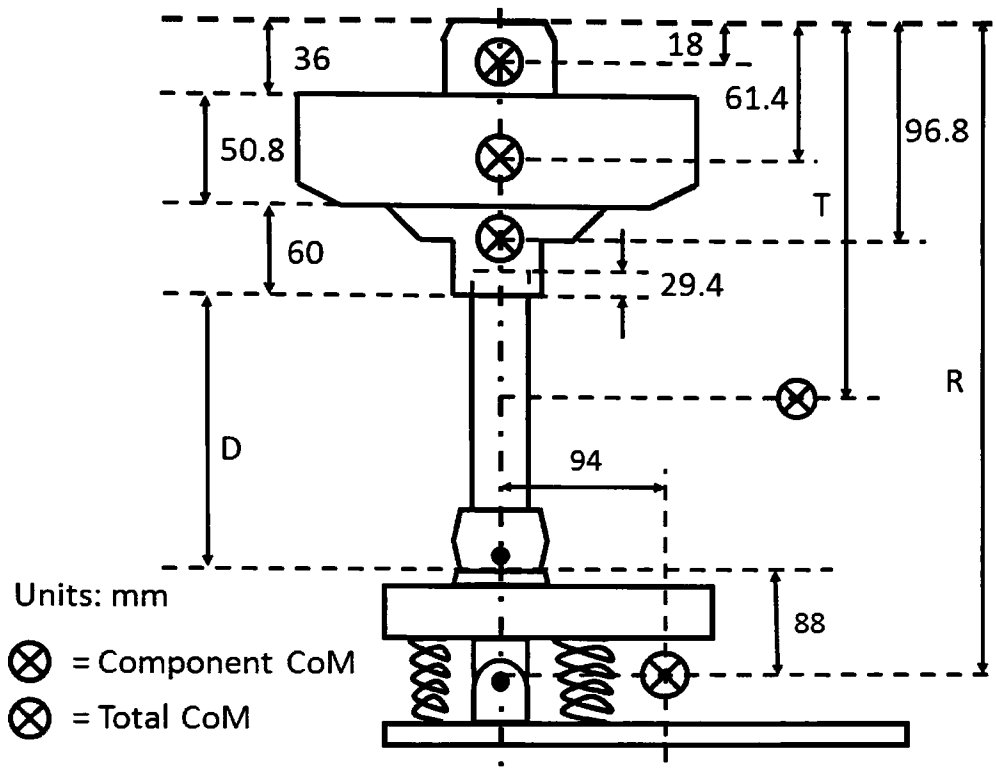

Figure 4.3.1.2. CoM locations and relevant dimensions of the components used in the assembly of the ITP. The total CoM position of the assembled ITP (T) is a function of the length of the pylon (D) as described by the following equation: $T=(18\times0.4+61.4\times1.07+96.8\times0.3+R\times1.2)/(0.4+1.07+0.3+1.2)$, *where* $R=(36+50.8+60+88+D)$ *and* D *is 29.4 (tube clamp recess) subtracted from the pylon length.*

4.4. Gait analysis protocol

This protocol describes the experimental methodology for human performance testing and gait analysis in order to investigate the research question posed earlier: how do alterations in the *AIPP* influence amputee performance during gait? In order to develop an understanding of how the *AIPP* affect amputee performance and if certain *AIPP* can improve performance under specific gait conditions, it was decided that a comprehensive investigation would utilise three methods of performance assessment:

1) biomechanical (i.e., joint kinematics and kinetics, temporal-spatial gait parameters),

2) physiological (i.e., energy expenditure), and
3) subjective feedback (i.e., visual analogue scales).

To conduct this study in a controlled manner, the experimental gait analysis trials were undertaken in a motion analysis laboratory at the University of Salford using the CFAM (see section 4.2), ITP (see section 4.3), a passive-marker motion analysis system[17], and a multiple-speed/grade treadmill[18]. Table 4.4.1 describes the three methods of assessment, how they were quantified, and the equipment used to measure them.

Table 4.4.1. Experimental measures and associated laboratory equipment.

Performance Assessment	Quantification	Equipment
Biomechanical	Kinetics of prosthetic limb, kinematics of ankle, knee, and hip joint, temporal-spatial parameters of gait	ITP, 10 Camera Vicon motion capture system
Physiological	Metabolic energy expenditure (i.e., oxygen consumption)	Polar portable heart rate monitor[19] and MetaMax gas analyser[20]
Subjective Feedback	Subjective ratings on comfort, exertion, and stability	Visual analogue scales (see Appendix D.3)

Based on the design of the CFAM, a 2X2 factorial design was utilised, in which all permutations of two levels of rearfoot stiffness and two levels of forefoot stiffness would be tested during four walking conditions:

1) self-selected walking speed on the level,
2) fast walking speed on the level (between 133 to 150% of self-selected speed, depending on what could be tolerated by the subject),
3) self-selected walking speed on a 5% grade incline, and
4) self-selected walking on a 5% grade decline.

[17] Vicon, Vicon Motion Systems Ltd, Oxford, UK
[18] Treadmill model T9450HRT, Vision Fitness, Lake Mills, WI, USA
[19] Polar S610i, Polar Electro Oy, Vantaa, Finland
[20] MetaMax 3B, Cortex Biophysik, Leipzig, Germany

4.4.1. Amputee subjects

Amputee subjects were recruited from the Disablement Services Centres (DSC) in Leeds, Liverpool, Preston, Manchester, Sheffield, the Wirral (as UK National Health Service (NHS) patients), and from the University of Salford BSc programme in Prosthetics and Orthotics (as 'professional amputees'). Prior to recruitment, ethical approval was obtained from the UK NHS National Research Ethics Service (see Appendix D.1) and the University of Salford. Rehabilitation consultants at the DSCs and academics at the University of Salford were provided four documents to enable them to make an informed decision regarding the selection of potentially suitable amputee subjects: 1) an explanation of the testing protocol (Protocol Sheet), 2) subject identification criteria, (Participant Identification Sheet), 3) information on the study to be distributed to the amputee subject prior to testing (Participant Information Sheet), and 4) consent form to be signed by the amputee subject (see Appendix D.2). Once suitable amputee subjects were identified, these individuals were approached informally by their respective rehabilitation consultant or Salford academic to establish whether they were willing to receive a formal request for possible inclusion in the study. If the identified amputee subject was willing to participate, then their contact details were supplied to the Principal Investigator of the study and they were subsequently provided with the Participant Information Sheet and the first of three visits were arranged. The recruitment process and participant involvement is described in Figure 4.4.1.1.

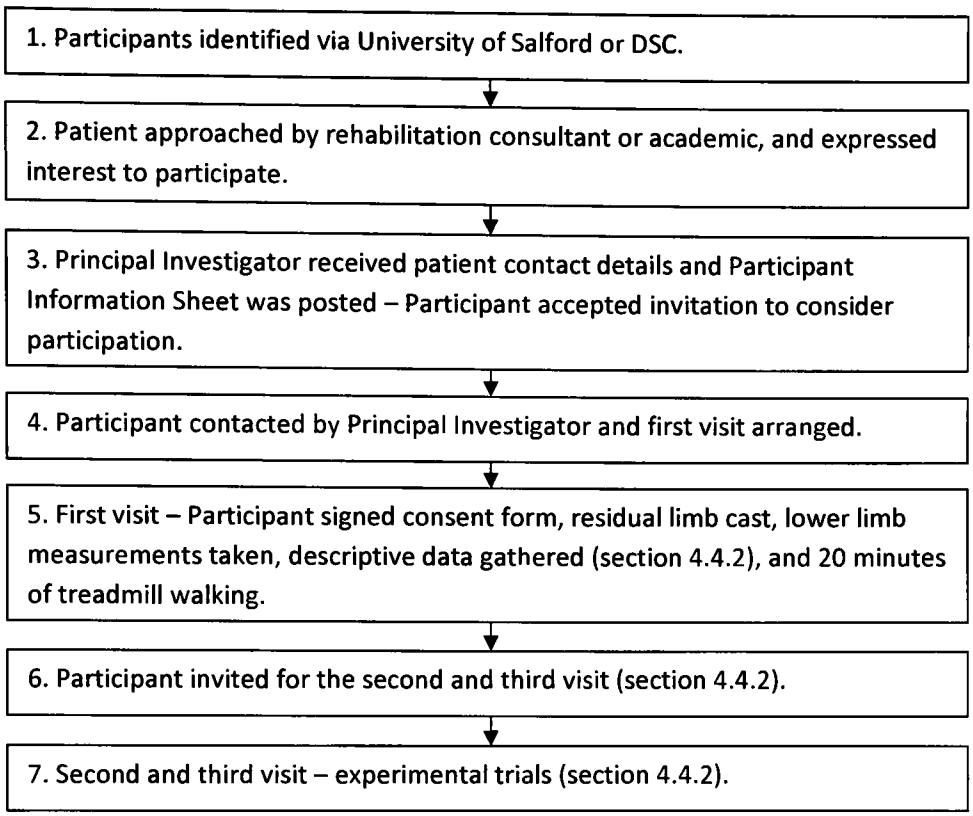

Figure 4.4.1.1. Recruitment process (1-4) and participant involvement (5-7).

The subject selection criteria were:

1. Unilateral trans-tibial amputee due to trauma; dysvascular amputees not permitted in order to avoid complicating health factors;
2. At least 29 centimetres of clearance between the end of the residuum and the ground (minimum distance allowed by full assembly of the ITP including socket);
3. Good general health and relatively active;
4. No significant medical conditions other than amputation;
5. No significant walking pathologies unrelated to prosthesis use;
6. Residuum in good condition (i.e., no adherent scars, infections, etc.);
7. Non-amputated side in good condition;
8. Full range of joint motion at both hips and knees;
9. More than one year experience of ambulation with a prosthesis;
10. Able to walk for at least 10 minutes continuously without suffering from fatigue;
11. Able to walk at a speed slightly faster than normal walking;

12. Able to walk on both moderate incline and decline surfaces;
13. Between the age of 18 and 80 years;
14. Can adequately understand verbal or written information in English;
15. Without special communication needs.

4.4.2. Experimental procedure

Amputee subjects were required to attend three visits to the University of Salford on separate days in order to complete the experimental procedure. These visits are described in detail below:

First visit

At the start of the first visit, the subject was required to sign the consent form. After consent was obtained, the subject's residual limb was cast using the Icecast procedure described in section 4.3, lower limb measurements were taken and descriptive data were recorded by a prosthetist, who also oversaw subsequent socket manufacture prior to the second visit and the ITP alignment on the second visit. Measurement of and descriptive data on subjects included:

1. Name (already obtained during recruitment);
2. Contact details (already obtained during recruitment);
3. Date of birth;
4. Gender;
5. Date of amputation;
6. Specific reason for amputation;
7. Side of amputation;
8. Medical conditions;
9. Occupation;
10. Hobbies and activities;
11. Current prosthetic prescription (i.e., type of foot, pylon etc.);

12. Body height;
13. Body weight;
14. Residuum length;
15. Residuum circumferences;
16. Distance from end of residual limb to ground;
17. Distance from sound side mid patella tendon to ground;
18. Foot length.

The casting and measuring were then followed by 20 minutes of walking on the treadmill, at a self-selected speed that the subject considered to be "comfortable and safe," while using their own prosthesis. The subject performed at least 10 minutes of continuous walking in order to allow the subject to become accustomed to the treadmill, and hence confident with performing the forthcoming experimental trials during the second and third visit. During this time, the subject's self-selected walking speed was recorded which would be used for the experimental trials. Additionally, the subject tried on three different sizes of the mask used for the gas analyser to measure oxygen consumption in order to confirm which size was a best fit for the following two visits. The first visit was approximately 1 hour in duration.

Second and third visit

The second visit involved the first set of experimental trials and was approximately 2 hours and 30 minutes in duration. Upon arrival, the subject changed into a pair of shorts provided and received the ITP with the custom socket which was fitted and adjusted by a prosthetist. Static and dynamic alignment adjustments took place in the clinic room across the corridor from the motion analysis laboratory. During fitting and alignment, the subject wore a comfortable trainer on their sound foot which would be used during the experimental trials. As there was no footwear on the amputated side, the prosthesis length was adjusted accordingly so that the effective leg lengths were the same on both sides. If the amputated side remained slightly longer, shoe insoles were used on the sound side until equal limb lengths were achieved.

Following the fitting procedure, the subject was then given at least 10 minutes for getting

accustomed to the ITP by walking the length of the clinic room. The subject was then led into the motion analysis laboratory and set up with the body-worn testing equipment (heart rate monitor, oxygen consumption monitor, and retro-reflective markers). The heart rate monitor belt was worn across the chest, just inferior to the pectoral muscles, and a silicon mask worn across the nose and mouth for gas analysis. Data from the heart rate monitor were transmitted wirelessly to the gas analyser. A volume transducer was press fit into the end of the silicon mask to measure oxygen consumption, and connected via a plastic tube to the gas analyser that remained on a moveable trolley in front of the treadmill. This trolley also carried the laptop for recording heart rate and oxygen data in real-time within the Metasoft software[21]. A schematic of the laboratory setup is displayed in Figure 4.4.2.1. The four treadmill markers placed on the static, rigid frame of the treadmill were used to define the walking surface plane for calculating the instantaneous Centre of Pressure (CoP) during gait as detailed in Appendix C.1.The load-cell cable attaches from the ITP to a power supply and main computer (operating motion analysis software[22]) located behind cameras 6, 7 and 8.The treadmill is surrounded by padded gym mates in case the subject suffers a fall from the treadmill. The trolley in front of the treadmill houses the gas analyser and laptop. Cameras 1-4 and 7-10 were raised to the maximum height allowed by their supporting tripods, whilst cameras 5 and 6 were lowered to minimum height allowed in order to minimise marker occlusion from the front support bars of the treadmill. The plastic tube connects the silicon mask to the gas analyser.

Potential modes of danger for the subject whilst walking on the treadmill were considered and, if necessary, addressed before any experimental testing took place. These can be found in Appendix B.1.3.

[21] Metasoft software, Cortex Biophysik, Leipzig, Germany

[22] Vicon Workstation, Vicon Motion Systems Ltd, Oxford, UK

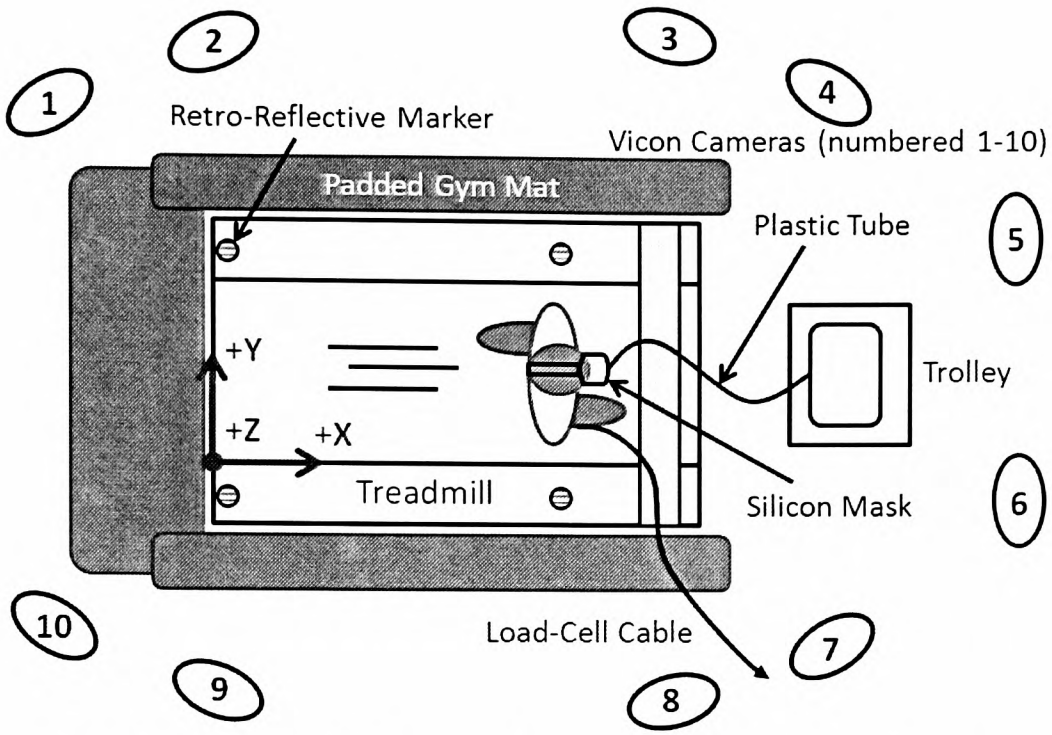

Figure 4.4.2.1. Schematic illustration of motion analysis laboratory setup (top-down view). Global axes are displayed (with +z-axis pointing toward the ceiling) as set by the Vicon calibration frame placed on the lower-left corner of the treadmill belt (as seen from above).

Using hypoallergenic, self-adhesive tape, Velcro and a neoprene belt, retro-reflective markers for tracking the subject's motion were attached to the ITP, CFAM, pelvis and both lower limbs, including specific anatomic landmarks, either as groups of four on rigid marker plates or individually (Figure 4.4.2.2). Three markers were attached to the load-cell in the configuration displayed in Figure 4.4.2.3. These were used to form a local reference frame on the load-cell in order to locate the instantaneous position of the geometric centre of the load-cell and define the local z-axis of the load-cell (aligned with the longitudinal axis of the pylon). This information is used to calculate the instantaneous CoP during gait as detailed in Appendix C.1.

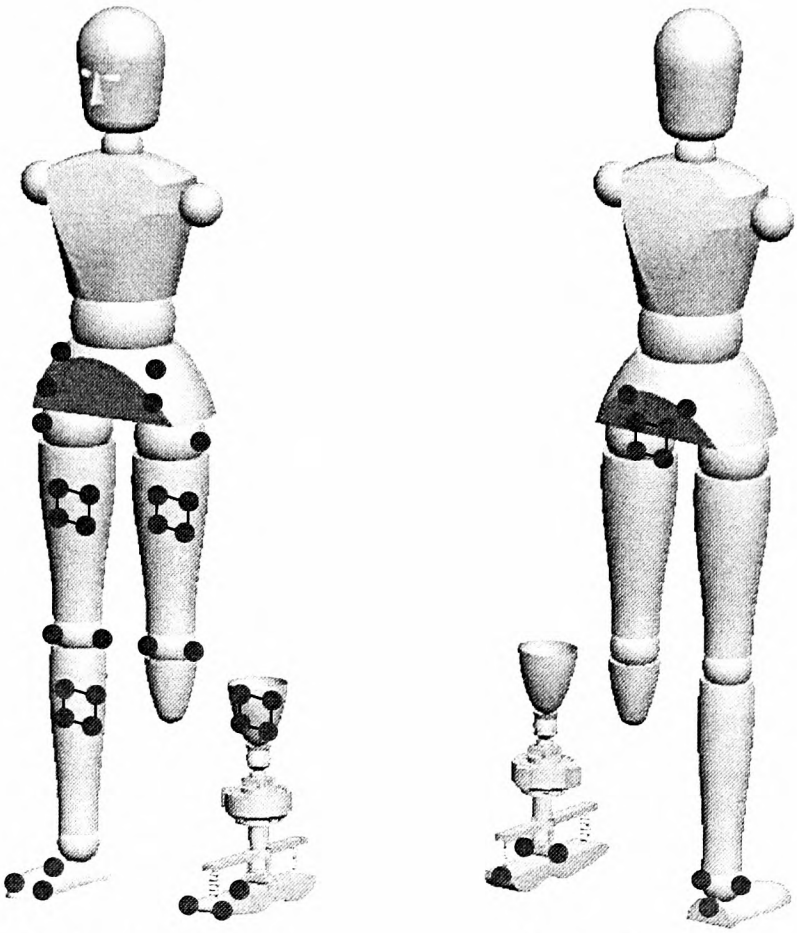

Figure 4.4.2.2. Schematic illustration of retro-reflective markers (represented as circles) on skin, ITP, and the CFAM. Markers connected by lines represent rigid marker-plates. A full list of the markers, including the ones removed during testing is provided in Appendix E.1.The articulated joint of the CFAM allowed for the same marker set as used on the sound foot to be used to measure the prosthetic ankle joint motion. No markers shown in either view are repeated in the opposing view.

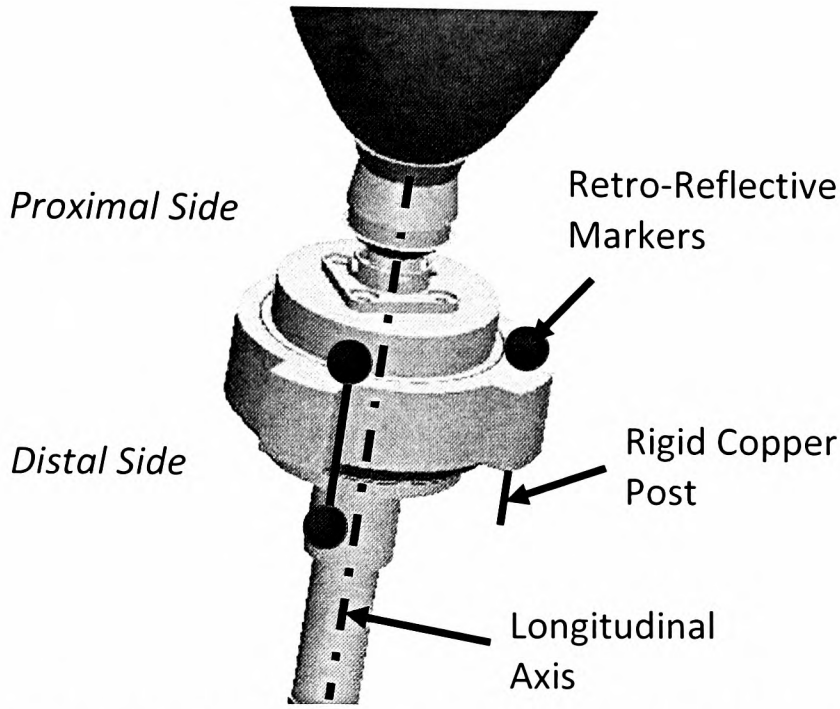

Figure 4.4.2.3. Load-cell marker set used to calculate the geometric centre of the load-cell and define local z-axis (aligned with longitudinal axis of the pylon). The markers are fixed to rigid copper posts that are pressed against the load-cell ports as shown. The markers on the proximal side of the load-cell are resting on the load-cell surface. During gait analysis, the load-cell is rotated such that the markers are on the lateral side to minimise marker occlusion.

The testing order of the four CFAM setups were randomized for each subject prior to testing with custom Matlab[23] software in order to reduce the potential for order bias. For each test, the self-selected walking and fast walking on the level were the first two walking conditions tested, consecutively, to further accommodate the subject to the equipment and reduce the time needed for testing. The last two tested walking conditions (incline and decline) were randomised prior to testing in order to reduce order bias. Two CFAM setups were tested under the four walking conditions during the second visit, and the remaining two during the third visit (Figure 4.4.2.4). As it was often difficult to schedule subjects for two consecutive days, the ITP had to be realigned for the third visit.

[23] Matlab, C-Motion Inc., Germantown, MD, USA

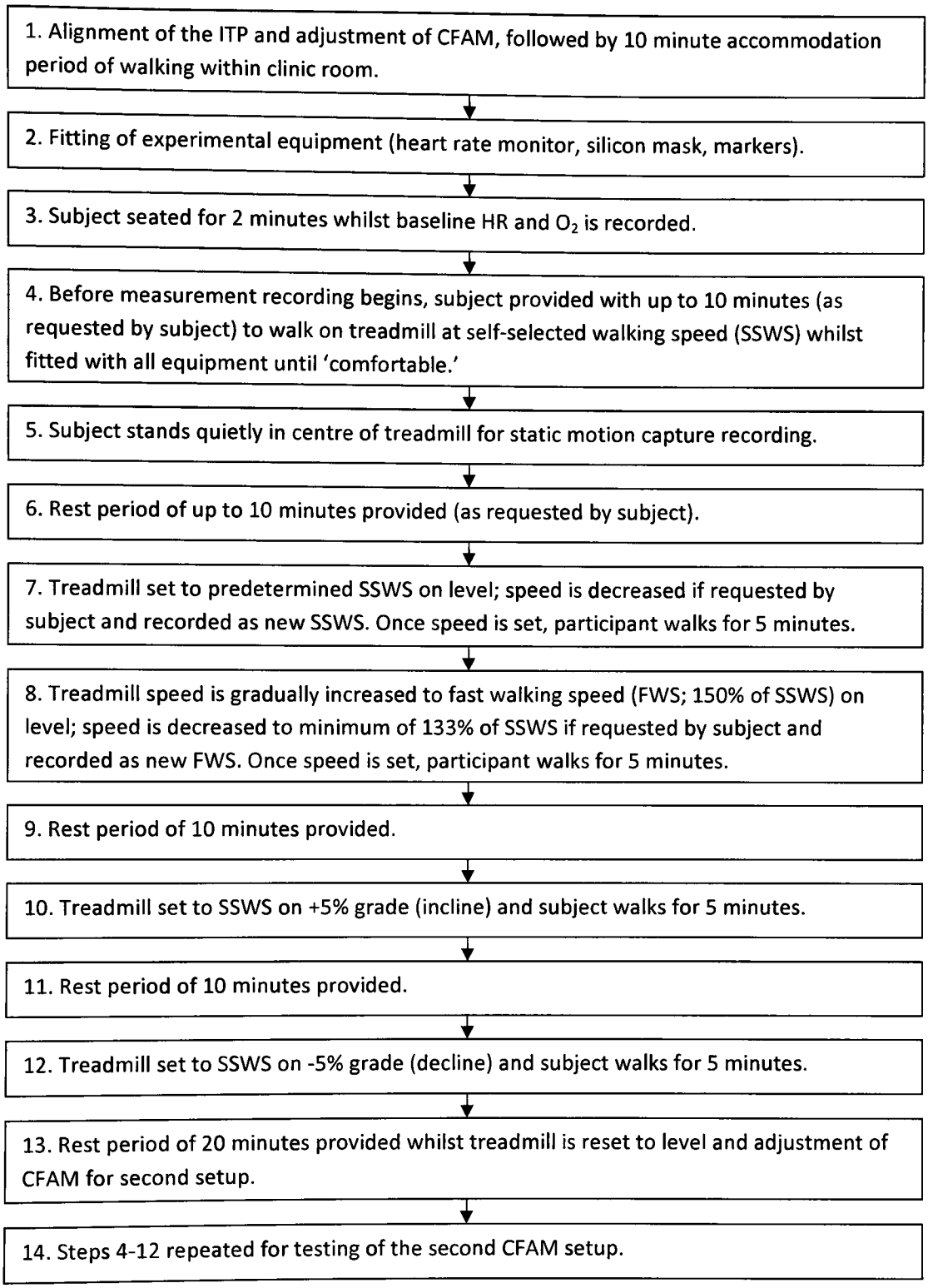

Figure 4.4.2.4. Experimental testing procedure for the second and third visit. Heart rate (HR) and oxygen consumption (O_2) data are recorded continuously for the final minute of each five minute walking condition, of which motion data is recorded for final 10 seconds.

4.5. Data analysis

4.5.1. Post-processing

In an attempt to avoid the transitory effects observed in treadmill gait parameters (Owings and Grabiner, 2003), data collection for each experimental condition only commenced once the subject had completed at least 400 steps. Calculation of the kinematic, kinetic and temporal-spatial data for each experimental condition was then performed over 12 continuous steps (6 right and 6 left). Consequently, the prosthetic and sound side kinematic data and prosthetic side kinetic data were averaged over 6 steps and the temporal-spatial parameters of each subject were calculated over all 12 steps, unless indicated otherwise.

The stance phase of gait was separated into two phases for the purpose of analysis: 1) loading phase, defined as the period between heel-strike (0% of stance) and the start of terminal stance (50% of stance), and 2) unloading phase, defined as the period between the start of terminal stance (50% of stance) and toe-off (100% of stance) (Perry, 1992). Maximum knee flexion of both limbs was calculated during the first part of stance before the knee began its second phase of knee flexion as seen during late stance.

Sign conventions for reported kinetics and kinematics are based on those defined by Whittle (1991). Kinetic and kinematic data were sampled at 1000 Hz and 100 Hz, respectively, and the kinetic data was re-sampled to 100 Hz prior to low-pass filtering. A Butterworth low-pass filter was applied to the kinetic and kinematic data with cut-off frequencies at 25 Hz and 6 Hz, respectively.

4.5.2. Lower extremity joint kinematics

Ankle and knee joint centres were calculated using the medial and lateral malleolus and condyle markers, respectively, and the method presented in Cappozzo et al. (1995). The hip joint centres were calculated using the anterior superior iliac spine and the posterior superior iliac spine markers and regression equations adapted from Bell et al. (1989; 1990).

The instantaneous joint centre locations and marker plate trajectories were used within a custom model in the Visual 3D software[24] to calculate the kinematics of the ankle, knee, and hip joints. Instantaneous location of the ankle, knee, and hip joint centre were determined in Visual 3D with use of the Calibrated Anatomical Systems Technique (Cappozzo et al., 1995).

4.5.3. Prosthetic limb kinetics

The integrated load-cell of the ITP records force and moment data at the distal end of the socket, which is converted into ground reaction forces as detailed in Appendix C.1 using custom software developed in Matlab. From these data, the maximum vertical and horizontal ground reaction forces during the loading and unloading phase of stance were identified. For the purpose of discussion, the horizontal ground reaction forces during the loading and unloading phase of stance are referred to as the braking and propulsive forces, respectively.

4.5.4. Temporal-spatial gait parameters

As there were no kinetics recorded for the sound leg, a method by O'Connor et al. (2007), was applied to identify the heel-strike and toe-off of both the sound foot and CFAM utilising only kinematic data. These gait events, as calculated by custom software developed in Matlab, allowed for determination of the following temporal-spatial gait parameters: step width, step length, step time, and single-support stance time (or swing time) of both limbs. Definitions of the spatial parameters are displayed in Figure 4.5.1. Step time is defined as the time between the heel-strike of one foot and the heel-strike of the contralateral foot. Coefficient of Variation (CV), defined as the individual subject's standard deviation divided by their mean, was calculated for each of these temporal-spatial parameters. A 'symmetry ratio' was defined as the ratio of the subject's mean swing time of the sound limb divided by the mean swing time of the prosthetic limb.

[24] Visual 3D, C-Motion Inc., Germantown, MD, USA

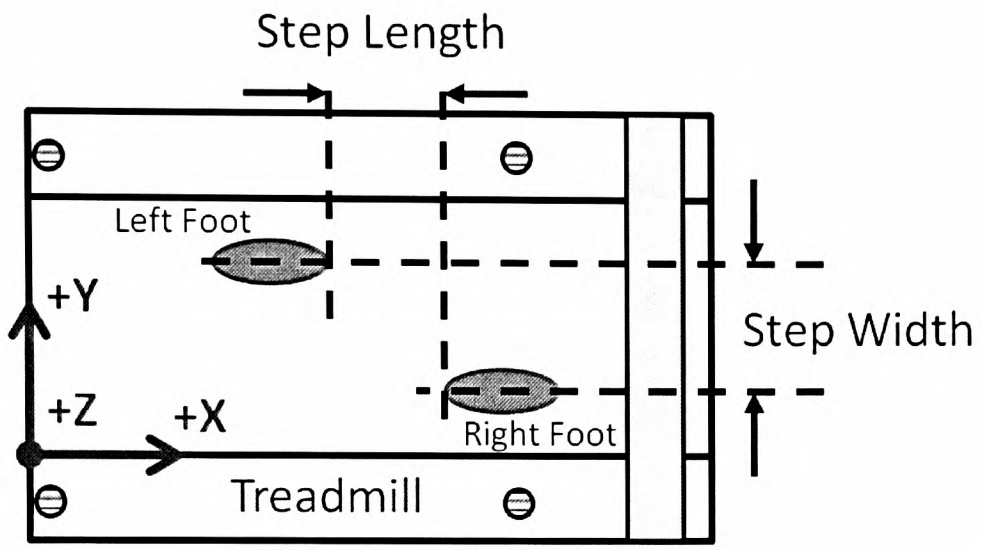

Figure 4.5.1. Schematic illustration of spatial measures. A modified definition of step length as seen in the study by Owings and Grabiner (2003), is used in this study due to use of the treadmill: the distance along the global x-axis between the toe-off of one foot and the heel-strike of the contralateral foot. Step width is defined as the distance along the global y-axis between the heel-strike of one foot and heel-strike of the contralateral foot.

4.5.5. Metabolic energy expenditure

Oxygen consumption and heart rate data was averaged over the final minute of each five minute walking trial. Oxygen consumption data was normalised by the subject's body weight (millilitres O_2/kilogram/minute) to calculate metabolic rate and then walking speed (millilitres O_2/kilogram/metre) to calculate metabolic cost of transport.

4.5.6. Subjective ratings

Following each five minute walking trial, subjects were asked to record their perceived level of stability, exertion, and comfort using a Visual Analogue Scale (VAS; see Appendix D.3). Each scale ranged from 1 to 10, in which extremes (level 1 and 10) for stability, exertion, and comfort were defined as: Very unsteady and at immediate risk of falling / Completely Stable and Confident, No exertion at all / Maximal exertion, and No pain at all and very comfortable / Unbearable discomfort, respectively.

4.5.7. Statistical analysis

Effects of rearfoot and forefoot stiffness (i.e., CFAM setups one through four) on the measured kinematic, kinetic, energy expenditure, temporal-spatial, and VAS parameters were statistically analysed with the Friedman test for non-parametric repeated measures analysis-of-variance using SPSS statistical software[25]. The Friedman statistical test is used to determine the effects of more than two 'treatments' on a single factor of paired data (Ennos, 2007). This test reduces the effects of intra-subject variance on statistical analysis. The value of critical α for this statistical analysis was set at 0.1, in which any p-value at or below this critical α was considered worthy of discussion. Therefore, if significance at or below a p-value of 0.1 was determined with the Friedman test, the Nemenyi post-hoc test was used to identify the significant relationships (Zar, 1996). If a significant p-value resulting from the Nemenyi test was greater than that which resulted from the Friedman test, then relationships are significant at that new p-value. Bivariate correlations were determined with the Spearman's rank correlation coefficient method for non-parametric variables using SPSS. Results from regression analyses using SPSS were tested for violation of the assumptions of residual normality and homoscedasticity (Petrie and Sabin, 2000). Normality was assessed using the Shapiro-Wilk test with a critical α set at 0.05. If the residual distribution was found to be different than the normal distribution at a p-value of less than 0.05, this was reported. As recommended with non-parametric and small data sets, all available data points of each data set were used in the statistical analysis, including those identified as outliers (Burke, 2001). Outliers within a data set were identified as values which were located a distance from the edges of the inter-quartile range box (i.e., lower or upper quartile) equal to or greater than 1.5 times the inter-quartile range.

[25] SPSS version 16, SPSS Inc., an IBM Company Headquarters, Chicago, IL, USA

5. Chapter Five: In-vivo results

A raw form of the results from the human performance study described in Chapter Four is presented in Appendix F, which is displayed in the form of box plots showing the effects of CFAM setup on gait performance measures and the results from the statistical analysis (see section 4.5.7). These results are separated into biomechanical (Appendices F.1.1 – F.1.20), physiological (Appendices F.1.21 – F.1.22), and subjective measures (Appendices F.1.23 – F.1.25). Based on these results, certain inferences can be made about how the forefoot and rearfoot stiffnesses affect amputee gait performance and if certain trends exist which indicate a preference for low or high stiffness. The discussion in the remainder of this chapter is based on observation of the median values and results from the statistical analysis. For this discussion, the CFAM setups are abbreviated as seen in Table 5.1 and the walking conditions are abbreviated as seen in Table 5.2.

Table 5.1. CFAM setup abbreviations.

Forefoot Stiffness	Rearfoot Stiffness	Foot Setup
LO	LO	*LOLO*
LO	HI	*LOHI*
HI	LO	*HILO*
HI	HI	*HIHI*

Table 5.2. Walking condition abbreviations.

Walking Condition	Definition
SSWS	Self-selected walking speed on level
FWS	Fast walking speed on level
INC	Self-selected walking speed on 5% incline
DEC	Self-selected walking speed on 5% decline

As a general note, for the reasons discussed in Chapter Two, the results from this study are difficult to compare with previous human performance investigations. First, very few studies provide any data on the mechanical properties of the prosthetic feet used during human performance testing. Therefore, it is impossible to establish correlations between the mechanical function of the prosthesis and gait performance measures when the only information available to distinguish between these feet are their commercial trade names.

Second, many human performance studies compare 'conventional' and 'energy storage and return' (ESAR) feet, in which the Solid Ankle Cushion Heel (SACH) foot is often representative of a conventional foot and the Flex-Foot is representative of an ESAR foot. These two prosthetic foot types are often tested because of their primary difference in design and function: an ESAR foot is constructed of materials, often in the form of leaf springs, that are capable of efficiently storing energy during the loading phase of stance and returning this energy during late stance, whilst the conventional foot is made of a non-articulated or single axis ankle joint and is only meant to provide a stable base of support and appropriate roll-over characteristics during the stance phase of gait (Seymour, 2002). However, the primary objective of this study was to observe the influence of prosthetic ankle joint stiffness on gait performance, without concurrently changing other prosthesis properties. For example, in comparison to the *AIPP* characterisation results for the Flex-Foot presented in Figure 3.3.3 of Chapter Three, the CFAM is significantly more damped (see Figure 4.2.3.2) and possesses approximately the same level of damping for all setups. Therefore, the results of this study are primarily due to differences in forefoot and rearfoot stiffness. Consequently, it is difficult to compare the results of this study to those which compare different commercial feet (e.g., ESAR and SACH) where several different prosthesis properties are likely to be changed concurrently. However, despite this issue, the results of this study have been related to the outcomes of previous research wherever possible.

Study participants

Following recruitment, eight subjects were identified as suitable participants and attended the first visit to the University. Following the first visit, one subject was deemed unsuitable due to a relatively slow and shuffling gait, one subject withdrew from the study after feeling uncomfortable with walking on the treadmill, and one subject withdrew due to the time commitment involved. Selected measured and descriptive data for the remaining five (male) subjects are available in Table 5.3.

Table 5.3. Descriptive and measured data of amputee subjects. The current foot prescription is labelled in brackets as either conventional, C, or energy-storage and return, E.

Subject Number	1	2	3	4	5	Average (SD)
Age (yrs)	56	44	56	39	44	48 (8)
Time since Amputation (yrs)	46	2	53	6	27	27 (23)
Side of amputation	Left	Left	Right	Left	Left	-----
Height (mm)	1836	1840	1847	1839	1766	1826 (34)
Weight (kg)	93	85	91	96	76	88 (8)
Residuum length (mm)	125	170	170	130	120	143 (25)
Foot length (mm)	280	280	290	260	250	272 (16)
Self-selected walking speed (m/min)	42.9	51.0	42.9	56.3	40.2	46.7 (6.7)
Fast walking speed (m/min)	64.4	75.1	64.4	83.2	53.6	68.1 (11.3)
Resting heart rate (beats/min)	58	62	62	73	76	66 (8)
Resting oxygen consumption (ml O_2/kg/min)	2.828	3.776	2.297	3.375	3.487	3.153 (0.589)
Current foot prescription	Otto Bock SACH (C)	Endolite Elite (E)	Hanger Quantum (E)	Össur Ceterus (E)	Otto Bock Trias (E)	-----

5.1. Effects of *AIPP* variation on gait kinetics and kinematics

5.1.1. Peak vertical ground reaction force during loading

Figures 5.1.1.1 and 5.1.1.2 display the effects of rearfoot and forefoot stiffness on the peak vertical ground reaction force on the prosthetic limb during the loading phase of stance (0-50% of stance), respectively. With one exception, across all walking conditions, it is clear that low forefoot with low rearfoot stiffness (LOLO) tends to reduce the peak loading force. The exception is the incline condition where LOLO and LOHI produced similar results. When

combined with a high forefoot stiffness, the vertical ground reaction force during loading is seen to increase with low rearfoot stiffness during the fast, incline, and decline walking conditions (Figure 5.1.1.1). This agrees with the finding in the study by (Lehmann et al., 1993b) which reported a direct relationship between a decrease in prosthetic heel stiffness and an increase in peak vertical ground reaction forces during prosthetic limb loading.

Referring to Figure 5.1.1.2, with the exception of the fast walking condition with high rearfoot stiffness, high forefoot stiffness leads to higher loading forces. The study by Lehmann et al. (1993b) also found that the prosthetic foot with the greatest forefoot stiffness produced the greatest maximum vertical ground reaction force during loading. Considering that the prosthetic ankle joint moves into dorsiflexion during the loading phase of stance (0-50% of stance, see Figure 5.1.1.3), it is possible that forefoot stiffness is having an effect on the loading characteristics of the prosthetic limb following heel-strike, particularly if there is a slow rate of loading. With one exception, the HILO CFAM setup produced the highest loading forces. In fact, for the fast walking condition, HILO produced greater peak loading forces than LOLO with a statistical significance of $p=0.001$. Overall, it appears that forefoot stiffness is the better predictor of loading forces, in which low forefoot stiffness produced lower peak loading forces across almost all walking conditions (Figure 5.1.1.2). The only walking condition in which high forefoot stiffness tended to reduce peak loading forces is during the fast walking speed condition, in which HIHI reduced the peak loading forces almost to the equivalent of those with the LOLO setup. Overall, a stiffer forefoot elevates the loading forces on the prosthetic side. Although this is not excessive for this set of controlled walking conditions, it could be more harmful for the prosthetic limb at increased walking speeds.

For self-selected walking speed on the level, the median value of the peak vertical ground reaction force on the prosthetic limb during the loading phase of stance (defined as 0-50% of stance) was approximately 1.0 times body weight across all foot setups. This is lower than the peak vertical ground reaction force reported for healthy individuals at a self-selected walking speed of 82 m/min on a level surface, which is approximately 1.1 times body weight (Perry, 1992). However, the forces in this study are more reflective of those seen in healthy individuals when walking at a slower speed of 60 m/min, in which peak vertical ground

reaction forces during loading do not exceed 1.0 times body weight (Perry, 1992). Previously reported prosthetic side peak forces for unilateral trans-tibial amputees during the loading phase of stance when walking overground have ranged from approximately 1.01 to 1.21 times body weight during self-selected walking speeds between 63.3 and 102.0 m/min (Menard et al., 1992; Powers et al., 1994; Snyder et al., 1995; Torburn et al., 1990).The average self-selected treadmill walking speed for this study (46.7 m/min) was lower than the previous reported studies for overground walking. However, despite a slower walking speed, the kinetic results from this study are found to lie within the range of previously reported values for ground reaction forces on the prosthetic limb during the loading phase of stance.

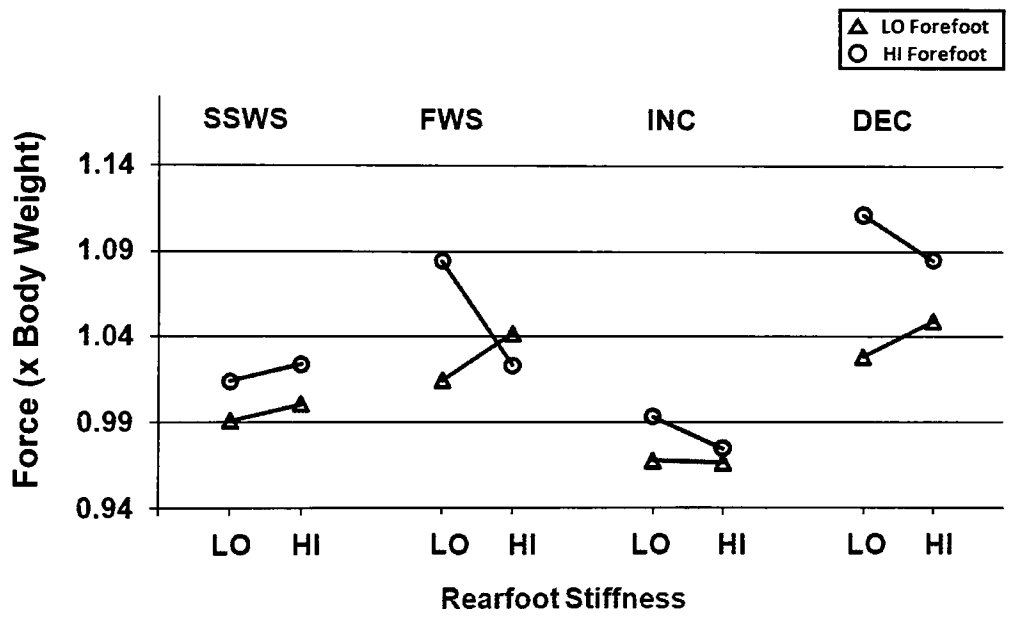

Figure 5.1.1.1 Effects of rearfoot stiffness on peak vertical ground reaction force (median) during loading phase of stance.

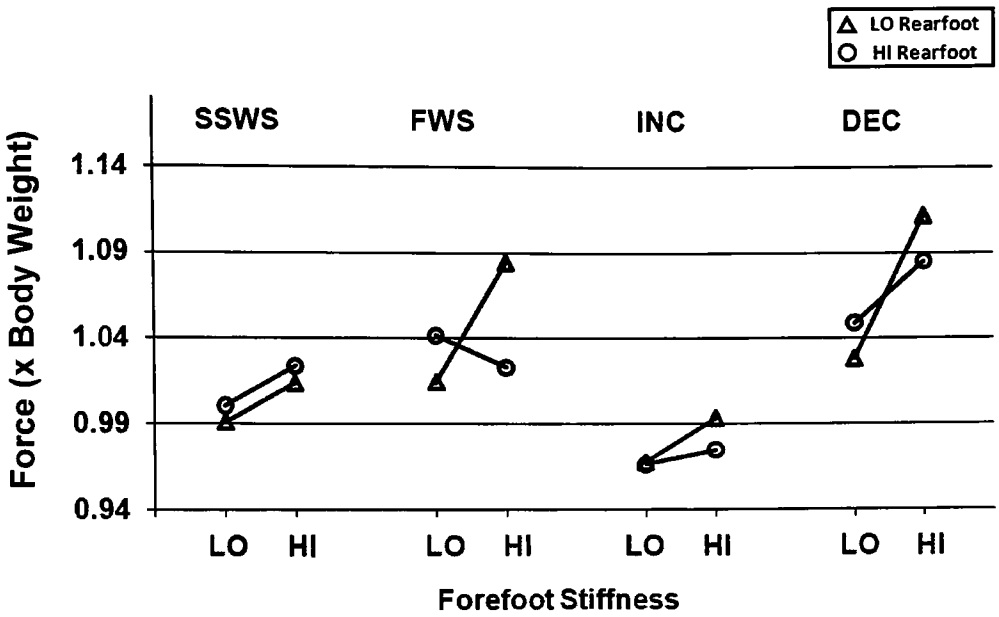

Figure 5.1.1.2 Effects of forefoot stiffness on peak vertical ground reaction force (median) during loading phase of stance.

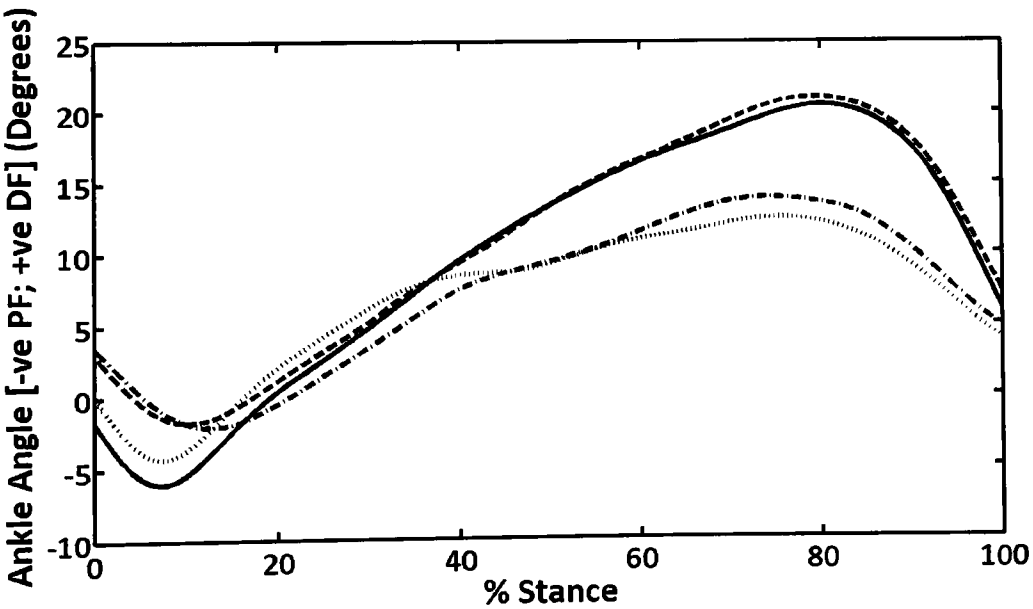

Figure 5.1.1.3. Single case results of in-vivo prosthetic ankle joint kinematics for four CFAM setups during prosthetic stance (0% and 100% approximating heel-strike and toe-off, respectively); solid line=LOLO, dash line=LOHI, dotted line=HILO, dash-dot line=HIHI.

5.1.2. Peak vertical ground reaction force during unloading

Figures 5.1.2.1 and 5.1.2.2 display the effects of rearfoot and forefoot stiffness on the peak vertical ground reaction force on the prosthetic limb during the unloading phase of prosthetic limb stance (50-100% of stance), respectively. These figures clearly show that high forefoot stiffness produced an increase in peak unloading forces across all walking conditions. This agrees with the findings in the study by Lehmann et al. (1993b), in which there was a direct relationship between increasing prosthetic forefoot stiffness and greater vertical force on the prosthetic limb during terminal stance. Given that a high forefoot stiffness also produces greater forces during loading of the prosthetic limb, it is postulated that the elevated unloading forces could be having a direct impact on the swing kinematics of the prosthetic limb and hence the loading forces after heel-strike.

For self-selected walking speed on the level, the median value of the peak vertical ground reaction force on the prosthetic limb during the unloading phase of stance (defined as 50-100% of stance) was approximately 1.04 times body weight across all foot setups. This is lower than the peak vertical ground reaction force reported for healthy individuals at self-selected walking speed of 82 m/min on a level surface, which is approximately 1.1 times body weight (Perry, 1992). As with the loading forces, the unloading forces in this study are more reflective of those seen in healthy individuals when walking at a slower speed of 60 m/min, in which peak vertical ground reaction forces during unloading do not exceed 1.0 times body weight (Perry, 1992). Previously reported prosthetic side peak forces for unilateral trans-tibial amputees during the unloading phase of stance when walking overground have ranged from approximately 0.98 to 1.05 times body weight during self-selected walking speeds between 66.9 and 102.0 m/min (Menard et al., 1992; Powers et al., 1994; Snyder et al., 1995; Torburn et al., 1990). Once again, even though the average self-selected treadmill walking speed for this study (46.7 m/min) was lower than the previous reported studies for overground walking, the kinetic results are found to lie within the range of previously reported values for ground reaction forces on the prosthetic limb during the unloading phase of stance.

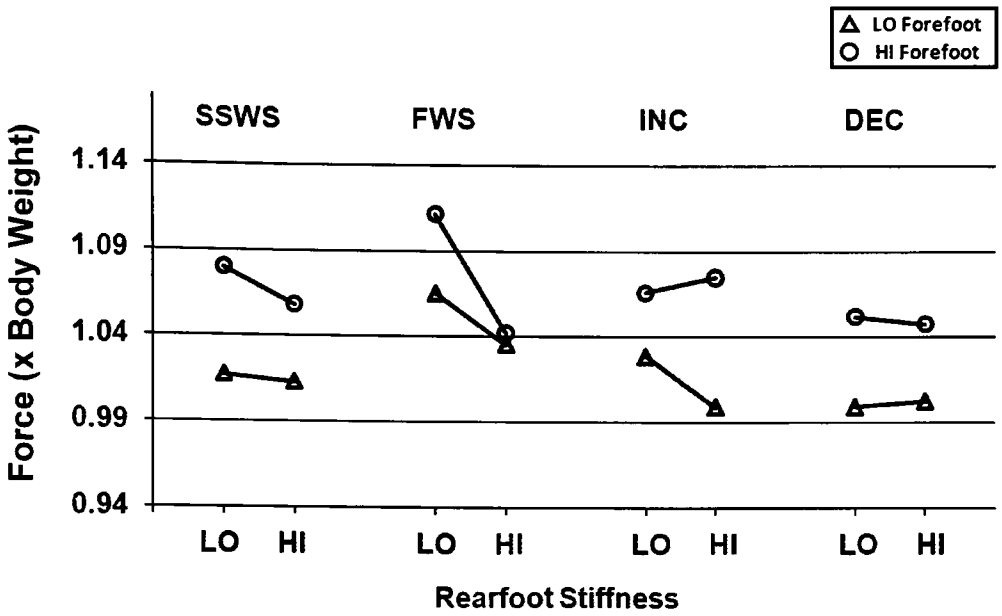

Figure 5.1.2.1. Effects of rearfoot stiffness on peak vertical ground reaction force (median) during unloading phase of stance.

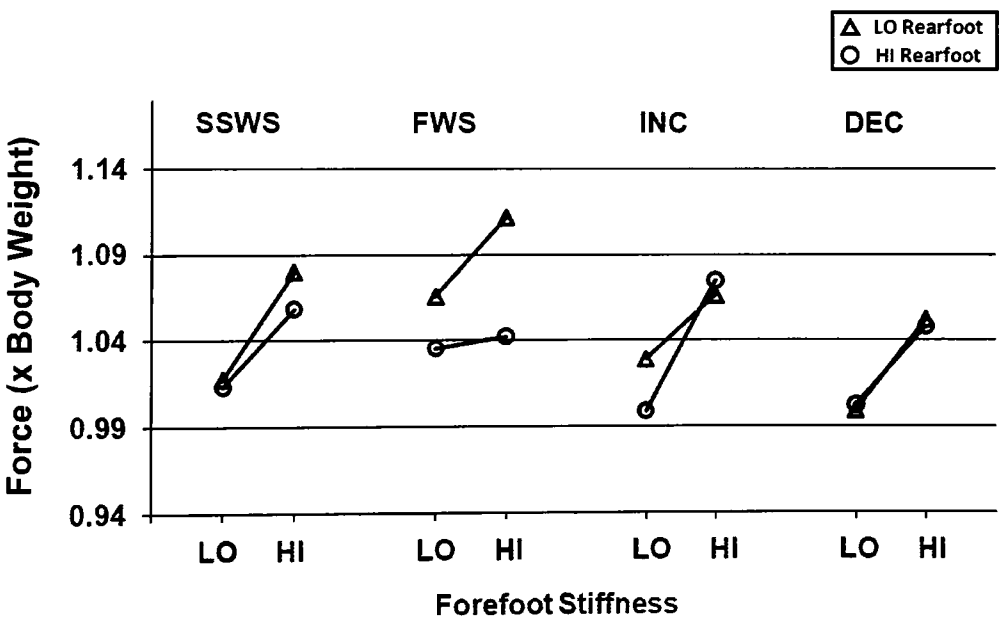

Figure 5.1.2.2. Effects of forefoot stiffness on peak vertical ground reaction force (median) during unloading phase of stance.

5.1.3. Peak horizontal ground reaction force during loading (braking force)

Figures 5.1.3.1 and 5.1.3.2 display the effects of rearfoot and forefoot stiffness on the peak horizontal ground reaction force on the prosthetic limb during the loading phase of stance (i.e., braking force). Once again, forefoot stiffness appears to be a good predictor of peak braking forces, in which high forefoot stiffness tends to increase the peak braking force for all walking conditions and this corresponds with the general increase found in the peak vertical forces. For example, during the fast walking condition, HILO produced greater peak braking force than LOHI with a statistical significance of p=0.054. In addition to this, low rearfoot stiffness tended to produce an increase in braking forces, which would again align with the results in the study by Lehmann et al. (1993b) that reported an increase in loading of the prosthetic limb during the loading phase of stance with lower rearfoot stiffness. Overall, it would appear that a high forefoot stiffness and low rearfoot stiffness would generally increase loading of the prosthetic limb.

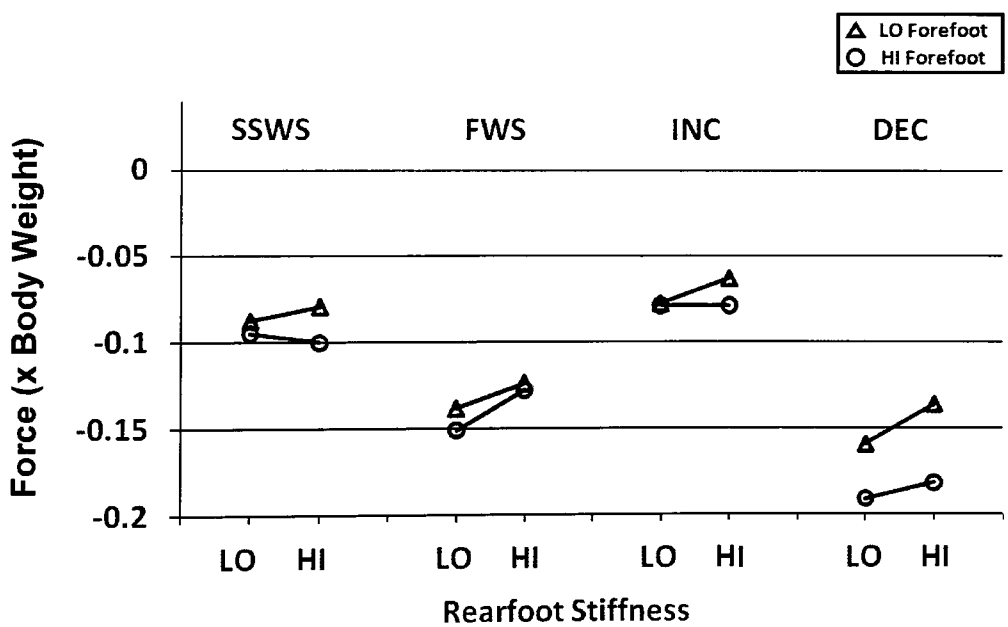

Figure 5.1.3.1. Effects of rearfoot stiffness on peak horizontal ground reaction force (median) during loading phase of stance (i.e., braking force).

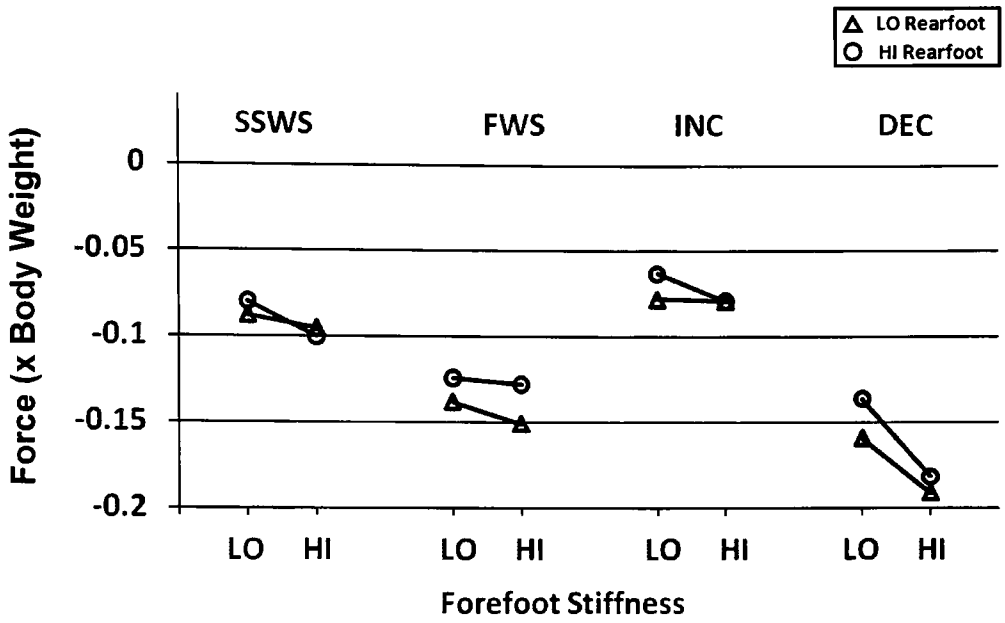

Figure 5.1.3.2. Effects of forefoot stiffness on peak horizontal ground reaction force (median) during loading phase of stance (i.e., braking force).

5.1.4. Peak horizontal ground reaction force during unloading (propulsive force)

Figures 5.1.4.1 displays the effects of forefoot stiffness on the peak horizontal ground reaction force on the prosthetic limb during the unloading phase of stance (i.e., propulsive force). Once again, forefoot stiffness appears to be a good predictor of peak propulsive forces, in which high forefoot stiffness generally tends to increase the peak propulsive force for all walking conditions and this corresponds with the general increase found in the peak vertical unloading forces. Overall, a high forefoot stiffness elevated all peak vertical and horizontal ground reaction forces on the prosthetic limb during stance.

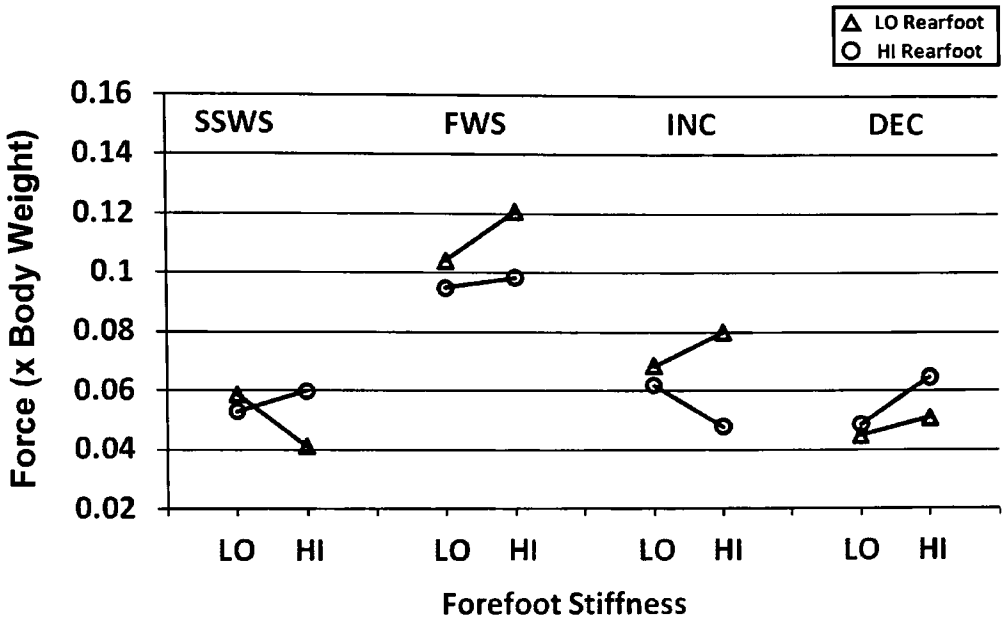

Figure 5.1.4.1. Effects of forefoot stiffness on peak horizontal ground reaction force (median) during unloading phase of stance (i.e., propulsive force).

5.1.5. Maximum plantar flexion and dorsiflexion angles for the CFAM ankle joint during stance

Figures 5.1.5.1 and 5.1.5.2 display the effects of rearfoot and forefoot stiffness on the maximum plantar flexion (PF) and dorsiflexion (DF) angles of the CFAM ankle joint during prosthetic limb stance, respectively. Results indicate that the maximum PF and DF angle were significantly influenced by the stiffness setup. The maximum PF angle observed during stance differed significantly between CFAM setups ($p<=0.033$ for self-selected and fast walking, $p<=0.077$ for incline and decline walking), with greatest PF associated with low rearfoot stiffness. On average, low rearfoot stiffness produced 2.4 degrees more maximum PF than high rearfoot stiffness during early stance. Similarly, the maximum DF angle observed during stance differed significantly between CFAM setups ($p<=0.006$ for all walking conditions), with greatest DF associated with low forefoot stiffness. On average, low forefoot stiffness produced 8.1 degrees more maximum DF than high forefoot stiffness during terminal stance. An increase in range of motion of the CFAM would potentially be beneficial for all walking conditions, as the prosthetic side is allowed to explore its full range of ankle joint motion. Furthermore, a low stiffness prosthetic foot would facilitate ease of

tibial progression over the prosthetic foot during stance. The physiological ankle joint typically produces a maximum of 7 degrees PF during the loading phase of stance and 10 degrees DF during the unloading phase of stance when walking on level ground at a self-selected speed (Perry, 1992). As seen in Figures 5.1.5.1 and 5.1.5.2, during self-selected walking speed on the level, low rearfoot stiffness produced a maximum prosthetic PF angle of 8.2 degrees which closely matched that of the physiological ankle joint, and low forefoot stiffness produced a maximum prosthetic DF angle of 20.4 degrees which exceeded that of the physiological ankle joint.

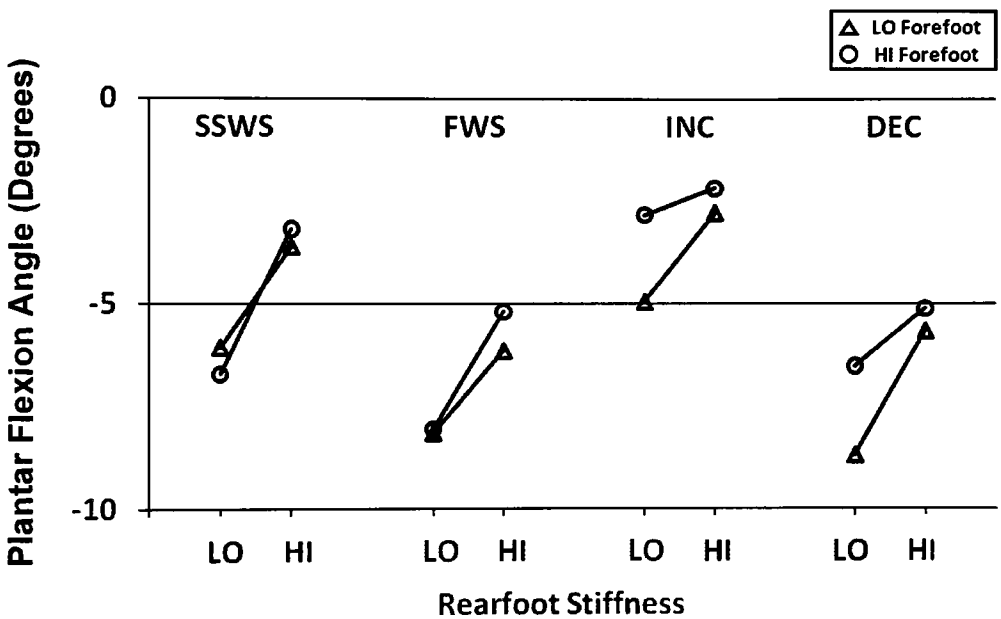

Figure 5.1.5.1. Effects of rearfoot stiffness on maximum PF angle (median) of the CFAM ankle joint during stance.

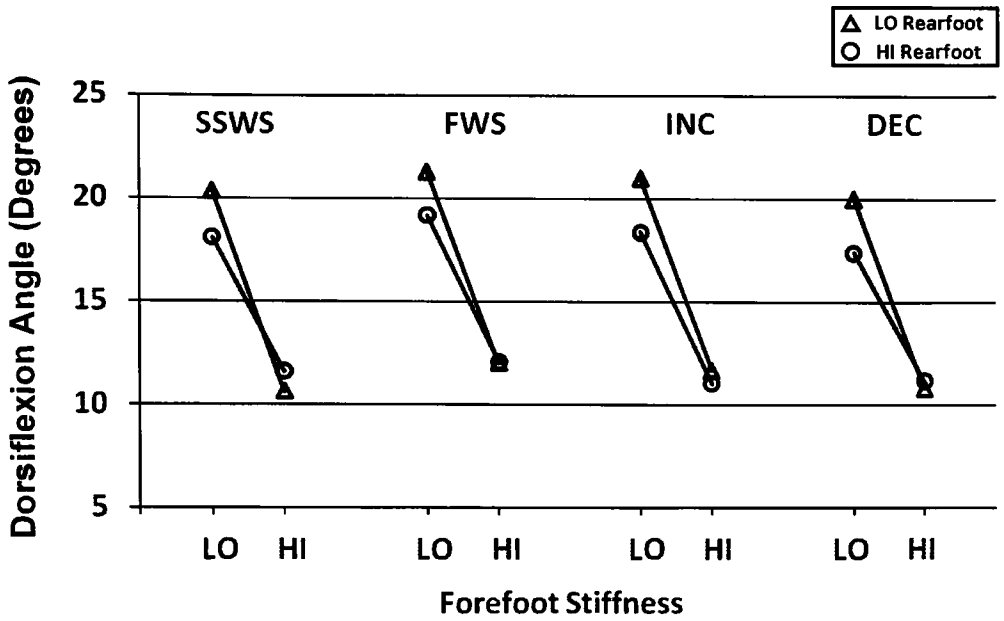

Figure 5.1.5.2. Effects of forefoot stiffness on maximum DF angle (median) of the CFAM ankle joint during stance.

5.1.6. Time to maximum plantar flexion of the CFAM ankle joint during stance

Figure 5.1.6.1 clearly shows that low rearfoot stiffness leads to a reduced time to foot flat (i.e., maximum PF) when compared with high rearfoot stiffness ($p<=0.021$ for fast and decline walking, and $p=0.054$ for incline walking), and this also corresponds to the increases seen in maximum PF. The average time to foot flat was reduced by 2.4 percent of stance. The time to foot flat has previously been considered an indicator of relative prosthetic stability in which a reduction in the time required to achieve foot flat would be beneficial as the foot can quickly obtain contact with the ground to provide a stable platform for forward progression of weight over the prosthetic limb (Perry et al., 1997). This would be more critical for decline walking, in which the ankle joint has to travel through a greater range of PF in order to achieve foot flat and, most importantly, stability is essential to avoid falling down the slope.

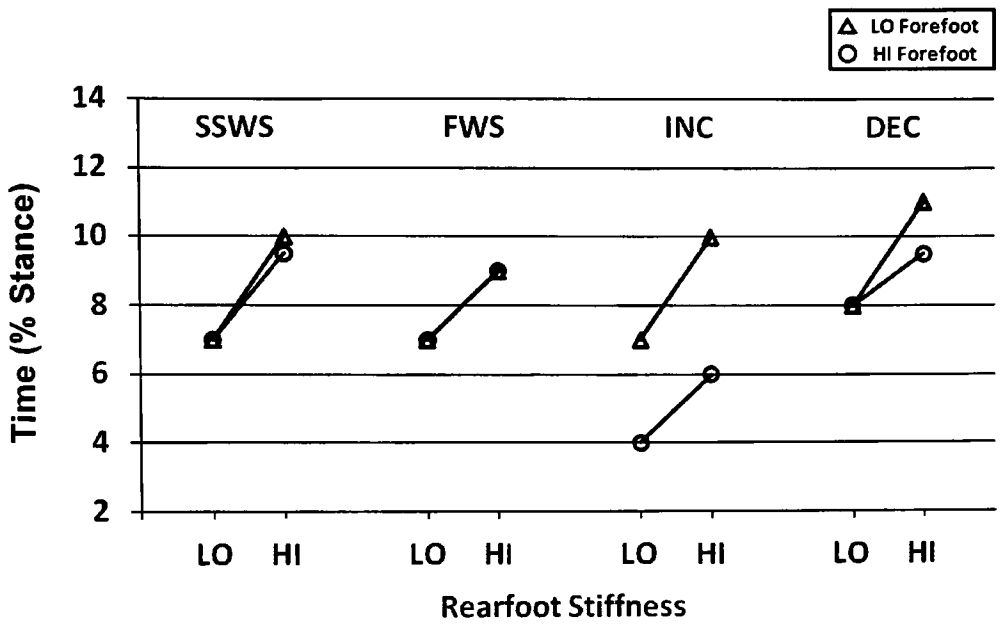

Figure 5.1.6.1. Effects of rearfoot stiffness on the time to maximum PF angle (median) of the CFAM ankle joint during stance.

5.1.7. Maximum plantar flexion and dorsiflexion angles for the sound ankle joint during stance

As seen in Figure 5.1.7.1, during self-selected and fast walking on the level, high forefoot stiffness tended to decrease the maximum PF of the sound side ankle joint, in which some subject's produced no PF during sound limb stance (seen as a positive PF value in Figure 5.1.7.1). This indicates that high forefoot stiffness is preventing normal progression over the prosthetic foot and this leads to the sound side foot being in DF at the moment of heel-strike, which is not seen in normal gait. This decrease in PF, leading to a DF position of the sound side ankle joint in early stance may be the result of a reduced stance time of the prosthetic limb. As well as allowing a greater range of motion (ROM) of the prosthetic side ankle, low forefoot stiffness also tends to increase ROM of the sound side ankle. During incline walking, the sound foot never went into PF for any setup. This is as expected considering the foot meets with the inclined surface in a dorsiflexed position. As seen in Figure 5.1.7.2, in the majority of walking conditions, high rearfoot stiffness increased the maximum DF of the sound side ankle joint. This increase in DF may be the result of prolonged stance time of the sound limb, compensating for reduced ROM of the prosthetic

ankle joint resulting from high rearfoot stiffness. However, the only statistically significant difference found in the maximum DF of the sound side ankle joint was between the HILO and LOLO setup during decline walking, in which HILO produced lower DF by approximately two degrees (p=0.034).

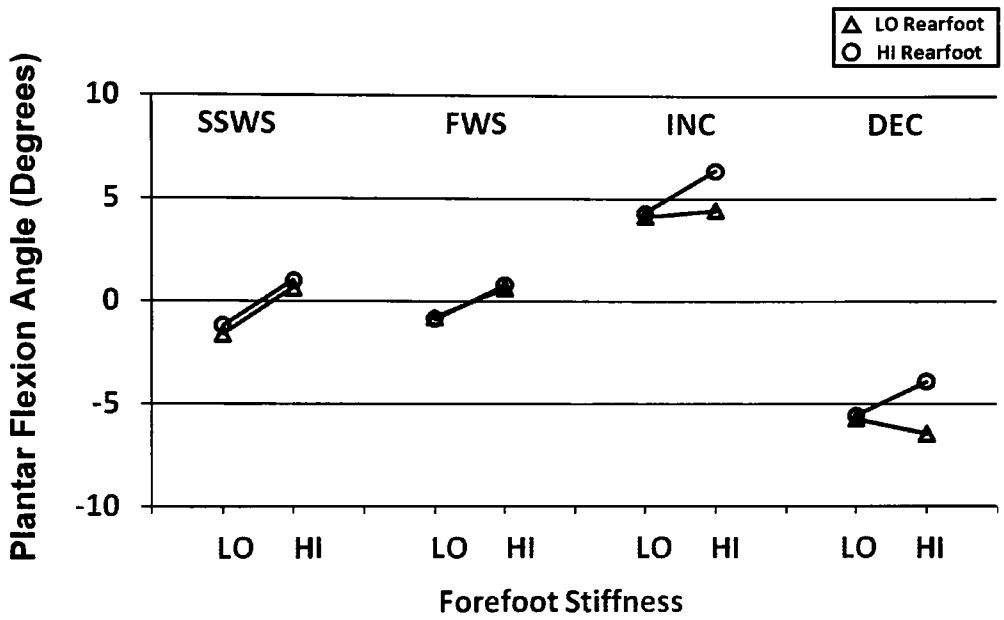

Figure 5.1.7.1. Effects of forefoot stiffness on the maximum PF angle (median) of the sound ankle joint during stance.

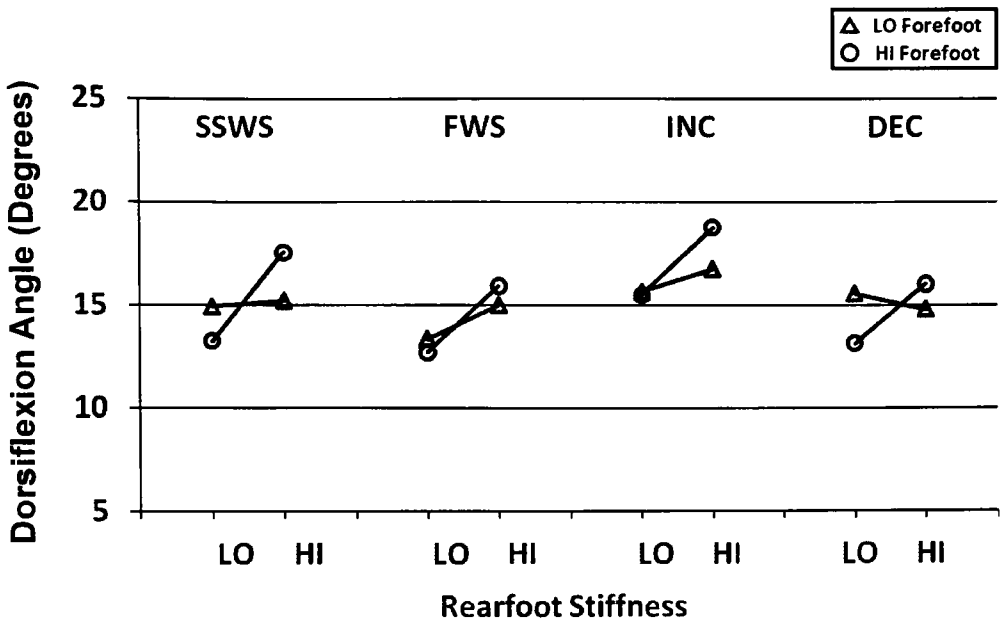

Figure 5.1.7.2. Effects of rearfoot stiffness on the maximum DF angle (median) of the sound ankle joint during stance.

5.1.8. Prosthetic side knee flexion during stance

Despite changes in the CFAM ankle joint kinematics, the prosthetic side knee joint appears to be unaffected by changes in prosthetic ankle joint stiffness during self-selected and fast walking. This agrees with previous research in which trans-tibial amputees displayed no noticeable change in maximum knee flexion during prosthetic limb stance between feet that produced significantly different maximum ankle DF (Torburn et al., 1990) or PF (Perry et al., 1997). This generally applies to the incline and decline walking condition, as well. Only the HILO CFAM setup produced noticeably greater maximum prosthetic side knee joint flexion for the incline condition by 6.7 degrees. Regarding the incline walking condition, a high forefoot stiffness would make it difficult to achieve the additional DF required in late stance. In this case, increased hip and knee flexion may help to force the prosthetic foot into DF in late stance. Overall, the prosthetic side knee flexion was significantly greater in this study than those reported by previous studies, which have reported maximum knee flexion angles during loading of between 9 and 12 degrees (Perry et al., 1997; Powers et al., 1998).

5.1.9. Sound side knee flexion during stance

However, despite little change in the prosthetic side knee joint kinematics, the sound side knee joint displayed significant changes between CFAM setups. As Figure 5.1.9.1 clearly shows, high forefoot stiffness significantly reduced the maximum flexion of the sound side knee joint during sound limb stance ($p<=0.006$ for fast, incline, and decline walking). Averaged across all walking conditions, low forefoot stiffness produced approximately 3.7 degrees more flexion of the sound side knee than high forefoot stiffness. The differences in maximum knee flexion of the sound limb are clearly due to the changes in the CFAM stiffnesses as each subject walked at the same controlled treadmill speeds for all CFAM setups.

Previous research has postulated as to why there is a change in sound side knee flexion during sound limb stance in unilateral trans-tibial amputee gait due to the use of different foot components; however, much of this discussion has been focused on sound limb loading. Several studies believe that a reduction in the DF of the prosthetic ankle joint, resulting from a stiffer forefoot, would require a greater heel rise in order to advance over the prosthetic limb (Perry and Shanfield, 1993; Powers et al., 1994; Snyder et al., 1995). This increase in heel rise would consequently produce a greater rise in the whole-body centre of mass and thus, a greater fall onto the sound limb, which would be reflected by an increase in peak vertical ground reaction force during loading. Indeed, many studies have reported a general, but not always consistent, trend for increasing peak vertical ground reaction force during the loading phase of sound limb stance with reduced prosthetic ankle DF during terminal prosthetic limb stance (Lehmann et al., 1993b; Perry and Shanfield, 1993; Powers et al., 1994). Consequently, an increase in peak sound limb loading would then require greater knee flexion in order to absorb this increased force. This is partially support in the study by Snyder et al. (1995) in which there was a trend for increased flexion of the sound knee during loading with prosthetic feet that produced greater sound limb forces during the loading phase of stance. However, this study did note that even though there was a direct relationship between maximum flexion of the sound limb and peak loading of the sound limb, such a relationship did not exist between these measures and maximum prosthetic

ankle DF. Therefore, some other factor is possibly influencing this increase in sound limb knee flexion.

The results from this study contradict these previous assumptions, in which the CFAM setups which allowed for increased DF of the prosthetic side ankle joint resulted in greater knee flexion of the sound limb. Considering that sound limb forces were not measured, an alternative route of investigation was taken. First, in order to verify if changes in forefoot stiffness, and hence changes in dorsiflexion ROM, influence vertical displacement of the whole-body centre of mass (CoM), the vertical height of the CoM of the pelvis (a representation of the whole-body CoM) was measured from time of heel-strike of the prosthetic limb (H_p) to the time of maximum height of the CoM (H_{max}) and the vertical displacement (Δ_1) was calculated as: $\Delta_1 = H_{max} - H_p$.

As displayed in Figure 5.1.9.2, there is an association between a stiffer forefoot and an increase in Δ_1. Therefore, reduced DF is producing greater vertical displacement and subsequent height of the CoM when advancing over the prosthetic limb. Furthermore, high forefoot stiffness was associated with decreased sound limb knee flexion at heel-strike during sound limb stance for the fast, incline, and decline walking condition (Figure 5.1.9.3). Therefore, it appears that in order to maintain a relatively symmetric gait, the subjects were compensating for the increase in CoM vertical displacement during prosthetic limb stance (Δ_1) by meeting the ground at sound limb heel-strike with a more extended knee. This extension then remains throughout stance, resulting in reduced sound knee flexion. Overall, symmetry is being maintained by reducing the ROM of the sound limb knee. Such a strategy would also help minimise the overall displacement of the CoM, which is important for minimising metabolic cost (Perry, 1992). Therefore, this might help explain why a stiffer forefoot is reducing the maximum flexion of the sound side knee.

However, this result does not eliminate the importance of sound limb loading in influencing sound limb knee flexion during amputee gait. An explanation which aligns with the results of this study is found in a study by Hansen et al. (2006). The authors indicated that higher sound limb loading was found with reduced roll-over shape arc lengths, which would reduce the maximum DF moment at the prosthetic ankle joint and produce a "drop-off" effect of

the prosthetic foot, in which the prosthetic limb is rapidly unloaded during terminal stance. Therefore, the amputee experiences a more abrupt loading on the sound side following unloading on the prosthetic side (Hansen et al., 2006) and this might produce increased knee flexion for loading absorption. As seen in Figure 5.1.9.4, a low stiffness forefoot reduced the amount of time spent on the forefoot of the CFAM. In addition, it also decreased the amount of time required for the centre of pressure (CoP) to progress from the longitudinal axis of the pylon (x=0, Figure 5.1.9.4) to the anterior end of the in-vivo roll-over shape. On average, low forefoot stiffness reduced this time by 1.5, 2.75, 5 and 2.5 percent of stance time for the self-selected, fast, incline and decline walking conditions, respectively. Even though the roll-over shape arc length did not noticeably reduce, this might produce kinematics that are similar to "drop-off," producing a more abrupt transfer of load onto the sound limb and consequently increase sound limb knee flexion. If this were the case, it would appear that sound side knee flexion is used as a compensatory mechanism to both aid in shock absorption and minimise whole-body CoM displacement due to the terminal stance kinematics of the prosthetic foot. However, further investigation is needed to confidently identify if sound limb loading is influenced in such a manner by changes in forefoot stiffness.

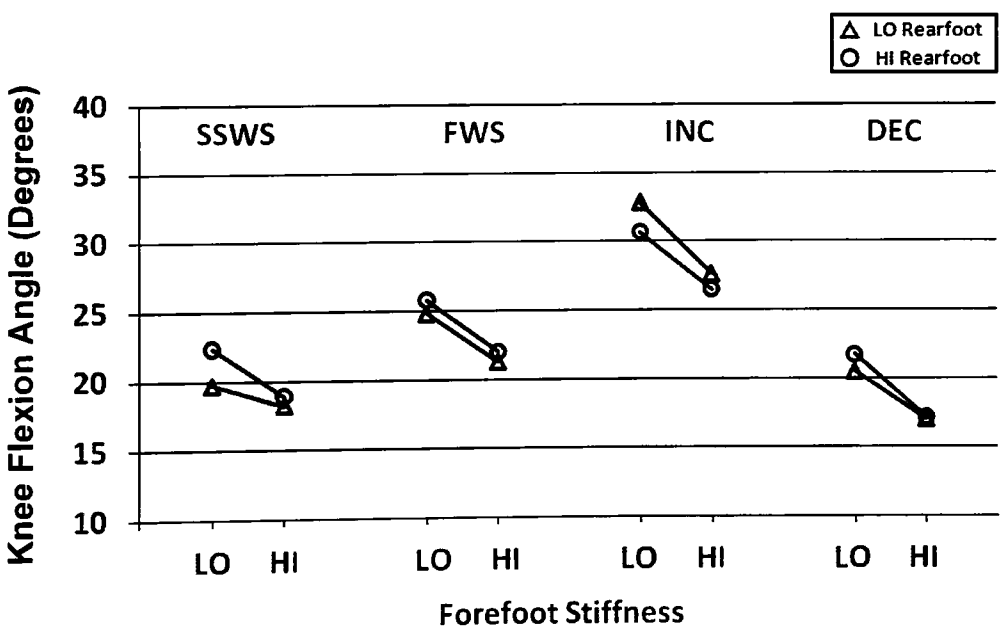

Figure 5.1.9.1. Effects of forefoot stiffness on maximum flexion angle (median) of the sound side knee joint during stance.

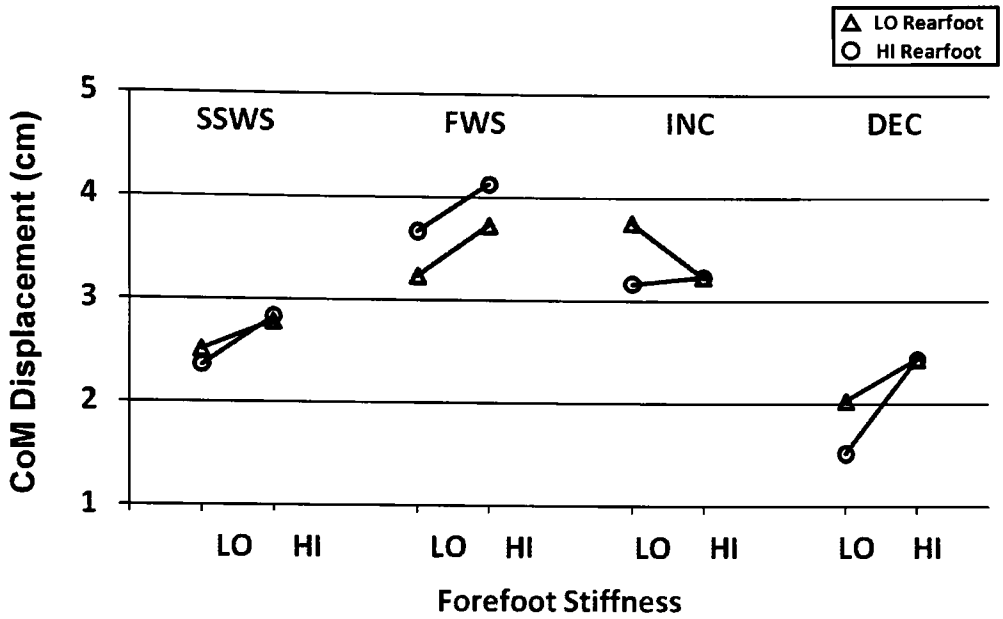

Figure 5.1.9.2. Effects of forefoot stiffness on the vertical displacement of the CoM (median) between time of heel-strike of the prosthetic limb and the time of maximum height of the CoM (Δ_1).

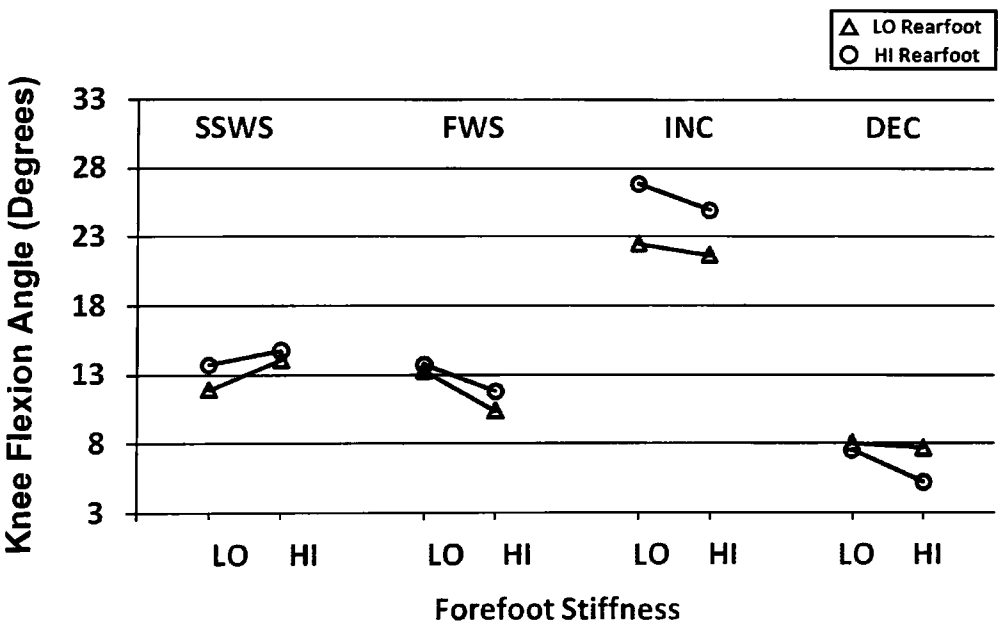

Figure 5.1.9.3. Effects of forefoot stiffness on the flexion angle (median) of the sound side knee at the time of heel-strike.

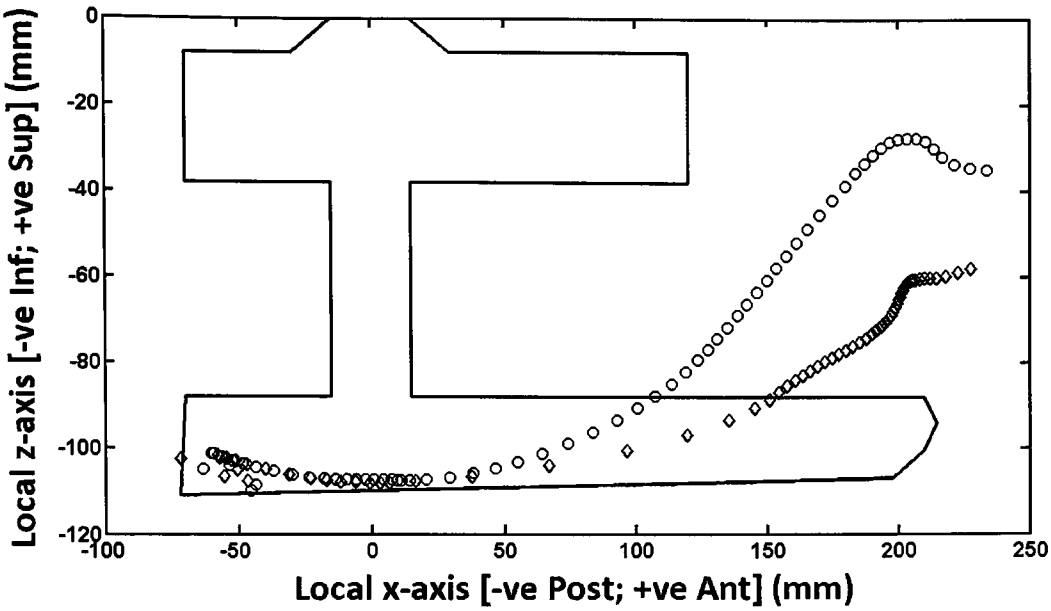

Figure 5.1.9.4. Example in-vivo roll-over shapes for HIHI (diamond markers) and LOHI (circle markers) CFAM setups. Roll-over shapes are sampled at a frequency of 100 Hz and progression of time can essentially be measured along the positive x-axis or along the roll-over curve from heel-strike to toe-off. Therefore, more markers (i.e., instantaneous position of the centre of pressure) within a shorter distance along the curve (i.e., more densely packed) represent more time being spent in that region of the CFAM during stance.

5.1.10. In-vivo roll-over shapes (based on single case study)

The appearance of the in-vivo roll-over curves across all walking conditions (see Appendices F.1.13 and F.1.14 and Figure 5.1.10.1) support the kinematic results for maximum DF and PF as low stiffness produced an increase in both compression and roll-over shape curvature. This increase in compression is less apparent in the rearfoot section of the CFAM as compared to the forefoot. Irrespective of walking condition, there does not appear to be any significant difference in the anterior-posterior length of the roll-over shape as a result of changes in ankle joint stiffness. However, high rearfoot stiffness tended to produce a small anterior change in the centre of pressure (CoP) position at heel-strike as compared to low rearfoot stiffness, possibly as a result of the amputee compensating for the limited PF of the CFAM ankle joint allowed by a high rearfoot stiffness. Figure 5.1.10.1 also includes the physiological roll-over curve, approximated as an arc with a radius of 15% of body height

(Hansen and Childress, 2004; Hansen et al., 2004) and shifted only in the z-axis such that the bottom of the arc aligns with the CFAM roll-over curves. When viewed alongside the CFAM roll-over curves, the physiological roll-over curve is seen to closely match the curve of the LOLO setup.

Overall, the in-vivo roll-over shapes appear to be very repeatable, which is a reflection of the repeatability of kinematic and kinetic measures on the prosthetic side during continuous walking. As a recognised measure of relative stability is the variability in temporal-spatial measures across consecutive steps during gait (Hausdorff, 2005), the repeatability of the roll-over shape could act as an indirect measure of gait stability; any significant variability in the kinetic and kinematic profiles, both in timing and magnitude, would potentially produce different in-vivo roll-over shapes. Consequently, repeatable roll-over shapes in both curvature and length would correspond to consistency in loading and ROM, respectively, of the prosthetic limb during stance. This concept is further explored in the section 6.3.1.

Furthermore, in order to stress the differences between the *AIPP* and in-vivo roll-over shapes, Figure 5.1.10.2 displays ten *AIPP* roll-over curves which were measured with the method described in Figure 5.1.10.3. This method was used as it produces results that are entirely equivalent to those obtained from the in-vivo method (i.e., continuous rolling and high sampling frequency); however, the prosthesis is subject to controlled quasi-static loading at a constant vertical force whilst rolling through a simulated stance phase of gait. This reinforces the fact that the in-vivo roll-over curve is a combination of *AIPP* and subject-specific gait factors. For example, compared to the in-vivo roll-over curves displayed in Figure 5.1.10.1, we see that varying magnitude in the ground reaction force during terminal stance has produced a sudden relief in compression of the forefoot, warping the smooth shape displayed in Figure 5.1.10.2. Additionally, it is important to note that additional warping results from varying compression of the treadmill belt during walking which is meant to act as a suspension system. Considering that the markers have been placed on the static frame, this varying level of compression will either under or over estimate the distance from the load-cell geometric centre to the surface of the treadmill belt.

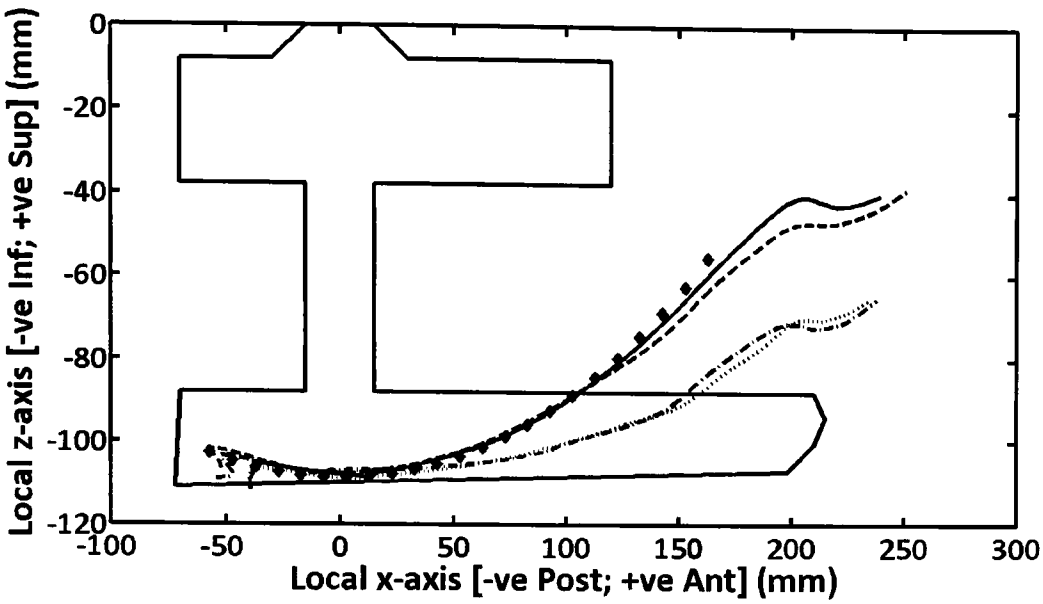

Figure 5.1.10.1. Example in-vivo roll-over curves for one representative subject (#2) during the self-selected walking on a level surface condition; solid line=LOLO, dash line=LOHI, dotted line=HILO, dash-dot line=HIHI, diamonds=approximated physiological roll-over curve.

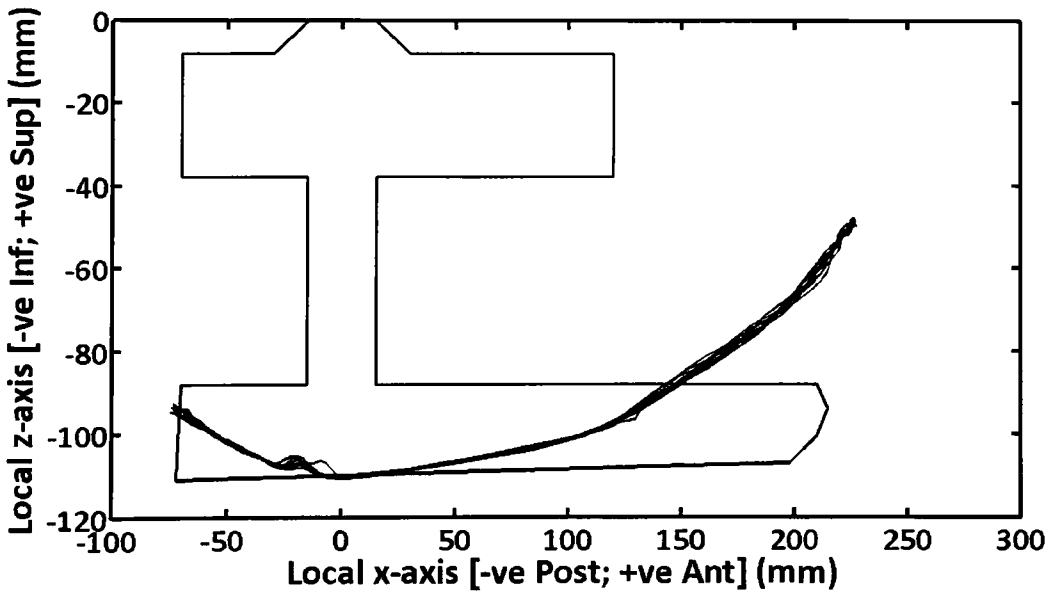

Figure 5.1.10.2. Ten CFAM roll-over curves for setup LOLO when measured on level ground with quasi-static loading of 400 N and independent of the amputee.

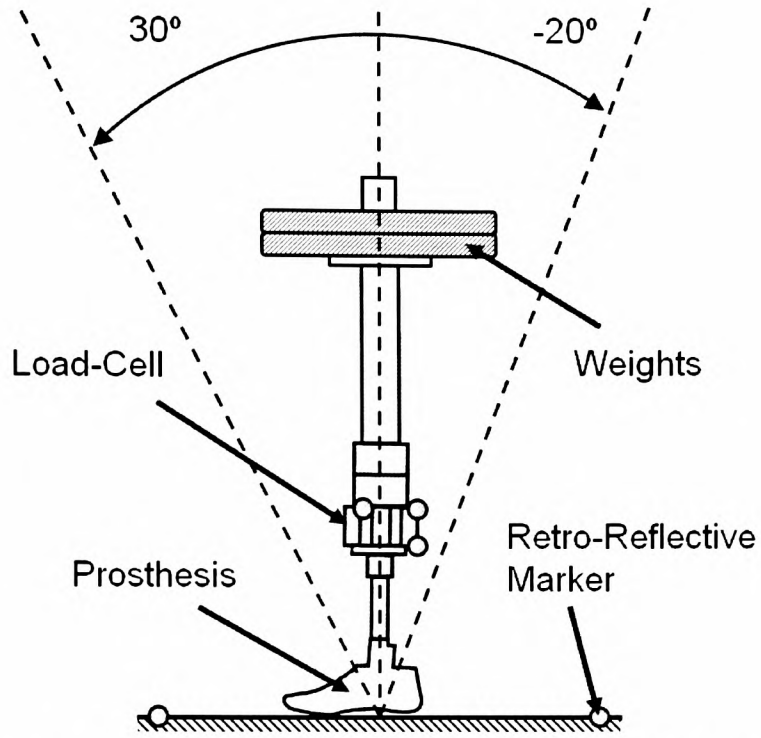

Figure 5.1.10.3. Schematic illustration of the apparatus used to mimic the stance phase of gait in order to measure simulated in-vivo roll-over curve. Weights are placed on top and foot is rolled from heel-strike (-20°) to toe-off (30°).

5.2. Effects of *AIPP* variation on temporal-spatial gait parameters

Previous research has shown that correlations exist between the variability of temporal-spatial gait parameters and instability and risk of falling in a number of populations (Hausdorff, 2005). An example of this relationship is that an increase in the variability of stride time and swing time was significantly correlated retrospectively ($p<0.0001$ for both measures) and prospectively ($p<0.04$ and $p<0.02$, respectively) with older adults who suffered a fall (Hausdorff et al., 1997; Hausdorff et al., 2001). Furthermore, there was a direct correlation between gait variability and time in which an individual suffered a fall (increased variability predicted that a fall was likely to occur sooner) (Hausdorff et al., 2001). More relevant to this research, the standard deviation/mean, known as the coefficient of variation (CV), of prosthetic limb swing time has previously proven to be a distinguishing factor between trans-tibial amputee fallers and non-fallers (fallers displayed increased CV)

(Vanicek et al., 2009). Gait stability is a critical component of amputee mobility, as previous research has reported that lower limb amputees are at increased risk of falling as compared to age-matched healthy controls and have reduced confidence in their balance (Miller et al., 2001a; Miller et al., 2001b). Of 435 lower limb amputees interviewed, 52.4% fell within one year, 49.2% expressed a fear of falling, and 76.2% of those with a fear of falling 'avoided activities' due to this fear (Miller et al., 2001a; Miller et al., 2001b). This increased risk and fear of falling contributes to restricted mobility, activity, and participation. Furthermore, in order to fully explore stability and fall risk in amputee populations, methods used previously to do so in normal populations must now include elements of prosthetic mechanical behaviour, as it is reasonable to assume that amputee gait is affected by *AIPP*.

5.2.1. Temporal gait symmetry

Figure 5.2.1.1 displays the effects of forefoot stiffness on temporal gait symmetry. In the majority of walking conditions, low forefoot stiffness tended to improve symmetry (i.e., a symmetry ratio closer to one), which might be explained by the easier progression through stance as a result of a lower resistance to DF. This relationship was significant for self-selected walking condition between the LOHI and HILO and LOLO and HILO setup ($p=0.034$) and for the fast walking condition between the LOLO and HIHI and LOHI and HIHI setup ($p=0.087$).This agrees with previous research that has reported a significant increase ($p<0.001$) in the symmetry of prosthetic and sound limb stance time in trans-tibial amputees when using a prosthetic foot with greater dorsiflexion ROM (a multi-axial foot) as compared to a foot with less dorsiflexion ROM (SACH foot) (Marinakis, 2004). Apart from the self-selected walking condition which had the opposite trend, low rearfoot stiffness also tended to improve temporal gait symmetry (Figure 5.2.1.2).

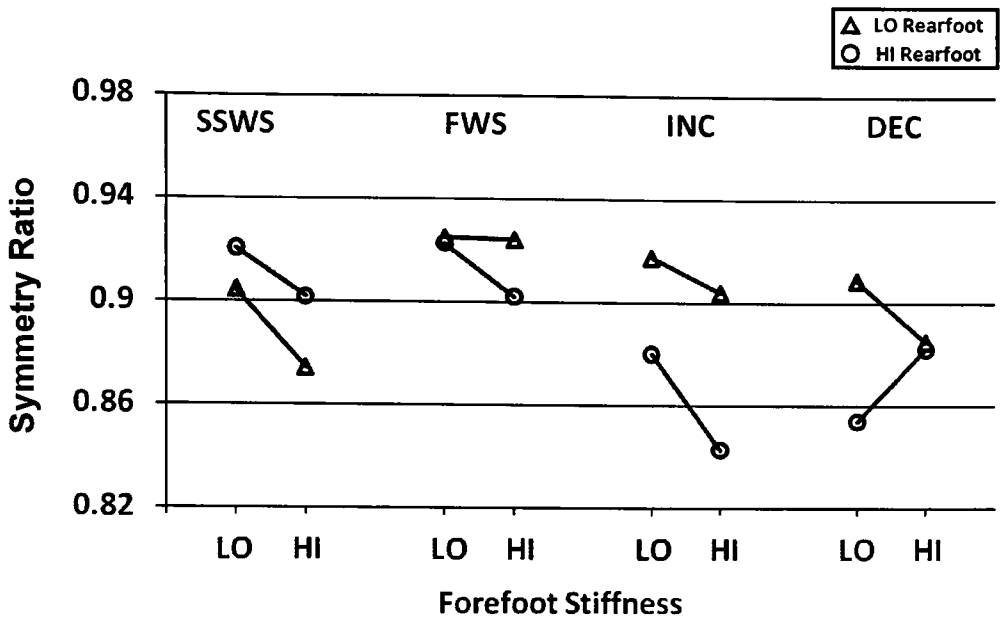

Figure 5.2.1.1. Effects of forefoot stiffness on the temporal symmetry of gait (median). Values closer to one indicate greater symmetry.

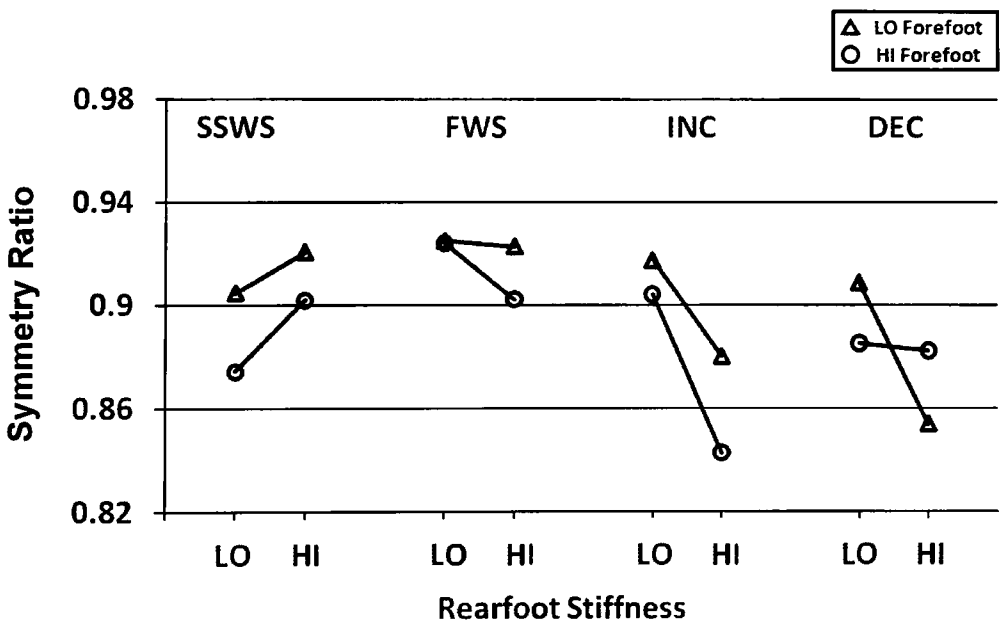

Figure 5.2.1.2. Effects of rearfoot stiffness on the temporal symmetry of gait (median). Values closer to one indicate greater symmetry.

5.2.2. CV of step time

Figure 5.2.2.1 displays the effects of rearfoot stiffness on the CV of step time. Generally, low rearfoot stiffness was associated with reduced CV. This effect was significant for both the fast ($p=0.013$) and incline walking conditions ($p=0.068$). In accordance with the research which has identified a correlation between an increase in step time CV and an increase in fall risk, it would appear that low rearfoot stiffness could reduce the risk of falls (Hausdorff et al., 1997; Hausdorff et al., 2001). However, this relationship between step time CV and amputee gait stability would have to be validated with future clinical studies before claiming this as a predictive factor of fall risk in amputee populations. It has been suggested in previous research that reducing the time to prosthetic foot flat would improve amputee gait stability by providing an early base of support for transferring weight onto the prosthetic limb during stance (Perry et al., 1997). The results from this study would support that, as low rearfoot stiffness as associated with a reduction in step time CV and also a decrease in time to foot flat of the prosthesis by an average of 2.4 percent of stance across all walking conditions. As seen in Figure 5.2.2.2, low forefoot stiffness did tend to reduce the step time CV, but this trend is certainly not as clear as seen with rearfoot stiffness. In fact, there tends to be a modest decrease with high forefoot stiffness in decline walking, which might be explained by the need for reduced DF motion during decline walking in order to restrict rapid forward motion and provide a stable base of support.

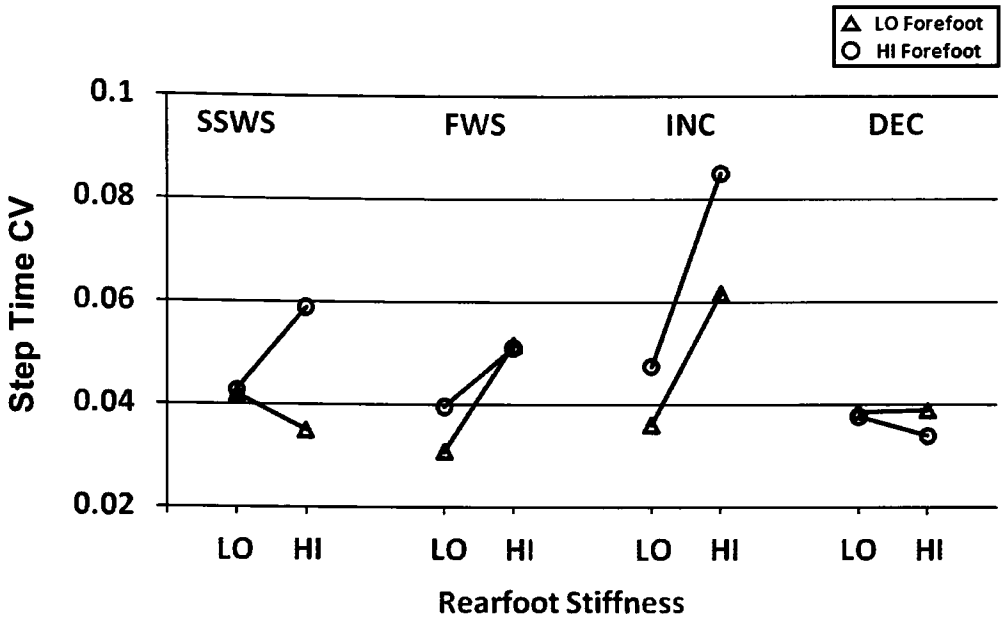

Figure 5.2.2.1. Effects of rearfoot stiffness on the CV of step time (median).

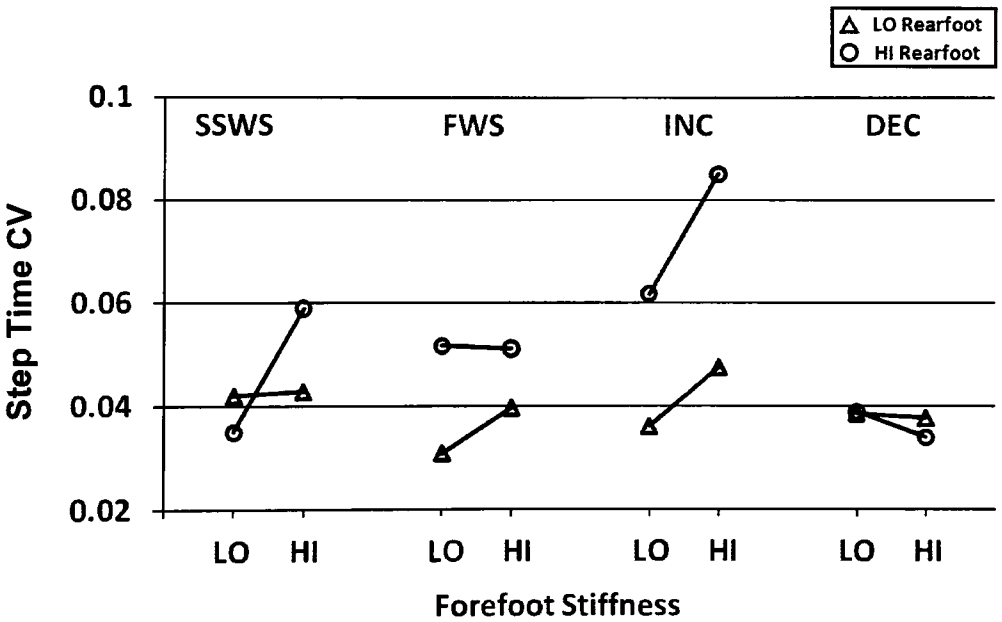

Figure 5.2.2.2. Effects of forefoot stiffness on the CV of step time (median).

5.2.3. CV of swing time

Low forefoot stiffness tended to reduce prosthetic limb swing time CV in most walking conditions (Figure 5.2.3.1). This relationship was significant for the self-selected walking

condition, in which the CFAM setup of HILO displayed an increase in prosthetic limb swing time CV as compared to LOHI (p=0.099). However, contrary to the changes seen in step time CV, a low rearfoot stiffness tended to increase the CV of the prosthetic limb swing time (Figure 5.2.3.2). The effects of forefoot stiffness on the CV of the sound limb swing time were similar to those for the prosthetic limb (Figure 5.2.3.3.), in which low forefoot stiffness was associated with a reduction in CV. In accordance with the kinematic results, this would indicate that the forefoot stiffness of the prosthesis influenced the temporal variability of both limbs. Vanicek et al. (2009), reported that trans-tibial amputees who had suffered a fall within the past year displayed a significant increase ($p<0.05$) in the CV of prosthetic limb swing time when compared with non-fallers. Accordingly, the results from this study would indicate that a low forefoot stiffness would generally improve walking stability of trans-tibial amputees over the four walking conditions tested. Considering that the low forefoot stiffness setups were associated with an increase of maximum DF during terminal stance (average increase of 8.1 degrees), this might indicate that greater forefoot flexibility leads to easier progression through stance as a result of a lower resistance to DF and, indirectly, to an improved start to the swing phase.

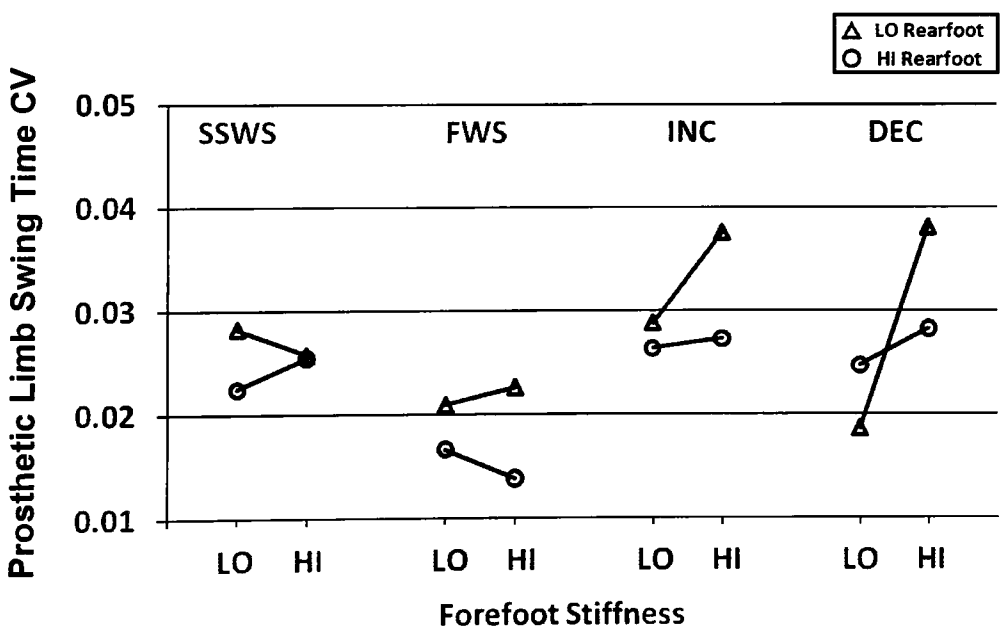

Figure 5.2.3.1. Effects of forefoot stiffness on the CV of prosthetic limb swing time (median).

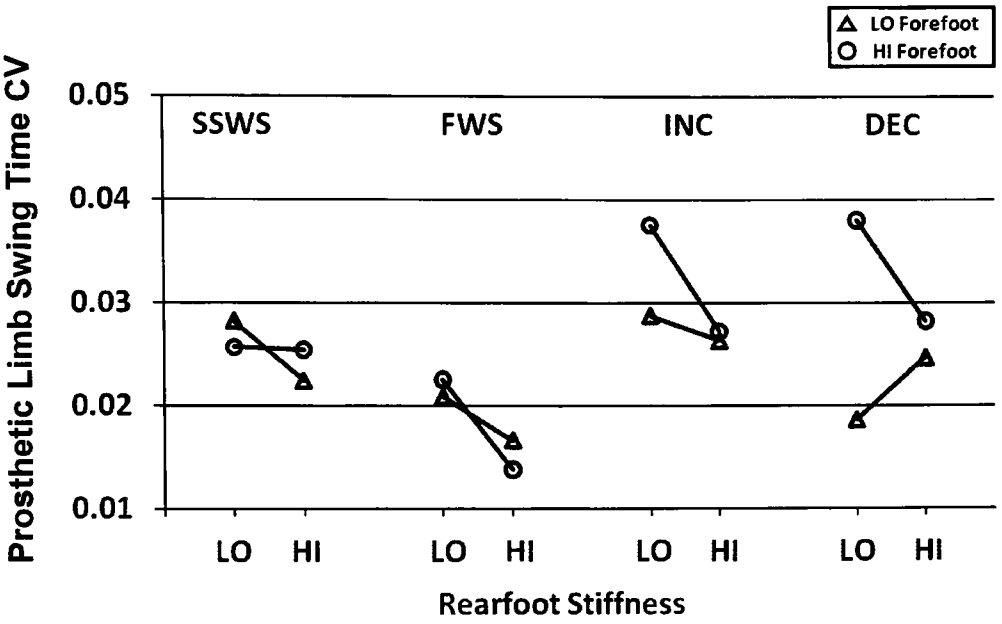

Figure 5.2.3.2. Effects of rearfoot stiffness on the CV of prosthetic limb swing time (median).

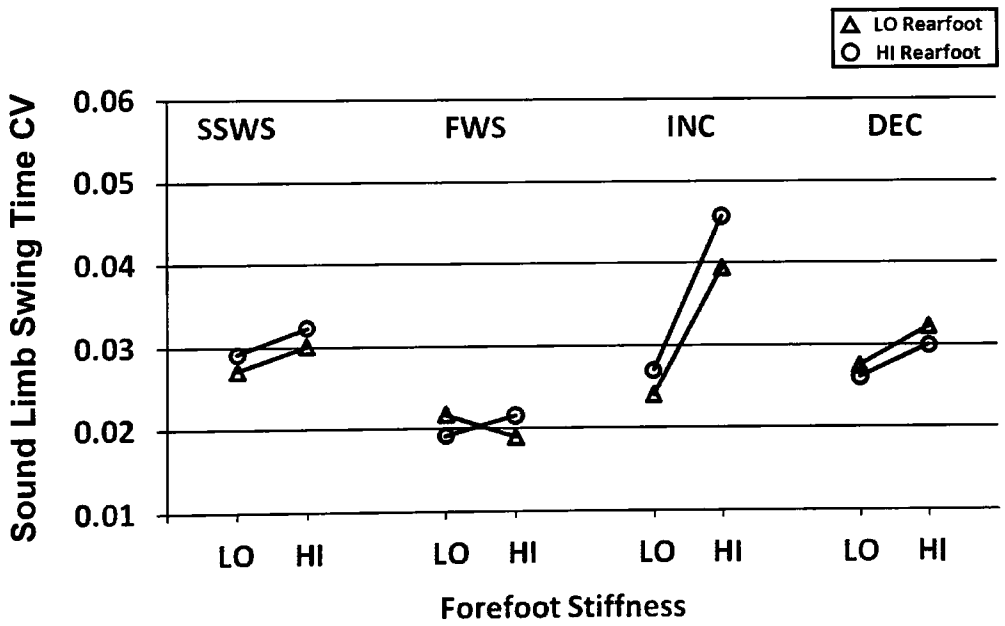

Figure 5.2.3.3. Effects of forefoot stiffness on the CV of sound limb swing time (median).

5.2.4. Relevance to clinical studies on relative stability

By observing the effects of rearfoot and forefoot stiffness on step time CV and prosthetic limb swing time CV, there appears to be a disconnect between these two temporal

measures of gait variability. As increases in both of these temporal gait parameters have been proven to be predictors of falls in older individuals (step time CV - (Hausdorff et al., 1997; Hausdorff et al., 2001) and trans-tibial amputees (prosthetic limb swing time CV - (Vanicek et al., 2009)), one might assume that they would be similarly affected by changes in rearfoot and forefoot stiffness. However, low rearfoot stiffness was seen to both decrease step time CV and increase prosthetic limb swing time CV. Furthermore, low forefoot stiffness tended to decrease prosthetic limb swing time CV for all walking conditions, but did not have a consistent effect on step time CV. Therefore, the results for step time CV and prosthetic limb swing time CV seem to indicate contradictory trends in gait stability. This might also be the reason why step time CV was correlated with the symmetry ratio ($p<0.001$, $\rho=-0.686$), whereas prosthetic limb swing time CV was not ($p>0.831$, $\rho<-0.025$).

The disconnect between these two parameters has been commented on in previous research. For example, the study by Donker and Beek (2002) reported that the symmetry between prosthetic and sound side step time improved with increasing walking speed in trans-femoral amputees whilst the symmetry between prosthetic and sound side swing time showed no difference. Furthermore, where a significant difference ($p<0.05$) was found in prosthetic limb swing time CV between trans-tibial amputee fallers and non-fallers, the difference in step frequency (steps per minute) was not significant (Vanicek et al., 2009).

Considering that variability in temporal measures of gait are used as indicators of relative gait stability and fall risk (Hausdorff, 2005), it is critical to choose the most valid measure in order to ensure that relative stability of amputee gait is being accurately assessed. Even though an important finding was made in the clinical study by Vanicek et al. (2009) (i.e., significant difference in prosthetic limb swing time CV), there were two important limitations: 1) the limited subject numbers, in which only 11 trans-tibial amputees (6 fallers and 5 non-fallers) participated, and 2) the subjects were not matched by age or cause of amputation. These limitations certainly warrant further investigation in order to confidently identify those factors which are predictive of falls (both retrospectively and prospectively) in amputee populations. Unfortunately, due to the limited information available on amputee gait stability and the contradictory findings of the effects of *AIPP* in this study, it is still

unclear as to whether step time CV and/or prosthetic limb swing time CV are appropriate measures of relative stability in trans-tibial amputee gait.

5.3. Effects of *AIPP* variation on physiological measures

5.3.1. Metabolic rate and cost of transport

Within each walking condition, there appears to be noticeable differences in metabolic cost between each CFAM setup. Figures 5.3.1.1 and 5.3.1.2 display the effects on metabolic rate (ml O_2/kg/min) of forefoot and rearfoot stiffness, respectively. The metabolic Cost of Transport (CoT; ml O_2/kg/m) displayed similar, albeit smaller, differences between CFAM setups and between walking conditions, however, they are more clearly observed in metabolic rate as this measure is not normalised by subject walking speed. Trends are not clear across all walking conditions; however, low forefoot stiffness generally reduced metabolic rate and CoT. Furthermore, differences in metabolic rate and CoT were only statistically significant for the self-selected walking condition, where metabolic rate and CoT were higher for the CFAM setup of HIHI compared to LOHI ($p<0.043$) and for the decline walking condition where metabolic rate and CoT were higher for the CFAM setup of LOHI compared to LOLO and HILO for ($p<0.044$). Figures 5.3.1.1 and 5.3.1.2 indicate that forefoot stiffness had a clear effect on metabolic rate during self-selected, fast, and incline walking, and rearfoot stiffness had the clearest effect on metabolic rate during incline walking. During level and incline walking, a low forefoot stiffness would facilitate roll-over at terminal stance with an increase in dorsiflexion ROM. A high forefoot stiffness would present a particular challenge for incline walking, during late stance, as the amputee would have to overcome increased DF resistance to produce the necessary progression of the pylon over the prosthetic foot and this is reflected in the large difference in metabolic rate (Figure 5.3.1.1). Compensatory strategies associated with this action would potentially increase metabolic energy expenditure.

The differences in metabolic rate between CFAM setups were more pronounced for the fast and incline walking condition, displaying a range of 2.59 and 3.94 ml O_2/kg/min, respectively, than for the self-selected and decline walking condition, displaying a range of 1.43 and 1.19 ml O_2/kg/min, respectively. These two conditions with greater range also required the greatest metabolic rate. This would indicate that differences in CFAM stiffness can have a larger impact on metabolic rate during more demanding walking conditions (i.e., conditions that require more metabolic energy per minute). This agrees with previous research in which differences in metabolic rate and CoT between different prosthetic feet were more pronounced at higher walking speeds (e.g., 67 m/min (Hsu et al., 2006; Nielsen et al., 1989) and 68 m/min (Casillas et al., 1995)), which were equivalent to the fast walking speeds achieved in this study (average of 68.1 m/min).

Overall, these results highlight the difficulty in attempting to completely separate effects of rearfoot and forefoot stiffness on metabolic rate and CoT. There appears to be certain CFAM setups which perform better with regards to metabolic energy expenditure for certain walking conditions. For all walking conditions, these measures are within acceptable limits and all five subjects were capable of accommodating to each CFAM setup despite the limited time provided during the experimental protocol in order to do so (maximum of 20 minutes).

There are several studies in which comparison between their results and those of this study are possible (Barth et al., 1992; Lehmann et al., 1993b; Torburn et al., 1990). Not coincidentally, one of these studies (Lehmann et al., 1993b) is that from which mechanical characterisation data was taken to determine the levels of high and low rearfoot and forefoot stiffness of the CFAM. In Lehmann et al. (1993b), use of the SACH foot resulted in a slight increase of metabolic CoT compared to use of the Seattle Foot and Flex-Foot, and this difference was not found to be statistically significant at $p=0.05$. By translating the trade names into definitions of high and low forefoot stiffness for each prosthetic foot, these results indicate than an increase in metabolic CoT resulted from using a HILO setup (i.e., SACH foot) as compared to a LOHI (i.e., combination of Flex-Foot forefoot stiffness and Seattle Foot rearfoot stiffness). These results agree with the trends found in metabolic rate for this study at a comparable walking speed (i.e., fast walking). However, when normalising walking speed, no noticeable difference in metabolic CoT were observed. The authors in the

study by Lehmann et al. (1993b) believe that a possible reason for this minimal difference in metabolic CoT is that ESAR feet do not return stored energy at an appropriate time during stance in order to aid with push-off.

Even though the *AIPP* of the prostheses used during testing was not measured for the remaining two studies (Barth et al., 1992; Torburn et al., 1990), their results may be used for indirect comparison as the prosthetic ankle ROM was reported. For the CFAM, maximum PF and DF were associated with low rearfoot and forefoot stiffness, respectively. Accordingly, even though many of the commercial feet tested do not possess an articulated ankle joint, late stance ankle DF may provide some indication of forefoot stiffness. This relationship would be less clear for maximum PF during the loading phase of stance and rearfoot stiffness considering that most prosthetic feet will experience some level of linear compression which may not directly contribute to ankle PF. In the study by Barth et al. (1992), while one prosthetic foot displayed significantly greater ($p<0.05$) maximum DF of the prosthetic ankle compared to the sound ankle and another displayed significantly less, there were minimal differences in metabolic rate. On the contrary, a study by Torburn et al. (1990), found the Flex-Foot to provide a significant increase in maximum prosthetic ankle DF in late stance compared to four other feet ($p=0.003$) and this foot also produced one of the lowest values of metabolic rate, although not statistically significant at $p<0.05$. This supports the findings in this study, in which a reduction in metabolic rate was associated with an increase in maximum prosthetic ankle DF in late stance as provided by low forefoot stiffness.

Any differences observed in metabolic rate and CoT in this study are solely due to the changes in prosthetic foot-ankle stiffness, as each subject walked at the same speed for each CFAM setup. Previous human performance studies have shown that if walking speed is not controlled, trans-tibial amputees will walk at different self-selected speeds during the same walking condition corresponding to different prosthetic feet (Casillas et al., 1995; Lehmann et al., 1993a; Nielsen et al., 1989; Torburn et al., 1990). Thus, it is possible that if given the opportunity, subjects would choose an alternative walking speed for each CFAM setup within the same walking condition and this would consequently affect their metabolic cost. It is possible that energy expenditure was partly influenced by forcing subjects to walk at a speed which was not necessarily comfortable for the particular CFAM setup being tested.

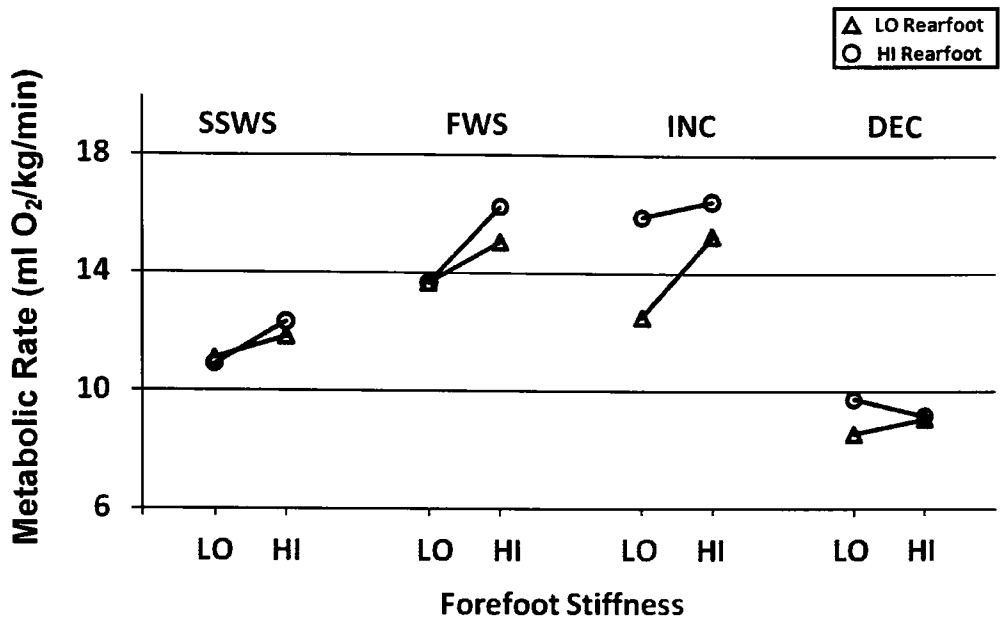

Figure 5.3.1.1. Effects of forefoot stiffness on metabolic rate (median).

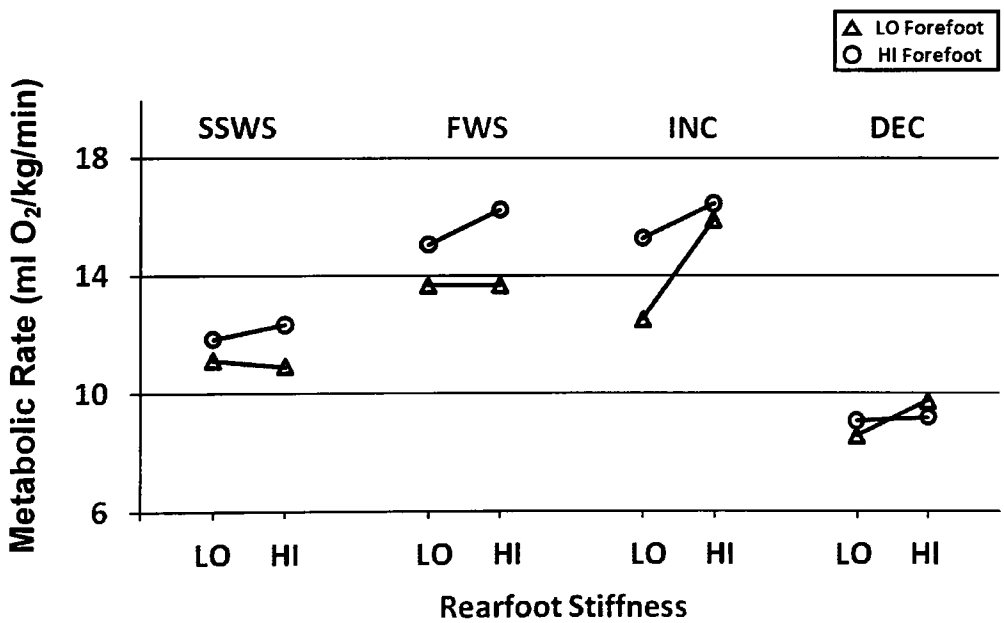

Figure 5.3.1.2. Effects of rearfoot stiffness on metabolic rate (median).

5.3.2. Physiological Cost Index

The Physiological Cost Index (PCI) has been shown to be correlated with metabolic energy expenditure in both normal (MacGregor, 1981; Nene, 1993) and amputee (Chin et al., 1999; Engsberg et al., 1994) populations, and has been used to assess changes in energy expenditure of lower limb amputees during use of different prosthetic components (Hachisuka et al., 1999; Jepson et al., 2008) and monitor progress of rehabilitation interventions (Rau et al., 2007). The PCI is calculated through the following equation:

$$PCI = \frac{HR_A - HR_R}{S}, \tag{5.1}$$

where HR_A and HR_R are the steady-state active and resting heart rates of the subject, respectively, and S is the walking speed (MacGregor, 1981). As the only measures required to calculate the PCI are steady-state heart rate and walking speed, this provides an alternative means to calculating metabolic CoT without the use of the cumbersome and expensive methods involved in gas analysis. Even though PCI has been used in previous investigations, the regression equations for the amputee population which participated in this study (i.e., adult traumatic trans-tibial amputees) have not been previously reported. Therefore, PCI has been investigated in this study and subsequently reported on in order to overcome some of the limitations of assessing metabolic energy expenditure in future studies where access to a gas analyser is not feasible (e.g., clinical trials). For this study, the PCI was significantly correlated with metabolic CoT for all walking conditions independently and when all conditions are grouped. Figure 5.3.2.1 displays the metabolic CoT versus PCI as separated by walking condition and the corresponding regression equations are listed in Table 5.3.2.1 together with the statistical results for the regression analysis (coefficient of determination, R^2, test statistic, F, and statistical significance, p) and correlation analysis (Spearman's correlation coefficient, ρ, and statistical significance, p). Figure 5.3.2.1 also clearly displays the changes in metabolic CoT between walking condition, where the subjects were most efficient during decline walking, followed by fast walking, self-selected walking, and incline walking.

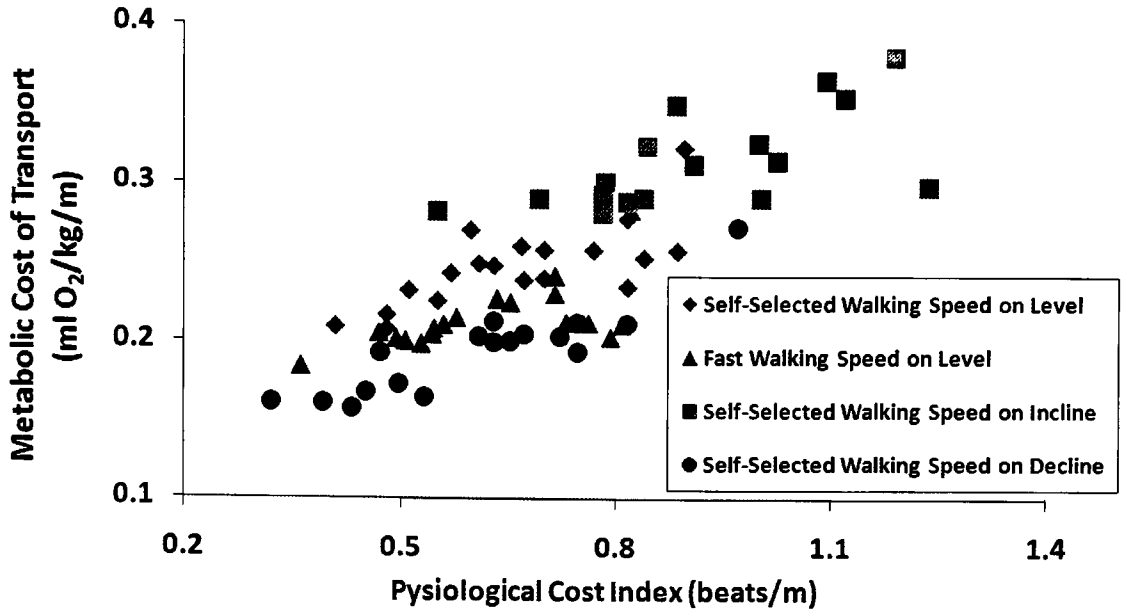

Figure 5.3.2.1. Metabolic CoT versus PCI as separated by walking condition.

Table 5.3.2.1. Correlation analysis between metabolic CoT (ml O_2/kg/m) and PCI (beats/min) as separated by walking condition and grouped over all walking conditions. Conditions are abbreviated as: SSWS (self-selected walking speed on level), FWS (fast walking speed on level), INC (self-selected walking speed on incline), and DEC (self-selected walking speed on decline).

		Regression			Correlation	
Walking Condition	**Regression Equation**	**R^2**	**p**	**F**	**ρ**	**p**
SSWS	*MCoT=0.134×PCI+0.159*	0.536	<0.001	19.603	0.695	0.001
FWS	*MCoT=0.101×PCI+0.153*	0.386	0.006	10.046	0.670	0.002
INC	*MCoT=0.129×PCI+0.201*	0.406	0.006	10.251	0.720	0.001
DEC	*MCoT=0.180×PCI+0.090*	0.801	<0.001	60.483	0.846	<0.001
All Conditions Grouped	*MCoT=0.228×PCI+0.088*	0.649	<0.001	127.609	0.772	<0.001

5.4. Effects of *AIPP* variation on subjective measures

As is seen in Figure 5.4.1, it is clear that low rearfoot stiffness is particularly important for improved comfort. Across all walking conditions, low rearfoot stiffness was associated with an increase in perceived level of comfort. More specifically, the LOHI setup was rated as the least comfortable and the LOLO the most comfortable. Additionally, the difference in perceived level of comfort becomes more pronounced for the incline and decline walking conditions and this is partly due to the fact that subjects reported higher levels of discomfort for these conditions overall, or in other words, a greater range of VAS values. Similar to perceived levels of comfort, low rearfoot stiffness was particularly important for an improvement in perceived level of exertion (Figure 5.4.2). Overall, subjects rated CFAM setups with low rearfoot stiffness as requiring less exertion across all walking conditions, and although not as clear, this trend applied to low forefoot stiffness as well (Figure 5.4.3). In the majority of walking conditions, HIHI was rated as requiring the most exertion and this is most likely attributed to the increased resistance to DF and PF, and hence limited ROM, of the prosthetic ankle joint produced by high rearfoot and forefoot stiffness. For self-selected and fast walking on the level, low forefoot stiffness was rated as the most stable (Figure 5.4.4). However, the trends for the incline and decline walking condition are not as clear. For the incline condition, the LOHI setup was rated as the least stable with the remaining three setups rated approximately the same; although, the reasons for this are not entirely clear. Additionally, the setup of HILO was rated as the least stable for the decline walking condition.

It is possible that the perceived level of stability in this study is also influenced by a subject's general balance confidence irrespective of the tested walking conditions. In this study, certain subjects consistently reported higher or lower levels of perceived stability compared to others and this was statistically significant ($p<0.001$) with differences between three groups of subjects (high, medium, and low perceived level of stability). A study by Hausdorff et al. (2001), found that stride time variability was associated with "confidence in one's ability to perform activities without falling." Therefore, it would be interesting to consider each subject's general level of confidence regarding balance and stability during gait and

how this affects their values of CV. Previous work has shown that lower limb amputees generally have reduced confidence in their balance (Miller et al., 2001a; Miller et al., 2001b) contributing to their restricted mobility, activity and participation. Consequently, the mobility of amputee patients might benefit from rehabilitation programmes which not only focus on improving the physical factors related to balance (e.g., strength and motor control), but also psychological factors as well (e.g., mental health and confidence).

Observation of Figures 5.4.1 and 5.4.2 indicate that rearfoot stiffness is a consistent factor in perceived levels of comfort and exertion, and more importantly, these differences appear more pronounced in the sloped walking conditions (i.e., incline and decline). This agrees with previous results that differences in perceived level of walking difficulty for trans-tibial amputees were more pronounced for uphill walking when compared to less challenging environments (Alaranta et al., 1994; Macfarlane et al., 1991b).

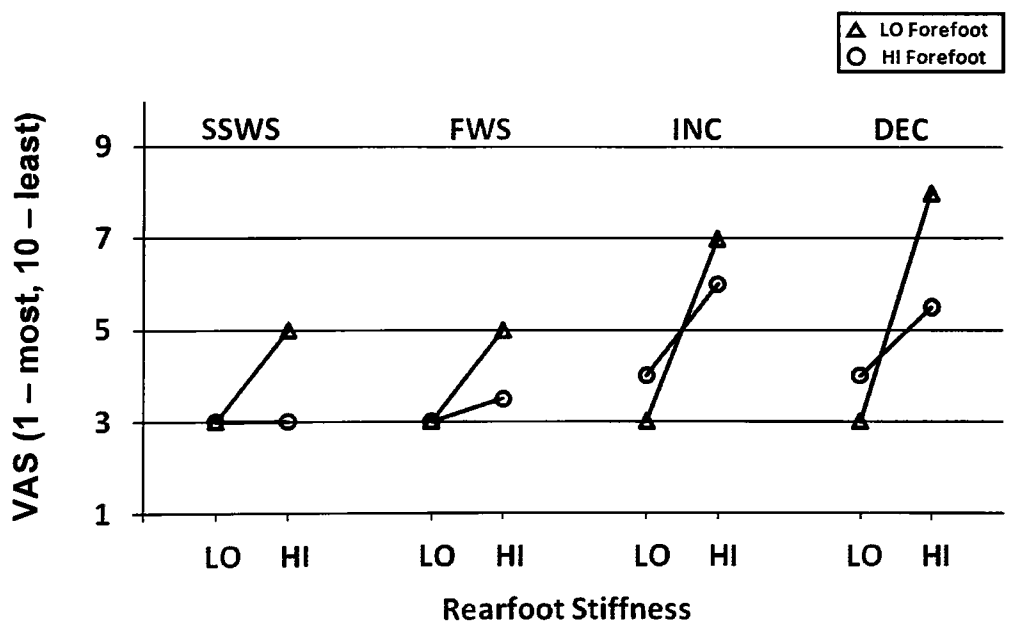

Figure 5.4.1. Effects of rearfoot stiffness on the perceived level of comfort (median) based on the Visual Analogue Scale (VAS) results from 1 (most comfortable) to 10 (least comfortable).

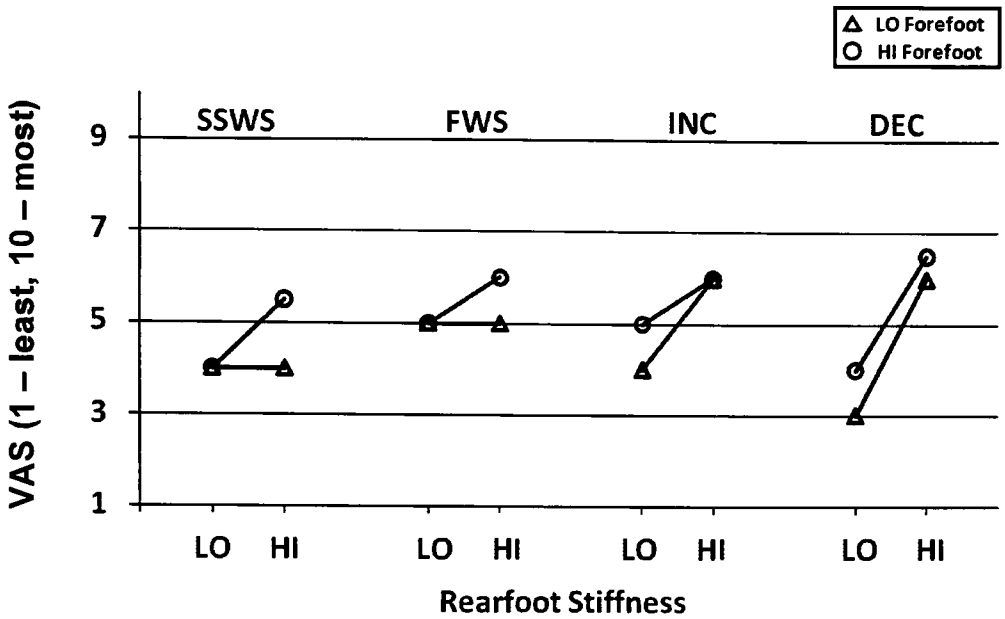

Figure 5.4.2. Effects of rearfoot stiffness on the perceived level of exertion (median) based on the Visual Analogue Scale (VAS) results from 1 (least exertion) to 10 (most exertion).

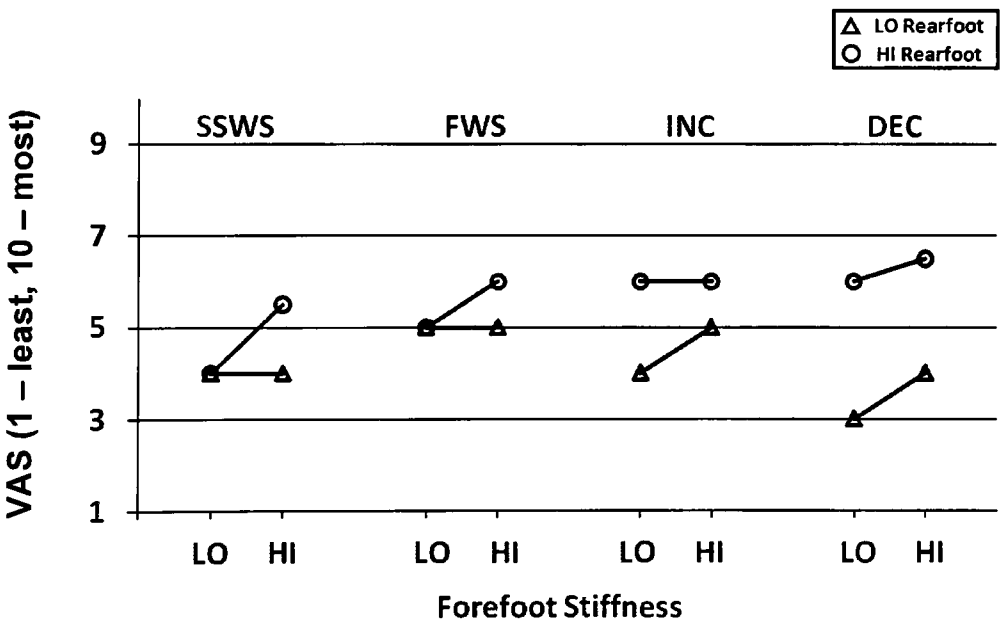

Figure 5.4.3. Effects of forefoot stiffness on the perceived level of exertion (median) based on the Visual Analogue Scale (VAS) results from 1 (least exertion) to 10 (most exertion).

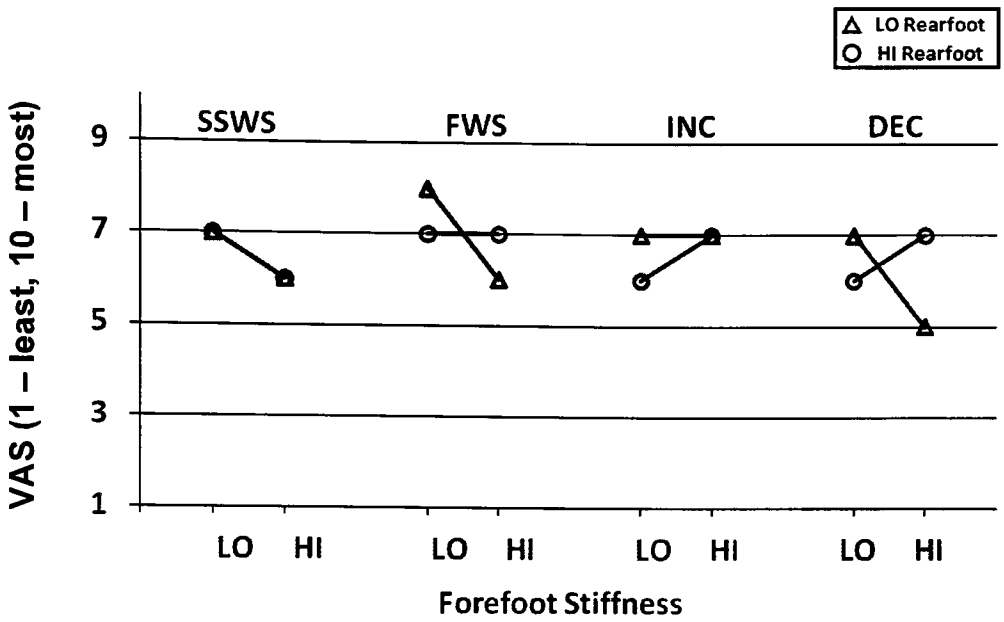

Figure 5.4.4. Effects of forefoot stiffness on the perceived level of stability (median) based on the Visual Analogue Scale (VAS) results from 1 (least stable) to 10 (most stable).

5.5. Correlations between subjective feedback and gait performance measures

A correlation analysis between gait performance measures and subjective feedback (i.e., perceived level of comfort, exertion, and stability) revealed several interesting relationships. Such relationships provide some insight into which measured gait parameters are relevant to perceived performance. When all conditions are grouped, level of comfort was correlated with the peak propulsive forces during terminal stance (significant at $p=0.005$, Spearman's $\rho=-0.346$) in which increases in propulsive forces were perceived as more comfortable. When related to the CFAM setups, high forefoot stiffness tended to increase propulsive forces. This unexpected result may indicate that the amputees often felt that there was too little propulsive force in late stance due to the lack of musculature to actively produce such forces. In contrast, a study by Alaranta et al. (1994), reported that amputees preferred devices that 'transmitted less shock' which indicated that amputees are sensitive to changes in applied loads on the prosthetic limb.

The level of exertion was correlated with metabolic rate (ml O_2/kg/min) for the self-selected (significant at p=0.042, Spearman's p=0.471) and incline walking conditions (significant at p=0.016, Spearman's ρ=0.545), as well as when all walking conditions are grouped (significant at p=0.087, Spearman's ρ=0.198). As would be expected, this indicated that the subjects perceived an increase in the amount of oxygen that is consumed per minute as indicating more exertion. However, in addition to metabolic rate, level of exertion was also correlated with the symmetry ratio (significant at p<0.001, Spearman's ρ=-0.473) and maximum flexion of the prosthetic side knee during the loading phase of stance (significant at p=0.001, Spearman's ρ=-0.402) with all walking conditions grouped. When related to the CFAM setups, high forefoot stiffness tended to decrease symmetry, whilst maximum knee flexion of the prosthetic side knee was not clearly associated with any CFAM setup and would therefore be affected more by subject or walking condition. A study by Casillas et al. (1995) reported that trans-tibial amputees were most satisfied with a foot that reduced metabolic rate (ml O_2/kg/min) and possessed greater ankle ROM (forefoot compliance), even though this claim was not supported by mechanical characterisation. This supports the findings of this study in which the subjects were able to identify the CFAM setup that required the least amount of metabolic cost, which was generally associated with greater ankle ROM (i.e., LOLO).

With all walking conditions grouped, the level of stability was correlated with the symmetry ratio (significant at p<0.001, Spearman's ρ=0.668), the CV of step length (significant at p=0.006, Spearman's ρ=-0.313), CV of step time (significant at p<0.001, Spearman's ρ=-0.481), time to maximum plantar flexion of the prosthesis (significant at p=0.001, Spearman's ρ=-0.432), and maximum flexion of the prosthetic side knee during the loading phase of stance (significant at p=0.004, Spearman's ρ=0.335). When related to the CFAM setups, a decrease in forefoot stiffness tended to increase symmetry, whilst a decrease in rearfoot stiffness tended to decrease the CV of step time and time to maximum plantar flexion of the prosthesis during stance. However, maximum flexion of the prosthetic side knee and CV of step length were not clearly associated with any particular CFAM setups.

All of the above correlations, which are summarised in Table 5.5.1, seem reasonable with the possible exception of propulsive loading of the prosthetic limb. In particular, one would

expect that an increase in oxygen consumption reflects more exertion which would be amplified by attempts to maintain a symmetric gait; and increases in the temporal-spatial variability of gait and the time required for the prosthetic foot to reach foot flat have been established as factors related to decreased stability. Furthermore, with all walking conditions grouped, level of comfort was correlated with level of stability (significant at $p=0.001$, Spearman's $\rho=-0.389$), indicating a close relationship between these two subjective measures. This result supports a previous finding that trans-tibial amputees ranked both the 'absence of stump pain,' which would be a critical factor in the overall comfort of the prosthesis, and 'stability while walking' as the most important functional factors when choosing an appropriate prosthetic foot (Postema et al., 1997b). Temporal gait symmetry and maximum knee flexion on the prosthetic side during loading appear to be highly correlated factors in both perceived level of exertion and stability, in which increases in both measures were perceived as requiring less effort and being more stable. Therefore, these two factors appear to be a significant conscious and desirable influence on the perceived mobility of the user. If the aim of trans-tibial amputee rehabilitation is to improve the patient's perceived level of stability and exertion, then these two factors might prove to be important outcome measures on which to focus.

Based on the above correlations with VAS results, it would appear that the VAS method used in this study was successful in reliably recording the patient's perceived levels of comfort, exertion, and stability and would be useful for future clinical and laboratory based studies. A review by Hafner (2005) concluded that if perceptive analysis is going to be used to evaluate the performance of prosthetic feet, then a better method of collecting subjective data would be through numerical rating scales (e.g., visual analogue scales) as they provide a standardised method of data collection with the added possibility of performing statistical analyses. Such reliable and easily collected information would not only provide a means of quantifying outcome measures of the rehabilitation process, but also assist with appropriate prescription of prosthetic components based on user feedback.

Table 5.5.1. Summary of correlations between subjective feedback and gait performance measures. For each subjective measure, gait performance measures are ordered (top to bottom) by their absolute value of ρ from greatest to least.

Subjective Feedback	Correlated Gait Performance Measure (ρ)
Comfort	1. Peak propulsive force (-0.346)
Exertion	1. Symmetry ratio (-0.473), 2. Metabolic rate (0.471 for self-selected; 0.545 for incline, 0.198 for all conditions grouped), 3. Maximum prosthetic side knee flexion during stance (-0.402)
Stability	1. Symmetry ratio (0.668), 2. Step time CV (-0.481), 3. Time to maximum plantar flexion of the prosthetic ankle joint during stance (-0.432), 4. Maximum prosthetic side knee flexion during stance (0.335), 5. Step length CV (-0.313)

5.6. Effects of walking conditions

When grouping the CFAM setups by walking condition, the effects of each walking condition on both subjective feedback and gait performance measures become more apparent. For the purpose of discussion and based on the correlations identified in section 5.5, the effects of walking conditions on gait performance can be grouped under the three measures of subjective feedback (i.e., comfort, exertion, and stability). Figures 5.6.1, 5.6.2 and 5.6.3, display the effects of walking condition on the median value of a selection of factors related to comfort, exertion, and stability, respectively. Considering that several measures are being graphed within the same plot, each possessing their own respective scale, some measures have been scaled and offset in order to view alongside others (see captions of Figures 5.6.1, 5.6.2, and 5.6.3).

5.6.1. Effects of walking conditions on comfort

Considering that perceived level of comfort was found to correlate with propulsive force and amputees have previously reported a preference for prosthetic devices that 'transmit less shock' (Alaranta et al., 1994), the VAS of comfort is displayed with all ground reaction forces on the prosthetic limb during the loading and unloading phases of stance (Figure 5.6.1). The self-selected and fast walking conditions were rated as equally comfortable, with the incline and decline conditions rated as more uncomfortable ($p<0.001$ for incline and decline greater than self-selected and fast walking). Unsurprisingly, there is a trend for peak ground reaction forces during the loading phase of stance (i.e., loading and braking force) to increase during fast walking ($p<0.001$ for fast walking greater than self-selected and incline walking conditions) and also during decline walking ($p<0.001$ for decline greater than self-selected and incline walking). However, peak ground reaction forces during the unloading phase of stance do not follow the same trend. Whereas peak unloading and peak propulsion forces do increase during fast walking (for unloading, $p=0.055$ for fast walking greater than all other walking conditions and for propulsion, $p<0.001$ for fast walking greater than all other walking conditions and incline greater than self-selected and decline walking conditions), they decrease with decline walking. This is unsurprising, as gravity aids in forward movement by propelling the amputee down the slope, reducing the need for propulsive forces.

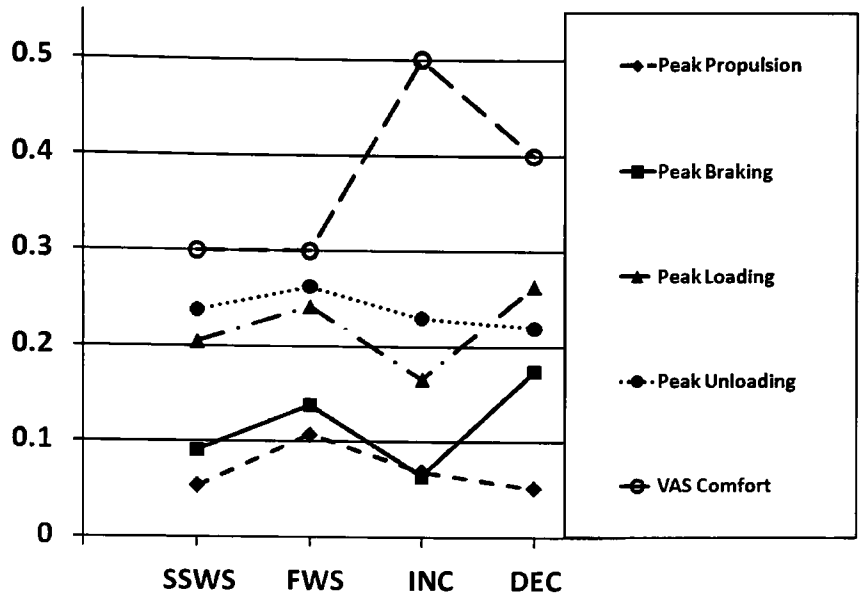

Figure 5.6.1. Effects of walking condition on measures related to gait comfort. 'Peak Loading' and 'Peak Braking' are the maximum vertical and horizontal forces occurring during the loading phase of stance, respectively. 'Peak Unloading' and 'Peak Propulsion' are the maximum vertical and horizontal forces occurring during the unloading phase of stance, respectively. An increase in 'VAS Comfort' indicates a greater level of perceived discomfort. The unadjusted data can be calculated from the presented data [in bold] through the following operations: Peak Braking (x Body Weight) = ***Peak Braking*** *x -1; Peak Loading (x Body Weight) =* ***Peak Loading*** *+ 0.8; Peak Unloading (x Body Weight) =* ***Peak Unloading*** *+ 0.8; VAS Comfort =* ***VAS Comfort*** *x 10. Peak Propulsion (x Body Weight) has not been adjusted.*

5.6.2. Effects of walking conditions on exertion

As perceived level of exertion was found to correlate with both metabolic rate and symmetry, these factors including metabolic CoT are displayed in Figure 5.6.2. The perceived level of exertion was found to increase during the fast, incline, and decline walking conditions compared to the self-selected ($p=0.001$ for incline and decline greater than self-selected walking). The same trends are seen in metabolic rate, apart from a decrease with decline walking in which metabolic rate is actually less than for self-selected ($p<0.001$ for fast walking greater than self-selected and decline, incline greater than self-selected and

decline, and self-selected greater than decline). However, the subjects still perceived this walking condition as requiring more exertion than the self-selected walking condition. A possible explanation for this elevated perception of exertion is that the decline walking condition, as well as the incline condition, presented a greater challenge for the subject as reflected by a decrease in symmetry ($p=0.01$ for fast walking greater than all other walking conditions). The metabolic CoT for the incline walking condition was the greatest, with fast and decline walking as the lowest ($p<0.001$ for incline greater than all other walking conditions, and for self-selected greater than fast and decline walking). Considering that the fast walking condition required less metabolic CoT (metabolic energy expenditure per unit distance travelled) compared to the self-selected walking condition, it would appear that this increased walking speed (133 to 150% of self-selected) is a more efficient speed for level walking on a treadmill.

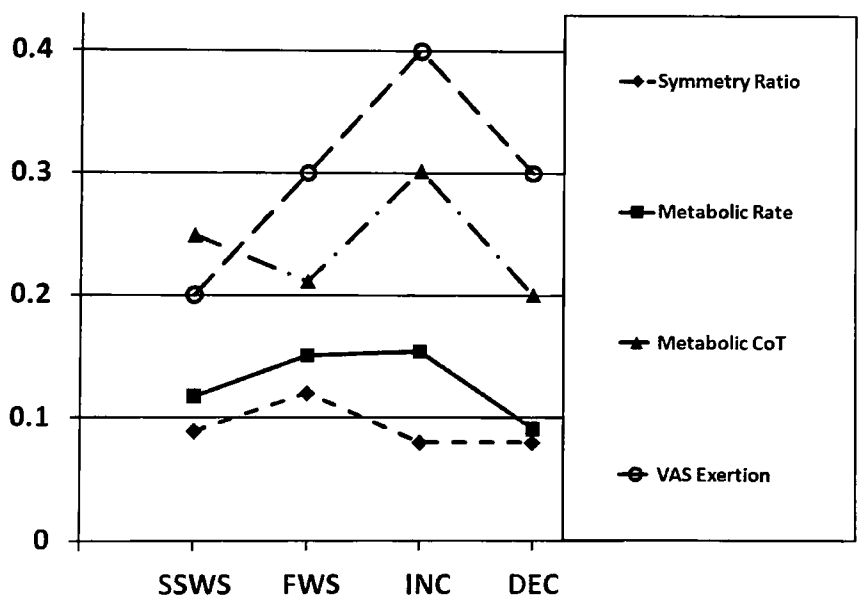

*Figure 5.6.2. Effects of walking condition on measures related to gait exertion. An increase in 'VAS Exertion' indicates a greater level of perceived exertion. The unadjusted data can be calculated from the presented data [in bold] through the following operations: Symmetry Ratio = **Symmetry Ratio** + 0.8; Metabolic Rate (ml O_2/kg/min) = **Metabolic Rate** x 100; VAS Exertion = (**VAS Exertion** + 0.2) x 10. Metabolic CoT (ml O_2/kg/m) has not been adjusted.*

5.6.3. Effects of walking conditions on stability

Perceived level of stability was found to correlate with several different performance measures, the majority of which are categorised as temporal-spatial measures of gait (Table 5.5.1). Therefore, these measures and the time to maximum plantar flexion of the prosthetic ankle joint are displayed with perceived level of stability in Figure 5.6.3. The perceived level of stability as indicated by the median VAS was equal across all walking conditions. Despite the inconclusive subjective results, differences in related performance measures were observed. The fast walking condition is the most symmetric ($p=0.01$ for fast walking greater than all other walking conditions), has the lowest step length CV ($p=0.002$ for all other conditions greater than fast walking), and lowest values of both prosthetic limb swing time CV ($p=0.018$ for incline walking greater than fast walking condition) and sound limb swing time CV ($p=0.002$ for all other conditions greater than fast walking). Conversely, the incline and decline conditions are the least symmetric and have the greatest step length CV. Step time CV was greatest for the incline condition when compared to the other three conditions ($p=0.002$ for incline greater than all other walking conditions), least for the decline condition, and displayed a modest increase from self-selected to fast walking.

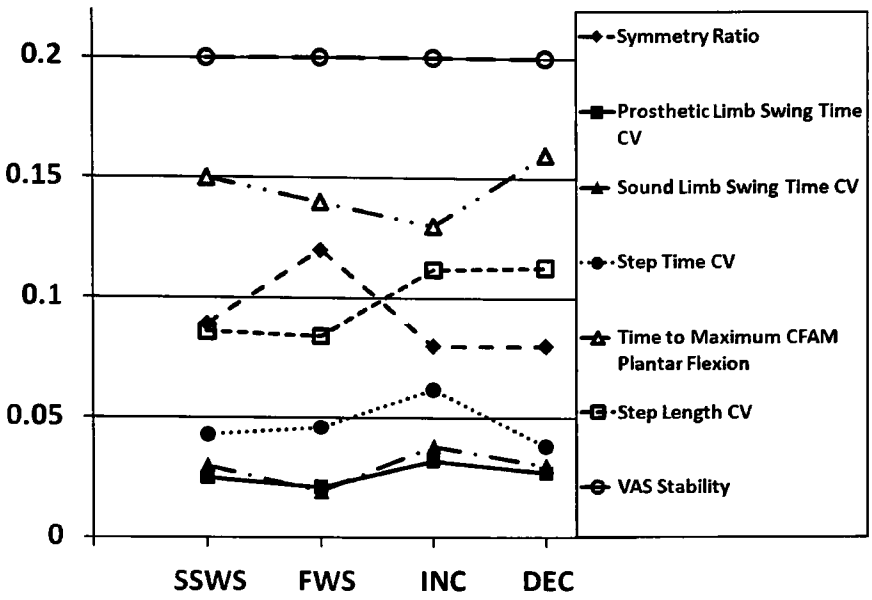

*Figure 5.6.3. Effects of walking condition on measures related to gait stability. An increase in 'VAS Stability' indicates an increase in perceived level of stability. The unadjusted data can be calculated from the presented data [in bold] through the following operations: Symmetry Ratio = **Symmetry Ratio** + 0.8; Time to Maximum CFAM Plantar Flexion (% Stance) = (**Time to Maximum CFAM Plantar Flexion** – 0.06) x 100; VAS Stability = (**VAS Stability** + 0.5) x 10. All CV data have not been adjusted.*

5.6.4. Conclusions

Overall, the most apparent conclusion is that the vast majority of the selected performance measures in Figures 5.6.1, 5.6.2, and 5.6.3, apart from peak loads, displayed an improvement during the fast walking condition compared to the self-selected walking condition. Specifically, the metabolic CoT decreased (i.e., lower metabolic cost per unit distance travelled), the symmetry ratio increased (i.e., greater temporal symmetry), the time to maximum plantar flexion of the prosthesis decreased (i.e., achieving earlier foot flat), and the CV of step length, prosthetic limb swing time, and sound limb swing time decreased (i.e., less gait variability and increased stability). Generally, this aligns with a study by Yamasaki et al. (1991), which reported a U-shaped relationship between walking speed and step time and step length CV, where an optimal speed can be located to minimise gait variability. Additionally, a study by Jordan et al. (2007), reported a reduction in step time CV and step

length CV with increased walking speed up to 120% of self-selected walking speed in healthy individuals. A similar U-shape relationship is also found in metabolic energy expenditure, where an optimal walking speed is seen in trans-tibial amputee gait whilst on a treadmill which will minimise metabolic CoT (Hsu et al., 1999). However, some other studies have reported that trans-femoral amputees displayed no difference in symmetry between prosthetic limb and sound limb swing time with increasing walking speed (Donker and Beek, 2002) or that swing time variability was not affected in healthy controls and Parkinson's patients when subjected to increased treadmill walking speeds between 80 and 110% of their self-selected speed (Frenkel-Toledo et al., 2005).

It is likely that the self-selected speeds chosen by the subjects in this study were slower than the speeds they normally use overground, and consequently, not their optimal treadmill speed. Previous research has reported that healthy individuals (Dal et al., 2009) and lower limb amputees (Traballesi et al., 2008) often chose a treadmill walking speed that is slower than what they would use overground and the authors have suggested that this is due to a conservative approach to gait when confronted with an unfamiliar or more risky walking scenario. As mentioned previously, the average self-selected walking speed in this study was 46.7 m/min, which is slower than previously reported self-selected walking speeds of between 63.3 m/min and 102.0 m/min for unilateral trans-tibial amputees when walking overground. In fact, the average fast walking speed of 68.1 in this study was within the range of self-selected overground walking speeds of previous studies. A conservative approach is most likely the reason for the relatively slow walking speed chosen by the subjects in this study, as they are unfamiliar with use of the experimental equipment involved (e.g., CFAM, treadmill, and gas analyser).

Although interesting differences were found between walking conditions, it should be remembered that these were based on grouping results for different CFAM setups. Clearly, different CFAM setups are likely to perform best for different walking conditions. Furthermore, interactions between the effects of walking condition and the effects of CFAM setup will reduce statistical significance when grouping results for different CFAM setups.

5.7. Effects of CFAM setup by walking condition

As indicated in section 5.6, there are interactions between the effects of walking condition and the effects of CFAM setup. By focussing on individual walking conditions, the relationships between CFAM setup and gait performance become more apparent. Furthermore, considering that the independent variables of prosthetic alignment and walking speed were held constant for each CFAM setup tested within each walking condition, any relative changes to subjective feedback and performance measures would be due to the differences in rearfoot and forefoot stiffness setups. Therefore, the ideal CFAM setup for a particular walking condition would optimise each of these parameters (e.g., reduce prosthetic limb swing time CV and increase the symmetry ratio and perceived level of comfort). The following sub-sections demonstrate the effects of CFAM setup (i.e., combinations of rearfoot and forefoot stiffness) on measures related to comfort, exertion and stability.

5.7.1. Effects of CFAM setup on self-selected walking

Figures 5.7.1.1, 5.7.1.2, and 5.7.1.3 display the effects of CFAM setup on measures related to comfort, exertion and stability at self-selected walking speed on the level. Regarding measures related to comfort, it would appear that even though the CFAM setup LOHI reduced most of the peak loading measures, it was rated as the least comfortable setup. Although there appears to be this contradiction between subjective feedback and loading, the changes in peak loading measures were relatively small and other factors are likely to be more dominant. Regarding measures related to exertion, the CFAM setup LOHI provided the greatest advantage as it showed the greatest temporal symmetry, lowest metabolic rate, and the second lowest value of metabolic CoT; which agrees with the low perceived level of exertion for this setup. Regarding measures related to stability, the CFAM setup LOHI again provided the greatest advantage, as it displayed the greatest level of temporal symmetry and the lowest values of step time CV and prosthetic limb swing time CV; which is in agreement with the higher perceived level of stability.

Overall, it appears that at ***self-selected walking speed on the level,*** the ***CFAM setup LOHI*** provided the greatest advantage for exertion and stability. However, when comfort is taken into account, the ***CFAM setup LOLO*** may have the better all round performance.

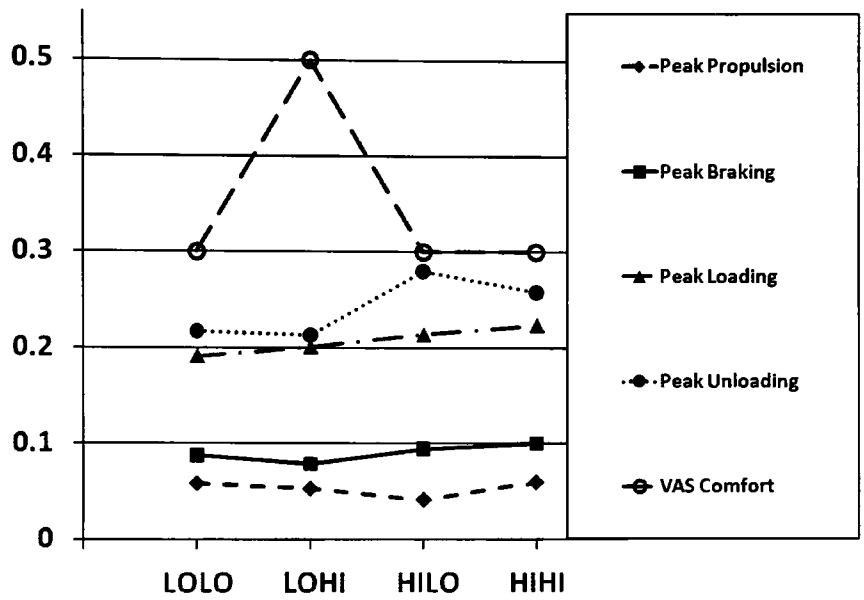

Figure 5.7.1.1. Effects of CFAM setup on measures related to gait comfort during the self-selected walking condition. 'Peak Loading' and 'Peak Braking' are the maximum vertical and horizontal forces occurring during the loading phase of stance, respectively. 'Peak Unloading' and 'Peak Propulsion' are the maximum vertical and horizontal forces occurring during the unloading phase of stance, respectively. An increase in 'VAS Comfort' indicates a greater level of perceived discomfort. The unadjusted data can be calculated from the presented data [in bold] through the following operations: Peak Braking (x Body Weight) = ***Peak Braking*** *x -1; Peak Loading (x Body Weight) =* ***Peak Loading*** *+ 0.8; Peak Unloading (x Body Weight) =* ***Peak Unloading*** *+ 0.8; VAS Comfort =* ***VAS Comfort*** *x 10. Peak Propulsion (x Body Weight) has not been adjusted.*

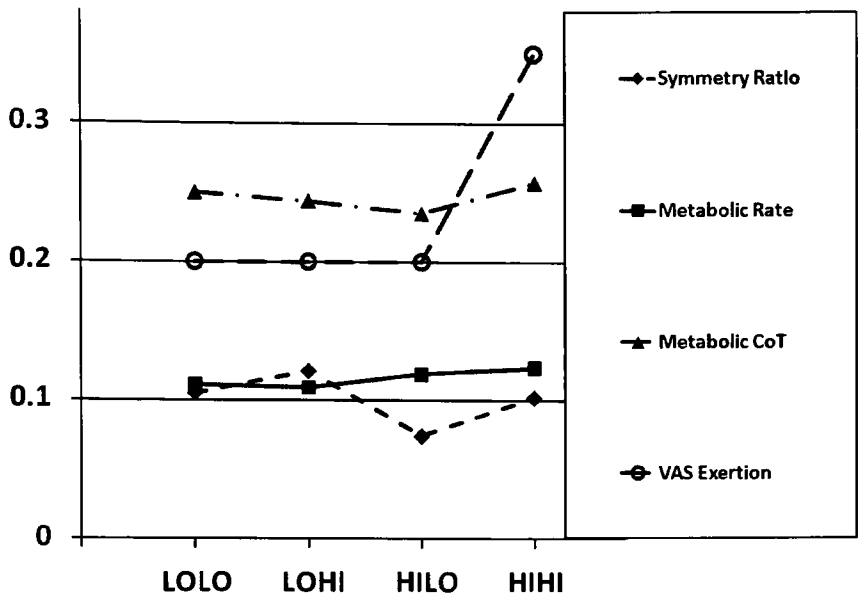

*Figure 5.7.1.2. Effects of CFAM setup on measures related to gait exertion during the self-selected walking condition. An increase in 'VAS Exertion' indicates a greater level of perceived exertion. The unadjusted data can be calculated from the presented data [in bold] through the following operations: Symmetry Ratio = **Symmetry Ratio** + 0.8; Metabolic Rate (ml O_2/kg/min) = **Metabolic Rate** x 100; VAS Exertion = (**VAS Exertion** + 0.2) x 10. Metabolic CoT (ml O_2/kg/m) has not been adjusted.*

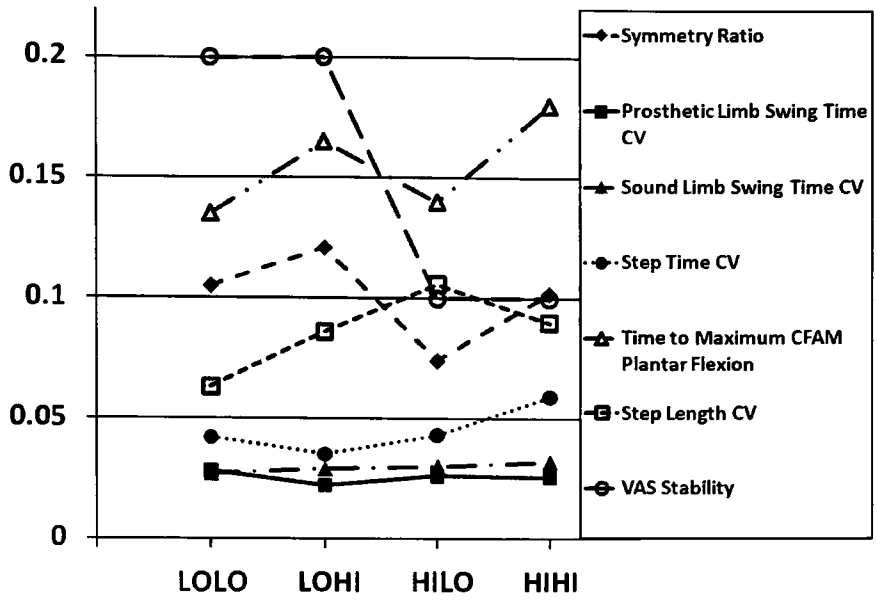

*Figure 5.7.1.3. Effects of walking condition on measures related to gait stability during the self-selected walking condition. An increase in 'VAS Stability' indicates an increase in perceived level of stability. The unadjusted data can be calculated from the presented data [in bold] through the following operations: Symmetry Ratio = **Symmetry Ratio** + 0.8; Time to Maximum CFAM Plantar Flexion (% Stance) = (**Time to Maximum CFAM Plantar Flexion** – 0.06) x 100; VAS Stability = (**VAS Stability** + 0.5) x 10. All CV data have not been adjusted.*

5.7.2. Effects of CFAM setup on fast walking

Figures 5.7.2.1, 5.7.2.2, and 5.7.2.3 display the effects of CFAM setup on measures related to comfort, exertion and stability at fast walking speed on the level. Regarding measures related to comfort, the CFAM setups of LOHI and HIHI reduced most of the peak loading measures. However, HIHI was rated as more comfortable, and might therefore be considered a better choice. Furthermore, LOLO and HILO were rated as being most comfortable; apparently contradicting the peak loading measures. However, in this context, it should be recalled that increasing peak propulsion force correlates with increasing comfort. Regarding measures related to exertion, no noticeable difference in metabolic CoT was seen across all CFAM setups. However, the CFAM setup LOLO provided the greatest advantage as it displayed the highest level of temporal symmetry and a relatively low metabolic rate; which agrees with the lower value of perceived exertion for this setup.

Regarding measures related to stability, the CFAM setup of LOLO provided the greatest advantage, as it displayed the highest level of temporal symmetry, and relatively low values of step time CV, step length CV and time to maximum plantar flexion; which agrees with the highest value of perceived stability.

Overall, it appears that during ***fast walking speed on the level,*** the ***CFAM setup LOLO*** provided the greatest advantage for exertion and stability. LOLO was also rated as being most comfortable, but the peak loading measures did not support this.

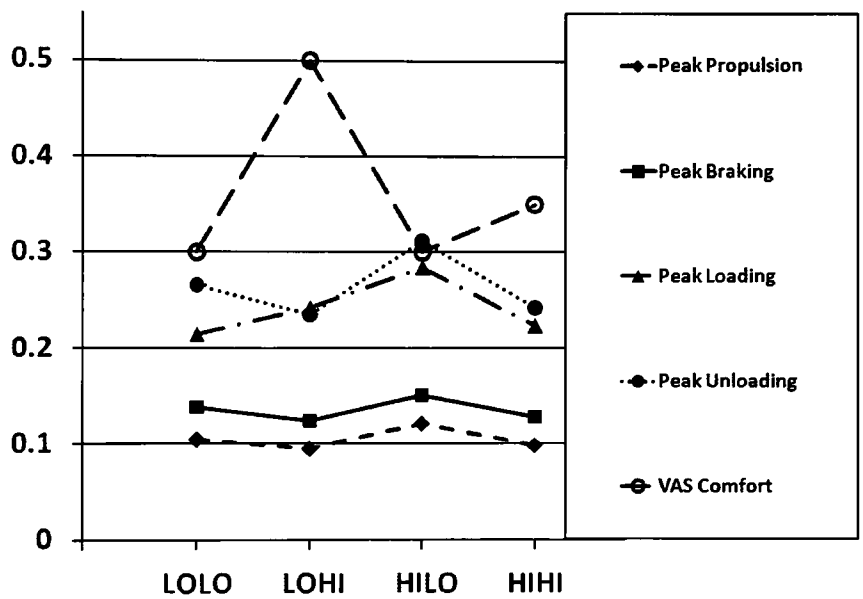

Figure 5.7.2.1. Effects of CFAM setup on measures related to gait comfort during the fast walking condition. 'Peak Loading' and 'Peak Braking' are the maximum vertical and horizontal forces occurring during the loading phase of stance, respectively. 'Peak Unloading' and 'Peak Propulsion' are the maximum vertical and horizontal forces occurring during the unloading phase of stance, respectively. An increase in 'VAS Comfort' indicates a greater level of perceived discomfort. The unadjusted data can be calculated from the presented data [in bold] through the following operations: Peak Braking (x Body Weight) = ***Peak Braking*** *x -1; Peak Loading (x Body Weight) =* ***Peak Loading*** *+ 0.8; Peak Unloading (x Body Weight) =* ***Peak Unloading*** *+ 0.8; VAS Comfort =* ***VAS Comfort*** *x 10. Peak Propulsion (x Body Weight) has not been adjusted.*

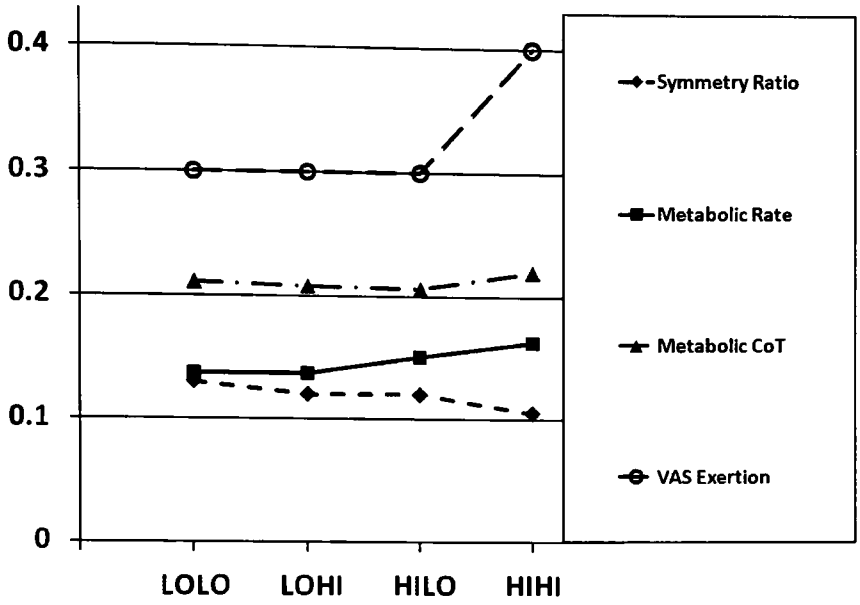

*Figure 5.7.2.2. Effects of CFAM setup on measures related to gait exertion during the fast walking condition. An increase in 'VAS Exertion' indicates a greater level of perceived exertion. The unadjusted data can be calculated from the presented data [in bold] through the following operations: Symmetry Ratio = **Symmetry Ratio** + 0.8; Metabolic Rate (ml O_2/kg/min) = **Metabolic Rate** x 100; VAS Exertion = (**VAS Exertion** + 0.2) x 10. Metabolic CoT (ml O_2/kg/m) has not been adjusted.*

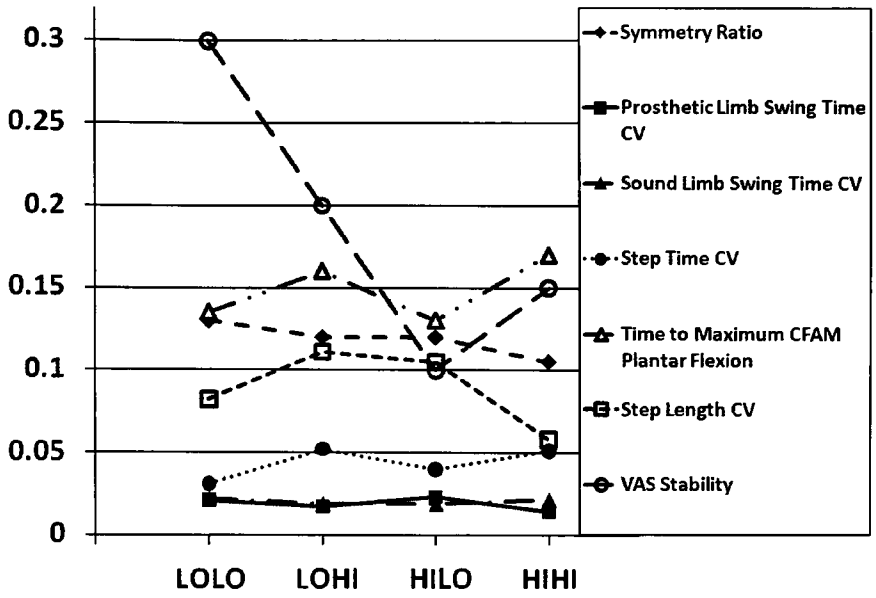

*Figure 5.7.2.3. Effects of walking condition on measures related to gait stability during the fast walking condition. An increase in 'VAS Stability' indicates an increase in perceived level of stability. The unadjusted data can be calculated from the presented data [in bold] through the following operations: Symmetry Ratio = **Symmetry Ratio** + 0.8; Time to Maximum CFAM Plantar Flexion (% Stance) = (**Time to Maximum CFAM Plantar Flexion** – 0.06) x 100; VAS Stability = (**VAS Stability** + 0.5) x 10. All CV data have not been adjusted.*

5.7.3. Effects of CFAM setup on incline walking

Figures 5.7.3.1, 5.7.3.2, and 5.7.3.3 display the effects of CFAM setup on measures related to comfort, exertion and stability during self-selected walking speed on the incline. Regarding measures related to comfort, even though the CFAM setup LOHI reduced most of the peak loading measures, it was rated as the least comfortable setup. The setup subjectively rated as most comfortable was LOLO. Therefore, as with self-selected walking on the level, there appears to be a contradiction between subjective feedback and loading. However, the changes in peak loading measures were relatively small and other factors are likely to be more dominant. Regarding measures related to exertion, the CFAM setup LOLO clearly provided the greatest advantage by displaying the lowest values of metabolic rate and CoT, and the greatest value of temporal symmetry; which is in agreement with the lowest reported value of perceived exertion for this setup. Regarding measures related to stability,

the CFAM setup LOLO clearly provided the greatest advantage, as it displayed the highest level of temporal symmetry, the lowest value of step length CV, step time CV, sound limb swing time CV, and a relatively low value of prosthetic swing time CV; which is in agreement with the higher value of perceived stability.

Overall, it appears that during ***self-selected walking speed on the incline,*** the ***CFAM setup LOLO*** provided the greatest advantage for exertion and stability. LOLO was also rated as being most comfortable, but the peak loading measures did not support this.

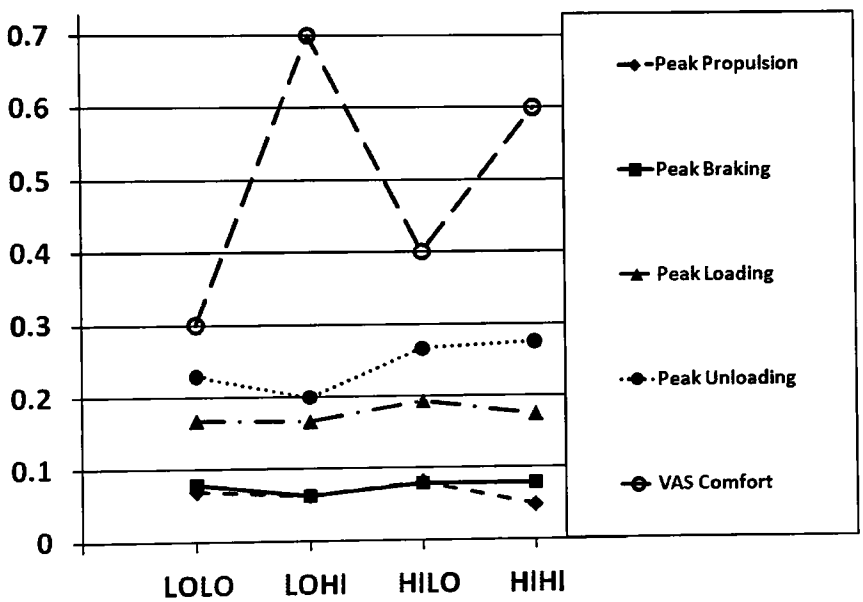

Figure 5.7.3.1. Effects of CFAM setup on measures related to gait comfort during the incline walking condition. 'Peak Loading' and 'Peak Braking' are the maximum vertical and horizontal forces occurring during the loading phase of stance, respectively. 'Peak Unloading' and 'Peak Propulsion' are the maximum vertical and horizontal forces occurring during the unloading phase of stance, respectively. An increase in 'VAS Comfort' indicates a greater level of perceived discomfort. The unadjusted data can be calculated from the presented data [in bold] through the following operations: Peak Braking (x Body Weight) = ***Peak Braking*** *x -1; Peak Loading (x Body Weight) =* ***Peak Loading*** *+ 0.8; Peak Unloading (x Body Weight) =* ***Peak Unloading*** *+ 0.8; VAS Comfort =* ***VAS Comfort*** *x 10. Peak Propulsion (x Body Weight) has not been adjusted.*

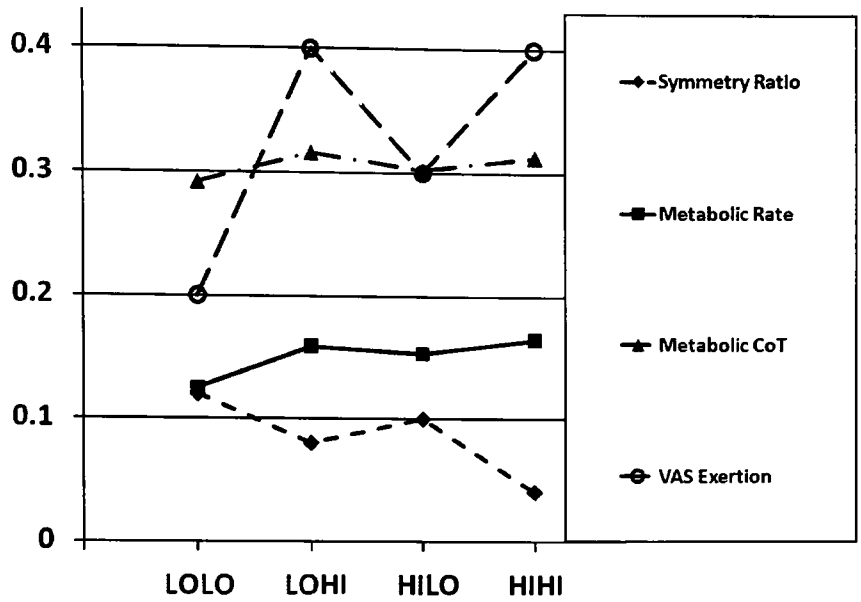

*Figure 5.7.3.2. Effects of CFAM setup on measures related to gait exertion during the incline walking condition. An increase in 'VAS Exertion' indicates a greater level of perceived exertion. The unadjusted data can be calculated from the presented data [in bold] through the following operations: Symmetry Ratio = **Symmetry Ratio** + 0.8; Metabolic Rate (ml O_2/kg/min) = **Metabolic Rate** x 100; VAS Exertion = **(VAS Exertion** + 0.2) x 10. Metabolic CoT (ml O_2/kg/m) has not been adjusted.*

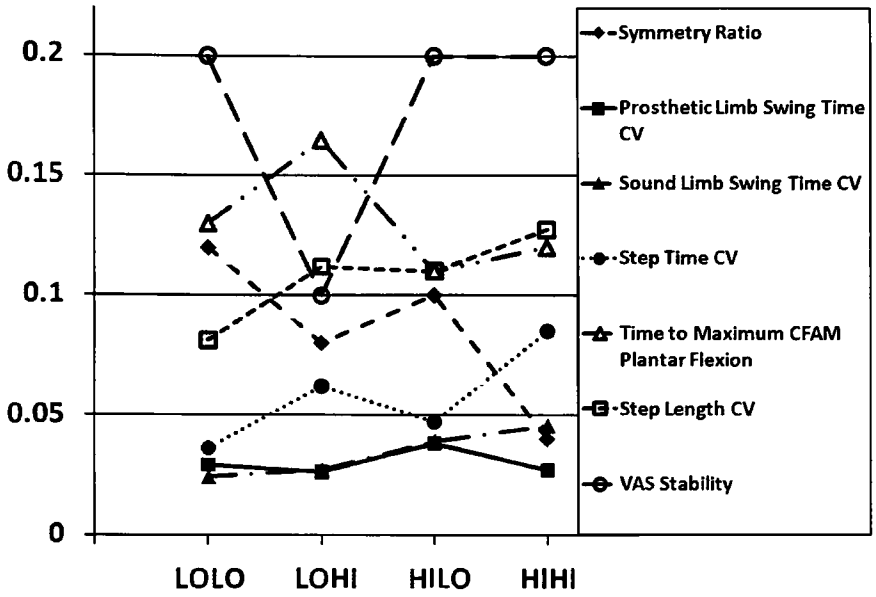

*Figure 5.7.3.3. Effects of walking condition on measures related to gait stability during the incline walking condition. An increase in 'VAS Stability' indicates an increase in perceived level of stability. The unadjusted data can be calculated from the presented data [in bold] through the following operations: Symmetry Ratio = **Symmetry Ratio** + 0.8; Time to Maximum CFAM Plantar Flexion (% Stance) = (**Time to Maximum CFAM Plantar Flexion** – 0.06) x 100; VAS Stability = (**VAS Stability** + 0.5) x 10. All CV data have not been adjusted.*

5.7.4. Effects of CFAM setup on decline walking

Figures 5.7.4.1, 5.7.4.2, and 5.7.4.3 display the effects of CFAM setup on measures related to comfort, exertion and stability at self-selected walking speed on the decline. Regarding measures related to comfort, the CFAM setups LOLO and LOHI reduced peak loading measures. However, as the CFAM setup LOLO was subjectively rated as more comfortable, this might be the better setup. Regarding measures related to exertion, the CFAM setup LOLO clearly provided the greatest advantage by displaying the lowest values of metabolic rate and CoT, and the greatest value of temporal symmetry; which is in agreement with the lowest reported value of perceived exertion for this setup. Regarding measures related to stability, the CFAM setup LOLO provided the greatest advantage, as it displayed the highest level of temporal symmetry and the lowest value of sound limb swing time CV and prosthetic limb swing time CV; which is in agreement with the higher value of perceived stability for

this setup. However, despite a lower value of temporal symmetry, it is worth noting is that the CFAM setup HIHI displayed a reduced step length CV and step time CV and was rated equally as stable as the LOLO setup.

Overall, it appears that during ***self-selected walking speed on the decline,*** the ***CFAM setup LOLO*** provided the greatest advantage for comfort, exertion, and stability.

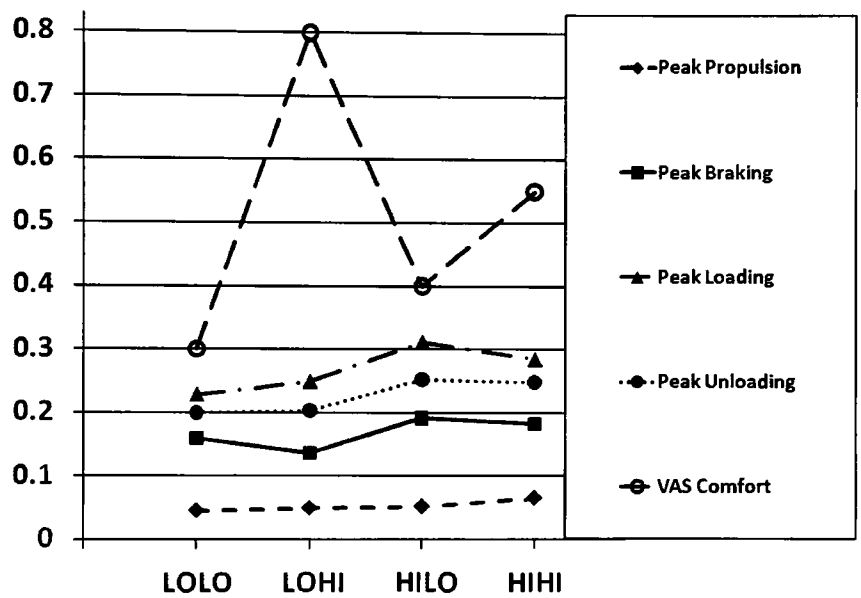

Figure 5.7.4.1. Effects of CFAM setup on measures related to gait comfort during the decline walking condition. 'Peak Loading' and 'Peak Braking' are the maximum vertical and horizontal forces occurring during the loading phase of stance, respectively. 'Peak Unloading' and 'Peak Propulsion' are the maximum vertical and horizontal forces occurring during the unloading phase of stance, respectively. An increase in 'VAS Comfort' indicates a greater level of perceived discomfort. The unadjusted data can be calculated from the presented data [in bold] through the following operations: Peak Braking (x Body Weight) = ***Peak Braking*** *x -1; Peak Loading (x Body Weight) =* ***Peak Loading*** *+ 0.8; Peak Unloading (x Body Weight) =* ***Peak Unloading*** *+ 0.8; VAS Comfort =* ***VAS Comfort*** *x 10. Peak Propulsion (x Body Weight) has not been adjusted.*

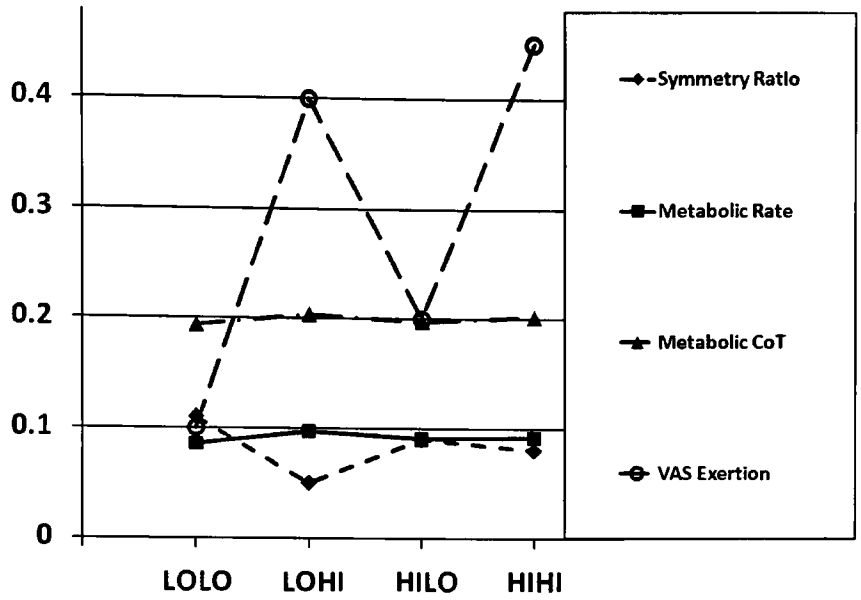

*Figure 5.7.4.2. Effects of CFAM setup on measures related to gait exertion during the decline walking condition. An increase in 'VAS Exertion' indicates a greater level of perceived exertion. The unadjusted data can be calculated from the presented data [in bold] through the following operations: Symmetry Ratio = **Symmetry Ratio** + 0.8; Metabolic Rate (ml O_2/kg/min) = **Metabolic Rate** x 100; VAS Exertion = (**VAS Exertion** + 0.2) x 10. Metabolic CoT (ml O_2/kg/m) has not been adjusted.*

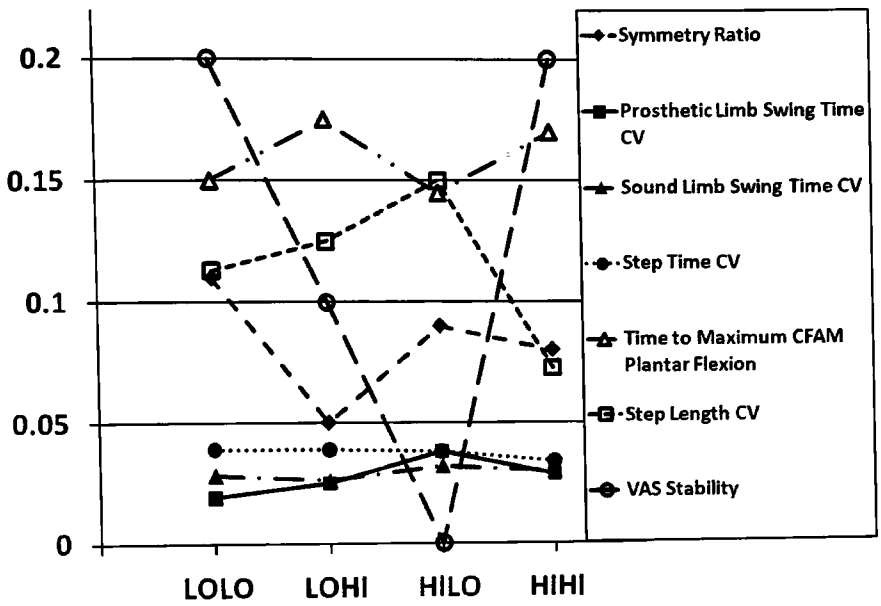

*Figure 5.7.4.3. Effects of walking condition on measures related to gait stability during the decline walking condition. An increase in 'VAS Stability' indicates an increase in perceived level of stability. The unadjusted data can be calculated from the presented data [in bold] through the following operations: Symmetry Ratio = **Symmetry Ratio** + 0.8; Time to Maximum CFAM Plantar Flexion (% Stance) = (**Time to Maximum CFAM Plantar Flexion** – 0.06) x 100; VAS Stability = (**VAS Stability** + 0.5) x 10. All CV data have not been adjusted.*

5.7.5. Relevance to prescription

The analysis above introduces a technique by which the effects of different CFAM setups can be compared in order to identify those setups that optimise gait performance. By identifying the CFAM setup which provides the greatest performance advantage for a particular walking condition, this information could inform prescription guidelines for prosthetic components (i.e., selecting commercial feet and pylons). Even though the results from this study apply to a generalised group of relatively active, traumatic, trans-tibial amputees, such a method could be applied to an individual patient. With ample time for trialling a variety of different prosthetic components (i.e., time for accommodation and gait analysis), a combination of modular prosthetic components could be tested and subsequently chosen by a prosthetist that will best optimise their patient's gait performance.

Overall, the small differences in metabolic rate and CoT and limited statistical significance found across all walking conditions in this study are not surprising. Numerous studies that have investigated the effects of different commercially available prosthetic feet (i.e., varying types of conventional and ESAR feet) on metabolic rate and CoT of unilateral trans-tibial amputees have reported inconclusive results (Barth et al., 1992; Hsu et al., 2006; Lehmann et al., 1993a; Lehmann et al., 1993b; Perry and Shanfield, 1993; Torburn et al., 1990; Torburn et al., 1995). Whereas differences in metabolic rate and CoT were not very conclusive in this study, temporal gait symmetry proved to be a better factor in distinguishing between CFAM setups. Therefore, in regards to prescription of prostheses for the patient population in this study, perhaps selection of an effective prosthesis should be based on optimisation of alternative gait measures, such as stability and comfort, as opposed to focussing on reducing energy expenditure. Not only would this relate to selection of commercial prosthetic components, but also assist in the identification of effective *AIPP* for the design of improved prostheses as described in the proposed design process of Chapter Two.

A summary of the results from the above analysis is provided in Table 5.7.5.1. When observing the results presented in this chapter as a whole, a low forefoot stiffness seems to be a key factor in improving trans-tibial gait performance. A possible explanation for this might be the fact that a low forefoot stiffness was associated with substantially increased DF in late stance (average increase of 8.1 degrees), which may correspond to an easier and more natural progression through stance. The typical maximum DF observed in normal gait on a level surface during late stance has been reported as 10 degrees by Perry (1992) and as 15 degrees by Whittle (1991), the latter of which is equivalent to the average DF observed for the sound ankle in this study (15.3 degrees, averaged over all walking conditions and CFAM setups). For this study, low forefoot stiffness produced an average of 19.2 and 20.2 degrees of DF for the self-selected and fast walking (on a level surface) conditions, respectively, whereas high forefoot stiffness only produced an average of 11.1 and 12.1 degrees of DF for the same conditions, respectively. Consequently, low forefoot stiffness is allowing DF motion during late stance that is within the range of healthy gait and beyond that of the sound side ankle joint, which may be contributing to the improvement seen in overall gait performance.

Furthermore, based on the summary of results in Table 5.7.5.1, it would appear that only one CFAM setup (LOLO) is necessary to provide optimal gait performance across all walking conditions. However, this result must be interpreted with caution as the experimental study in this investigation was limited to just four walking conditions and four CFAM setups. It is possible that during more severe walking conditions (i.e., speeds greater than 150% of self-selected and slopes greater than 5% grade), different CFAM setups would be required to provide the best performance.

Table 5.7.5.1. Summary of optimal CFAM setups per walking condition.

Walking Condition	Optimal CFAM Setup
Self-selected walking speed on the level	LOHI or LOLO
Fast walking speed on the level	LOLO
Self-selected walking speed on the incline	LOLO
Self-selected walking speed on the decline	LOLO

5.8. Study limitations

One significant limitation of this study is that the same experimental custom foot-ankle mechanism (CFAM) was used for each subject. Commercial prosthetic feet and associated characteristics (i.e., length and stiffness grade) are prescribed for patients depending on their foot length, weight, and activity level. Unfortunately, the same prosthetic foot length and stiffness setups were used for each subject in this study despite their difference in height, weight, and activity level. A mismatch in length between the prosthetic foot and sound foot could have adverse effects on the gait of the amputee. However, the foot length of the subjects in this study ranged from 250 to 290 mm, with an average of 272 and a median of 280 mm, and the length of the CFAM was 283 mm. Therefore, it can be said that the CFAM generally covered the foot length of all the subjects, and was 3.3 cm longer than the sound foot in the worst case scenario. Additionally, the stiffness settings used were adapted from the mechanical characterisation results from a study by Lehmann et al. (1993b), which were presumably based on the loading response of one foot per design, even though the study does not explicitly state this, nor does it mention the stiffness grade for each foot. Most likely, as the subject mass in this study ranged from 76 to 96 kilograms, the

CFAM stiffness setups would be different for each subject if they were actually adapted from the manufacturer recommended patient-specific stiffness grades for the Flex-Foot, SACH Foot, and Seattle Foot. An improved design of the CFAM would include adjustable foot length and an improved experimental design would include testing of stiffness setups that are subject-specific based on their weight.

A second limitation is that for each individual subject, only one fixed alignment of the prosthetic foot was used during the human performance testing regardless of the stiffness setup being tested. It has been documented that prosthetists will align prosthetic feet differently when their geometries and stiffnesses differ (Hansen et al., 2003), but unfortunately this is based on subjective criteria. However, for this study, adjustments in alignment were excluded in order to eliminate this element as a confounding variable and ensure that only the stiffness variable of *AIPP* was being (systematically) adjusted. However, this method might have undesirable effects, as the prosthesis might at times appear to the subject as mal-aligned, which would influence their perceived level of comfort and related gait performance. Thus, this would compromise the clinical relevance of the results in this study, emphasising that they must be interpreted with caution. Future extended studies might include variable alignment relative to the stiffness setup being tested in order to more clearly understand these effects.

A third limitation of this study is the limited number of subjects. Unfortunately, this limitation affects the statistical power of the study and was most likely the primary reason for limited statistical significance at $p<0.05$ for many of the gait measures. For this study to obtain ethical approval from the National Health Service (NHS), the subjects could not use any of the prosthetic components that they were prescribed by the NHS. Furthermore, for this study to be successfully carried out, the subjects used the ITP, CFAM, and the same type of socket to minimise confounding variables. Therefore, a custom socket had to be manufactured for each subject. Such a process required both an additional visit by the subject to the University of Salford for casting and at least one full week following casting to produce a finished socket. This required a significant amount of time and, together with the well known difficulties of recruiting large amputee cohorts, led to the low number of subjects. Naturally, future work of this type should include more subjects in order to

produce results of greater statistical confidence. However, even with only five subjects, significance was found in many of the gait measures, which reflects the strength of the experimental methodology in detecting differences in amputee gait performance.

The final limitation is that this study did not include a matched group of healthy controls with which to compare the amputee results. Even though the amputee subjects behaved as their own control when comparing the effects of varying prosthetic stiffness on gait performance, it would have been interesting to see if healthy subjects displayed similar changes in kinematics and metabolic energy expenditure when subjected to a similar testing protocol. Unfortunately, the scope of this current study did not extend to healthy controls, but this may be included in future research when investigating similar questions.

6. Chapter Six: Discussion

6.1. Correlations between *AIPP* and gait performance

As discussed in Chapter Two, one critical component of the proposed prosthesis design process is the development of methods for combined studies which include both *AIPP* characterisation and in-vivo gait performance. The experimental methods for *AIPP* characterisation and in-vivo testing presented in Chapters Three and Four, respectively, enable such an approach. Such studies could easily incorporate several commercially available prosthetic devices, rather than use of a custom device such as the CFAM. Consequently, correlations could be drawn between prosthetic mechanical behaviour (*AIPP*) and amputee gait performance.

To demonstrate one way in which such an approach could be applied, the coefficients (*A*, *B*, and *C*) of the second-order best fit ($y=Ax^2 + Bx + C$) to the roll-over points of each foot setup as measured by the test-rig (see Table 4.2.3.2) have been used in a multiple linear regression analysis for prediction of several in-vivo gait measures. All in-vivo gait parameters have been analysed as a function of *A*, *B*, *C*, subject body mass (*BM*; kg), subject walking speed (*WS*; m/min), and a regression constant. The results of this regression analysis (i.e., regression equation, coefficient of determination, R^2, test statistic, F, and statistical significance, p), separated by walking condition, are presented in Tables 6.1.1, 6.1.2, 6.1.3, 6.1.4, and 6.1.5. Walking conditions are abbreviated as: SSWS (self-selected walking speed on level), FWS (fast walking speed on level), INC (self-selected walking speed on incline), and DEC (self-selected walking speed on decline).

Based on these results, it appears that the *AIPP* roll-over shape provides useful information for predicting certain measures of gait performance. Therefore, *AIPP* could be useful for predicting the effects of prosthetic components on amputee gait performance. This might provide some insight for prescription of such components based on *AIPP* (measured independent of the amputee) and only requiring minimal data from the patient (i.e., body

mass and self-selected walking speed). For such a technique to be effective, this would require that the manufacturers of such prosthetic components provide information on the *AIPP* roll-over shape through similar methods as those described in Chapter Three. Considering that roll-over shape coefficients are reflective of the rearfoot and forefoot stiffness by way of the curvatures, it would seem obvious that some measures of gait should be significantly correlated, such as maximum DF and PF (Table 6.1.1 and 6.1.2, respectively). The regression equation for maximum PF was more heavily dependent on the *AIPP* coefficients (reflected by a significance of $p<0.05$ for all walking conditions) than for maximum DF, which was more dependent on body mass and walking speed. However, for the majority of walking conditions, the regression equations do a fair job of representing the data.

Peak vertical load during the unloading phase of stance was significantly dependent on walking speed ($p<=0.01$) and metabolic rate was significantly dependent on both body mass ($p<=0.062$) and walking speed ($p<=0.012$, apart from the decline condition where $p=0.314$). Additionally, the regression equation for the fast walking condition was significantly dependent on *AIPP* coefficients ($p<=0.026$), which would indicate that they have a greater influence on the peak unloading forces. As mentioned, the fast walking condition has been established as the most optimal when compared to self-selected walking speed in terms of symmetry, gait variability and metabolic cost (see section 5.6.4) and is perhaps more reflective of the subject's natural gait outside the laboratory. However, despite the small contribution of the *AIPP* coefficients in the regression equations for the other walking conditions, their addition to the regression analysis improved the overall fit in all cases.

This regression analysis provides insight into how measures of the mechanical properties of prostheses independent of the amputee (*AIPP*) might be useful in predicting trans-tibial amputee gait performance, which could be used in prescription. However, because of the limited in-vivo data set, it should be emphasised that only a small correlation study has been undertaken to illustrate the concept. As discussed in the following section, it would be extremely difficult to undertake a comprehensive study of the effects of *AIPP* on amputee gait by any means other than simulation.

Table 6.1.1. Maximum dorsiflexion of the CFAM (M_{DF}; Degrees).

Walking Condition	Regression Equation	R^2	F	p
SSWS	$M_{DF} = -1636.645 + 0.059 \times BM + 0.279 \times WS - 1839.668 \times A + 242.690 \times B + 14.645 \times C$	0.787	9.592	0.001
FWS	$M_{DF} = -649.156 + 0 \times BM + 0.193 \times WS - 5018.753 \times A + 55.385 \times B + 5.812 \times C$	0.807	10.858	<0.001
INC	$M_{DF} = 2188.103 + 0.092 \times BM + 0.265 \times WS - 13403.6 \times A - 455.920 \times B - 19.799 \times C$	0.789	9.717	<0.001
DEC	$M_{DF} = -1313.672 + 0.111 \times BM + 0.243 \times WS - 1893.287 \times A + 161.208 \times B + 11.733 \times C$	0.758	8.152	0.001

Table 6.1.2. Maximum plantar flexion of the CFAM (M_{PF}; Degrees).

Walking Condition	Regression Equation	R^2	F	p
SSWS	$M_{PF} = -10001 - 0.031 \times BM + 0.064 \times WS + 32726.854 \times A + 1701.228 \times B + 90.086 \times C$	0.685	3.922	0.036
FWS	$M_{PF} = -11302.1 + 0.004 \times BM + 0.044 \times WS + 36919.137 \times A + 1923.939 \times B + 101.764 \times C$	0.901	16.313	<0.001
INC	$M_{PF} = -9395.905 + 0.106 \times BM + 0.070 \times WS + 31603.001 \times A + 1602.618 \times B + 84.542 \times C$	0.887	14.164	<0.001
DEC	$M_{PF} = -6400.230 - 0.044 \times BM + 0.021 \times WS + 23062.183 \times A + 1031.538 \times B + 57.713 \times C$	0.595	2.643	0.097

Table 6.1.3. Peak vertical ground reaction force on the prosthetic limb during unloading phase of stance (F_{UN}; Newtons).

Walking Condition	Regression Equation	R^2	F	p
SSWS	$F_{UN}=-55.376-0.002\times BM+0.007\times WS+196.763\times A+10.556\times B+0.507\times C$	0.659	4.255	0.021
FWS	$F_{UN}=87.085-0.007\times BM+0.009\times WS-281.686\times A-14.858\times B-0.775\times C$	0.586	3.110	0.054
INC	$F_{UN}=-57.109-0.002\times BM+0.008\times WS+185.598\times A+11.017\times B+0.521\times C$	0.506	2.249	0.122
DEC	$F_{UN}=-177.264+0\times BM+0.008\times WS+592.222\times A+32.635\times B+1.602\times C$	0.814	9.614	0.001

Table 6.1.4. Metabolic Cost of Transport (MCoT; ml O_2/kg/m).

Walking Condition	Regression Equation	R^2	F	p
SSWS	$MCoT=-12.443-0.001\times BM-0.002\times WS+49.182\times A+2.417\times B+0.116\times C$	0.586	3.678	0.027
FWS	$MCoT=2.748-0.001\times BM-0.001\times WS+9.024\times A-0.460\times B-0.021\times C$	0.561	3.319	0.038
INC	$MCoT=0.355-0.002\times BW-0.001\times WS+24.092\times A-0.726\times B+0.003\times C$	0.393	1.681	0.208
DEC	$MCoT=40.820-0.001\times BM-0.003\times WS-108.397\times A-8.025\times B-0.362\times C$	0.723	6.798	0.003

Table 6.1.5. Metabolic Rate (MR; ml O_2/kg/min).

Walking Condition	Regression Equation	R^2	F	p
SSWS	$MR=-2600.146+0.133\times BM-0.058\times WS+8581.248\times A+472.264\times B+23.510\times C$	0.620	4.234	0.017
FWS	$MR=-4097.071-0.078\times BM+0.165\times WS+14049.380\times A+730.049\times B+37.006\times C$	0.909	25.944	<0.001
INC	$MR=-2354.835-0.109\times BM+0.254\times WS+8415.667\times A+393.208\times B+21.353\times C$	0.619	4.219	0.017
DEC	$MR=81.092-0.067\times BM+0.038\times WS+595.276\times A-48.648\times B-0.574\times C$	0.439	2.034	0.140

6.2. The use of *AIPP* in amputee gait simulation

Results from the *AIPP* characterisation and in-vivo gait study provide data that could be used to validate numerical gait simulations. As is clear from the in-vivo results presented in Chapter Five, it is not feasible to undertake a comprehensive experimental study of the relationships between *AIPP* and amputee gait. Because of the number of *AIPP* variables, the design space is too large to be explored by in-vivo experimentation. Therefore, as mentioned in Chapter Two, numerical simulation of amputee gait is essential in order to conduct a comprehensive and systematic investigation of the effects of *AIPP* on amputee gait and hence inform the design process. Such a gait simulation approach would be similar to that developed by Srinivasan et al. (2009) and Zmitrewicz et al. (2007) involving forward dynamic modelling, but would incorporate the comprehensive *AIPP* model of Chapter Three (i.e., normal stiffness, shear stiffness, and normal damping properties). Both of the forward dynamic simulations in the studies by Srinivasan et al. (2009) and Zmitrewicz et al. (2007) modelled amputee gait, however, one significant difference between the two is the method by which the prosthesis was modelled. In the study by Srinivasan et al. (2009) the prosthesis-ground interface was modelled as a rigid (i.e., non-dynamic) roll-over shape, whereas the study by Zmitrewicz et al. (2007) modelled the prosthesis as an articulated ankle joint that

behaved as a visco-elastic torsional spring. Referring to the different types of *AIPP* models discussed in Chapter Two, the model used in the study by Srinivasan et al. (2009) is a roll-over shape model, whereas Zmitrewicz et al. (2007) used a lumped parameter model.

The study by Zmitrewicz et al. (2007) is quite relevant to this study as the prosthetic model used for simulation is entirely reflective of the manner in which the CFAM operates. As described in Chapter Four, the CFAM is essentially an articulated ankle joint in which the PF and DF motions are independently controlled by a specified rotational stiffness. For the simulation in the study by Zmitrewicz et al. (2007) the equation used to calculate the torsion of the prosthetic ankle joint was derived from the *AIPP* characterisation data in the study by Lehmann et al. (1993b). Coincidentally, this is the same study in which the rotational stiffness values were derived to form the four CFAM setups used for in-vivo gait testing. Unfortunately, the study by Zmitrewicz et al. (2007) does not specify which of the three prostheses in the study by Lehmann et al. (1993b) the torsion equation was modelled on, only referring to it as a 'nominal ESAR prosthesis.' Selected kinematic results from the gait simulation are displayed in Figure 6.2.1. Comparative results from the in-vivo gait analysis of this study are displayed in Figure 6.2.2 and 6.2.3. The in-vivo prosthetic side knee kinematics appear to match well in both magnitude and profile with the simulated kinematics. However, the in-vivo prosthetic ankle kinematics from this study display a period of PF following heel-strike, which is not present in the simulated kinematics.

In conclusion, the results from combined *AIPP* characterisation and in-vivo gait studies could be used as a means of validating results from numerical gait simulations that incorporate *AIPP*-based prosthesis models. An improved numerical simulation could build on the studies by Srinivasan et al. (2009) and Zmitrewicz et al. (2007) using the *AIPP* model of Chapter Three which combines the geometric elements of roll-over shape with the visco-elastic properties of lumped parameter models. Therefore, the effects of *AIPP* on both joint kinetics (e.g., forces, moments, powers, and work) and kinematics (e.g., angular displacements) could be accurately represented. This would enable comprehensive studies of the effects of *AIPP* on amputee gait performance, which are not possible through experimental studies because of the size of the design space (too many *AIPP* variables).

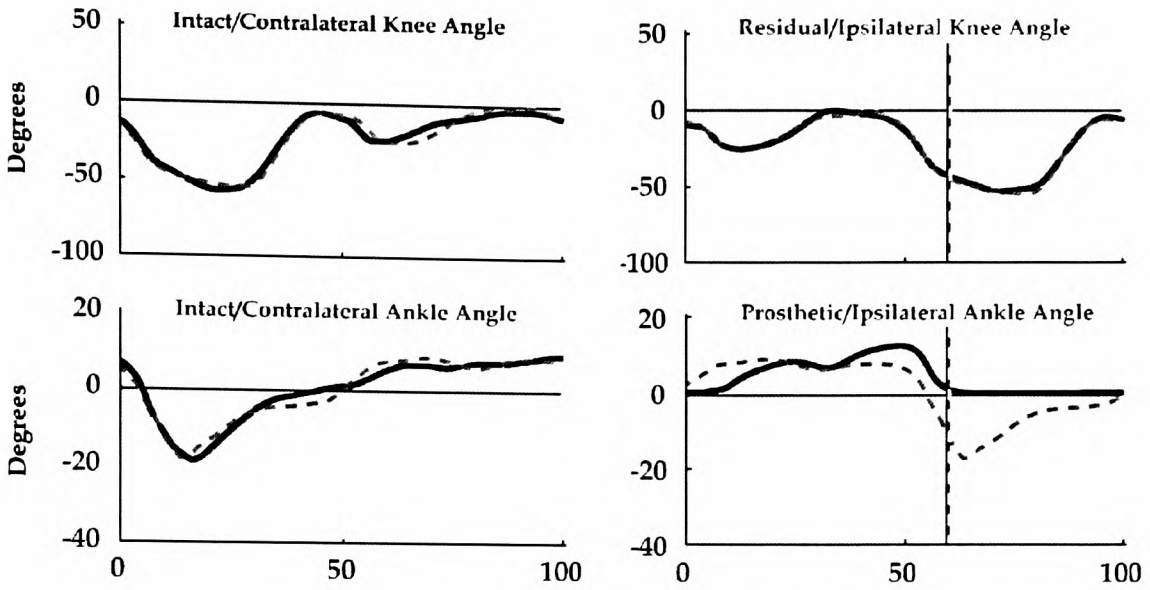

Figure 6.2.1. Select kinematic results from the amputee gait simulation study of Zmitrewicz et al. (2007). Results from the amputee and non-amputee gait simulation are represented as a solid and dashed line, respectively. The solid vertical line denotes the end of the residuum leg stance phase. The x-axis units of each plot are percentage of the residual leg gait cycle.

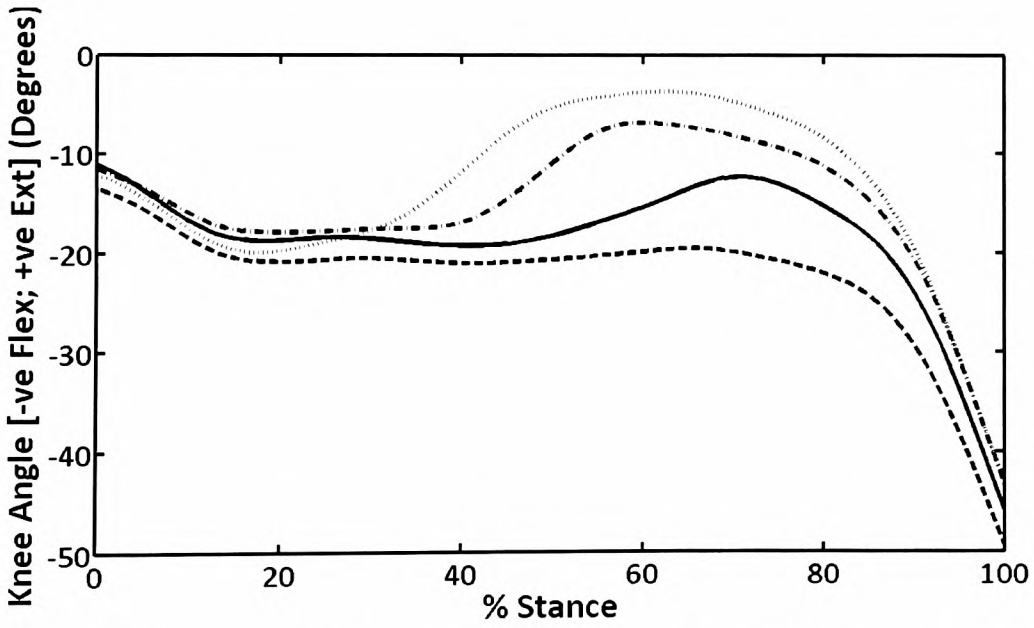

Figure 6.2.2. Single case results of in-vivo prosthetic side knee joint kinematics for four CFAM setups during prosthetic stance (0% and 100% approximating heel-strike and toe-off, respectively); solid line=LOLO, dash line=LOHI, dotted line=HILO, dash-dot line=HIHI.

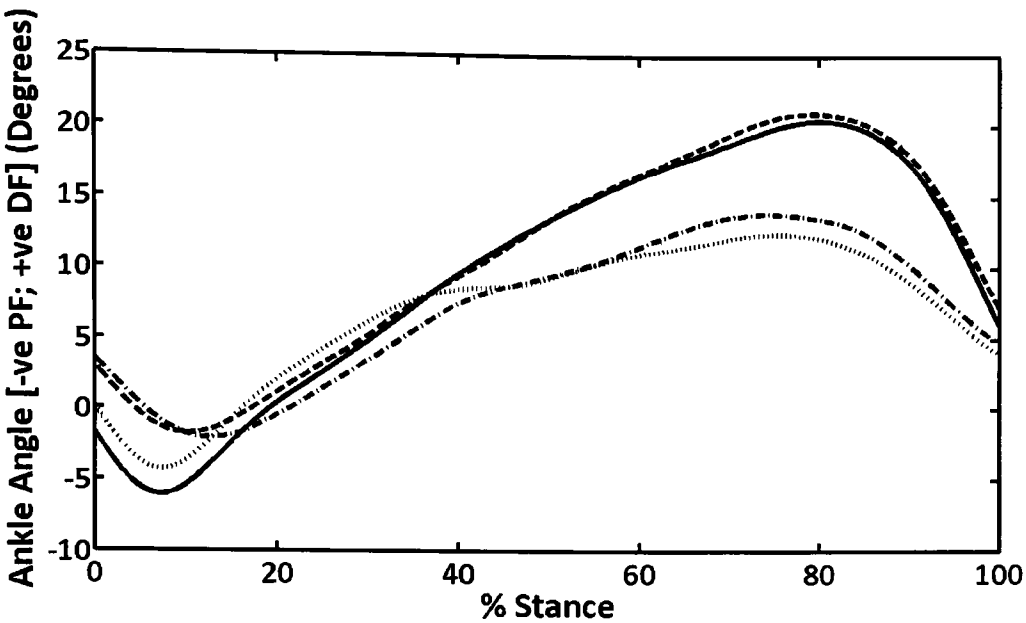

Figure 6.2.3. Single case results of in-vivo prosthetic ankle joint kinematics for four CFAM setups during prosthetic stance (0% and 100% approximating heel-strike and toe-off, respectively); solid line=LOLO, dash line=LOHI, dotted line=HILO, dash-dot line=HIHI.

6.3. Future work

6.3.1. Use of the in-vivo roll-over shape as a predictor of gait measures

The in-vivo roll-over shape is essentially a spatial mapping of the CoP during the stance phase of gait relative to a reference frame attached to the prosthesis, and calculated from kinematic and kinetic measures. Such measures provide useful information on the gait performance of prosthesis users, such as prosthetic ankle ROM, time to foot flat, and repeatability of kinematics and kinetics of the prosthetic limb. Therefore, if such information can be derived from the in-vivo roll-over shape and without collecting data through the use of conventional gait analysis techniques (i.e., motion capture equipment and force plates), this would increase the ease of measuring gait performance and allow measurement in the real world. In this study, motion capture equipment was used to measure the instantaneous distance between the load-cell geometric centre and the ground along the longitudinal axis of the pylon, accelerations of the prosthesis CoM, and angle of the longitudinal axis of the

pylon with respect to the plane normal to the walking surface in order to calculate the in-vivo roll-over shape. However, if other techniques could be used to measure these parameters which did not rely on motion capture equipment and was self-contained within the prosthesis assembly, then this would eliminate the need for all conventional gait analysis equipment for capturing in-vivo roll-over shape.

Consequently, the in-vivo roll-over shape could provide a useful tool for clinical evaluation of gait dynamics and repeatability. For example, a paper by Kendell et al. (2010), established a technique for measuring stability in trans-tibial amputee gait through use of the medial-lateral and anterior-posterior CoP traces under the prosthetic foot. In this study, a pressure insole was inserted between the prosthetic foot and shoe in order to measure the CoP. However, the in-vivo roll-over shape is essentially a CoP trace, which could be measured in the medial-lateral and anterior-posterior direction, and hence provide the information needed for this technique. Additionally, it could be measured with and without the use of footwear, which would not be possible with an insole unless adhered to the prosthetic foot.

The in-vivo roll-over shape provides an indirect means of measuring the gait kinematics and kinetics of the prosthetic limb, as well as the mechanical behaviour of the prosthesis during gait. Table 6.3.1.1 demonstrates through a regression analysis how the in-vivo roll-over shape can be used to predict the time to prosthesis foot flat. For all walking conditions, the difference between time at heel-strike and time at the minimum point of the roll-over curve correlates significantly ($p<0.001$) with the time it takes to achieve foot flat. Time to foot flat has been referred to as a measure of prosthetic stability (Perry et al., 1997) and has been shown in this study to be correlated with step time CV and perceived level of stability. Therefore, the in-vivo roll-over shape could present useful information with which to predict such factors.

Table 6.3.1.1. Correlations between time to foot flat (FF; % Stance) and time to the minimum point of the roll-over curve (M; % Stance) following time at heel-strike as separated by walking condition and grouped over all walking conditions. Conditions are abbreviated as: SSWS (self-selected walking speed on level), FWS (fast walking speed on level), INC (self-selected walking speed on incline), and DEC (self-selected walking speed on decline).

		Regression			Correlation	
Walking Condition	**Regression Equation**	**R^2**	**F**	**p**	**ρ**	**p**
SSWS*	$FF=0.579\times M-1.220$	0.832	74.224	<0.001	0.869	<0.001
FWS	$FF=0.451\times M-0.405$	0.661	29.230	<0.001	0.802	<0.001
INC	$FF=0.683\times M-3.010$	0.830	73.150	<0.001	0.867	<0.001
DEC	$FF=0.611\times M-1.166$	0.841	79.498	<0.001	0.903	<0.001
All Conditions Grouped	$FF=0.556\times M-1.132$	0.741	188.704	<0.001	0.846	<0.001

*The Shapiro-Wilk test revealed that the residual distribution differed from the normal distribution at a significance of p=0.042.

6.3.2. Studies of functional amputee stability

Regarding the general results from this study, it would appear that for this particular population of trans-tibial amputees more focus should be placed on prosthetic designs which optimise functional stability rather than metabolic energy expenditure. Even though forefoot stiffness tended to reduce both metabolic rate and CoT, the subjects were able to accommodate to all of the CFAM setups given a limited amount of acclimation time and maintain their energy expenditure within acceptable limits. Therefore, for such active trans-tibial amputees, it is more important to improve their functional stability rather than reducing their metabolic energy expenditure. However, even though it is reasonable to assume that functional amputee stability is influenced by various factors, such as gait symmetry, proprioception of the residual limb, lower-extremity motor control, muscle strength, and mechanical properties of the prosthesis, the underlying mechanisms of functional amputee stability are still not well understood. Consequently, this limits the

knowledge of predictive factors that might distinguish between fallers and non-fallers among prosthesis users. Even though it has been shown that variability in temporal-spatial gait parameters is correlated with instability and risk of falling in a number of different populations (Hausdorff, 2005), as mentioned previously, such information for amputee populations is rather limited. Once again, the only study which identified a single distinguishing factor in gait variability between transtibial amputee fallers and non-fallers (Vanicek et al., 2009) had significant limitations: this study was limited to only 11 subjects (6 fallers and 5 non-fallers) and they were not matched by age or cause of amputation. Furthermore, the effects of *AIPP* on step time CV and prosthetic limb swing time CV produced conflicting results. For example, low rearfoot stiffness both decreased step time CV, indicating increased stability (Hausdorff et al., 1997; Hausdorff et al., 2001) and increased prosthetic limb swing time CV, indicating reduced stability (Vanicek et al., 2009). Therefore, further investigation with an extended pool of properly matched amputee subjects would likely provide more conclusive results, helping to identify predictive factors of falls in amputees and providing a means of assessing functional stability.

Most importantly, this study only observed the influence of *AIPP* on stability during gait and not on standing. Results indicated that a more flexible prosthetic forefoot, allowing increased dorsiflexion and ankle ROM during the stance phase of gait, generally reduced variability in swing time of the prosthetic limb, indicating an improvement in gait stability. However, a more flexible prosthetic forefoot could have an adverse effect on stability during standing by limiting restriction to forward motion over a stable base of support. The inverse relationship will presumably hold true for a less compliant prosthesis. Further research is required to fully explore these relationships in order to develop prosthetic designs that will assist lower limb amputees in maintaining relative stability throughout all forms of daily activity (i.e., walking, standing, and sit-to-stand).

Therefore, the objectives of future research into functional amputee stability should focus on: 1) identifying key predictive factors that clearly distinguish between transtibial amputee fallers and non-fallers (both retrospectively and prospectively), and 2) investigating the relationship between *AIPP* and user stability during gait, quiet standing and other activities. Further insight into the stability of prosthesis users would assist in identifying amputee

patients who are at risk of falling, help develop rehabilitation programs that could improve functional stability and motor control, and improve prescription guidelines of prosthetic devices that would foster a more stable, and hence safer, gait.

6.3.3. Adaptive trans-tibial prostheses

Although the summary of results in Table 5.7.5.1 gives the impression that one CFAM setup (LOLO) might be suitable for all walking conditions, this is unlikely to be the case in practise. The experimental study was limited to just four walking conditions and four CFAM setups and, therefore, it is not sensible to draw such a strong conclusion. In particular, the incline and decline conditions were on slopes of only 5% grade and more severe slopes would almost certainly require different CFAM setups for best performance. Therefore, it may be appropriate that future designs of prosthetic foot-ankle mechanisms adjust their ankle joint stiffness based on the current walking condition in order to maximise amputee gait performance.

The input variables for an ankle stiffness control system could be kinetics, kinematics, temporal parameters and metabolic measures. Temporal parameters and kinetics could be measured using an integrated load-cell similar to the one used in the ITP of this study. Lower-extremity kinematics could be measured through a combination of accelerometers and goniometers. As discussed earlier, with the appropriate built-in sensors, it may be possible to estimate the in-vivo roll-over shape in real-time. As demonstrated in section 5.3.2, metabolic CoT can be estimated from the physiological cost index, in which metabolic efficiency can be measured using a heart rate monitor. These gait performance measures could be monitored continuously and this information used by a controller to identify the current gait condition and thus set the ankle joint stiffness in order to provide optimal amputee performance.

7. Chapter Seven: Conclusion

This thesis has presented: 1) a new method for the measurement of Amputee Independent Prosthesis Properties (*AIPP*); 2) experimental methods for systematically exploring the effects of *AIPP* on trans-tibial amputee gait performance; and 3) the results of in-vivo testing using the aforementioned methodology. Chapter Two discussed previous methods used to characterise *AIPP* and the problems associated with these methods (e.g., lack of consistency in models and methods used), which make comparison of results very difficult. Essentially, two types of characterisation model have been used in previous research: 1) lumped parameter and 2) roll-over shape. As discussed, both models have their merits. Lumped parameter models are good for characterising mechanical properties, such as stiffness and damping, whereas roll-over shape is good for capturing dynamic geometry including the effects of alignment. The *AIPP* model proposed in this work combines the features of both types of model, thus overcoming the limitations of both types. Chapter Two also introduced a framework for developing improved prosthesis designs, in which the most effective *AIPP* could be identified through a combination of *AIPP* characterisation, human performance studies, and amputee gait simulation.

Chapter Three described the methodology developed for measuring the *AIPP* of the combined trans-tibial prosthetic components distal to the socket (i.e., pylon and foot-ankle mechanism) which attempts to address the limitations of previous methods of *AIPP* characterisation. This was accomplished by developing the Salford *AIPP* model, a modified version of the original roll-over shape model (Hansen et al., 2000; Knox, 1996) which incorporates aspects of lumped parameter models. A custom test-rig was built in order to measure the parameters of this model, which include: 1) dynamic geometry (roll-over shape), 2) normal stiffness, 3) shear stiffness, and 4) normal damping at several points along the plantar surface of the prosthetic foot, corresponding to a range of pylon angles reflective of those incurred during the stance phase of gait. This improved *AIPP* roll-over shape model provides comprehensive information on the mechanical properties of the foot which are relevant to 1) experimental studies of the correlations between *AIPP* and gait performance, and 2) prosthesis model implementation for gait simulation. An additional feature of the

test-rig is that all prosthetic components within the test-rig (i.e., 3-axis load-cell, pylon, and foot) can be directly attached to a socket in order to form the Instrumented Trans-tibial Prosthesis (ITP) used during human performance testing. Therefore, a method for seamless transition between *AIPP* characterisation and in-vivo gait measurement has been established. This method allows for the patient-specific alignment of the prosthetic components distal to the socket to be maintained during *AIPP* characterisation, as alignment has a direct effect on the *AIPP* roll-over curves. As demonstrated in Chapter Four, the ITP is capable of measuring the forces and moments applied to the distal end of the socket in three axes, kinematics of the prosthetic limb (using markers attached to the ITP with a camera system) , and hence the in-vivo roll-over shape.

Chapter Four described the methods developed for undertaking a systematic study of the effects of *AIPP* on amputee performance using an approach which is decoupled from the use of commercial devices. The motivation for this arose from the inconclusive results of previous human performance studies that have often failed to clearly identify the biomechanical and physiological advantage of one prosthetic design over another. Furthermore, the vast majority of these studies did not include *AIPP* characterisation of the prostheses used during in-vivo testing, and therefore did not provide information on the effects of prosthesis properties. The protocol for the human performance study was designed to obtain biomechanical (i.e., kinetics, kinematics, and temporal-spatial gait parameters), physiological (i.e., metabolic energy expenditure), and subjective (i.e., ratings on comfort, exertion, and stability) performance measures during four walking conditions reflective of those encountered during daily activity: self-selected walking speed (SSWS) on the level, fast walking speed on the level, SSWS on a 5% grade incline, and SSWS on a 5% grade decline. A Custom Foot-Ankle Mechanism (CFAM) was developed to be used during this human performance study which allowed for independent modulation of the forefoot and rearfoot stiffness of the prosthetic foot. The CFAM was based on a single-axis ankle joint and the adjustable positions of two linear compression springs relative to the pivot determined the forefoot and rearfoot stiffnesses. Four CFAM setups were tested during each of the four walking conditions described previously. The four setups were based on a full-factorial design using high and low forefoot stiffness and high and low rearfoot stiffness. The

AIPP of all four setups (stiffness combinations) were measured in the test-rig prior to the in-vivo testing.

Chapter Five then discussed the results from the human performance testing (i.e., biomechanical, physiological, and subjective feedback), with particular focus on where trends were identified to clearly demonstrate the effects of forefoot and rearfoot stiffness on various measures of gait performance. Additionally, the effects of walking condition and CFAM setup on measures specifically related to amputee comfort, exertion, and stability during gait were discussed. Results from this combined study offer a more comprehensive understanding of how *AIPP* directly influence certain measures of amputee gait performance and how such information can be used to inform prescription of prosthetic components, and as validation for amputee gait simulation. As described in Chapter Two, the first stage of an effective design process for creating improved prosthetic components is the identification of desired *AIPP* through combined experimental studies such as that presented in Chapter Four and through comprehensive exploration of the *AIPP* design space and *AIPP* optimisation via amputee gait simulation. Chapter Six discussed correlations between *AIPP* and gait performance, concepts in amputee gait simulation, and ideas for future work. The future work section included discussion on the potential for using the in-vivo roll-over shape for prediction of gait measures, extended work on investigating amputee stability during various activities, and the concept of an adaptive prosthesis that modifies ankle joint stiffness properties based on the current gait condition in order to maximise amputee gait performance.

7.1. Original contributions

The major and original contributions of this work can be summarised as follows:

1. A new methodology for characterising the *AIPP* of the combined trans-tibial prosthetic components distal to the socket, which includes the new Salford *AIPP* model and a new *AIPP* test-rig.
2. A Custom-Foot Ankle Mechanism (CFAM) for exploring the influence of *AIPP* on amputee gait performance decoupled from the use of commercial devices.

3. Methods for investigating the effects of *AIPP* on amputee gait performance using the CFAM and an instrumented trans-tibial prosthesis (ITP).
4. Comprehensive in-vivo results on how *AIPP* affect amputee gait performance.

Appendix A

A.1. Calibration of the six-channel load-cell

The load-cell was independently calibrated in-house to account for measurement differences between those recorded during the calibration procedure performed by the manufacturer and those recorded within the University of Salford human performance laboratory. The test-rig used for calibration is displayed in Figure A.1.1. Calibration was performed for all force and moment components of the load-cell apart from the moment around the local z-axis (i.e., axis aligned with the longitudinal axis of the pylon).

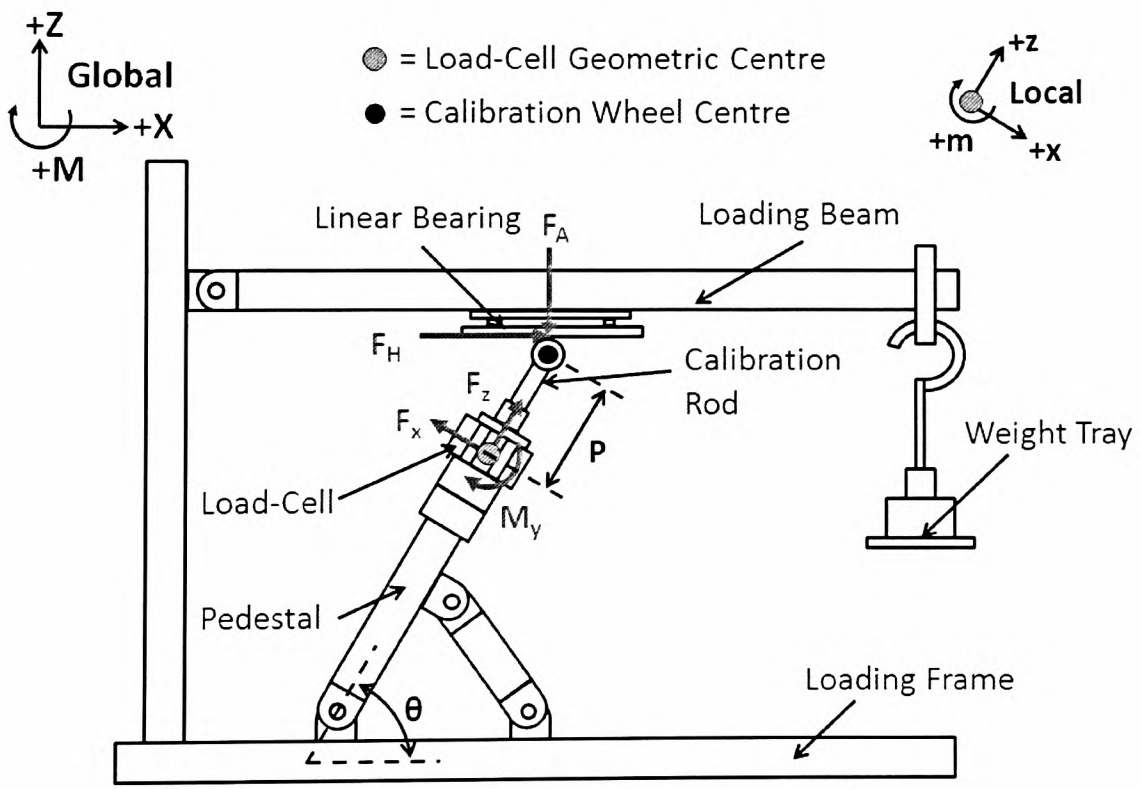

Figure A.1.1. Test-rig used for the calibration procedure. All forces and moments (F_z, F_x, M_y, F_A, and F_H) are shown to be acting on the load-cell. The shear force, F_H, is assumed to be negligible (F_H =0) due to the interface between the linear bearing and free wheel of the calibration rod. P is the distance between the load-cell geometric centre and calibration wheel centre.

The calibration process for the forces and moments in one plane is performed in three steps:

1. *Calibration of force along local z-axis, F_z*

Two adaptors were connected to each end of the load-cell to ensure that all loads were passing through the load-cell with none applied to its aluminium outer-casing. The load-cell was placed on level ground with the positive local z-axis pointing toward the ceiling and a systematic increase of known loads from 0 to 80 kg with increments of 10 kg was applied to the top adaptor. A linear best fit was applied to the data of known vertical force, F_z' , versus recorded vertical force, F_z, as calculated by the manufacturer's decoupling matrix. The resulting equation and associated coefficients, A and C, of the linear best fit served as the new calibration equation as shown:

$$F_z' = A \times F_z + C \tag{A.1}$$

where the true force, F_z' , is calculated from the load-cell reading, F_z.

2. *Calibration of force along local x-axis, F_x*

Following calibration of F_z, the load-cell was than assembled within the test-rig as shown in Figure A.1.1. The local z-axis is aligned with the longitudinal axis of the pedestal and the local x-z plane is aligned with the global x-z plane. A calibration rod with a free rotating wheel at the end was attached to the load-cell. Through use of the free rotating wheel and the linear bearing of the test-rig, only vertical forces were being applied at one single point (at the outer diameter of the wheel) with negligible shear forces. With the test-rig linear bearing aligned with the global x-axis (verified with a spirit level), the load-cell was then loaded through the calibration rod at four known pedestal angles with respect to the global x-axis (θ), ranging from 68 to 90 degrees with average increments of 7 degrees. At each loading angle, the known force, F_x' , could be calculated as follows:

$$F_x' = F_z'' + \tan\theta \tag{A.2}$$

where F_z' is the known force resulting from the calibration equation in step one. A linear best fit was applied to the data of known force, F_x', versus recorded force, F_x, as calculated by the manufacturer's decoupling matrix. Similar to step one, the resulting equation from this linear best fit was used as the calibration equation to solve for the true force.

3. *Calibration of moment acting on load-cell along y-axis, M_y*

Using the same data as recorded in step two, the known moment along the local z-axis acting at the load-cell geometric centre for each loading angle, M_y', as produced by the applied force, F_A, was calculated as follows:

$$M_y' = P \times \cos\theta \times F_A \tag{A.3}$$

where $F_A = \sqrt{F_x' + F_z'}$ and P is the distance from the load-cell geometric centre to the calibration wheel centre (see Figure A.1.1). A linear best fit was applied to the data of known moment, M_y', versus recorded moment, M_y, as calculated by the manufacturer's decoupling matrix. Similar to step one, the resulting equation from this linear best fit was used as the calibration equation to solve for the true moment.

In order to calibrate the force along the local y-axis, F_y, and moment along the local x-axis, M_x, steps 1-3 were performed with the load-cell rotated 90 degrees along the local z-axis such that the local y-z plane aligned with the global x-z plane. Table A.1.1 summarises the calibration equation coefficients of each load-cell component as derived.

Table A.1.1. Coefficients of the calibration equations used to solve for the true force or moment value ([true value] = A × [load-cell reading value] + C).

	Load-Cell Component				
Equation Coefficient	F_z	F_x	F_y	M_y	M_x
A	1.07	1.17	1.10	1.02	1.00
C	0.91	2.16	13.05	-0.61	2.53

Appendix B

B.1. Potential modes of failure and danger during in-vivo gait analysis

B.1.1. Potential modes of failure of the CFAM

Scenario 1: Bolts fastening the central joint to the upper and lower aluminium profiles loosened and separated

The central joint was attached to the lower profile through a single threaded bolt and fitted into an extruded profile to ensure it would not rotate relative to the lower profile. This single threaded bolt was securely tightened and Loctite was inserted into the threads to ensure it did not loosen. The central joint was attached to the upper profile by bolting into an aluminium sliding block that fit into a channel of the upper profile. The sliding block was secured down through a clamping mechanism when the threaded bolt passing through the central joint was tightened. This sliding block is the width of the channel, restricting any potential for rotation relative to the upper profile. Additionally, the threaded bolt which holds the central joint in place was securely tightened and Loctite was inserted into the threads to ensure it did not loosen. Both the upper and lower profile were permanently adhered to the central joint with Araldite[26].

Scenario 2: Rear spring translated past the heel end of the lower profile during walking and detached from the foot

The rear (and front) spring were held in place through a post which was secured to the upper profile through a clamping mechanism. The springs were permanently adhered to the inner post with Araldite.

[26] Araldite, Huntsman Advanced Materials Co. Ltd., Hong Kong

Scenario 3: The male pyramid adaptor which secured the test-foot to the pylon rotated and separated

The Otto Bock adaptor which was attached to the female end of the pylon was secured to the CFAM by bolting into an aluminium sliding block that fit into a channel of the upper profile. The sliding block was secured down through a clamping mechanism when the threaded bolt passing through the adaptor was tightened. This sliding block is the width of the channel, restricting any potential for rotation relative to the upper profile. An additional threaded bolt was run through the adaptor and attached to the upper profiles through a similar sliding block/clamping mechanism to ensure that no rotation of the adaptor occurred relative to the upper profile. Additionally, the threaded bolts which held these components in place were securely tightened and Loctite was inserted into the threads to ensure they did not loosen.

B.1.2. Potential modes of failure of the ITP

Scenario 1: Adaptor which attached the load-cell to the pylon detached from the load-cell mounting surface

A custom adaptor was built that secured the distal surface of the load-cell to the pylon. The pylon was attached to this adaptor through a standard tube-clamp mechanism which did not pose any threat of detaching. Additionally, the custom adaptor was secured to the distal surface of the load-cell through a series of six of threaded bolts and did not pose any threat of detaching. However, the tube-clamp was attached to the custom adaptor through a single threaded bolt that passes through a washer in the tube-clamp and the custom adaptor. At the end of the threaded bolt are two nuts. When the nuts were tightened, a clamping mechanism secured the tube-clamp in place. Two nuts were used to ensure that axial rotation produced during walking did not loosen the clamping mechanism, which would have resulted in detachment of the tube clamp from the custom

adaptor (and hence load-cell). Loctite was also applied to the threads of this central threaded bolt to further ensure that it would not loosen from the nuts. A small rod attached firmly to the custom adaptor was inserted through one of the holes of the tube-clamp, which restricted any rotation of the tube clamp relative to the custom adaptor.

B.1.3. Potential danger during walking on the treadmill

Scenario 1: Subject experienced a fall whilst walking on the treadmill

The subjects walked on the treadmill during four different conditions: self-selected speed on level surface, fast walking speed on level surface, self-selected speed on an inclined surface, and self-selected speed on a declined surface. Thus, there was potential of falling during any of these conditions as the subject might not have been familiar with treadmill walking and the ITP they were using during testing. To increase familiarity with the treadmill and prosthesis, the subject was provided with twenty minutes of treadmill walking during the first visit with their own prosthesis. During the second and third session of testing, ten minutes of walking with the custom prosthesis were provided for each of the four test-foot conditions. If the subject wandered too far back on the treadmill, a tethered safety cord which was attached between the subject and the treadmill would detach from the treadmill, forcing the treadmill belt to come to a gradual stop. If the subject fell, padded gym mats were placed around the treadmill (sides and back) to soften the impact with the ground. Furthermore, the volume transducer which was attached to the gas analyser unit via a plastic tube, was press fit into the silicon mask worn by the subject and would detach immediately if a sufficient pull was applied. Additionally, a cable was attached from the ITP load-cell to the central computer and power supply. Approximately 1.2 meters of length of cable were provided between the load-cell and computer/power supply, and thus eliminated any potential of the subject's movement being restricted by the stationary equipment.

Appendix C

C.1. In-vivo force and moment calculations

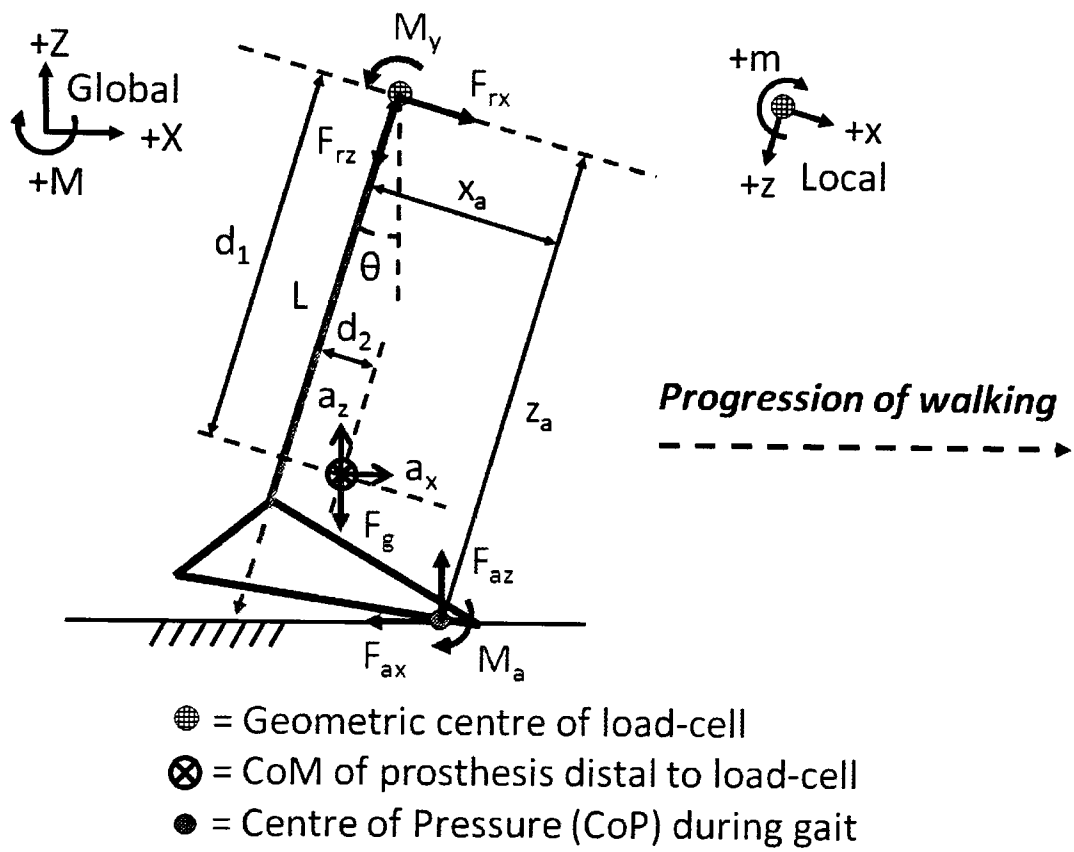

Figure C.1.1. Free-body diagram of the ITP during gait in the sagittal plane. All forces are shown to act on the ITP. The local axis shown in this figure relates to the setup for a left amputee. For a right amputee setup, the load-cell is rotated 180° along the local z-axis, thereby switching the direction of +m and +x in the local reference frame.

Terms of the free-body diagram in Figure C.1.1 are defined below:

M_y Moment around local y-axis applied by load-cell (as measured by load-cell with same sign)

F_{rz} Force in local z-axis applied by load-cell (resolved forces [see Appendix C.2] as measured by load-cell with sign switched)

F_{rx} Force in local x-axis applied by load-cell (resolved forces [see Appendix C.2] as measured by load-cell with sign switched)

θ Angle of local z-axis with respect to the plane normal to the walking surface plane

d_1 Distance in local z-axis from geometric centre of the load-cell to the CoM of the ITP components distal to the load-cell

d_2 Distance in local x-axis from geometric centre of the load-cell to the CoM of the ITP components distal to the load-cell

L Magnitude distance between geometric centre of load-cell and intersection point of the local z-axis vector with the walking surface plane

a_z Acceleration of the CoM of the ITP components distal to the load-cell in global z-axis

a_x Acceleration of the CoM of the ITP components distal to the load-cell in global x-axis

F_g Force due to gravity acting on the ITP components distal to the load-cell (mass (m) × acceleration due to gravity)

M_a Moment around global y-axis acting on the ITP at the CoP during gait ($M_a = 0$)

F_{az} Ground reaction force in global z-axis acting on the ITP at the CoP during gait

F_{ax} Ground reaction force in global x-axis acting on the ITP at the CoP during gait

z_a Distance in local z-axis from geometric centre of the load-cell to the CoP

x_a Distance in local x-axis from geometric centre of the load-cell to the CoP

The instantaneous ground reaction forces (F_{az} and F_{ax}) and CoP of the prosthetic foot in the local reference frame (x_a and z_a) were calculated with the following equations:

$$F_{ax} = F_{rx}\cos\theta - F_{rz}\sin\theta - m \times a_x \,, \tag{C.1}$$

$$F_{az} = F_{rx}\sin\theta + F_{rz}\cos\theta + F_g + m \times a_z \,, \tag{C.2}$$

$$z_a = L - x_a \times \tan\theta \,, \quad \text{and} \tag{C.3}$$

$$x_a = \frac{\begin{pmatrix} I_{com} \times \alpha + M_y + F_{rz} \times d_2 - F_{rx} \times d_1 - F_{ax} \times \cos\theta \times L + F_{ax} \times \cos\theta \times d_1 \\ + F_{ax} \times \sin\theta \times d_2 - F_{az} \times \cos\theta \times d_2 - F_{az} \times \sin\theta \times L + F_{az} \times \sin\theta \times d_1 \end{pmatrix}}{\left(-F_{ax} \times \cos\theta \times \tan\theta + F_{ax} \times \sin\theta - F_{az} \times \cos\theta - F_{az} \times \sin\theta \times \tan\theta\right)}, \tag{C.4}$$

where I_{CoM} is the moment of inertia of the ITP components distal to the load-cell around the CoM, m is the mass of the ITP components distal to the load-cell, and α is the angular acceleration of the ITP as defined by the second derivative of the angle between local z-axis with the global z-axis.

Following completion of human performance testing, the moment of inertia of the ITP components distal to the load-cell (i.e., pylon-load-cell adaptor, pylon, and CFAM) about the load-cell geometric centre was measured in the sagittal and coronal plane using a pendulum mechanism. The ITP was secured in the pendulum at the load-cell geometric centre, held at a 45 degree angle, and then released. The time required for one oscillation was then recorded and averaged over ten trials. This time (T) was used in the following equation to calculate the I_{CoM} :

$$I_{CoM} = (m \times a_g \times H \times T^2)/(4\pi^2) - (m \times H^2) \quad \text{(C.5)}$$

where a_g is the acceleration due to gravity and H is the distance between the load-cell geometric centre and the centre of mass of the ITP components distal to the load-cell. The moment of inertia about the load-cell geometric centre (I_{Geo}) and the I_{CoM} for each subject's setup are displayed in Table C.1.1.

Table C.1.1. ITP moment of inertia around the load-cell geometric centre (I_{Geo}) and centre of mass of the ITP components distal to the load-cell (I_{CoM}) in units of kg·m^2. Each subject's prosthetic setup differed only in the length of the pylon.

	Subject Number	1	2	3	4	5
Sagittal Plane	I_{Geo}	0.091	0.063	0.064	0.081	0.081
	I_{CoM}	0.018	0.016	0.014	0.020	0.018
Coronal Plane	I_{Geo}	0.089	0.058	0.059	0.075	0.077
	I_{CoM}	0.016	0.010	0.009	0.014	0.014

C.2. Assembly of load-cell and socket within ITP for in-vivo gait analysis

In order to allow for attachment and alignment adjustments of the ITP components distal to the load-cell during fitting, the Otto Bock female pyramid adaptor was aligned with the sagittal and coronal planes. Consequently, the load-cell was rotated 15° in the local z-axis as displayed in Figure C.2.1.

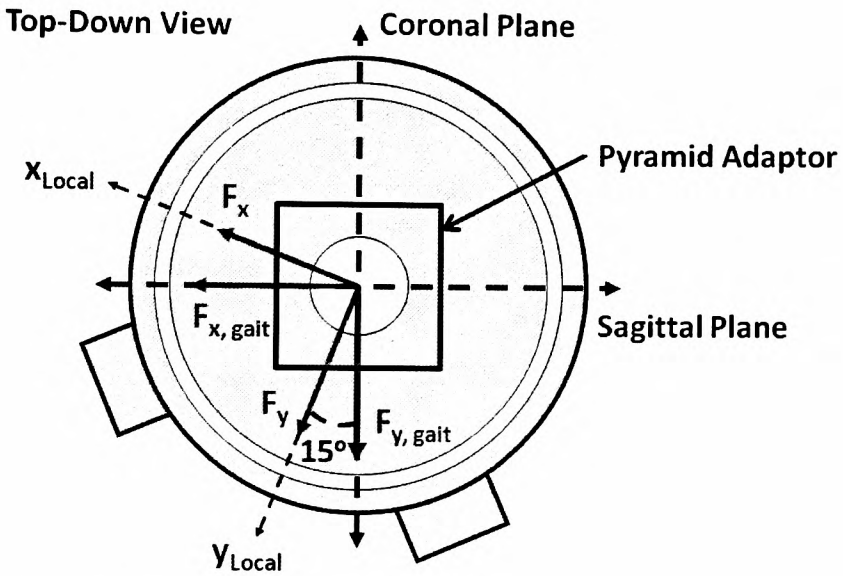

Figure C.2.1. Load-cell rotation during in-vivo testing.

For the calculations described in Appendix C.1, the load-cell force and moment measurements are assumed to be aligned with the sagittal (i.e., plane of walking progression) and coronal plane. Therefore, the load-cell forces F_x and F_y and moments M_x and M_y were resolved through the following equations in order to calculate forces and moments within the sagittal ($F_{x,gait}$ *and* $M_{y,gait}$) and coronal ($F_{y,gait}$ *and* $M_{x,gait}$) planes:

$$F_{x,gait} = F_x \cos(15°) + F_y \sin(15°) , \quad (C.6)$$

$$F_{y,gait} = -F_x \sin(15°) + F_y \cos(15°) , \quad (C.7)$$

$$M_{x,gait} = M_x \cos(15°) + M_y \sin(15°) \text{ , and} \quad (C.8)$$

$$M_{y,gait} = -M_x \sin(15°) + M_y \cos(15°) \quad (C.9)$$

Appendix D

D.1. NHS National Research Ethics Service ethical approval letter

Tameside & Glossop Local Research Ethics Committee

Room 181

Gateway House

Piccadilly South

Manchester

M60 7LP

Telephone: 0161 237 2336

Facsimile: 0161 237 2383

23 May 2008

Mr Matthew Major

PhD Student

University of Salford

Brian Blatchford Building

Frederick Rd

Salford

M66PU

Dear MR Major

Full title of study: **Investigation into the effects of the mechanical properties of trans-tibial prostheses on the biomechanical and physiological performance of the user.**

REC reference number: **08/H1013/19**

Thank you for your letter of 20 May 2008, responding to the Committee's request for further information on the above research and submitting revised documentation.

The further information has been considered on behalf of the Committee by the Chair.

Confirmation of ethical opinion

On behalf of the Committee, I am pleased to confirm a favourable ethical opinion for the above research on the basis described in the application form, protocol and supporting documentation as revised.

Ethical review of research sites

The Committee has designated this study as exempt from site-specific assessment (SSA). There is no requirement for other Local Research Ethics Committees to be informed or for site-specific assessment to be carried out at each site.

Conditions of the favourable opinion

The favourable opinion is subject to the following conditions being met prior to the start of the study.

Management permission or approval must be obtained from each host organisation prior to the start of the study at the site concerned.

Management permission at NHS sites ("R&D approval") should be obtained from the relevant care organisation(s) in accordance with NHS research governance arrangements. Guidance on applying for NHS permission is available in the Integrated Research Application System or at http://www.rdforum.nhs.uk.

Approved documents

The final list of documents reviewed and approved by the Committee is as follows:

Document	*Version*	*Date*
Application	5.5	13 March 2008
Investigator CV		13 March 2008
Protocol	1	13 March 2008
Protocol	2	20 May 2008
Participant Information Sheet	2	20 May 2008
Participant Consent Form	1	13 March 2008
Response to Request for Further Information		20 May 2008
reminder letter	1	20 May 2008
Participant Identification Sheet	2	20 May 2008
Indemnity arrangements		13 March 2008
CV - Dr Laurence Kenney		13 March 2008

Statement of compliance

The Committee is constituted in accordance with the Governance Arrangements for Research Ethics Committees (July 2001) and complies fully with the Standard Operating Procedures for Research Ethics Committees in the UK.

After ethical review

Now that you have completed the application process please visit the National Research Ethics Website > After Review

You are invited to give your view of the service that you have received from the National Research Ethics Service and the application procedure. If you wish to make your views known please use the feedback form available on the website.

The attached document "After ethical review – guidance for researchers" gives detailed guidance on reporting requirements for studies with a favourable opinion, including:

- Notifying substantial amendments
- Progress and safety reports
- Notifying the end of the study

The NRES website also provides guidance on these topics, which is updated in the light of changes in reporting requirements or procedures.

We would also like to inform you that we consult regularly with stakeholders to improve our service. If you would like to join our Reference Group please email referencegroup@nres.npsa.nhs.uk.

08/H1013/19	**Please quote this number on all correspondence**

With the Committee's best wishes for the success of this project

Yours sincerely

Dr Lorraine Lighton

Chair

Email: carol.ebenezer@northwest.nhs.uk

Enclosures: "After ethical review – guidance for researchers"

Copy to: *Dr Max Pilotti*

D.2. Patient consent form

Directorate of Prosthetics & Orthotics
University of Salford
Brian Blatchford Building
Salford M5 4WT

Matthew Major
Tel: 0161 295 2017
E-mail: m.j.major@pgr.salford.ac.uk

CONSENT FORM

Title of Project: Investigation into the effects of prosthesis properties on amputee gait.

Name of Researchers: Mr. Matthew Major, Prof. David Howard, Dr. Martin Twiste, Dr. Laurence Kenney

Please initial box

I confirm that I have read and understand the information sheet dated, for the above study and have had the opportunity to ask questions. ○

I understand that my participation is voluntary and that I am free to withdraw at any time, without giving any reason, without my medical care or legal rights being affected. ○

I understand that sections of any of my medical notes may be looked at by responsible individuals from my limb fitting centre or from regulatory authorities where it is relevant to my taking part in research. I give permission for these individuals to have access to my records. ○

I agree that the researcher may withdraw me from the study in the interests of my health or welfare. ○

I have been informed of any compensation arrangements that have been made. ○

I understand that my participation in this study is conditional upon the agreement of my consultant and I give permission for the researcher of this study to contact my consultant. ○

I have had enough time to think about the study, talk to relatives and friends about it and I agree to take part in the above study. ○

Name of Patient	Date	Signature
Name of Person taking consent (If different from researcher)	Date	Signature
Researcher	Date	Signature

1 for patient; 1 for researcher; 1 to be kept with hospital notes

Please rate your perceived level of comfort while walking during each test (how painful is the activity?)

Normal Walking		Fast Walking		Incline Walking		Decline Walking	
1	No pain at all and very comfortable	1	No pain at all and very comfortable	1	No pain at all and very comfortable	1	No pain at all and very comfortable
2		2		2		2	
3		3		3		3	
4		4		4		4	
5		5		5		5	
6		6		6		6	
7		7		7		7	
8		8		8		8	
9		9		9		9	
10	Unbearable discomfort	10	Unbearable discomfort	10	Unbearable discomfort	10	Unbearable discomfort

Setup: 1 2 3 4

Figure D.3.1. Visual Analogue Scale for perceived level of comfort.

Please rate your perceived exertion while walking during each test (how strenuous is the activity?)

Normal Walking	Fast Walking	Incline Walking	Decline Walking
1 No exertion at all	1 No exertion at all	1 No exertion at all	1 No exertion at all
2	2	2	2
3	3	3	3
4	4	4	4
5	5	5	5
6	6	6	6
7	7	7	7
8	8	8	8
9	9	9	9
10 Maximal exertion	10 Maximal exertion	10 Maximal exertion	10 Maximal exertion
			Setup: 1 2 3 4

Figure D.3.2. Visual Analogue Scale for perceived level of exertion.

Please rate your perceived stability while walking for each test (how steady and confident do you feel?)

Normal Walking		Fast Walking		Incline Walking		Decline Walking	
1	Very unsteady and at immediate risk of falling	1	Very unsteady and at immediate risk of falling	1	Very unsteady and at immediate risk of falling	1	Very unsteady and at immediate risk of falling
2		2		2		2	
3		3		3		3	
4		4		4		4	
5		5		5		5	
6		6		6		6	
7		7		7		7	
8		8		8		8	
9		9		9		9	
10	Completely Stable and Confident	10	Completely Stable and Confident	10	Completely Stable and Confident	10	Completely Stable and Confident

Setup: 1 2 3 4

Figure D.3.3. Visual Analogue Scale for perceived level of stability.

Appendix E

E.1. Retro-reflective marker list for in-vivo gait analysis testing

The fifty-one markers used during testing (5 plates, 24 individual body markers, 3 load-cell, and 4 treadmill) were as follows:

1. Pelvis (*10 markers*): sacrum marker plate, sound and amputated side anterior superior iliac spine, posterior superior iliac spine, iliac crest;
2. Upper Leg and Knee (*14 markers*): sound and amputated side greater trochanter, thigh marker plate, and the lateral and medial femoral condyles;
3. Lower Leg (*8 markers*): shank marker plate and socket marker plate;
4. Sound Foot and Ankle (*6 markers*): lateral and medial malleoli, posterior aspect of the shoe where the heel is located, and the dorsal aspect of the shoe at the location of the navicular, and the first and fifth tarsal-metatarsal joint;
5. Prosthetic Foot and Ankle (*6 markers*): lateral and medial side of the central joint, posterior surface to represent the heel, anterior-laterally and anterior-medially, and on the dorsal aspect of the platform between the two anterior markers and the central joint;
6. Miscellaneous markers (*7 markers*): Three on the load-cell, four on rigid top surface of treadmill that is approximately 19 millimetres superior to the treadmill belt (with a 110 kilogram load placed on top of belt to fully compress treadmill suspension).

Following the static trial, 16 markers were removed: sound and amputated side iliac crest, anterior superior iliac spine, posterior superior iliac spine, greater trochanter, lateral and medial femoral condyles, and lateral and medial malleoli.

Appendix F

F.1. Box plots and statistical results of the human performance study

The results of the in-vivo study are reported as follows: Biomechanical measures (F.1.1 – F.1.20), physiological measures (F.1.21 – F.1.22), and subjective measures (F.1.23 – F.1.25). Plots showing the descriptive statistics that summarise the group's data are provided for the biomechanical, physiological, and subjective measures of each CFAM setup and grouped by walking condition (self-selected walking speed on level, fast walking speed on level, self-selected walking speed on 5% incline and self-selected walking speed on 5% decline). Illustrative data for the in-vivo roll-over shape are shown for one representative subject. As indicated in Chapter Four, the CFAM setups are abbreviated as seen in Table F.1.1. Data for each CFAM setup as separated by walking condition are presented as box plots. The features of the plots are explained in Figure F.1.1.

Table F.1.1. CFAM setup abbreviations.

Forefoot Stiffness	Rearfoot Stiffness	Foot Setup
LO	LO	*LOLO*
LO	HI	*LOHI*
HI	LO	*HILO*
HI	HI	*HIHI*

Missing data and outliers

One subject's gait data (subject 5) for the HIHI CFAM setup has been removed from analysis for all walking conditions as the subject was observed to have held the front handrail of the treadmill. This behaviour has been shown to significantly affect gait parameters (Owings and Grabiner, 2004). For calculation of maximum knee flexion during the stance phase of gait, if a peak knee value was not identified between the events of heel-strike and toe-off, this subject's data point for the corresponding CFAM setup and walking condition was excluded from the data set presented in the box plot. Similarly, if either a maximum braking force

(identified as a negative magnitude) or maximum propulsive force (identified as a positive magnitude) was not identified, the data point for this subject was excluded from the data set. Furthermore, a single subject's data is missing from all force plots for CFAM setups LOLO and HILO as force data could not be recorded due to a hardware fault.

Outliers within a data set were identified as values which were located a distance from the edges of the inter-quartile range box (i.e., lower or upper quartile) equal to or greater than 1.5 times the inter-quartile range and are identified as shown in Figure F.1.1. Outliers denoted by a circle (O) are located a distance from the inter-quartile range box between 1.5 and 3.0 times the inter-quartile range, and outliers denoted by an asterisk (*) are located at a distance equal to or greater than 3.0 times the inter-quartile range. Outlier data points were included in calculation of the median, upper and lower quartile values and used in the inferential statistical analysis.

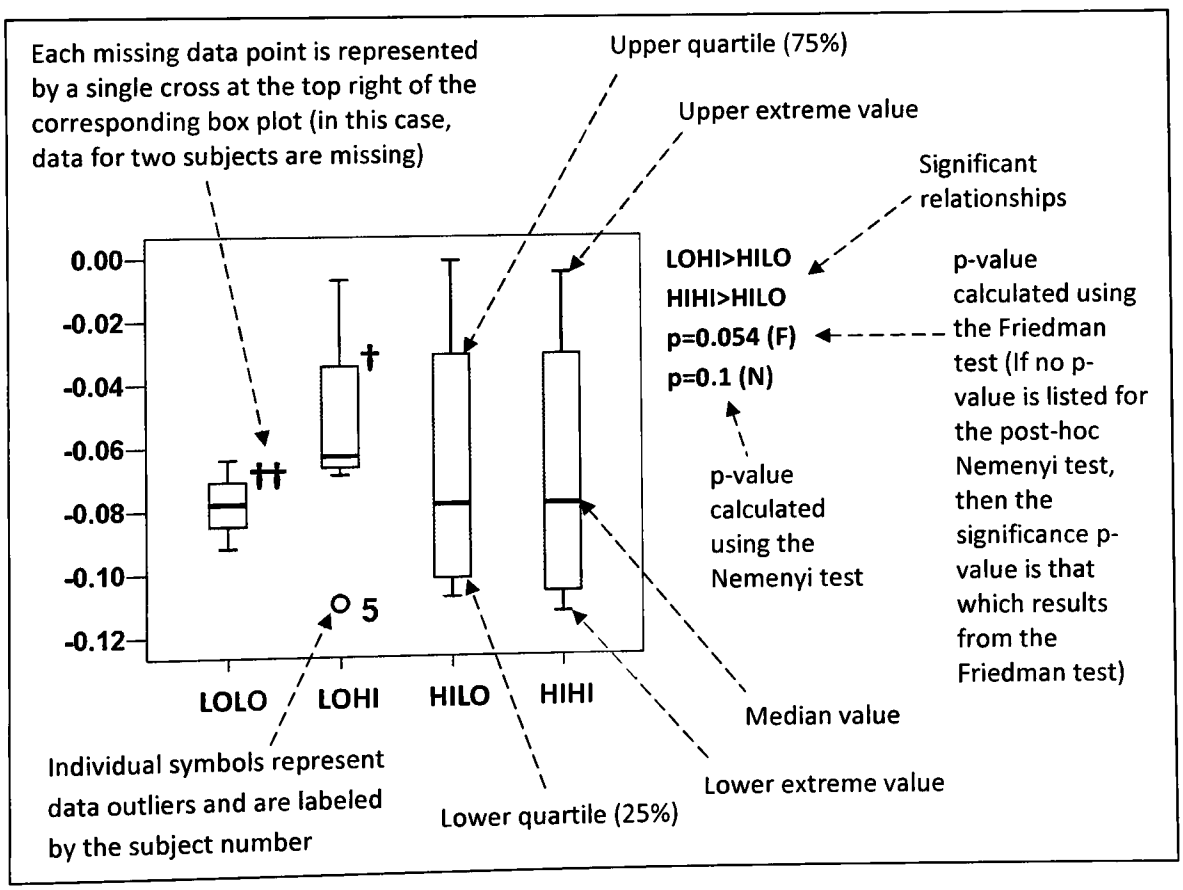

Figure F.1.1. Box plot legend.

F.1.1. Peak vertical ground reaction force on the prosthetic limb during loading phase of stance (x Body Weight)

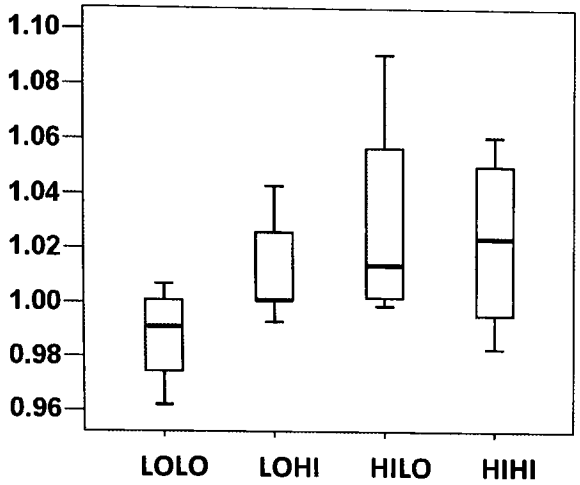

Figure F.1.1.1. Self-selected walking speed on level.

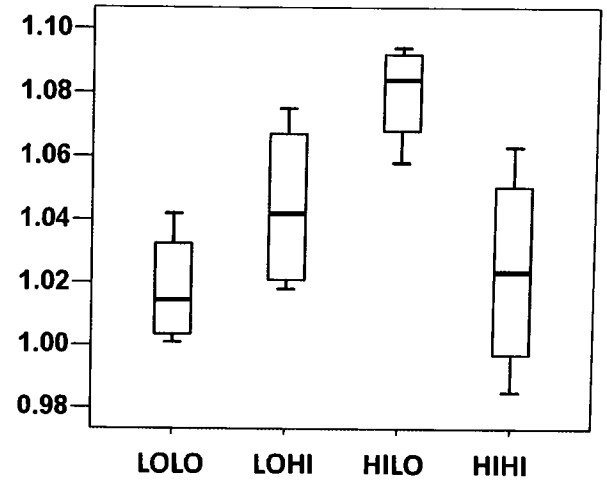

HILO>LOLO
p=0.001 (F)

Figure F.1.1.2. Fast walking speed on level.

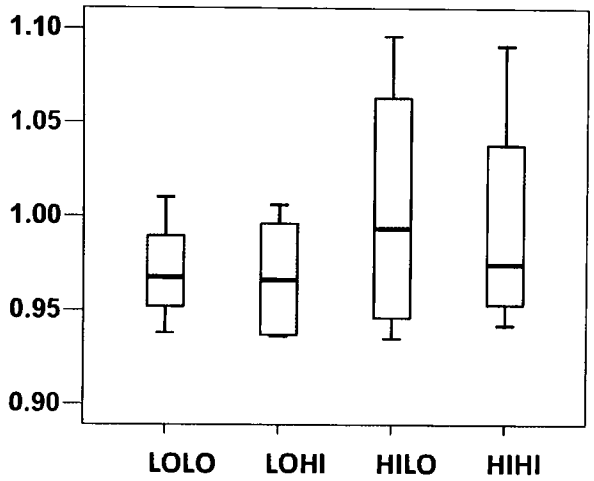

Figure F.1.1.3. Self-selected walking speed on incline.

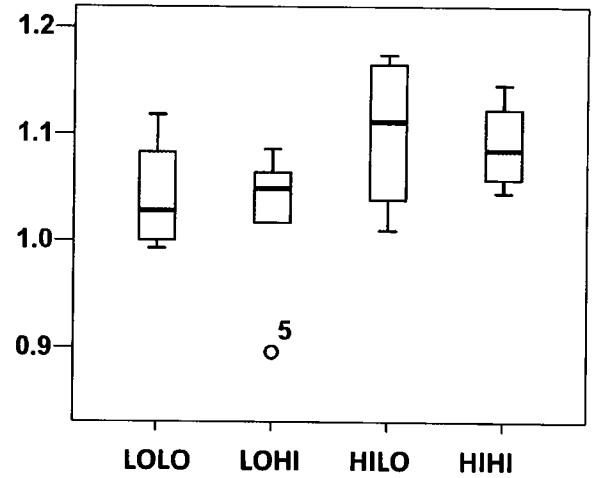

Figure F.1.1.4 Self-selected walking speed on decline.

F.1.2. Peak vertical ground reaction force on the prosthetic limb during unloading phase of stance (x Body Weight)

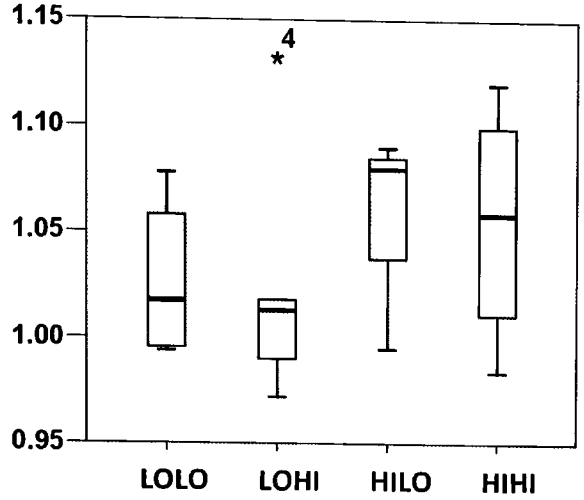

Figure F.1.2.1. Self-selected walking speed on level.

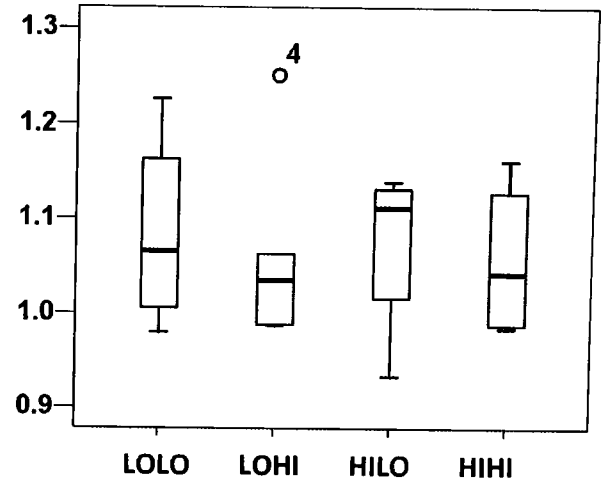

Figure F.1.2.2. Fast walking speed on level.

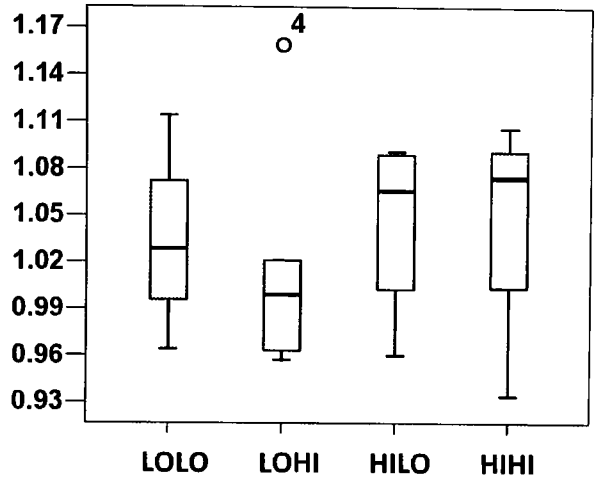

Figure F.1.2.3. Self-selected walking speed on incline.

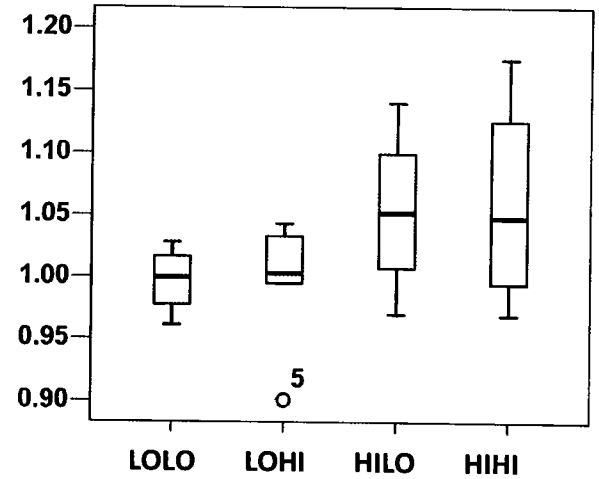

Figure F.1.2.4. Self-selected walking speed on decline.

F.1.3. Peak horizontal (braking) ground reaction force on the prosthetic limb during loading phase of stance (x Body Weight)

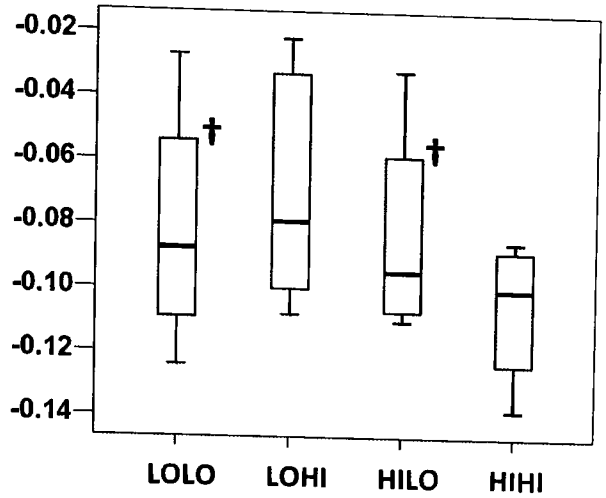

Figure F.1.3.1. Self-selected walking speed on level.

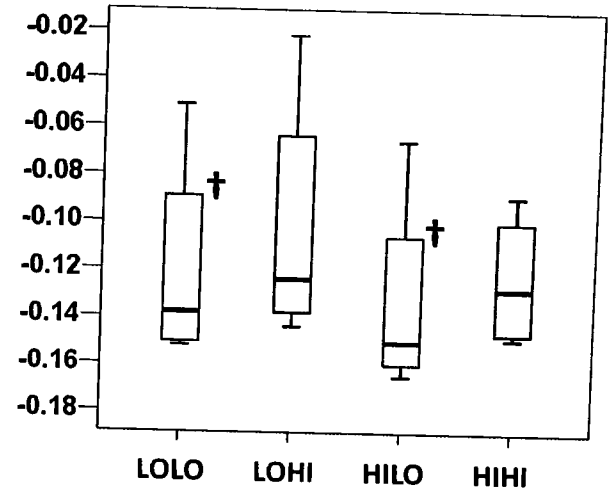

HILO>LOHI
p=0.054 (F)

Figure F.1.3.2. Fast walking speed on level.

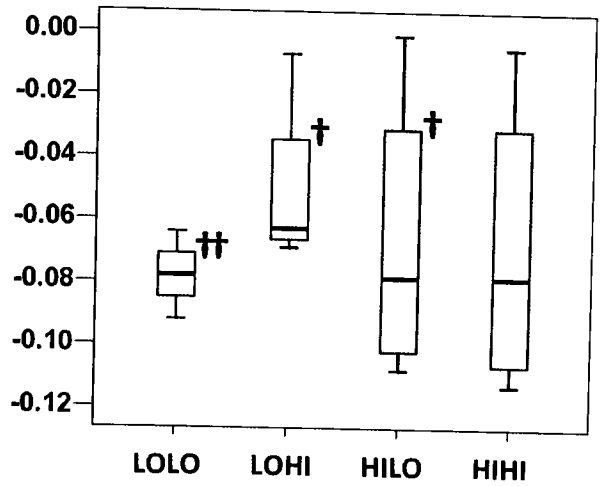

Figure F.1.3.3. Self-selected walking speed on incline.

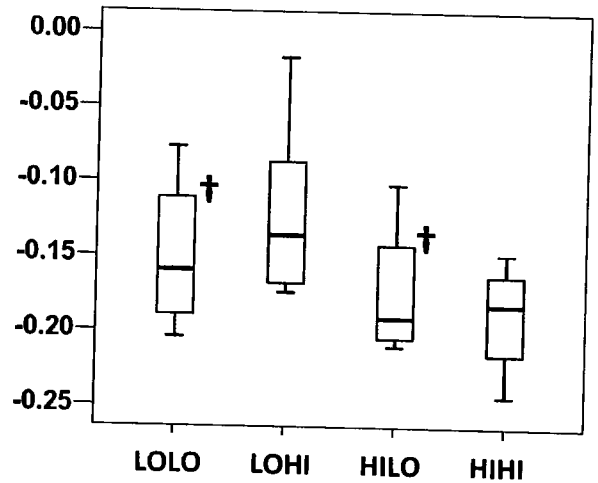

Figure F.1.3.4. Self-selected walking speed on decline.

F.1.4. Peak horizontal (propulsive) ground reaction force on the prosthetic limb during unloading phase of stance (x Body Weight)

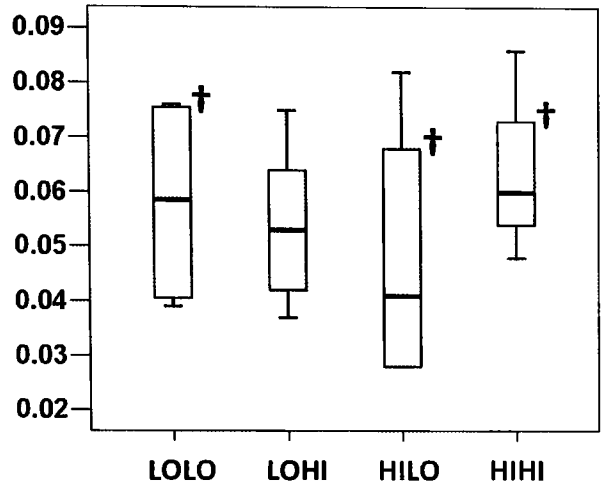

Figure F.1.4.1. Self-selected walking speed on level.

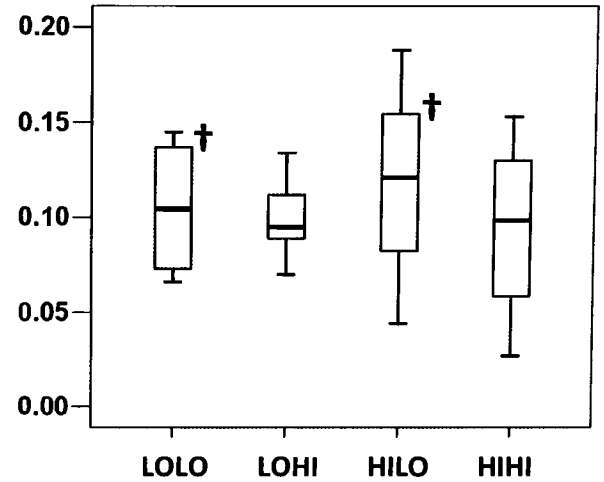

Figure F.1.4.2. Fast walking speed on level.

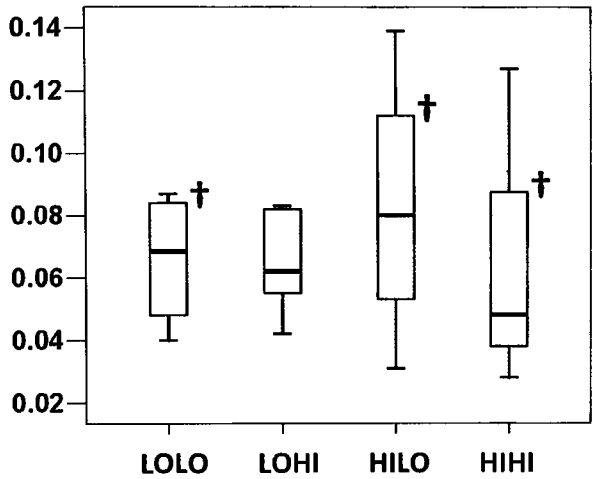

Figure F.1.4.3. Self-selected walking speed on incline.

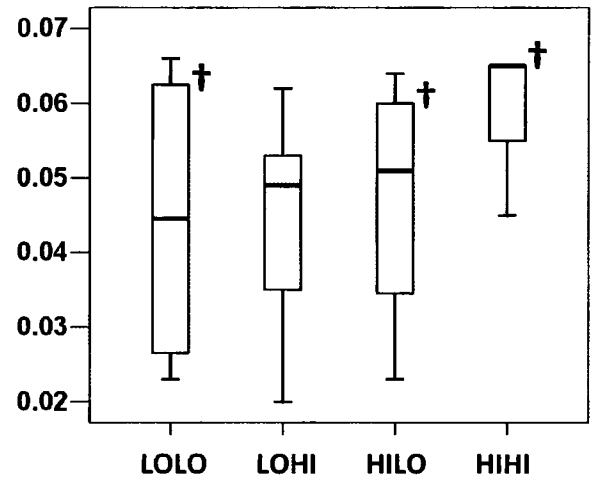

Figure F.1.4.4. Self-selected walking speed on decline.

F.1.5. Time to maximum plantar flexion of the sound ankle joint (% Stance)

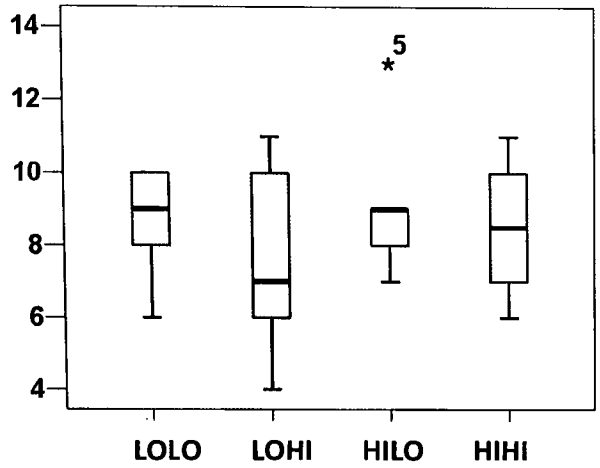

Figure F.1.5.1. Self-selected walking speed on level.

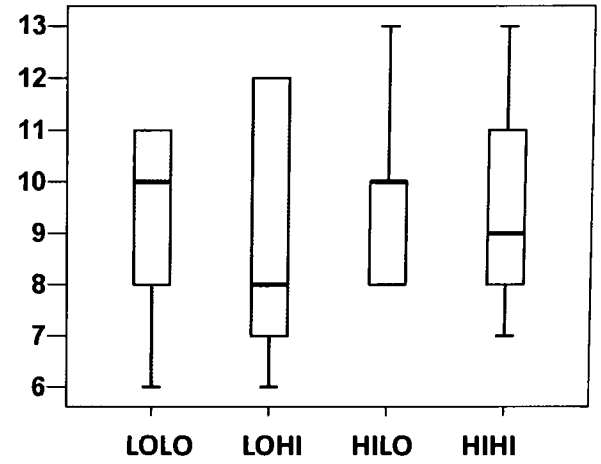

Figure F.1.5.2. Fast walking speed on level.

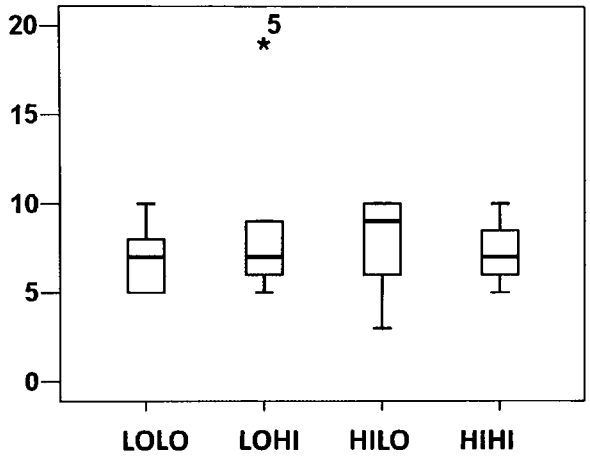

Figure F.1.5.3. Self-selected walking speed on incline.

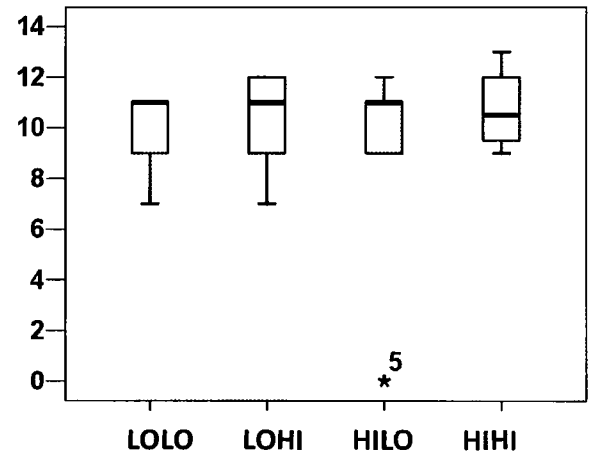

Figure F.1.5.4. Self-selected walking speed on decline.

F.1.6. Time to maximum plantar flexion of the prosthetic ankle joint (% Stance)

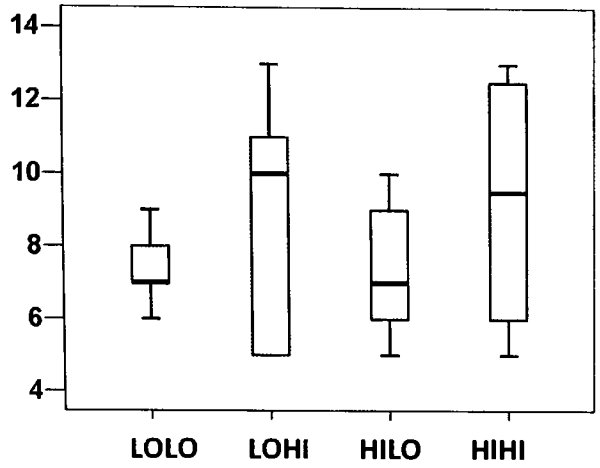

Figure F.1.6.1. Self-selected walking speed on level.

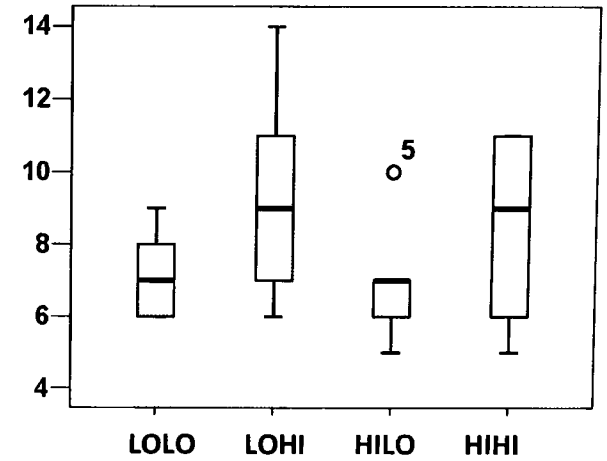

Figure F.1.6.2. Fast walking speed on level.

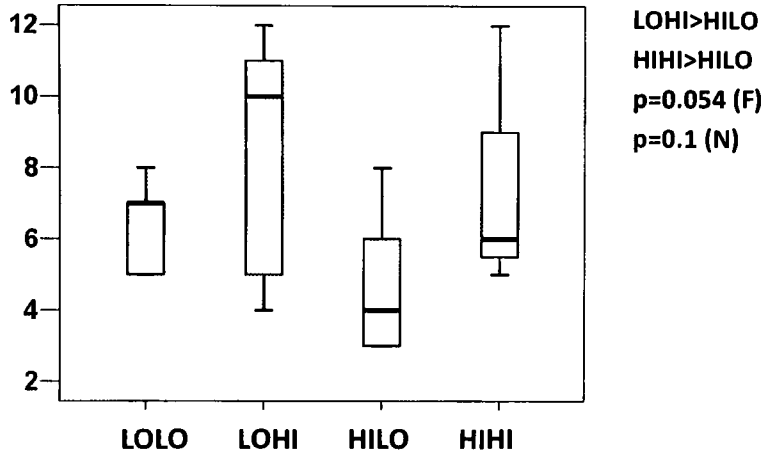

Figure F.1.6.3. Self-selected walking speed on incline.

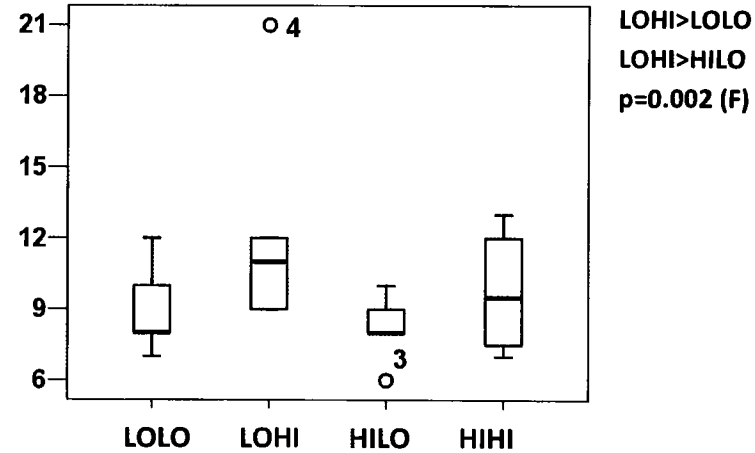

Figure F.1.6.4. Self-selected walking speed on decline.

F.1.7. Maximum plantar flexion of the sound ankle joint (Degrees)

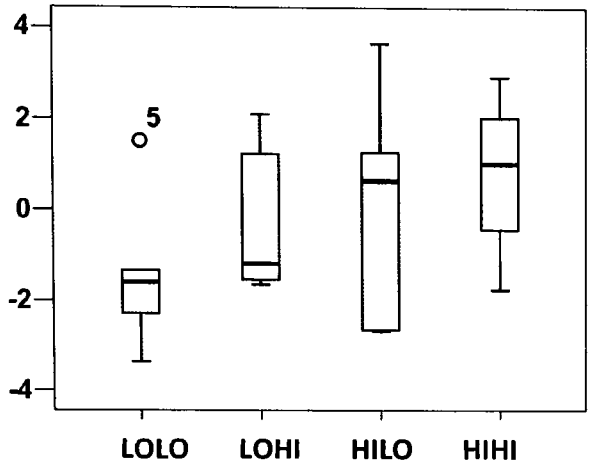

Figure F.1.7.1. Self-selected walking speed on level.

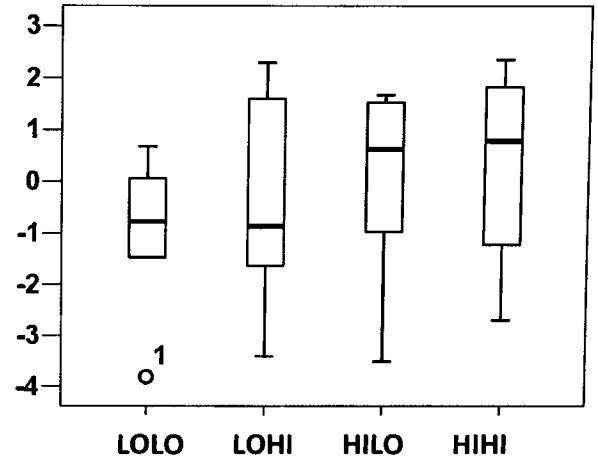

Figure F.1.7.2. Fast walking speed on level.

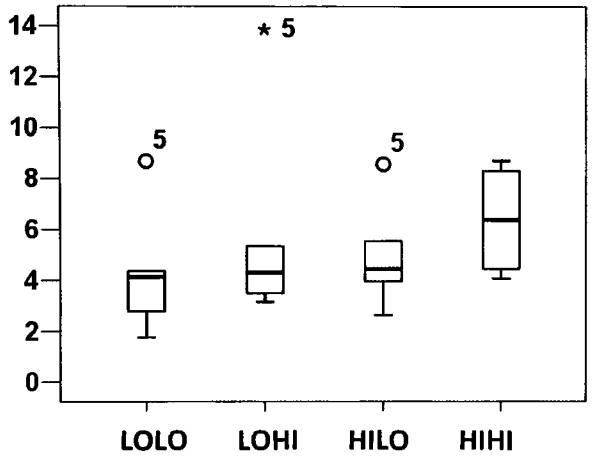

Figure F.1.7.3. Self-selected walking speed on incline.

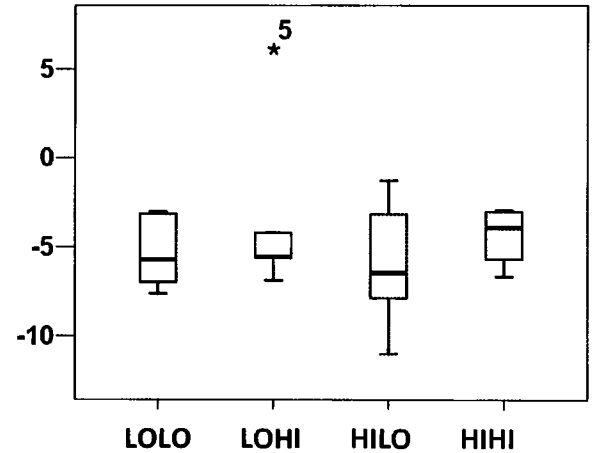

Figure F.1.7.4. Self-selected walking speed on decline.

F.1.8. Maximum plantar flexion of the prosthetic ankle joint (Degrees)

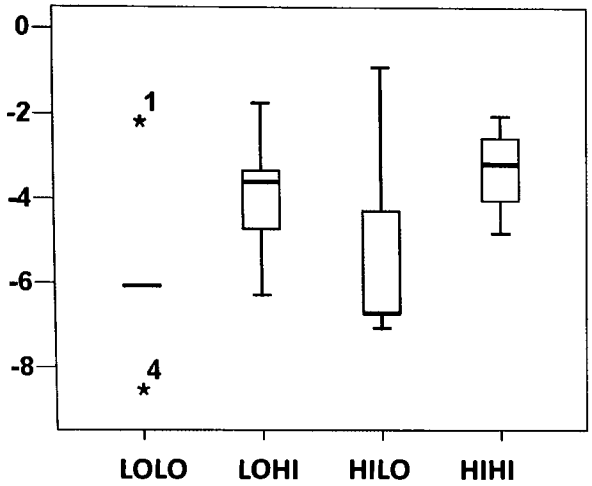

HILO>LOHI
LOLO>LOHI
HILO>HIHI
LOLO>HIHI
p=0.033 (F)
p=0.2 (N)

Figure F.1.8.1. Self-selected walking speed on level.

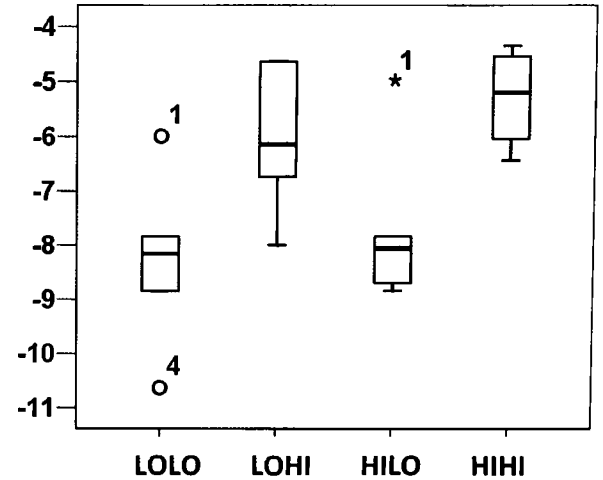

LOLO>LOHI
LOLO>HIHI
p=0.017 (F)
p=0.1 (N)

Figure F.1.8.2. Fast walking speed on level.

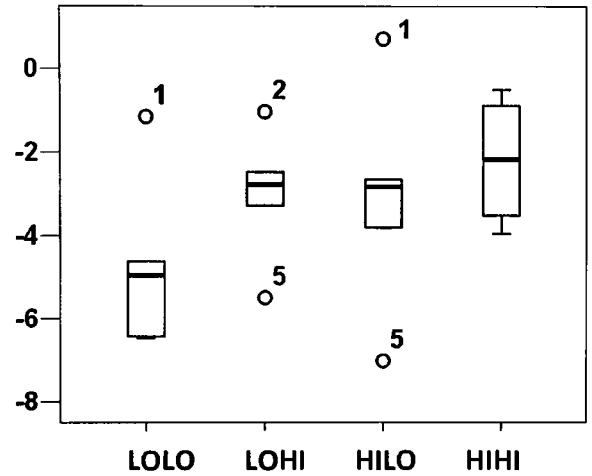

LOLO>LOHI
p=0.077 (F)
p=0.1 (N)

Figure F.1.8.3. Self-selected walking speed on incline.

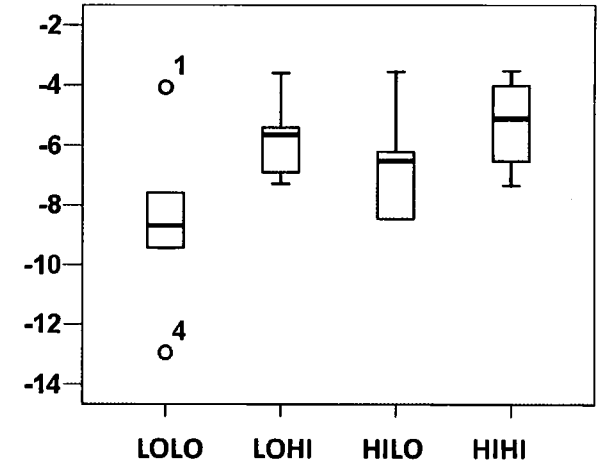

LOLO>HIHI
p=0.054 (F)
p=0.1 (N)

Figure F.1.8.4. Self-selected walking speed on decline.

F.1.9. Maximum dorsiflexion of the sound ankle joint (Degrees)

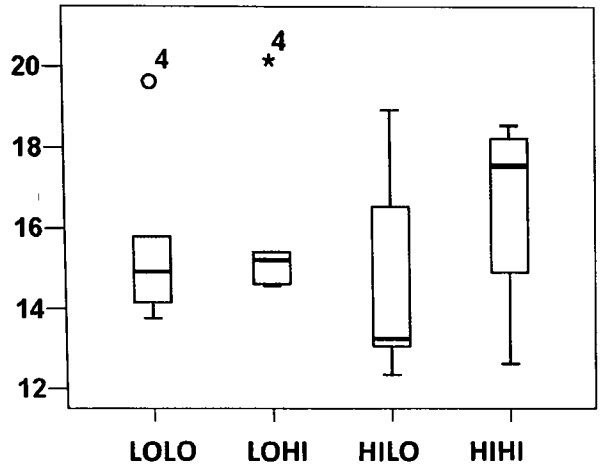

Figure F.1.9.1. Self-selected walking speed on level.

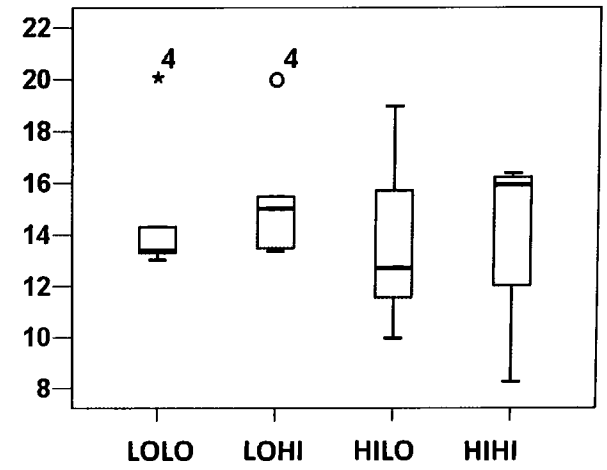

Figure F.1.9.2. Fast walking speed on level.

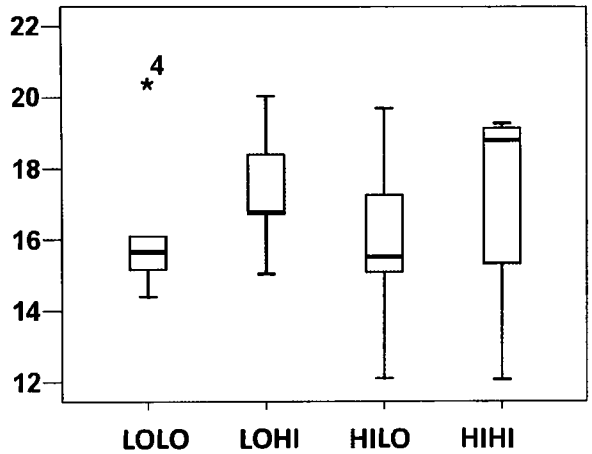

Figure F.1.9.3. Self-selected walking speed on incline.

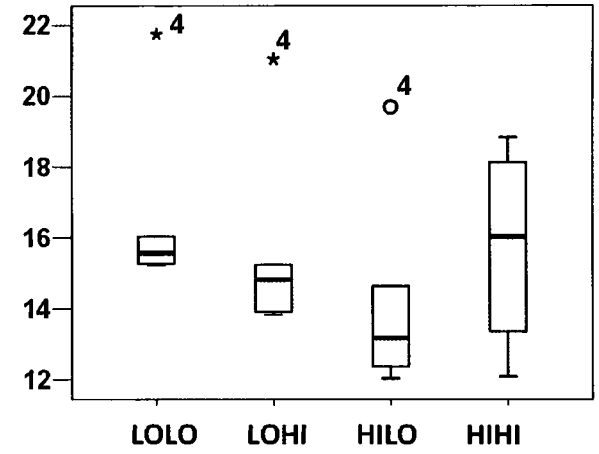

LOLO>HILO
p=0.034 (F)

Figure F.1.9.4. Self-selected walking speed on decline.

F.1.10. Maximum dorsiflexion of the prosthetic ankle joint (Degrees)

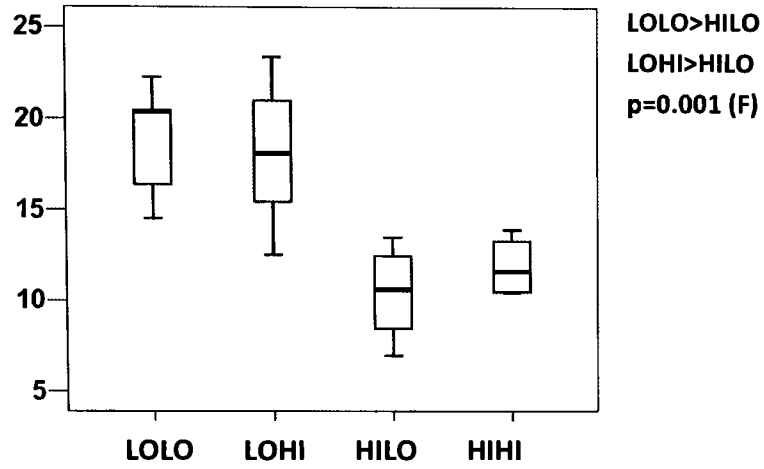

LOLO>HILO
LOHI>HILO
p=0.001 (F)

Figure F.1.10.1. Self-selected walking speed on level.

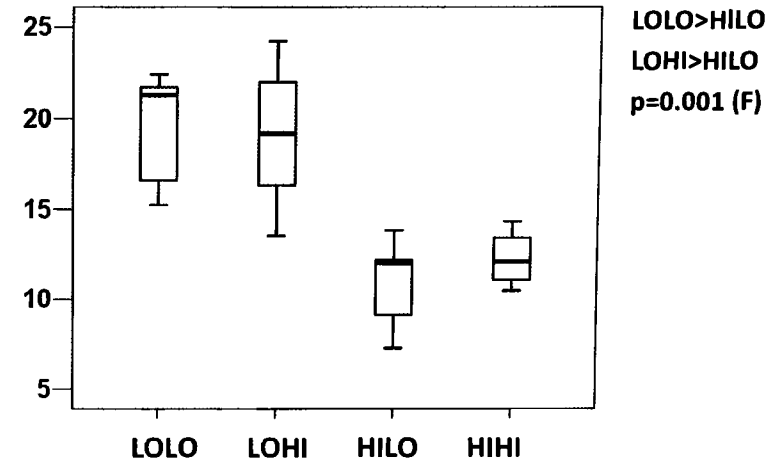

LOLO>HILO
LOHI>HILO
p=0.001 (F)

Figure F.1.10.2. Fast walking speed on level.

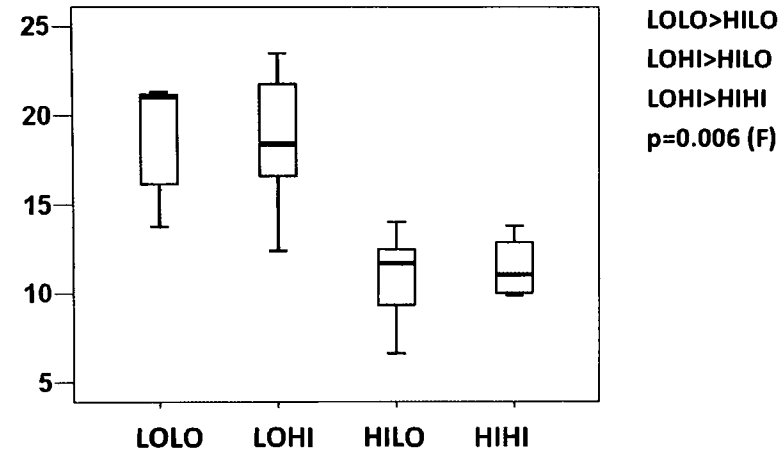

LOLO>HILO
LOHI>HILO
LOHI>HIHI
p=0.006 (F)

Figure F.1.10.3. Self-selected walking speed on incline.

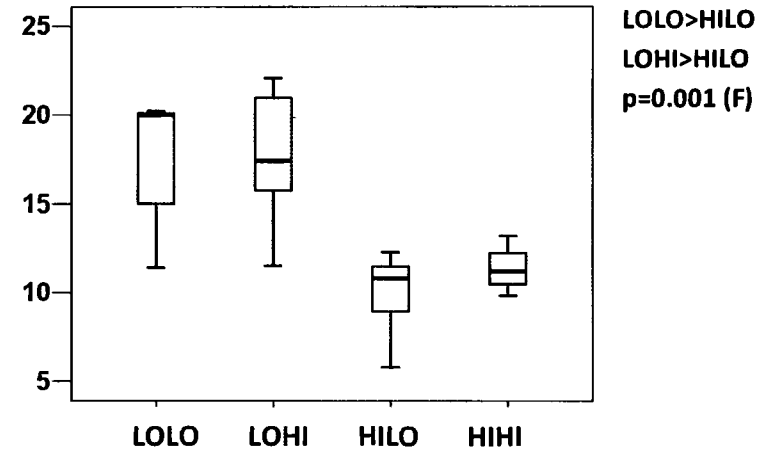

LOLO>HILO
LOHI>HILO
p=0.001 (F)

Figure F.1.10.4. Self-selected walking speed on decline.

F.1.11. Maximum flexion of the sound side knee joint during loading phase of stance (Degrees)

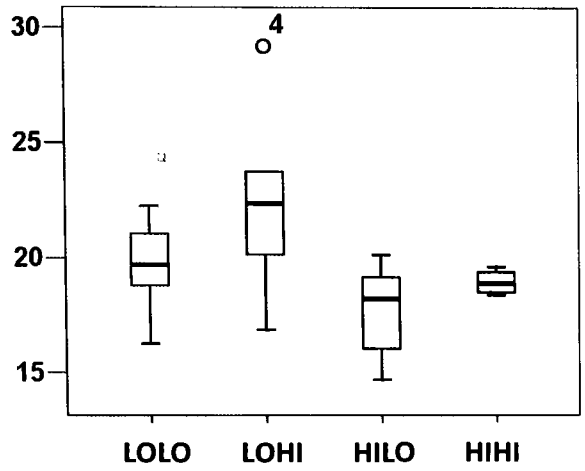

Figure F.1.11.1. Self-selected walking speed on level.

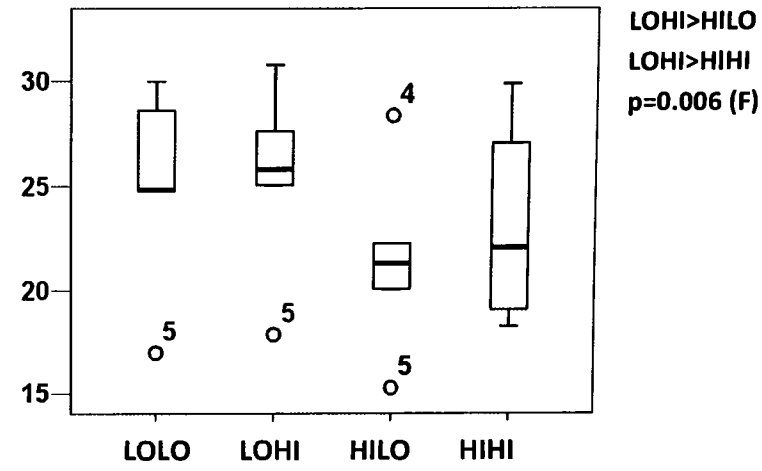

Figure F.1.11.2. Fast walking speed on level.

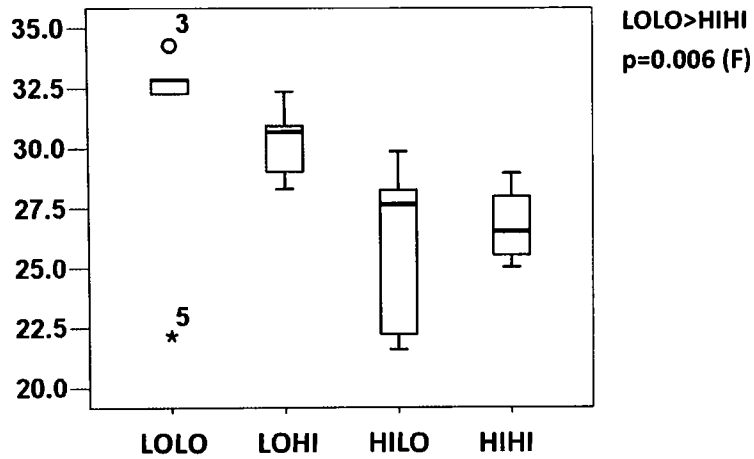

Figure F.1.11.3. Self-selected walking speed on incline.

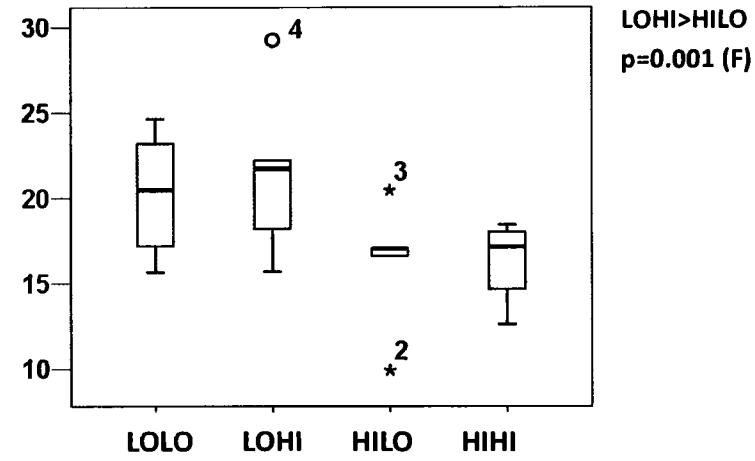

Figure F.1.11.4. Self-selected walking speed on decline.

F.1.12. Maximum flexion of the prosthetic side knee joint during loading phase of stance (Degrees)

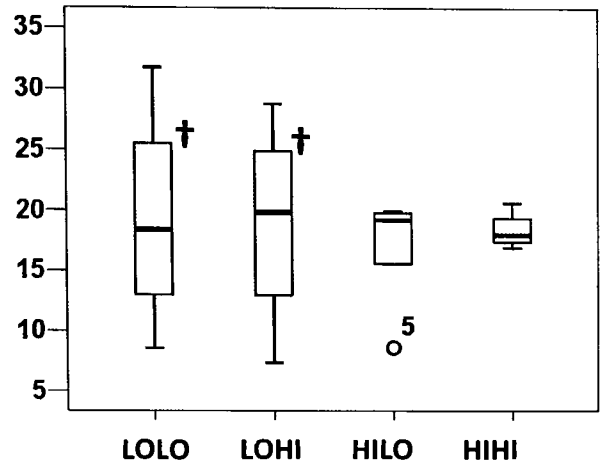

Figure F.1.12.1. Self-selected walking speed on level.

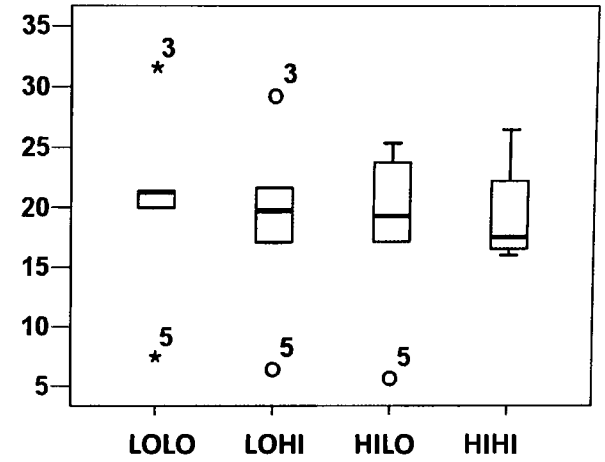

Figure F.1.12.2. Fast walking speed on level.

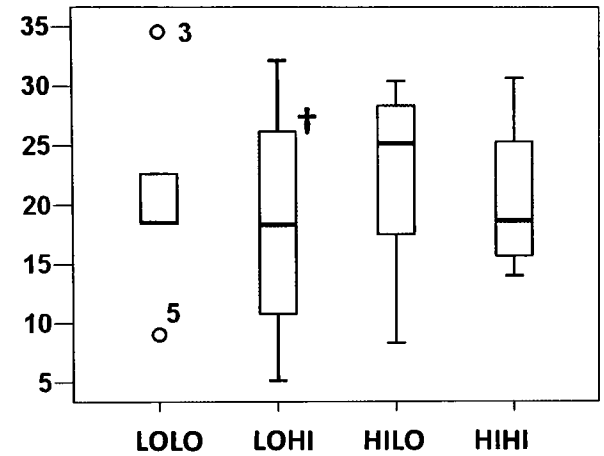

Figure F.1.12.3. Self-selected walking speed on incline.

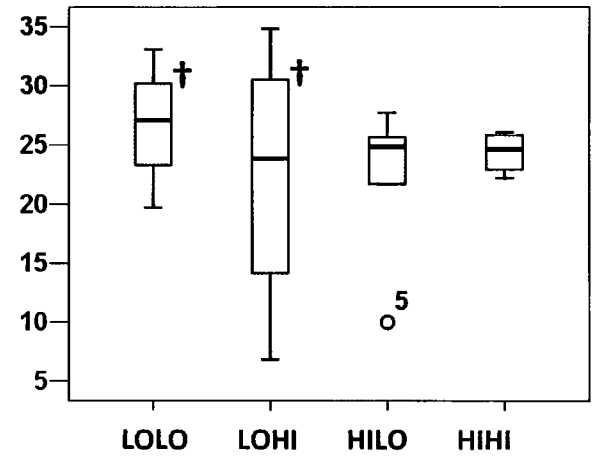

Figure F.1.12.4. Self-selected walking speed on decline.

F.1.13. Six in-vivo roll-over shapes per CFAM setup for one representative subject (#2)
(solid=LOLO; dash=LOHI; dot=HILO; dash-dot=HIHI)

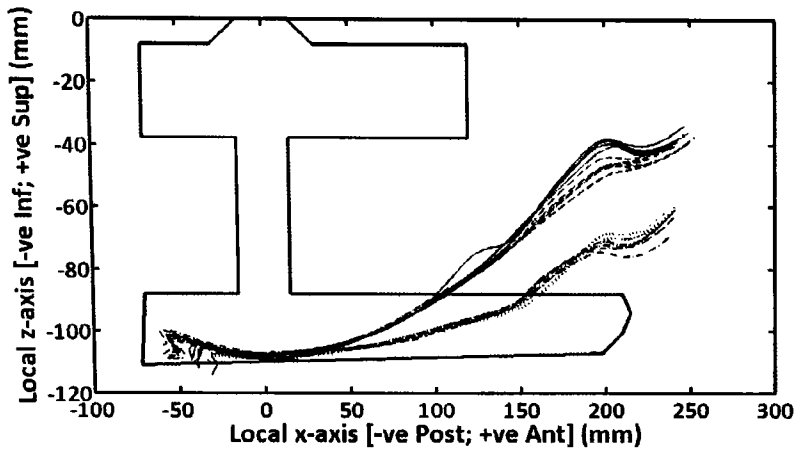

Figure F.1.13.1. Self-selected walking speed on level.

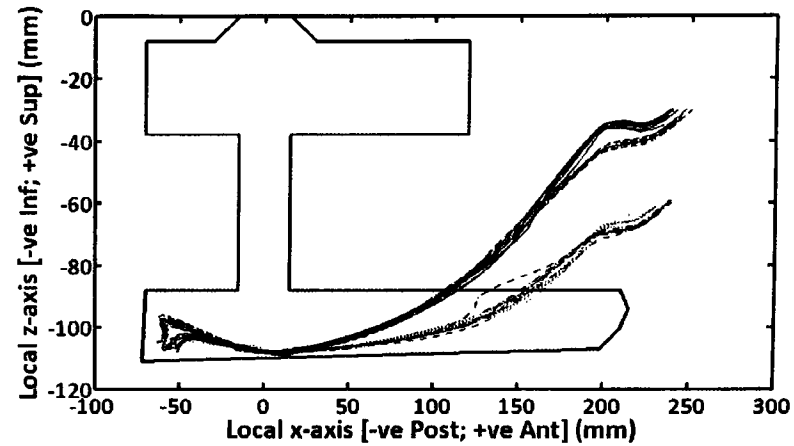

Figure F.1.13.2. Fast walking speed on level.

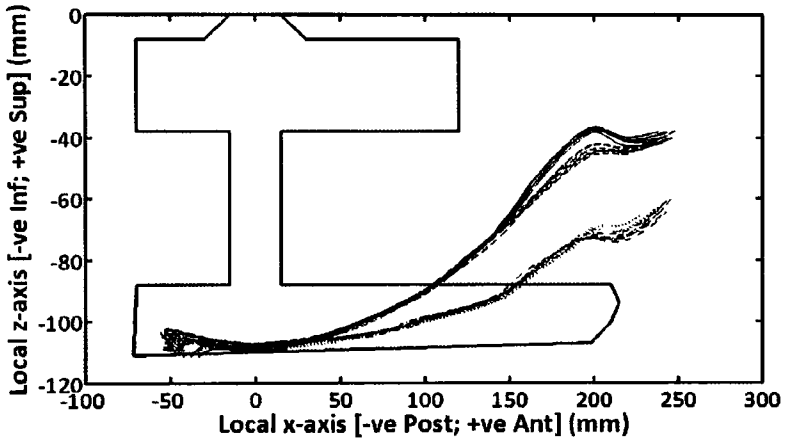

Figure F.1.13.3. Self-selected walking speed on incline.

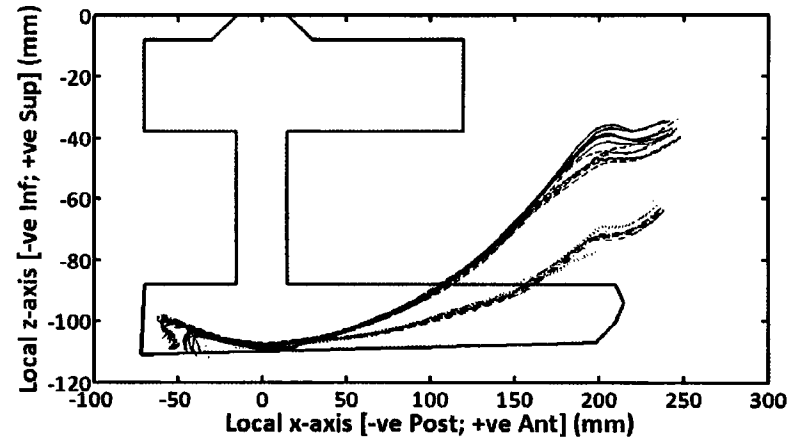

Figure F.1.13.4. Self-selected walking speed on decline.

F.1.14. Fourth-order best fit curve of each set of six in-vivo roll-over curves for one representative subject (#2)

(solid=LOLO; dash=LOHI; dot=HILO; dash-dot=HIHI)

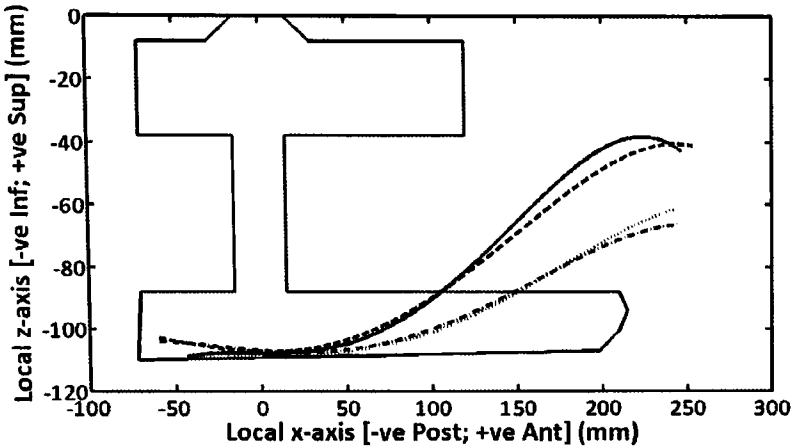

Figure F.1.14.1. Self-selected walking speed on level.

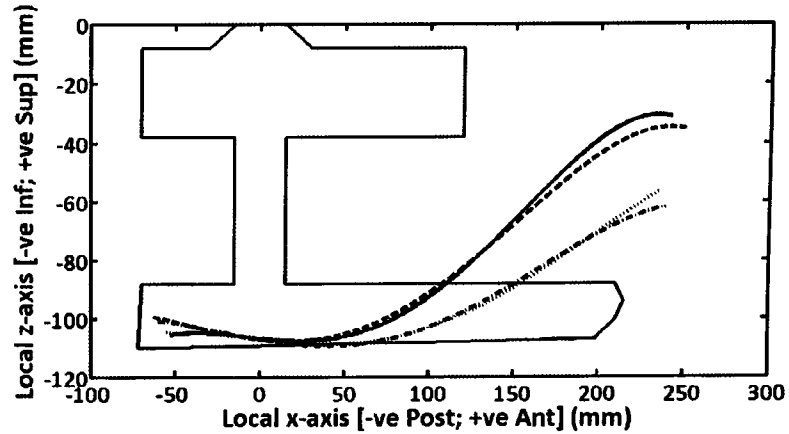

Figure F.1.14.2. Fast walking speed on level.

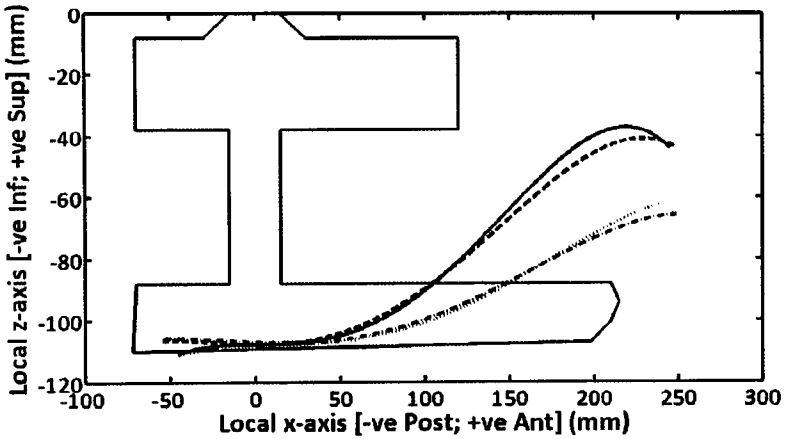

Figure F.1.14.3. Self-selected walking speed on incline.

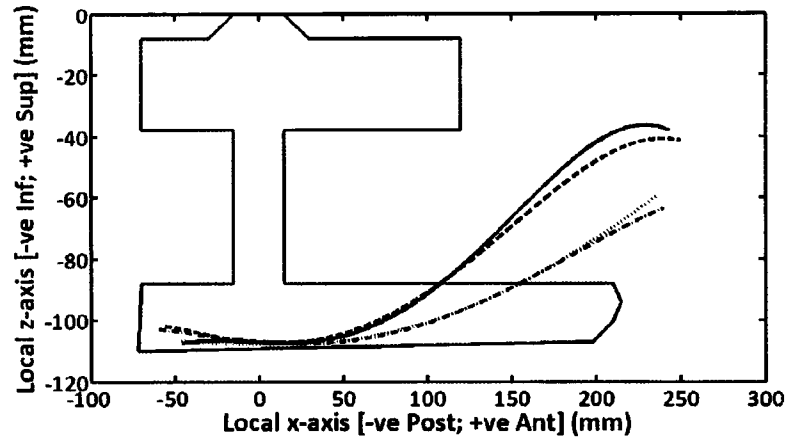

Figure F.1.14.4. Self-selected walking speed on decline.

F.1.15. Symmetry ratio (swing time of sound limb/swing time of prosthetic limb)

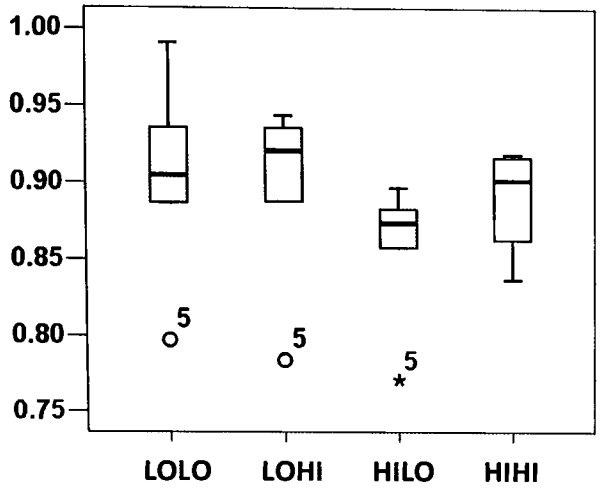

LOLO>HILO
LOHI>HILO
p=0.034 (F)

Figure F.1.15.1. Self-selected walking speed on level.

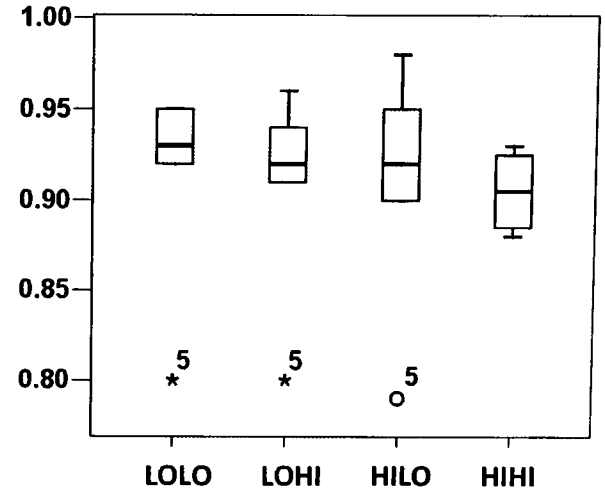

LOLO>HIHI
LOHI>HIHI
p=0.087 (F)
p=0.1 (N)

Figure F.1.15.2. Fast walking speed on level.

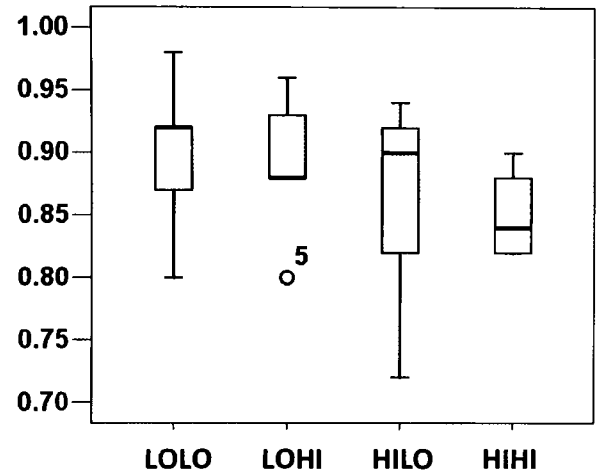

HILO>HIHI
p=0.083 (F)
p=0.1 (N)

Figure F.1.15.3. Self-selected walking speed on incline.

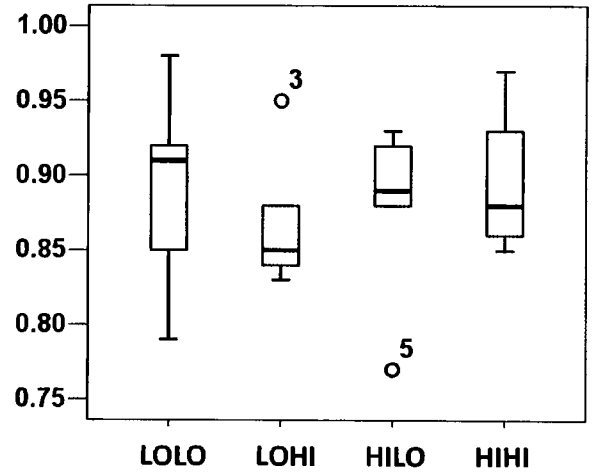

Figure F.1.15.4. Self-selected walking speed on decline.

F.1.16. Coefficient of variation (standard deviation/mean) of step width

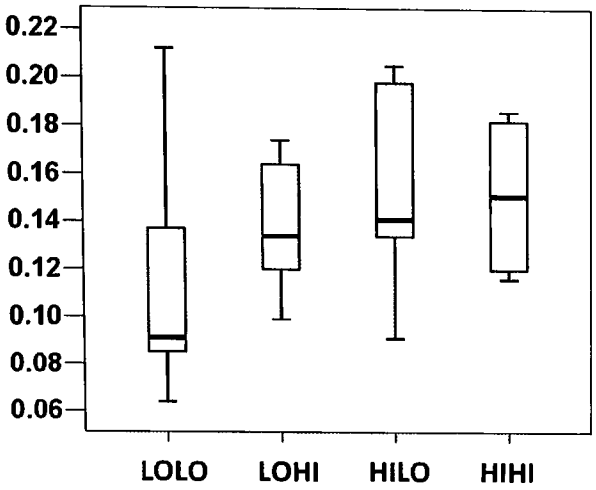

Figure F.1.16.1. Self-selected walking speed on level.

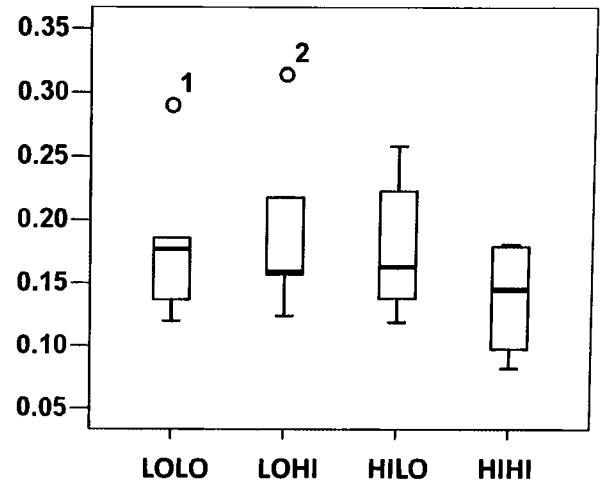

Figure F.1.16.2. Fast walking speed on level.

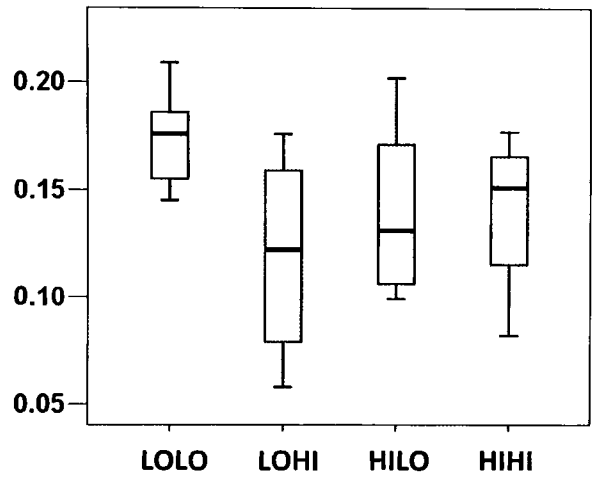

Figure F.1.16.3. Self-selected walking speed on incline.

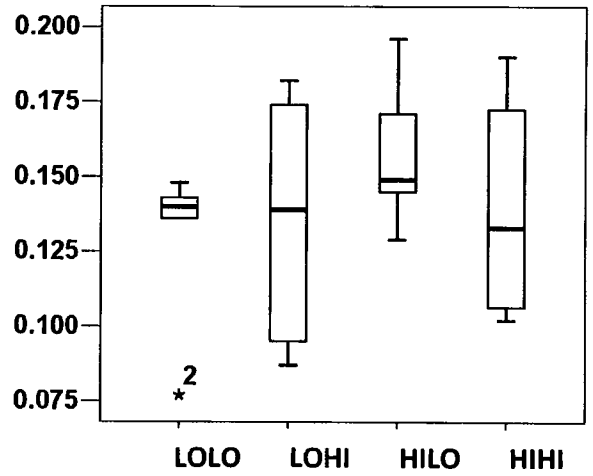

HILO>LOLO
HILO>LOHI
p=0.093 (F)
p=0.2(N)

Figure F.1.16.4. Self-selected walking speed on decline.

F.1.17. Coefficient of variation (standard deviation/mean) of step length

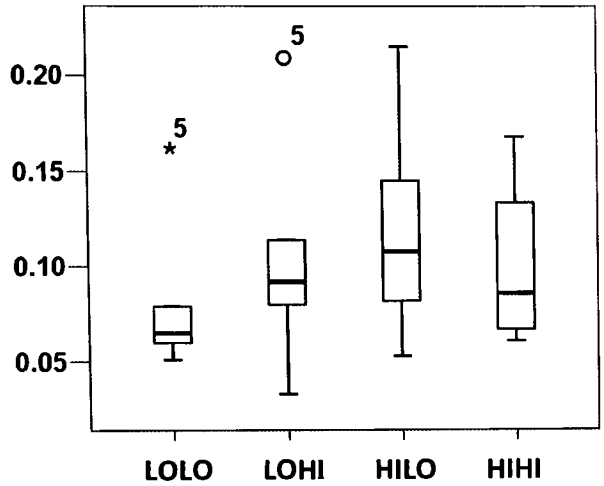

Figure F.1.17.1. Self-selected walking speed on level.

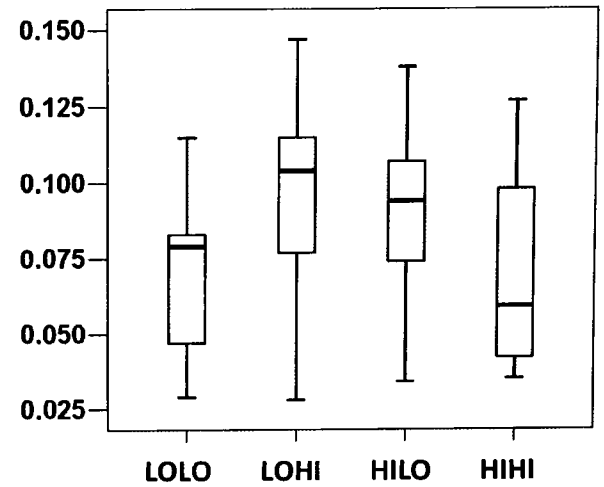

Figure F.1.17.2. Fast walking speed on level.

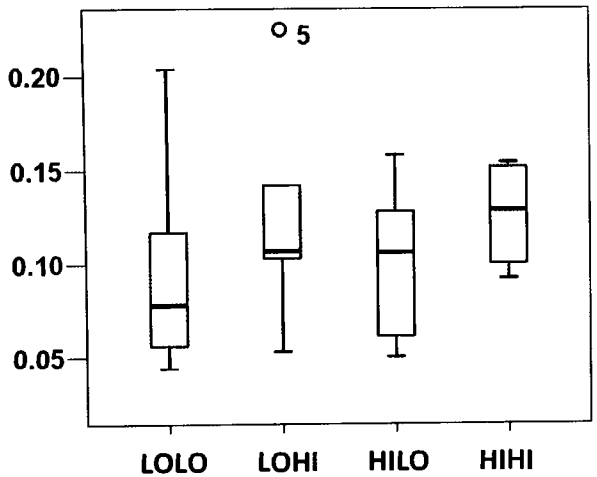

LOHI>LOLO
p=0.031 (F)
p=0.1 (N)

HIHI>LOLO
P<0.001 (F)

Figure F.1.17.3. Self-selected walking speed on incline.

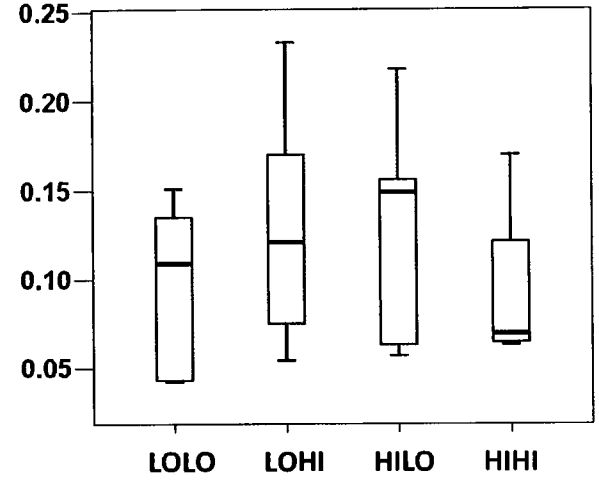

Figure F.1.17.4. Self-selected walking speed on decline.

F.1.18. Coefficient of variation (standard deviation/mean) of step time

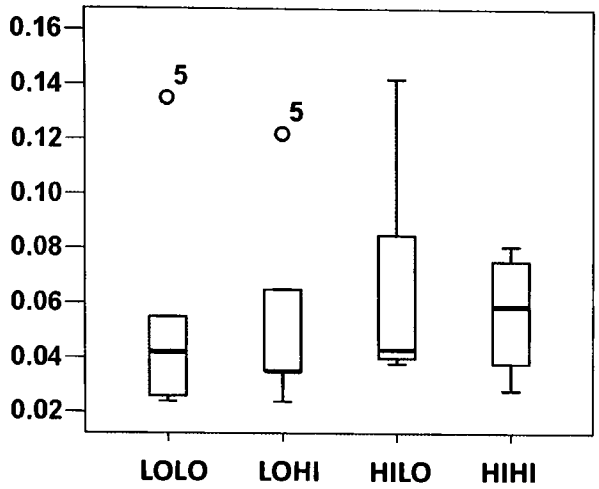

Figure F.1.18.1. Self-selected walking speed on level.

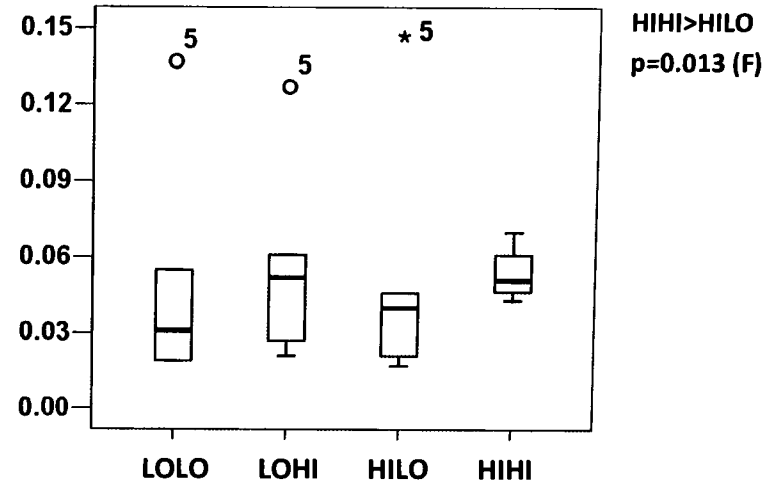

Figure F.1.18.2. Fast walking speed on level.

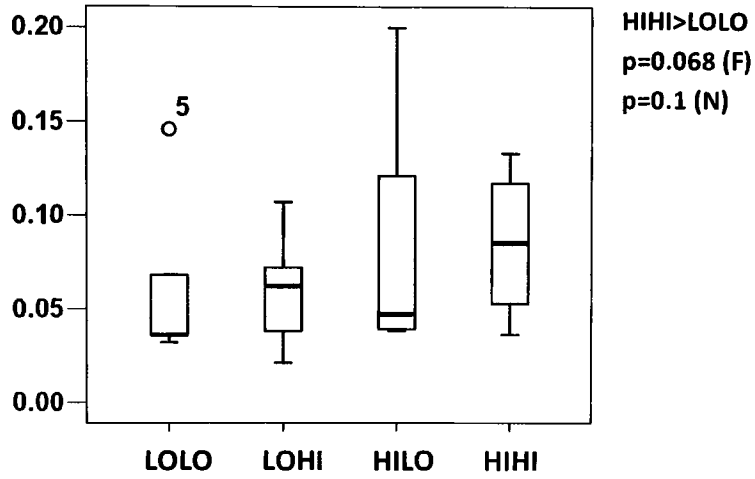

Figure F.1.18.3. Self-selected walking speed on incline.

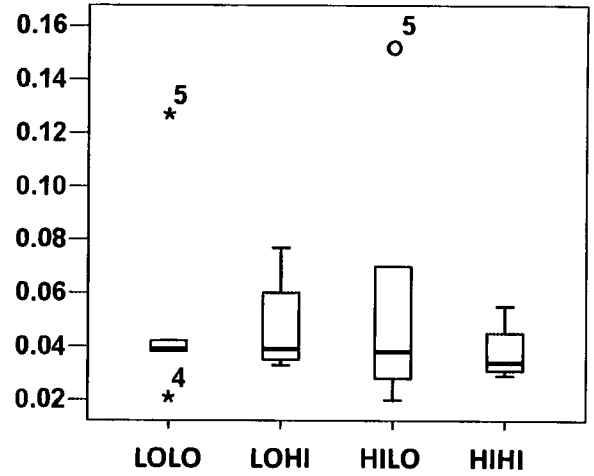

Figure F.1.18.4. Self-selected walking speed on decline.

F.1.19. Coefficient of variation (standard deviation/mean) of swing time of prosthetic limb or single-stance time of sound limb

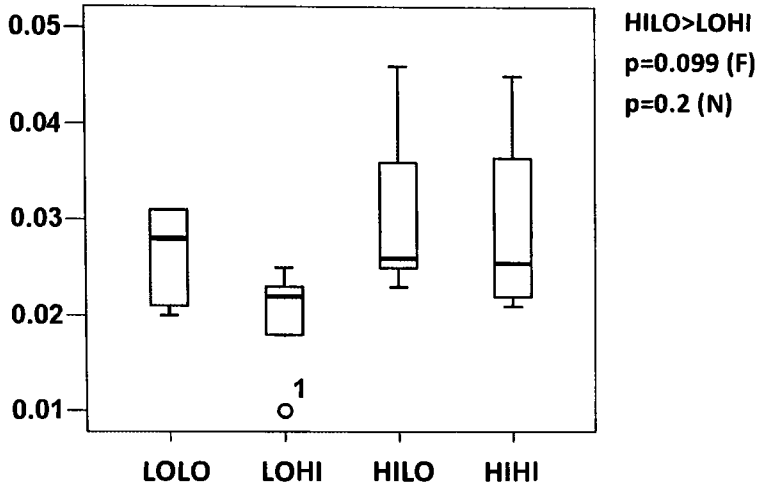

HILO>LOHI
p=0.099 (F)
p=0.2 (N)

Figure F.1.19.1. Self-selected walking speed on level.

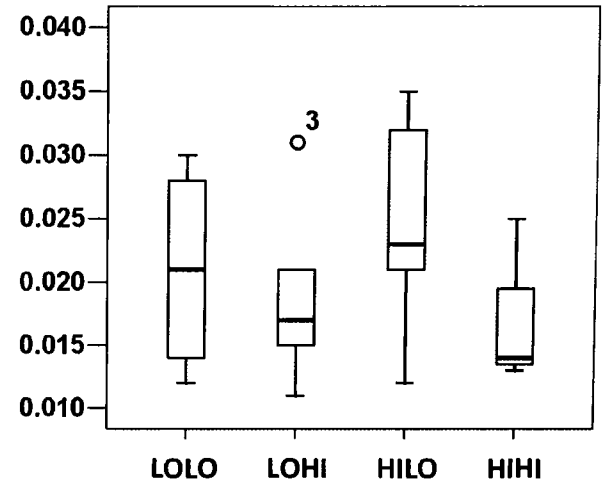

Figure F.1.19.2. Fast walking speed on level.

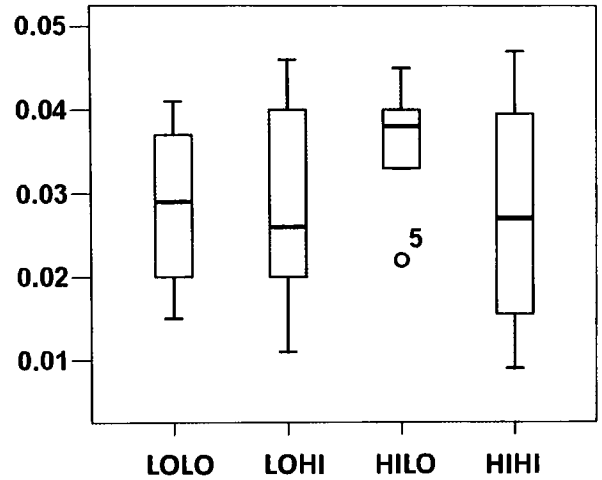

Figure F.1.19.3. Self-selected walking speed on incline.

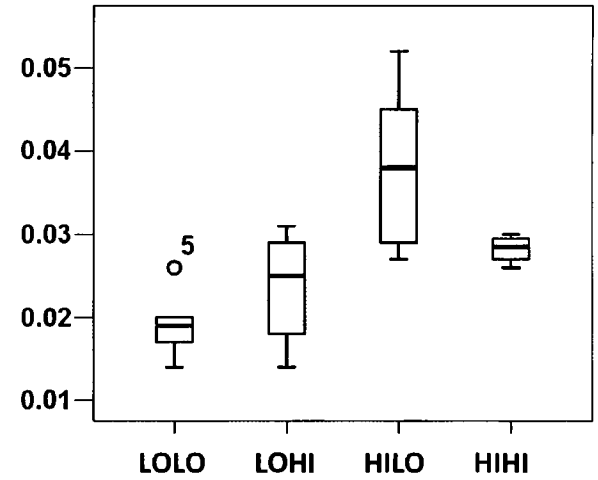

Figure F.1.19.4. Self-selected walking speed on decline.

F.1.20. Coefficient of variation (standard deviation/mean) of swing time of sound limb or single-stance time of prosthetic limb

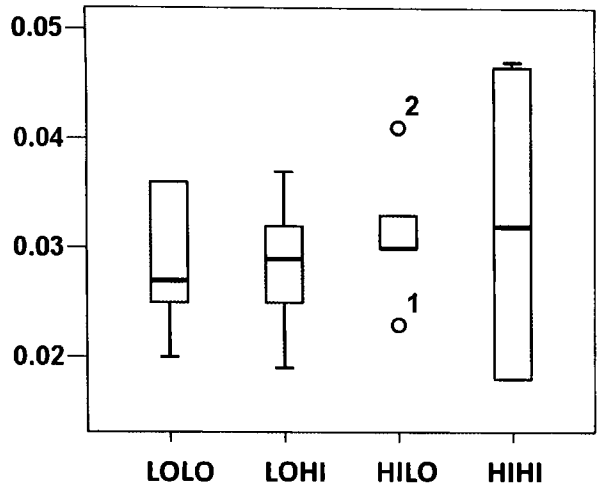

Figure F.1.20.1. Self-selected walking speed on level.

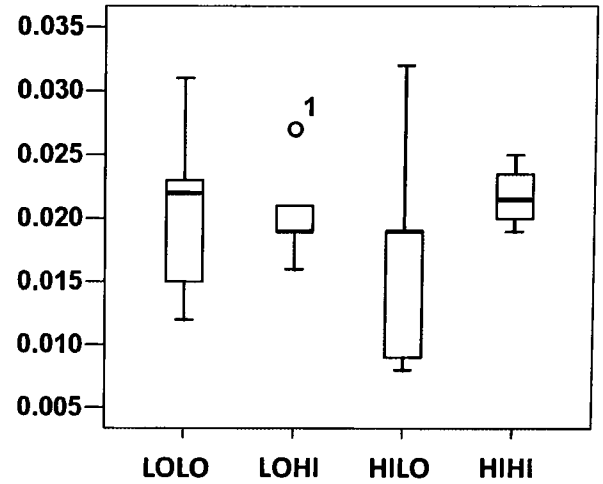

Figure F.1.20.2. Fast walking speed on level.

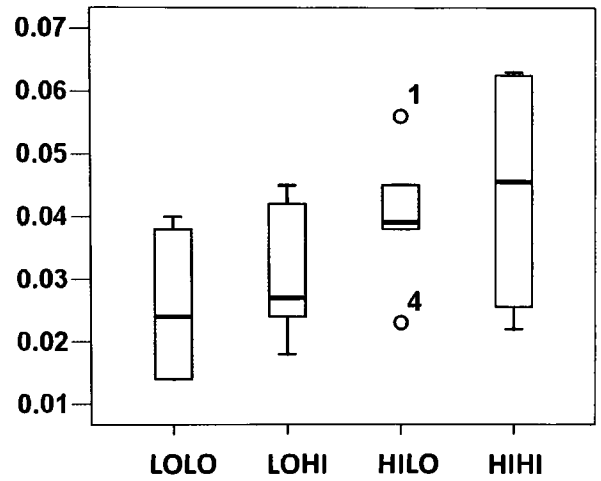

Figure F.1.20.3. Self-selected walking speed on incline.

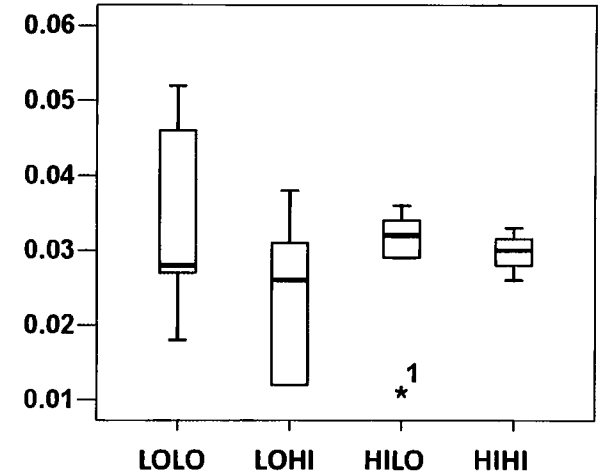

Figure F.1.20.4. Self-selected walking speed on decline.

F.1.21. Metabolic cost of transport (ml O_2/kg/m)

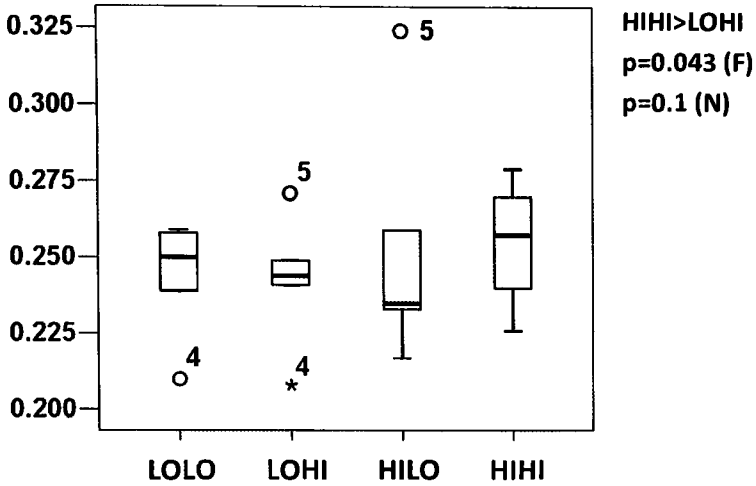

HIHI>LOHI
p=0.043 (F)
p=0.1 (N)

Figure F.1.21.1. Self-selected walking speed on level.

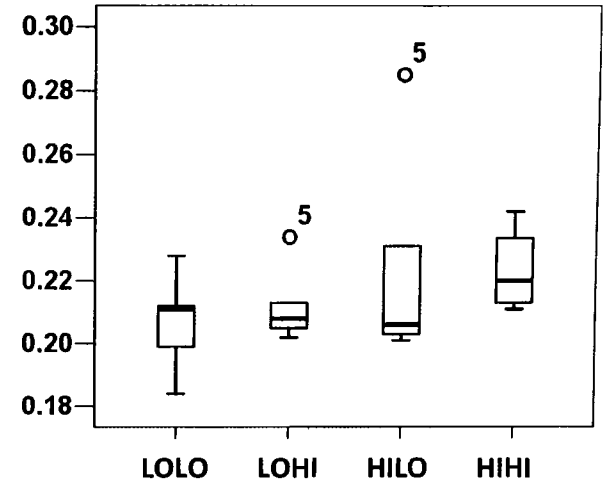

Figure F.1.21.2. Fast walking speed on level.

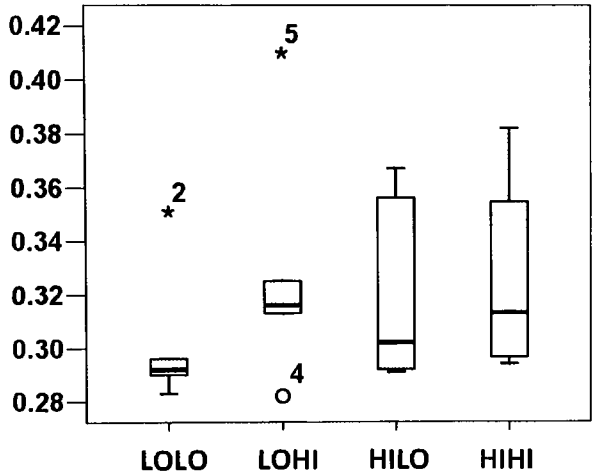

Figure F.1.21.3. Self-selected walking speed on incline.

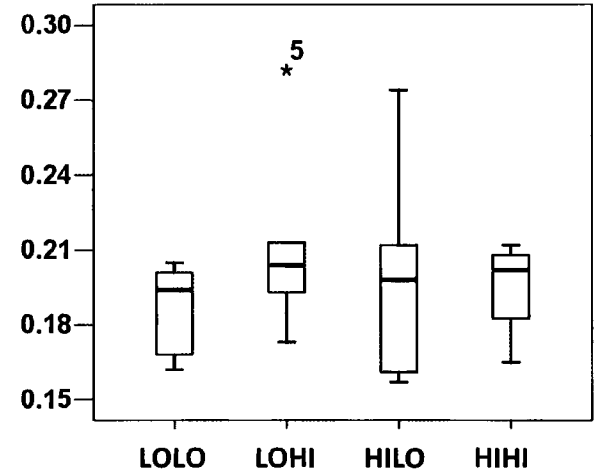

LOHI>LOLO
LOHI>HILO
p=0.011 (F)
p=0.1 (N)

Figure F.1.21.4. Self-selected walking speed on decline.

F.1.22. Metabolic rate (ml O_2/kg/min)

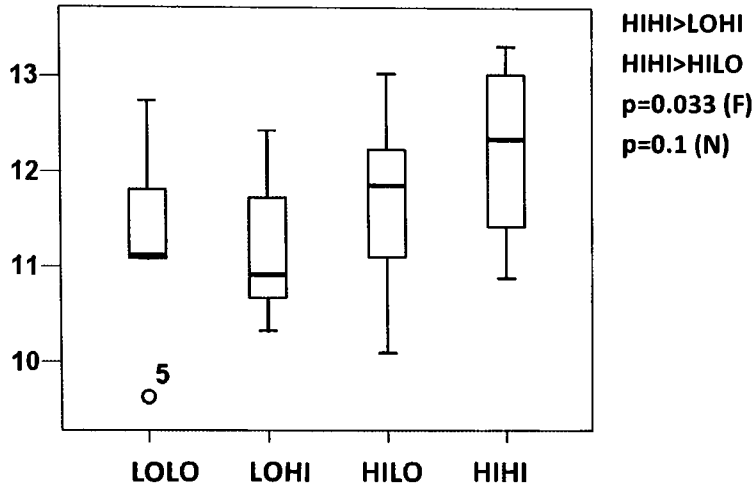

HIHI>LOHI
HIHI>HILO
p=0.033 (F)
p=0.1 (N)

Figure F.1.22.1. Self-selected walking speed on level.

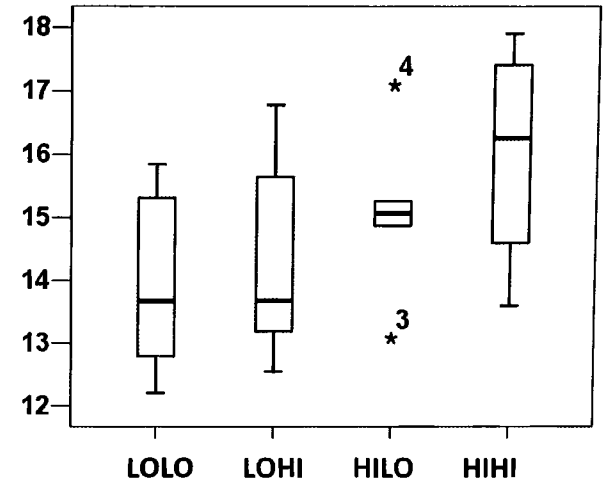

Figure F.1.22.2. Fast walking speed on level.

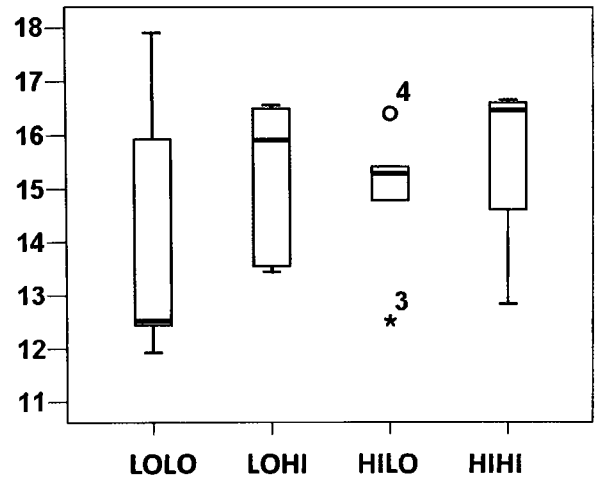

Figure F.1.22.3. Self-selected walking speed on incline.

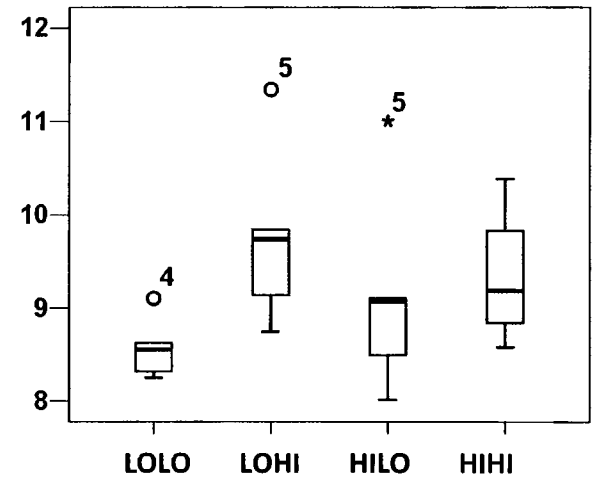

LOHI>LOLO
LOHI>HILO
p=0.044 (F)
p=0.1 (N)

Figure F.1.22.4. Self-selected walking speed on decline.

F.1.23. Perceived level of comfort (1-most, 10-least)

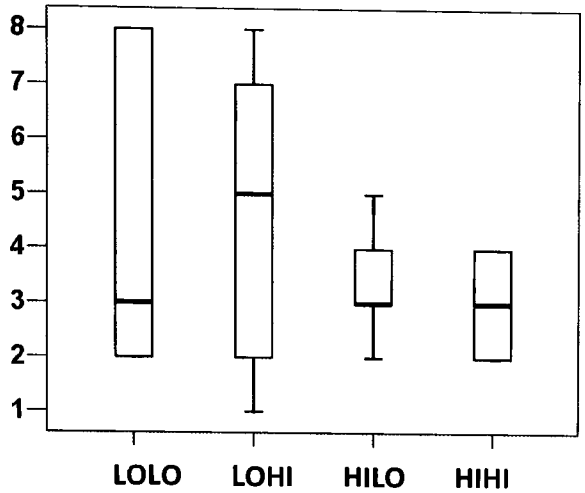

Figure F.1.23.1. Self-selected walking speed on level.

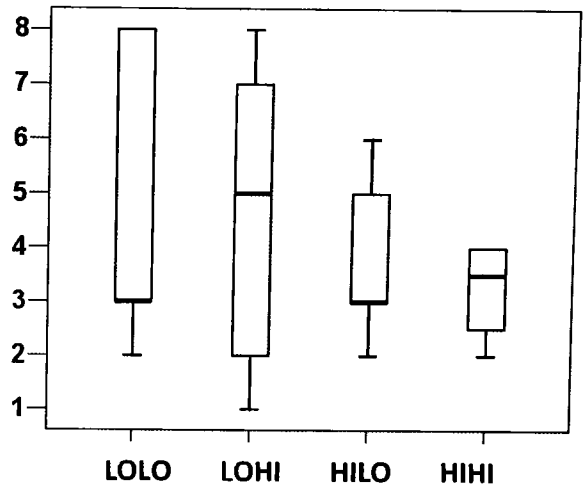

Figure F.1.23.2. Fast walking speed on level.

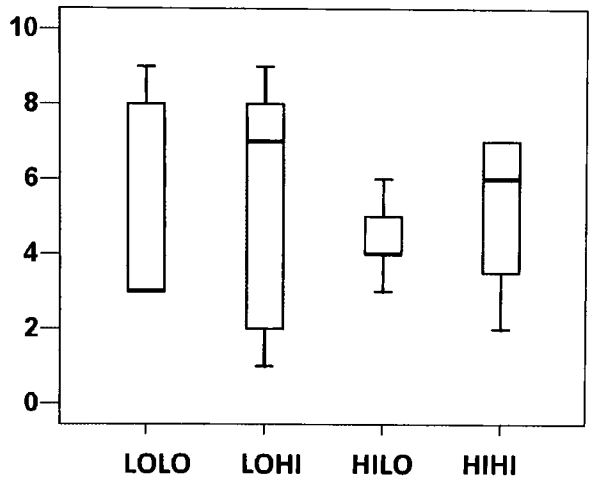

Figure F.1.23.3. Self-selected walking speed on incline.

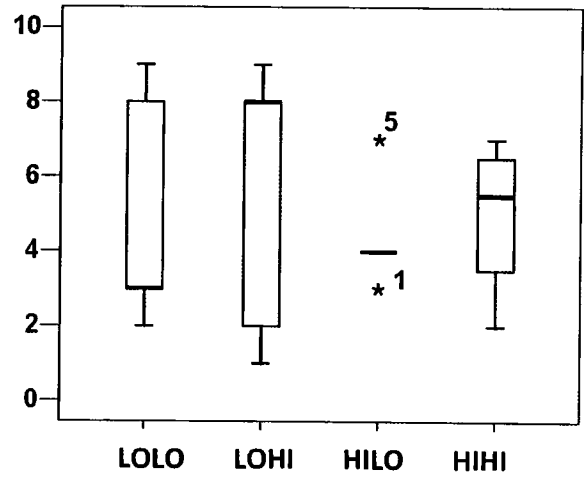

Figure F.1.23.4. Self-selected walking speed on decline.

F.1.24. Perceived level of exertion (1-least, 10-most)

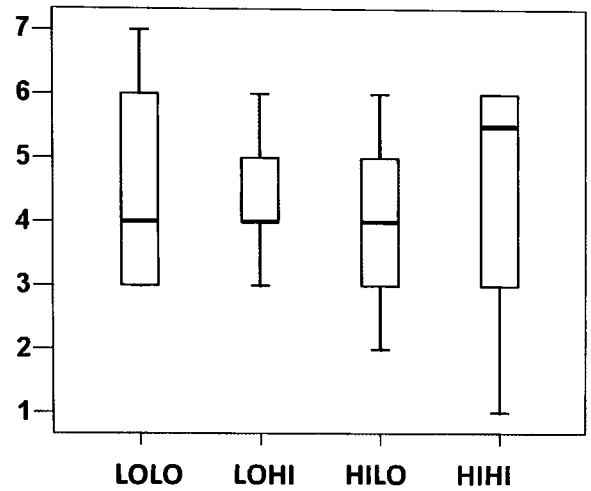

Figure F.1.24.1. Self-selected walking speed on level.

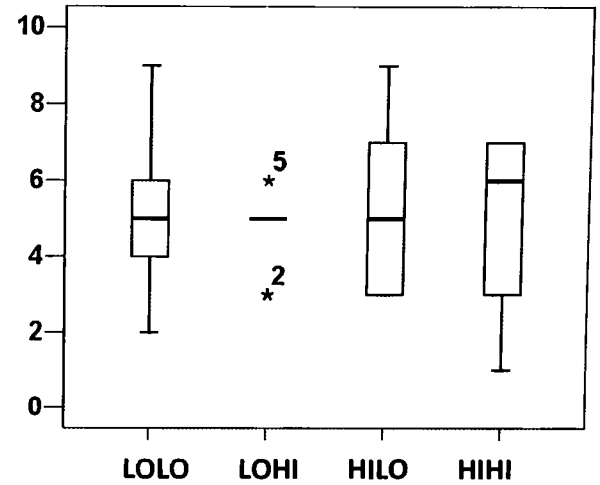

Figure F.1.24.2. Fast walking speed on level.

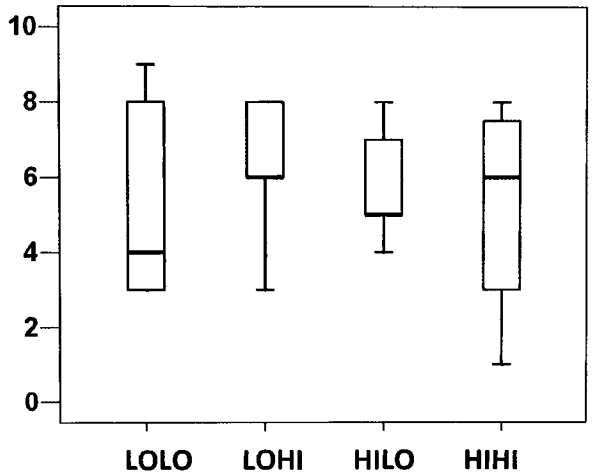

Figure F.1.24.3. Self-selected walking speed on incline.

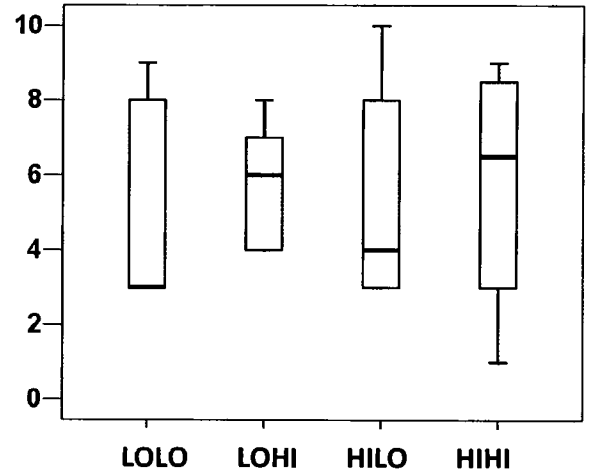

Figure F.1.24.4. Self-selected walking speed on decline.

F.1.25. Perceived level of stability (1-least, 10-most)

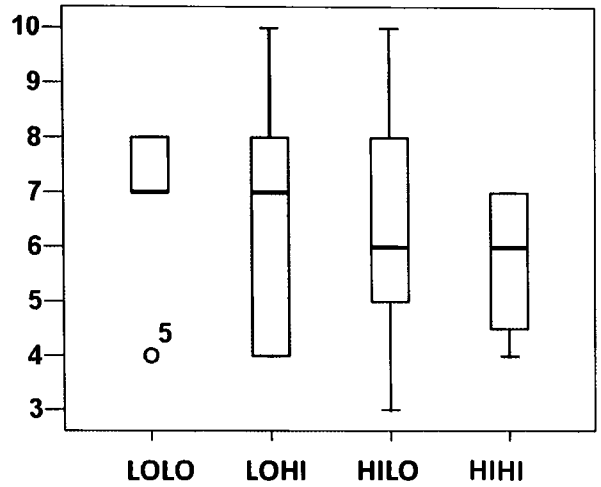

Figure F.1.25.1. Self-selected walking speed on level.

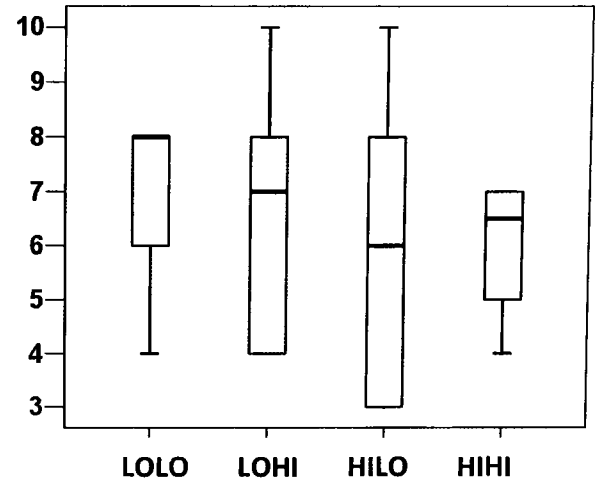

Figure F.1.25.2. Fast walking speed on level.

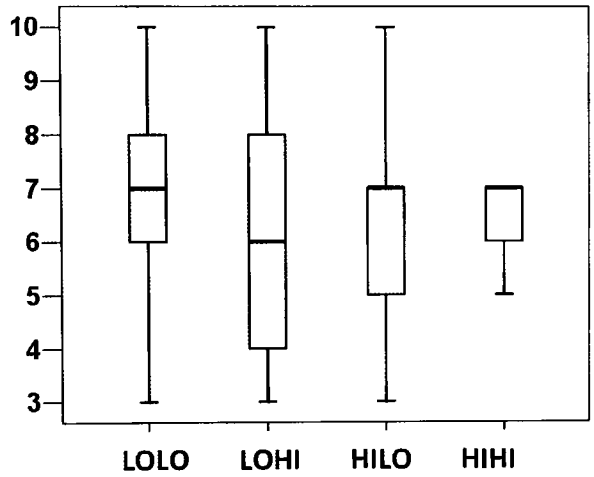

Figure F.1.25.3. Self-selected walking speed on incline.

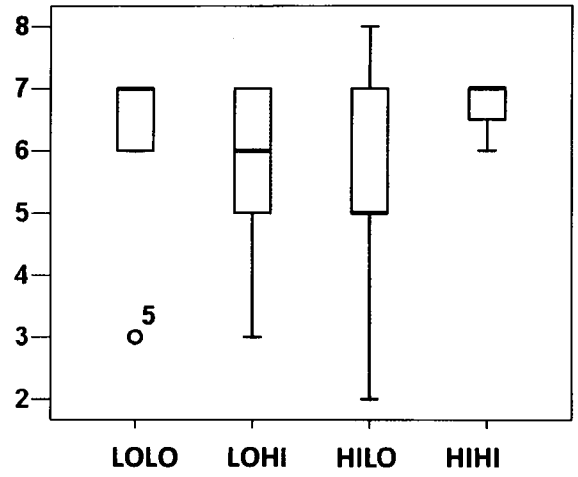

Figure F.1.25.4. Self-selected walking speed on decline.

References

Adderson, J. A., Parker, K. E., Macleod, D. A., Kirby, R. L., and McPhail, C., 2007. Effect of a shock-absorbing pylon on transmission of heel strike forces during the gait of people with unilateral trans-tibial amputations: a pilot study. Prosthetics and Orthotics International **31,** 384-93.

Alaranta, H., Kinnunen, A., Karkkainen, M., Pohjolainen, T., and Heliovaara, M., 1991. Practical benefits of flex-foot(tm) in below-knee amputees. Journal of Prosthetics and Orthotics **3,** 179-181.

Alaranta, H., Lempinen, V. M., Haavisto, E., Pohjolainen, T., and Hurri, H., 1994. Subjective benefits of energy storing prostheses. Prosthetics and Orthotics International **18,** 92-7.

Allard, P., Trudeau, F., Prince, F., Dansereau, J., Labelle, H., and Duhaime, M., 1995. Modelling and gait evaluation of asymmetrical-keel foot prosthesis. Medical and Biological Engineering and Computing **33,** 2-7.

Au, S., Berniker, M., and Herr, H., 2008. Powered ankle-foot prosthesis to assist level-ground and stair-descent gaits. Neural Networks **21,** 654-66.

Barr, A. E., Siegel, K. L., Danoff, J. V., McGarvey, C. L., 3rd, Tomasko, A., Sable, I., and Stanhope, S. J., 1992. Biomechanical comparison of the energy-storing capabilities of SACH and Carbon Copy II prosthetic feet during the stance phase of gait in a person with below-knee amputation. Physical Therapy **72,** 344-54.

Barth, D. G., Schumacher, L., and Thomas, S. S., 1992. Gait analysis and energy cost of below-knee amputees wearing six different prosthetic feet. Journal of Prosthetics and Orthotics **4,** 63-75.

Bell, A. L., Brand, R. A., and Pedersen, D. R., 1989. Prediction of hip joint center location from external landmarks. Human Movement Science **8,** 3-16.

Bell, A. L., Pedersen, D. R., and Brand, R. A., 1990. A comparison of the accuracy of several hip center location prediction methods. Journal of Biomechanics **23,** 617-621.

Berge, J. S., Czerniecki, J. M., and Klute, G. K., 2005. Efficacy of shock-absorbing versus rigid pylons for impact reduction in transtibial amputees based on laboratory, field, and outcome metrics. Journal of Rehabilitation Research and Development **42,** 795-808.

Berge, J. S., Klute, G. K., and Czerniecki, J. M., 2004. Mechanical properties of shock-absorbing pylons used in transtibial prostheses. Journal of Biomechanical Engineering **126,** 120-2.

Buckley, J. G., Jones, S. F., and Birch, K. M., 2002. Oxygen consumption during ambulation: comparison of using a prosthesis fitted with and without a tele-torsion device. Archives of Physical Medicine and Rehabilitation **83,** 576-80.

Burke, S., 2001. Missing values, outliers, robust statistics & non-parametric methods. In: "Statistics and Data Analysis." pp. 19-24. LC-GC Europe online supplement.

Cappozzo, A., Catani, F., Croce, U. D., and Leardini, A., 1995. Position and orientation in space of bones during movement: anatomical frame definition and determination. Clinical Biomechanics (Bristol, Avon) **10,** 171-178.

Casillas, J.-M., Dulieu, V., Cohen, M., Marcer, I., and Didier, J.-P., 1995. Bioenergetic comparison of a new energy-storing foot and SACH foot in traumatic below-knee vascular amputations. Archives of Physical Medicine and Rehabilitation **76,** 39-44.

Chin, T., Sawamura, S., Fujita, H., Nakajima, S., Ojima, I., Oyabu, H., Nagakura, Y., Otsuka, H., and Nakagawa, A., 1999. The efficacy of physiological cost index (PCI) measurement of a subject walking with an Intelligent Prosthesis. Prosthetics and Orthotics International **23,** 45-9.

Collins, S. H., and Kuo, A. D., 2010. Recycling energy to restore impaired ankle function during human walking. PLoS One **5,** e9307.

Culham, E. G., Peat, M., and Newell, E., 1986. Below-knee amputation: a comparison of the effect of the SACH foot and single axis foot on electromyographic patterns during locomotion. Prosthetics and Orthotics International **10,** 15-22.

Curtze, C., Hof, A. L., van Keeken, H. G., Halbertsma, J. P., Postema, K., and Otten, B., 2009. Comparative roll-over analysis of prosthetic feet. Journal of Biomechanics **42,** 1746-53.

Dal, U., Erdogan, T., Resitoglu, B., and Beydagi, H., 2009. Determination of preferred walking speed on treadmill may lead to high oxygen cost on treadmill walking. Gait and Posture **31,** 366-9.

Dempster, W. T., 1955. Space requirements of the seated operator: Geometrical, kinematic, and mechanical aspects of the body, with special reference to the limbs. In: "Technical report WADC-TR." pp. 55 -159. Wright-Patterson Air Force Base, Ohio.

Doane, N. E., and Holt, L. E., 1983. A comparison of the SACH and single axis foot in the gait of unilateral below-knee amputees. Prosthetics and Orthotics International **7,** 33-6.

Donker, S. F., and Beek, P. J., 2002. Interlimb coordination in prosthetic walking: effects of asymmetry and walking velocity. ACTA Psychologica (Amsterdam) **110,** 265-88.

Engsberg, J. R., Herbert, L. M., Grimston, S. K., Fung, T. S., and Harder, J. A., 1994. Relation among indices of effort and oxygen uptake in below-knee amputee and able-bodied children. Archives of Physical Medicine and Rehabilitation **75,** 1335-41.

Ennos, R., 2007. Statistical and data handling skills in biology. Pearson Education Limited, Harlow, England.

Frenkel-Toledo, S., Giladi, N., Peretz, C., Herman, T., Gruendlinger, L., and Hausdorff, J. M., 2005. Effect of gait speed on gait rhythmicity in Parkinson's disease: variability of stride time and swing time respond differently. Journal of Neuroengineering and Rehabilitation **2,** 23.

Fung, Y. C., and Tong, P., 2001. Classical and computational solid mechanics. World Scientific Publishing Co. Pte. Ltd., London, UK.

Gard, S. A., and Konz, R. J., 2003. The effect of a shock-absorbing pylon on the gait of persons with unilateral transtibial amputation. Journal of Rehabilitation Research and Development **40,** 109-24.

Geil, M. D., 2001. Energy loss and stiffness properties of dynamic elastic response prosthetic feet. Journal of Prosthetics and Orthotics **13,** 70-73.

Geil, M. D., 2002. An iterative method for viscoelastic modeling of prosthetic feet. Journal of Biomechanics **35,** 1405-1410.

Geil, M. D., Parnianpour, M., Quesada, P., Berme, N., and Simon, S., 2000. Comparison of methods for the calculation of energy storage and return in a dynamic elastic response prosthesis. Journal of Biomechanics **33,** 1745-50.

Goh, J. C., Solomonidis, S. E., Spence, W. D., and Paul, J. P., 1984. Biomechanical evaluation of SACH and uniaxial feet. Prosthetics and Orthotics International **8,** 147-54.

Hachisuka, K., Umezu, Y., Ogata, H., Ohmine, S., Shinkoda, K., and Arizono, H., 1999. Subjective evaluations and objective measurements of the ischial-ramal containment prosthesis. Journal of UOEH **21,** 107-18.

Hafner, B. J., 2005. Clinical prescription and use of prosthetic foot and ankle mechanisms: a review of the literature. Journal of Prosthetics and Orthotics **17,** 5-11.

Hafner, B. J., Sanders, J. E., Czerniecki, J., and Fergason, J., 2002. Energy storage and return prostheses: does patient perception correlate with biomechanical analysis? Clinical Biomechanics (Bristol, Avon) **17,** 325-44.

Hansen, A., 2008. Effects of alignment on the roll-over shapes of prosthetic feet. Prosthetics and Orthotics International **32,** 390-402.

Hansen, A. H., and Childress, D. S., 2004. Effects of shoe heel height on biologic rollover characteristics during walking. Journal of Rehabilitation Research and Development **41,** 547-54.

Hansen, A. H., Childress, D. S., and Knox, E. H., 2000. Prosthetic foot roll-over shapes with implications for alignment of trans-tibial prostheses. Prosthetics and Orthotics International **24,** 205-15.

Hansen, A. H., Childress, D. S., and Knox, E. H., 2004. Roll-over shapes of human locomotor systems: effects of walking speed. Clinical Biomechanics (Bristol, Avon) **19,** 407-14.

Hansen, A. H., Meier, M. R., Sam, M., Childress, D. S., and Edwards, M. L., 2003. Alignment of trans-tibial prostheses based on roll-over shape principles. Prosthetics and Orthotics International **27,** 89-99.

Hansen, A. H., Meier, M. R., Sessoms, P. H., and Childress, D. S., 2006. The effects of prosthetic foot roll-over shape arc length on the gait of trans-tibial prosthesis users. Prosthetics and Orthotics International **30,** 286-99.

Hausdorff, J. M., 2005. Gait variability: methods, modeling and meaning. Journal of Neuroengineering and Rehabilitation **2,** 19.

Hausdorff, J. M., Edelberg, H. K., Mitchell, S. L., Goldberger, A. L., and Wei, J. Y., 1997. Increased gait unsteadiness in community-dwelling elderly fallers. Archives of Physical Medicine and Rehabilitation **78,** 278-83.

Hausdorff, J. M., Rios, D. A., and Edelberg, H. K., 2001. Gait variability and fall risk in community-living older adults: a 1-year prospective study. Archives of Physical Medicine and Rehabilitation **82,** 1050-6.

Hofstad, C., Linde, H., Limbeek, J., and Postema, K., 2004. Prescription of prosthetic ankle-foot mechanisms after lower limb amputation. Cochrane Database of Systematic Reviews, CD003978.

Hsu, M. J., Nielsen, D. H., Lin-Chan, S. J., and Shurr, D., 2006. The effects of prosthetic foot design on physiologic measurements, self-selected walking velocity, and physical activity in people with transtibial amputation. Archives of Physical Medicine and Rehabilitation **87,** 123-9.

Hsu, M. J., Nielsen, D. H., Yack, H. J., and Shurr, D. G., 1999. Physiological measurements of walking and running in people with trans-tibial amputations with 3 different prostheses. Journal of Orthopaedic and Sports Physical Therapy **29**.

Jang, T. S., Lee, J. J., Lee, D. H., and Yoon, Y. S., 2001. Systematic methodology for the design of a flexible keel for energy-storing prosthetic feet. Medical and Biological Engineering and Computing **39,** 56-64.

Jepson, F., Datta, D., Harris, I., Heller, B., Howitt, J., and McLean, J., 2008. A comparative evaluation of the adaptive knee and catech knee joints: a preliminary study. Prosthetics and Orthotics International **32,** 84-92.

Jones, S. F., Twigg, P. C., Scally, A. J., and Buckley, J. G., 2006. The mechanics of landing when stepping down in unilateral lower-limb amputees. Clinical Biomechanics (Bristol, Avon) **21,** 184-93.

Jordan, K., Challis, J. H., and Newell, K. M., 2007. Walking speed influences on gait cycle variability. Gait and Posture **26,** 128-34.

Kabra, S. G., and Narayanan, R., 1991. Equipment and methods for laboratory testing of ankle-foot prostheses as exemplified by the Jaipur foot. Journal of Rehabilitation Research and Development **28,** 23-34.

Kendell, C., Lemaire, E. D., Dudek, N. L., and Kofman, J., 2010. Indicators of dynamic stability in transtibial prosthesis users. Gait and Posture **31,** 375-9.

Klute, G. K., and Berge, J. S., 2004. Modelling the effect of prosthetic feet and shoes on the heel-ground contact force in amputee gait. Proceedings of the Institution of Mechanical Engineers. Part H **218,** 173-82.

Klute, G. K., Berge, J. S., Orendurff, M. S., Williams, R. M., and Czerniecki, J. M., 2006. Prosthetic intervention effects on activity of lower-extremity amputees. Archives of Physical Medicine and Rehabilitation **87,** 717-22.

Klute, G. K., Berge, J. S., and Segal, A. D., 2004. Heel-region properties of prosthetic feet and shoes. Journal of Rehabilitation Research and Development **41,** 535-46.

Knox, E. H., 1996. The role of prosthetic feet in walking. Unpublished PhD thesis, Northwestern University.

Lehmann, J. F., Price, R., Boswell-Bessette, S., Dralle, A., and Questad, K., 1993a. Comprehensive analysis of dynamic elastic response feet: Seattle ankle/lite foot versus SACH foot. Archives of Physical Medicine and Rehabilitation **74,** 853-61.

Lehmann, J. F., Price, R., Boswell-Bessette, S., Dralle, A., Questad, K., and deLateur, B. J., 1993b. Comprehensive analysis of energy storing prosthetic feet: Flex foot and seattle foot versus standard SACH foot. Archives of Physical Medicine and Rehabilitation **74,** 1225-31.

Lehmann, J. F., Price, R., Okumura, R., Questad, K., de Lateur, B. J., and Negretot, A., 1998. Mass and mass distribution of below-knee prostheses: effect on gait efficacy and self-selected walking speed. Archives of Physical Medicine and Rehabilitation **79,** 162-8.

Lin-Chan, S. J., Nielsen, D. H., Yack, H. J., Hsu, M. J., and Shurr, D. G., 2003. The effects of added prosthetic mass on physiologic responses and stride frequency during multiple speeds of walking in persons with transtibial amputation. Archives of Physical Medicine and Rehabilitation **84,** 1865-71.

Macfarlane, P. A., Nielsen, D. H., Shurr, D. G., and Meier, K., 1991a. Gait comparisons for below-knee amputees using a flex-foot(TM) versus a conventional prosthetic foot. Journal of Prosthetics and Orthotics **3,** 150-161.

Macfarlane, P. A., Nielsen, D. H., Shurr, D. G., and Meier, K., 1991b. Perception of walking difficulty by below-knee amputees using a conventional foot versus the flex-foot. Journal of Prosthetics and Orthotics **3,** 114-119.

MacGregor, J., 1981. The evaluation of patient performance using long-term ambulatory monitoring technique in the domiciliary environment. Physiotherapy **67,** 30-3.

Marinakis, G. N., 2004. Interlimb symmetry of traumatic unilateral transtibial amputees wearing two different prosthetic feet in the early rehabilitation stage. Journal of Rehabilitation Research and Development **41,** 581-90.

Menard, M. R., McBride, M. E., Sanderson, D. J., and Murray, D. D., 1992. Comparative biomechanical analysis of energy-storing prosthetic feet. Archives of Physical Medicine and Rehabilitation **73,** 451-8.

Miller, L. A., and Childress, D. S., 1997. Analysis of a vertical compliance prosthetic foot. Journal of Rehabilitation Research and Development **34,** 52-7.

Miller, W. C., Deathe, A. B., Speechley, M., and Koval, J., 2001a. The influence of falling, fear of falling, and balance confidence on prosthetic mobility and social activity among individuals with a lower extremity amputation. Archives of Physical Medicine and Rehabilitation **82,** 1238-44.

Miller, W. C., Speechley, M., and Deathe, B., 2001b. The prevalence and risk factors of falling and fear of falling among lower extremity amputees. Archives of Physical Medicine and Rehabilitation **82,** 1031-7.

Moser, D., Abimosleh, F., Zahedi, S., Harris, G., Ross, J., and McCarthy, J., 2009. Biomechanical analysis of a novel automatically self-aligning ankle-foot prosthesis. Orthopädie-Technik Quarterly, English edition III, 10-15.

Nene, A. V., 1993. Physiological cost index of walking in able-bodied adolescents and adults. Clinical Rehabilitation **7,** 319 – 326.

Nielsen, D. H., Shurr, D. G., Golden, J. C., and Meier, K., 1989. Comparison of energy cost and gait efficiency during ambulation in below-knee amputees using different prosthetic feet - A preliminary report. Journal of Prosthetics and Orthotics **1,** 24-31.

O'Connor, C. M., Thorpe, S. K., O'Malley, M. J., and Vaughan, C. L., 2007. Automatic detection of gait events using kinematic data. Gait and Posture **25,** 469-74.

Owings, T. M., and Grabiner, M. D., 2003. Measuring step kinematic variability on an instrumented treadmill: how many steps are enough? Journal of Biomechanics **36,** 1215-8.

Owings, T. M., and Grabiner, M. D., 2004. Variability of step kinematics in young and older adults. Gait and Posture **20,** 26-9.

Perry, J., 1992. Gait Analysis: Normal and pathological function Slack Incorporated, Thorofare, NJ.

Perry, J., Boyd, L. A., Rao, S. S., and Mulroy, S. J., 1997. Prosthetic weight acceptance mechanics in transtibial amputees wearing the single axis, seattle lite, and flex foot. IEEE Transactions on Rehabilitation Engineering **5,** 283-9.

Perry, J., and Shanfield, S., 1993. Efficiency of dynamic elastic response prosthetic feet. Journal of Rehabilitation Research and Development **30,** 137-43.

Petrie, A., and Sabin, C., 2000. Medical statistics at a glance. Blackwell Science Ltd, Malden, MA.

Postema, K., Hermens, H. J., de Vries, J., Koopman, H. F., and Eisma, W. H., 1997a. Energy storage and release of prosthetic feet. Part 1: Biomechanical analysis related to user benefits. Prosthetics and Orthotics International **21,** 17-27.

Postema, K., Hermens, H. J., de Vries, J., Koopman, H. F., and Eisma, W. H., 1997b. Energy storage and release of prosthetic feet. Part 2: Subjective ratings of 2 energy storing and 2 conventional feet, user choice of foot and deciding factor. Prosthetics and Orthotics International **21,** 28-34.

Powers, C. M., Rao, S., and Perry, J., 1998. Knee kinetics in trans-tibial amputee gait. Gait and Posture **8,** 1-7.

Powers, C. M., Torburn, L., Perry, J., and Ayyappa, E., 1994. Influence of prosthetic foot design on sound limb loading in adults with unilateral below-knee amputations. Archives of Physical Medicine and Rehabilitation **75,** 825-9.

Prince, F., Winter, D. A., Sjonnesen, G., and Wheeldon, R. K., 1994. A new technique for the calculation of the energy stored, dissipated, and recovered in different ankle-foot prostheses. IEEE Transactions on Rehabilitation Engineering **2,** 247-255.

Rao, S. S., Boyd, L. A., Mulroy, S. J., Bontrager, E. L., Gronley, J. K., and Perry, J., 1998. Segment velocities in normal and transtibial amputees: prosthetic design implications. IEEE Transactions on Rehabilitation Engineering **6,** 219-26.

Rau, B., Bonvin, F., and de Bie, R., 2007. Short-term effect of physiotherapy rehabilitation on functional performance of lower limb amputees. Prosthetics and Orthotics International **31,** 258-70.

Sam, M., Hansen, A. H., and Childress, D. S., 2000. Mechanical characterisation of prosthetic feet using a prosthetic foot loading apparatus. In: "Engineering in Medicine and Biology Society." pp. 1968 -1971. IEEE, Chicago.

Sam, M., Hansen, A. H., and Childress, D. S., 2004. Characterisation of prosthetic feet used in low-income countries. Prosthetics and Orthotics International **28,** 132-40.

Sanders, J. E., Miller, R. A., Berglund, D. N., and Zachariah, S. G., 1997. A modular six-directional force sensor for prosthetic assessment: a technical note. Journal of Rehabilitation Research and Development **34,** 195-202.

Saunders, M. M., Schwentker, E. P., Kay, D. B., Bennett, G., Jacobs, C. R., Verstraete, M. C., and Njus, G. O., 2003. Finite element analysis as a tool for parametric prosthetic foot design and evaluation. Technique development in the solid ankle cushioned heel (SACH) foot. Computer Methods in Biomechanics and Biomedical Engineering **6,** 75-87.

Schmalz, T., Blumentritt, S., and Jarasch, R., 2002. Energy expenditure and biomechanical characteristics of lower limb amputee gait: the influence of prosthetic alignment and different prosthetic components. Gait and Posture **16,** 255-63.

Seymour, R., 2002. Prosthetics and orthotics: Lower limb and spinal. Lippincott Williams & Wilkins, Baltimore, MD.

Skinner, H. B., Abrahamson, M. A., Hung, R. K., Wilson, L. A., and Effeney, D. J., 1985. Static load response of the heels of SACH feet. Orthopedics **8,** 225-8.

Snyder, R. D., Powers, C. M., Fontaine, C., and Perry, J., 1995. The effect of five prosthetic feet on the gait and loading of the sound limb in dysvascular below-knee amputees. Journal of Rehabilitation Research and Development **32,** 309-15.

Srinivasan, S., Westervelt, E. R., and Hansen, A. H., 2009. A low-dimensional sagittal-plane forward-dynamic model for asymmetric gait and its application to study the gait of transtibial prosthesis users. Journal of Biomechanical Engineering **131,** 031003.

Tilley, A. R., 2002. The measure of man and woman: human factors in design. John Wiley & Sons, New York, New York.

Torburn, L., Perry, J., Ayyappa, E., and Shanfield, S. L., 1990. Below-knee amputee gait with dynamic elastic response prosthetic feet: a pilot study. Journal of Rehabilitation Research and Development **27,** 369-84.

Torburn, L., Powers, C. M., Guiterrez, R., and Perry, J., 1995. Energy expenditure during ambulation in dysvascular and traumatic below-knee amputees: a comparison of five prosthetic feet. Journal of Rehabilitation Research and Development **32,** 111-9.

Traballesi, M., Porcacchia, P., Averna, T., and Brunelli, S., 2008. Energy cost of walking measurements in subjects with lower limb amputations: a comparison study between floor and treadmill test. Gait and Posture **27,** 70-5.

Twiste, M., 2004. The effect of transverse rotation and longitudinal translation between prosthetic components during the gait of unilateral trans-tibial amputees. Unpublished PhD thesis, University of Salford.

Twiste, M., and Rithalia, S., 2003. Transverse rotation and longitudinal translation during prosthetic gait--a literature review. Journal of Rehabilitation Research and Development **40,** 9-18.

Twiste, M., Rithalia, S. V., and Kenney, L., 2004. A cam-displacement transducer device for measuring small two-degree of freedom inter-component motion in a prosthesis. Medical Engineering and Physics **26,** 335-40.

UK. 2007. Health survey for England 2007: Healthy lifestyles: knowledge, attitudes and behaviour (D. o. Health, Ed.). The Health and Social Care Information Centre Leeds.

Underwood, H. A., Tokuno, C. D., and Eng, J. J., 2004. A comparison of two prosthetic feet on the multi-joint and multi-plane kinetic gait compensations in individuals with a unilateral trans-tibial amputation. Clinical Biomechanics (Bristol, Avon). **19,** 609-16.

van der Linde, H., Hofstad, C. J., Geurts, A. C., Postema, K., Geertzen, J. H., and van Limbeek, J., 2004. A systematic literature review of the effect of different prosthetic components on human functioning with a lower-limb prosthesis. Journal of Rehabilitation Research and Development **41,** 555-70.

van Jaarsveld, H. W., Grootenboer, H. J., de Vries, J., and Koopman, H. F., 1990. Stiffness and hysteresis properties of some prosthetic feet. Prosthetics and Orthotics International **14,** 117-24.

Vanicek, N., Strike, S., McNaughton, L., and Polman, R., 2009. Gait patterns in transtibial amputee fallers vs. non-fallers: biomechanical differences during level walking. Gait and Posture **29,** 415-20.

Whittle, M., 1991. Gait analysis: An introduction. Butterworth-Heinemann Ltd, Oxford.

Yamasaki, M., Sasaki, T., and Torii, M., 1991. Sex difference in the pattern of lower limb movement during treadmill walking. European Journal of Applied Physiology and Occupational Physiology **62,** 99-103.

Zar, J. H., 1996. Biostatistical analysis. Prentice-Hall, Upper Saddle River, N.J.

Zeller, S., 2007. Stiffness properties of prosthetic feet under cross-slope conditions. Unpublished MSc thesis, Georgia Institute of Technology.

Zmitrewicz, R. J., Neptune, R. R., and Sasaki, K., 2007. Mechanical energetic contributions from individual muscles and elastic prosthetic feet during symmetric unilateral transtibial amputee walking: a theoretical study. Journal of Biomechanics **40,** 1824-31.